Faculty of Science and Engineering

Geochemical Modelling to Characterize Wettability of Oil-Brine-Rock Systems

Yongqiang Chen

This thesis is presented for the degree of

Doctor of Philosophy

of

Curtin University

July 2019

Declaration

To the best of my knowledge and belief, this thesis contains no material previously published by any other person except where due acknowledgement has been made.

This thesis contains no material, which has been accepted for the award of any other degree or diploma in any university.

Signature: ███████████ Yongqiang Chen)

Data: 30 - Jan - 2020

Copyright

I warrant that I have obtained, where necessary, permission from the copyright owners to use any third-party copyright material reproduced in the thesis (e.g. questionnaires, artwork, unpublished letters), or to use any of my own published work (e.g. journal articles) in which the copyright is held by another party (e.g. publisher. Co-author).

Signature: ▮▮▮▮▮▮ Yongqiang Chen)

Data: 30-Jan-2020

Acknowledgements

Abstract

Low salinity waterflooding appears to be a cost-effective and environmentally friendly means to improve oil recovery in both sandstone and carbonate reservoirs. Wettability alteration has been confirmed as an important physiochemical process behind low salinity waterflooding. While a few mechanisms have been proposed to interpret this physicochemical process, few works have been done to draw on any structured research into the interpretation of wettability alteration process. This research aimed to characterize and quantify the interaction of oil-brine-rock system by addressing a few knowledge gaps with a combination of experimental and numerical studies.

To predict low salinity waterflooding performance at subsurface, saturation functions (e.g., relative permeabilities and capillary pressure) need to be determined to model the wettability alteration, which is believed to be represented using geochemical reactions taking place on oil-brine-rock interfaces. Therefore, to characterize the oil-brine-rock interactions in sandstone and carbonate reservoirs, the hypothesis and methodologies in this work are as the following:

Firstly, while published work show that pH would increase during low salinity waterflooding in sandstone core plugs, the nature of the physics behind the pH increase has not been quantified, presenting a tremendous impediment to predict the low salinity EOR-Effect. To quantify the controlling factor of the pH increase, ion exchange process occurring at basal-charged clays is hypothesized to be a driver of the pH increase, which was tested using PHREEQC against literature data. Secondly, the effect of mineral dissolution and surface complexation on pH increase were also examined using 1D reactive transport modelling in PHREEQC against literature data. Thirdly, given that both edge-charged and basal-charged planes contribute to oil-mineral adhesion, a new geochemical model in light of adsorption theory was developed to quantify the relative contribution of the two type of minerals on the adhesion thus wettability by coupling PHREEQC and PEST against literature data. Fourthly, on the completion of the geochemical modelling characterization at sub-pore scale, the geochemical characterization was tested at pore-scale using Micro X-ray computed tomography.

Similar approach was also used to characterize the oil-brine-carbonate rock with the same assumption that the geochemical reactions on brine-rock-calcite interfaces likely governs the wettability alteration process. To test the hypothesis, a combination of contact angle measurements with and without carbonation together with geochemical modelling was conducted.

The geochemical reactions on oil-brine-rock interface have been validated and calibrated to characterize the wettability alteration during low salinity waterflooding. For sandstone reservoirs, the primary contributor of the pH increase during low salinity waterflooding would be ion exchange process in basal-charged plane minerals (e.g., illite, smectite and chlorite), followed by albite dissolution and surface complexation reactions. Also, the new geochemical model shows that basal adsorption ($>Na + BaseH^+ = >BaseH + Na^+$) dominates adsorption of basic component of oils at low pH (pH=5). Rather, edge adsorption controls adsorption mechanism at high pH (pH=8). Furthermore, the model shows that salinity plays a minor role in adsorption at a controlled pH system. Our new model quantifies the relative contribution of basal and edge planes on basic component adhesion thus wettability at different pH and salinity, providing insights and new geochemical data to existing geochemical database, thereby better model and predict the wettability alteration during low salinity waterflooding. Moreover, low salinity brine decreases adhesion of oil-kaolinite minerals at pore surfaces, accounting for the *in-situ* wettability alteration thus oil film detachment. This observation sheds

light on the significance of geochemical controls over wettability alteration at pore-scale through water film propagation, thus providing insights in oil coalescence, transport, banking and eventually recovery of oil at different length scale. In addition, geochemical modelling demonstrates that excess H^+ substantially substitutes exchangeable cations (>Na) embedded in muscovite thus decreasing electrostatic bridges between oil-brine-muscovite. This provides a first quantitative investigation on how water uptake of CO_2 depresses ion exchange process between oil/brine/basal-charged minerals and thus leading to wettability alteration.

For carbonate reservoirs, this research demonstrates that the conventional dilution approach likely triggers an oil-wet system at low pH, which may explain why the low salinity EOR-effect is not always observed by injecting low salinity water in carbonated reservoirs. Also, coupled surface complexation/CO_2 and mineral dissolution model provides a mechanistic rationale for the CO_2-induced wettability shift, and a means for coupling such observations into larger reservoir simulators. The latter might provide a path for more effectively tuning CO_2 EOR to increase oil recovery from carbonate reservoirs. We therefore argue that H^+ adsorption due to water uptake of CO_2 on the interface of oil/brine and brine/carbonate governs wettability alteration during CO_2-assisted EOR techniques. Our study sheds light on the significant influence of excess H^+ due to water uptake of CO_2 on oil-brine-carbonate system wettability thus enhancing hydrocarbon recovery in carbonate reservoirs.

To summarize, the wettability of oil-brine-rocks have been characterized with a combination of the experiments and geochemical modelling for both sandstone and carbonate reservoirs. The identified mechanisms can be further applied to explain wettability alteration in CO_2-assisted EOR. Moreover, the new geochemical model would be expected to be coupled with existing commercial reservoir simulators to model wettability alteration during low salinity waterflooding in subsurface.

Contents

List of Figures

List of Tables

Publications by the author

(Publication forming part of the thesis as standalone chapters)

<u>Chapter 1:</u>

Chen, Y., Xie, Q., Pu, W., & Saeedi, A. (2018). Drivers of pH increase and implications for low salinity effect in sandstone. Fuel, 218, 112-117. doi:https://doi.org/10.1016/j.fuel.2018.01.037

<u>Chapter 2:</u>

Chen, Y., Xie, Q., & Saeedi, A. (2019b). Role of ion exchange, surface complexation, and albite dissolution in low salinity water flooding in sandstone. Journal of Petroleum Science and Engineering, 176, 126-131. doi:https://doi.org/10.1016/j.petrol.2019.01.019

<u>Chapter 3:</u>

Chen, Y., Xie, Q., & Saeedi, A. (2019a). Electrostatic characterization of -NH^+-brine-kaolinite system: Implications for low salinity waterflooding in sandstone reservoirs. Journal of Petroleum Science and Engineering. doi:https://doi.org/10.1016/j.petrol.2019.04.056

<u>Chapter 5:</u>

Chen, Y., Xie, Q., Sari, A., Brady, P. V., & Saeedi, A. (2018). Oil/water/rock wettability: Influencing factors and implications for low salinity water flooding in carbonate reservoirs. Fuel, 215, 171-177. doi:https://doi.org/10.1016/j.fuel.2017.10.031

<u>Chapter 6:</u>

Chen, Y., Sari, A., Xie, Q., & Saeedi, A. (2019b). Insights into the wettability alteration of CO_2-assisted EOR in carbonate reservoirs. Journal of Molecular Liquids, 279, 420-426. doi:https://doi.org/10.1016/j.molliq.2019.01.112

<u>Chapter 7:</u>

Chen, Y., Sari, A., Xie, Q., Brady, P. V., Hossain, M. M., & Saeedi, A. (2018). Electrostatic Origins of CO2-Increased Hydrophilicity in Carbonate Reservoirs. Scientific Reports, 8(1), 17691. doi:10.1038/s41598-018-35878-3

<u>Chapter 8:</u>

Chen, Y., Sari, A., Xie, Q., & Saeedi, A. (2019a). Excess H^+ Increases Hydrophilicity during CO2-Assisted Enhanced Oil Recovery in Sandstone Reservoirs. Energy & Fuels, 33(2), 814-821. doi:10.1021/acs.energyfuels.8b03573

Introduction

Importance of Water-Assisted Enhanced Oil Recovery and Problem Statements

Waterflooding has been widely used to improve oil recovery by maintaining reservoir pressure over the past a few decades [1]. However, more than 70% of Original Oil in Place (OOIP) remains in reservoirs after conventional waterflooding [2]. Further improving the efficiency of waterflooding has long been a goal of reservoir engineers. One such technique that gains great interests from industry is termed low salinity water flooding, which is also called *LoSal* flooding by British Petroleum (BP) [3, 4], *Smart Water* flooding by its originators, Austad and co-workers, at the University of Stavanger, Saudi Aramco[5], and *Designer Water flooding* by Shell [6, 7]. Coreflooding experiments and field scale demonstrations show that low salinity waterflooding can recover additional 5-10% of OOIP after conventional waterflooding [8-12].

Since the inception of low salinity waterflooding, a number of mechanisms have been proposed to understand why low salinity water injection likely renders a measureable incremental oil recovery by the aid of coreflooding experiments. The proposed mechanisms include: fines mobilization [13], limited release of mixed-wet particles [13], increased pH and reduced IFT similar to the alkaline flooding [14], multi-component ion exchange (MIE) [4, 15-17], expansion of the double layer [18-20], salt-in effect [21], salting-out effect [22] and osmotic pressure [23]. Wettability alteration is thought to be one of the main physicochemical processes behind the additional oil recovery. In this context, wettability of oil/brine/rock system thus is of vital importance because system wettability governs subsurface multiphase flow behaviour, remaining oil saturation distribution, and thus hydrocarbon recovery. However, the controlling factor(s) which drives this process has yet to be clearly defined, which in return presents uncertainties to manage and predict low salinity effect at field scale [24]. For example, BP conducted four sets of test at Endicott in Alaska North Slope, showing that residual oil saturation after high salinity water flooding decreased from 41 to 27% followed by low salinity water injection [25]. Yet, corefloods and single well field pilot tests show a negligible low salinity effect in Snorre field at North Sea [26].

Therefore, there is a pressing need to draw on a structured research into this wettability alteration process, thus providing an overall framework to minimize the intrinsic uncertainty of low salinity waterflooding. In particular, the interaction of oil-brine-rock system needs to be systematically characterized with a goal to providing an interplant for the modelling the shift of relative permeability curves due to the wettability alteration process. To achieve this, existing reservoir simulators have been equipped with the simplified geochemical models without taking into account considering oil-brine-rock interactions. For example, modelling the shift of relative permeability curves as a function of salinity has been implemented in ECPLISE 100 [3]. Moreover, geochemical reactions in particular between fluid-rocks have been incorporated into CMG-GEM to model wettability alteration as a function of exchangeable cations for sandstone and the concentration of SO_4^{2-} in carbonate reservoirs [27-32]. However, existing accounts fail to incorporate the interaction of oil-brine-rock, which governs in-situ system wettability, thus calling for a closer examination of oil-brine-rock interactions from geochemical perspectives.

Research Objectives

This research aimed to characterize the oil-brine-rock interactions from geochemical aspect, which provides a lens to determine wettability alteration by shifting relative permeabilities as a function of brine composition and local pH. To achieve this, below were proposed

hypothesise, which have been tested in this research through a combination of laboratory experiments and geochemical modelling.

1. Given that effluent pH likely increases 1 to 3 unit during low salinity waterflooding in sandstone reservoirs [13, 18, 33-35], ion exchange process is assumed to be one the mechanisms to trigger the pH increase. Moreover, the increased pH would likely promote the detachment of oil film from basal-charged clays by reducing the bridges between oil-brine-rock interfaces.
2. Mineral dissolution in particular albite and surface complexation may also contribute to pH increase. It is assumed that the albite dissolution may contribute more pH increase than surface complexation reactions.
3. Published work show that both ion exchange and surface complexation reactions contribute to wettability alteration [36]. Yet, their relative contribution to wettability alteration has not been clearly defined. Therefore, a new geochemical model needs to be developed to couple ion exchange and surface complexation together.
4. Although contact angle tests and geochemical modelling predict wettability alteration, the wettability alteration has not been proven on pore scale. It is thus hypothesized that the geochemical induced wettability alteration at sub-pore scale would prevail at pore-scale in the presence of low salinity brine.
5. Literature shows that sandstone surface will be more water-wet in carbonated water. Based on the understanding of wettability alteration in low salinity water, pH decrease is hypothesized as the mechanism of wettability alteration in carbonated water. Specifically, the high concentration of H^+ competently adsorbed on sandstone surface, which leads to oil desorption in carbonated water.
6. In light of the role of pH in low salinity waterflooding in carbonate reservoirs, it is hypothesized that pH would play an important role in wettability alteration in carbonated water.

To test these hypotheses, the main methodologies used in this research are briefly listed as following:

1. To test hypothesis #1, the ion exchange process taking place at basal-charged clays was validated against RezaeDoust et al., (2011, Figure 2) during low salinity waterflooding by the aid of geochemical modelling through PHREEQC. Moreover, the equilibrium pH and oil-brine ion exchange were analysed to illustrate the pH increase in different salinity brines.
2. To verify hypothesis #2, pH profile from the same literature (RezaeDoust et al., (2011, Figure 2)) was matched to quantify the relative contribution of albite dissolution and surface complexation on pH increase during low salinity waterflooding using 1D reactive transport modelling in PHREEQC.
3. To test hypothesis #3, a new geochemical model coupling ion exchange and surface complexation is proposed to model base component adsorption on kaolinite surface against RezaeDoust et al., (2011, Figure 13) by combination of PHREEQC and PEST.
4. To test hypothesis #4, a tertiary low salinity waterflooding was conducted using Micro-CT scanning. Also, water cluster distribution was analysed to provide evidence of the wettability alteration at pore-scale.
5. To verify hypothesis #5, contact angle tests were conducted to measure wettability in carbonated brines with different salinities. Moreover, the influence of pH on chemical species distributions at oil-brine-rock interface was analysed by geochemical modelling in PHREEQC.
6. To teste hypothesis #6, wettability alteration was examined through contact angle tests in the presence of brines with and without carbonation. The surface charge properties were

then evaluated by surface complexation modelling to quantify the interface electrostatic forces.

Outline and Scope of work

To verify the above hypotheses, the following nine chapters were conducted to investigate the correlation between wettability and geochemical reactions on oil-brine-rock interface. In Chapter 1-3, geochemical modelling was carried on to screen the mechanisms of wettability alteration in sandstone reservoirs. Then the wettability alteration was examined at pore-scale by Micro-CT scanning in Chapter 4. Furthermore, to better understand wettability alteration on the calcite surface, contact angle tests and surface complexation modelling were evaluated to explain the wettability alteration on calcite surfaces in Chapter 5. Moreover, the role of pH on wettability alteration was examined in carbonated brines, and geochemical modelling was used to characterize geochemical reactions on oil-brine-rock interfaces in Chapters 6-9.

In Chapter 1, mechanism of pH increase was examined by calculation of ion exchange in PHREEQC. Furthermore, the correlation between amount of oil adsorption by ion exchange (bridging number) and oil recovery was evaluated to illustrate the correlation between ion exchange and oil recovery.

In Chapter 2, the relative contribution of the ion exchange, albite dissolution and surface complexation to pH increase was examined in reactive transport modelling by PHREEQC against RezaeiDoust et al.'s [33] experimental data. It shows that ion exchange is the primary mechanism of pH increase, while albite dissolution and surface complexation make secondary contribution.

In Chapter 3, a new geochemical model was proposed in light of electrostatic adsorption theory to quantify the adsorption of base polar component on kaolinite surfaces. Both ion exchange and surface complexation reaction were analysed to reflect their relative contribution to wettability alteration.

In Chapter 4, wettability alteration in pore scale was characterized by Micro-CT scanning and geochemical modelling. The distribution of water clusters was analysed from the CT images to quantify wettability alteration. Geochemical modelling was conducted to relate the physicochemical process at sub-pore scale to account for *in-situ* wettability alteration at the pore-scale.

In Chapter 5, wettability alteration on calcite surface was characterized by contact angle tests and surface complexation modelling. The results show that geochemical reactions on oil-brine-calcite interface may govern the wettability alteration on calcite surfaces in low salinity brines. Furthermore, surface complexation modelling indicates that pH would affect the electrostatic force, thus influencing wettability.

In Chapter 6, to further confirm the role of pH on wettability alteration on the calcite surface, contact angle tests were conducted in carbonated brines and pH fixed acidic brine. The results reveal that both calcite surfaces are strongly water-wet, which indicates that pH is the controlling mechanism of wettability alteration in carbonated water.

In Chapter 7. The role of pH on wettability alteration of calcite surface was applied to explain wettability alteration in carbonated water. Contact angle and surface complexation modelling reveal that the strong hydrophilicity of oil-brine-carbonate are caused by high concentration H^+ at oil-brine and brine-calcite surfaces. The low pH in carbonated water leads to strong repulsive force between oil-brine interfaces and calcite-brine interfaces due to the increase of electrostatic bridges.

In Chapter 8, the role of pH on wettability alteration on mica surface was used to explain wettability alteration in carbonated water. Contact angle tests show a strong water-wet mica surface in carbonated water. Further geochemical modelling indicates that excess H^+ would occupy the adsorption site at mica surfaces, which would desorb the oil film in carbonated brines.

Literature Review

Introduction

Waterflooding has been widely implemented to improve oil recovery for the past a few decades by maintaining reservoir pressure [1]. However, more than 70% OOIP remains in reservoirs after conventional waterflooding. To unlock the remaining oil, low salinity waterflooding has been proposed to further improve recovery efficiency for the past two decades. Literature shows that 5-10% additional oil may be recovered by low salinity waterflooding in tertiary mode in some carbonate and sandstone reservoirs (not for all reservoirs) from coreflooding experiments [8-10, 37-40].

History matching of coreflooding experiments indicates that the low salinity water likely accelerates oil production by shifting relative permeability curves towards a lower residual oil saturation [9, 41-46]. To predict the shift of the relative permeability curves during low salinity waterflooding, the mixed salinity is taken as an interpolant between two bounding curves (relative permeabilities in low and high salinity brines) [45]. Moreover, to better represent the fluid-rock interaction during low salinity waterflooding, ion exchange models together with mineral dissolution has been considered to model the low salinity effect [27-32]. For example, Dang et al. [29] used the equivalent ionic fraction of Na-X to model the shift of relative permeability curves. Esene et al. [31] extended the ionic fraction model to carbonate reservoirs. Furthermore, published work shows that wettability alteration is dependent on surface charge properties [47-49]. Their relation can be experimentally indicated by zeta potential measurement [50], AFM measurement [51, 52] and theoretically indicated by disjoining pressure calculation [53], SCM calculation [36] and molecular dynamics simulation [54, 55]. The experimental results and theoretical calculation reveal that the wettability is a function of surface charge properties. However, two limitations remain using ionic fraction to model wettability alteration: 1) the influence of oil-brine interface on oil adhesion is not accounted for in the modelling although published work shows that oil composition plays a significant role in oil-brine-rock interactions [56-58]. 2) While both ion exchange and surface complexation reactions contribute to oil adhesion on minerals [36, 59], only ion exchange process is considered in current models. Exclusion of surface complexation reactions would overlook the oil adsorption on edge-charged minerals, which likely underestimates the low salinity EOR potential for edge-charged minerals bearing sandstone reservoirs.

To address the two problems above, geochemical reactions occurring at oil-brine-rock interface need to be characterized. This work can be implemented in three different levels: 1) Geochemical modelling at oil-brine-rock interfaces; 2) Contact angle measurements (Sub-pore level); 3) Core flooding with Micro-CT scanning (Pore level). Brady et al. [36, 60, 61] calculated the geochemical surface species, and quantified the electrostatic force between oil-brine and brine-rock interfaces. Their work indicates that the geochemical reactions at oil-brine-rock interfaces control surface chemical species thus determining wettability alteration. To provide further evidence of the wettability alteration, zeta potential of brine-rock and oil-brine were measured and analysed using thermodynamic isotherm [47, 49, 57, 62-70], which show electrical double layer also contributes to the wettability alteration. However, limitations and uncertainties of geochemical modelling remain at molecular level for the characterization of the oil-brine-rock system thus wettability. To be more specific, experimental verification is needed to provide theoretical foundation for current geochemical models. Additionally, controlling factor of pH increase during low salinity water flooding needs to be quantified to predict the oil-brine and brine-rock surface species. Moreover, the prevailing of the geochemical controls at pore-scale, which accounts for the oil detachment, coalescence and transport in porous media, has not been systematically investigated.

Role of pH increase on wettability alteration

pH of effluent usually increases during low salinity water injection. For example, Zhang et al. [71] observed a pH increase from 0.5 to 1.5 units during low salinity water injection. Al-Saedi et al. [72] report 2-3 units of pH increase during low salinity waterflooding from sandstone columns. Strand et al. [34] observed an pH increase from 7 to 10 at 40°C during low salinity waterflooding.

To understand the pH increase during low salinity waterflooding in sandstone reservoirs, a few mechanism have been proposed. For example, Austad et al. [73] proposed a multicomponent ion exchange mechanism to explain how H^+ is consumed by ion exchange reaction between clays and brines thus increasing the local pH. Furthermore, reservoir simulators shows that the ion exchange on clay-brine interface can also increase the pH. Along with ion exchange mechanism at clays, strand et al. [34] proposed that ion exchange can take place on albite and plagioclase, which will consume H^+ in the brine and increase pH . However, much of research up to now has been descriptive in nature. Therefore, to predict wettability alteration, it is imperative to quantify pH increase from geochemical perspective by addressing the following two questions.

1. If ion exchange is one of the mechanisms of pH increase, how much will this process contribute to pH increase?
2. Given sandstone composed of dissolvable minerals and edge charged clays, what is the relative contribution of these factors to pH increase?

To answer the above two questions, a geochemical study was conducted in this research using PHREEQC in light of double layer diffuse theory against literature data reproted by RezaeiDoust et al. [RezaeiDoust A, Puntervold T, Austad T. Chemical Verification of the EOR Mechanism by Using Low Saline/Smart Water in Sandstone. Energy & Fuels. 2011;25(5):2151-62.]. A deeper understanding of factors controlling pH increase would help to quantify the wettability alteration in sandstone reservoirs.

Ion exchange and surface complexation reactions in low salinity brine

The geochemical reactions on oil-brine-clays include SCM and ion exchange modelling. SCM describes the electrostatic adsorption on clay edges and ion exchange reaction quantifies the adsorption by ion substitution [74]. Therefore SCM reactions are usually applied compute the adsorption on edge dominant clays such as kaolinite [75]. Ion exchange reactions are primarily used to characterize adhesion on basal dominant clays including illite, smectite and muscovite [76]. Ion exchange and surface complexation reactions control wettability alteration on sandstone surface [77]. Existing geochemical models can successfully predict the trend of the wettability alteration in most scenarios. However, the relative contribution of ion exchange and surface complexation on oil polarized component at minerals surfaces has not been systematically investigated. For example, surface complexation modelling describes the oil polar adsorption at edge-charged plane minerals by electrostatic force, and ion exchange process controls oil polar adsorption at basal-charged plane minerals using ion bridging. Surface complexation modelling reveals that oil adhesion at edge-charged minerals decreases with lowering salinity. Yet, ion exchange process likely increases oil adhesion on basal-charged planes with lowering salinity at a fixed pH. Given that usually sandstone reservoirs contain both edge-charged and basal-charged clay minerals, it is of vital importance to quantify the relative contribution of different adsorption mechanisms on oil adhesion by addressing the following questions.

1. Adsorption equilibrium constants for ion exchange proposed by Brady et al. [31] are assumed to be 1, which need to be calibrated against experimental data for a better prediction of wettability alteration during low salinity waterflooding.
2. A new geochemical model needs to be developed to capture the two oil adsorption reactions at basal and edge-charged plane minerals.

The new geochemical model would constrain the intrinsic uncertainty of the wettability alteration of sandstone reservoirs with various type and content of clay minerals.

Wettability alteration at pore-scale

To verify if wettability alteration could take place at pore scale, micro-model and micro-CT scanning have been conducted to evaluate the wettability in pore space, and examined how multiple mechanisms act together alternate wettability. For example, Khishvand et al. [78] measured the *in-situ* contact angle in micro-CT images. The *in-situ* contact angle decreases from 115° to 89° during low salinity water, which confirmed the wettability alteration in low salinity water. Song et al. [79] did low salinity waterflooding using a micromodel, and conclude that clays would significantly affect low salinity effect as a result of wettability alteration. While a few works have been done to describe wettability alteration at pore-scale, the existing accounts fail to link mechanisms at sub-pore and pore-scale. To gain a better understanding of the factors controlling the multiphase flow from sub-pore to pore-scale, the following questions need to be addressed:

1. How does wettability alteration from contact angle measurements using substrates represent *in-situ* wettability alteration at pore-scale?
2. How does wettability alteration trigger oil detachment from pore surfaces? Does the oil detachment lead to oil coalescence and transport in pore network thus oil banking?
3. More importantly, can we link electrostatic adhesion at sub-pore scale to wettability alteration at pore-scale?

It is worth noting that besides wettability alteration, emulsion generation and osmosis effect may also contribute to additional oil recovery at pore scale. For example, emulsion generation has been confirmed by CT intensity change [80] and microscope visual observation [11] in low salinity waterflooding, which can increase viscoelasticity and reduce oil trapping in the pore. Spontaneous imbibition tests (5 mol/L NaCl and distilled brine) by Sandengen et al. [81] in mini-core plugs show that osmosis could be a potential mechanism for additional oil recovery.

Controlling factors of wettability alteration in carbonate reservoirs

Apart from the geochemical characterization for sandstone reservoirs, this research also covers the geochemical characterization for oil-brine-carbonate systems. Published work shows that wettability alteration appears to be the main mechanism during low salinity waterflooding in carbonate reservoirs. Yet, the main driver of wettability alteration has not been thoroughly investigated. To decode the mechanistic of wettability alteration, the electrostatic properties on calcite-brine, and brine-oil interfaces has been studied by zeta potential measurements [67, 68, 82] and surface complexation modelling [83, 84]. For example, zeta potential measurements show that the concentration change of PDI (potential determining ions, including Ca^{2+}, Mg^{2+}, CO_3^{2-}, SO_4^{2-}) during low salinity water may lead to a more repulsive force between oil-brine and calcite-brine interface. Surface complexation modelling indicates that the change of surface species likely leads to variation of surface charge properties. However, controlling factor(s) of the oil-brine-carbonate wettability remains unclear in particular the contribution of pH, minerals likely anhydrite. Moreover, the implication of the

geochemical understanding in the application of CO_2-assited enhanced oil recovery has not been elucidated.

CO_2-assisted low salinity EOR in both sandstone and carbonate reservoirs

CO_2-assisted EOR can increase oil recovery effectively [85-90] and mitigate the anthropogenic greenhouse gas [91]. For example, Teklu et al., [92] show that subsequent CO_2 flooding after low salinity waterflooding produced 14.2% additional oil in carbonate core plugs. Carbonated waterflooding by Seyyedi et al., [93, 94] in the microfluidic model shows an oil recovery factor more than 60% OOIP recovery.

While wettability alteration has been observed as one of the main physicochemical processes behind CO_2-assisted EOR, the governing factor(s) behind this process has not been identified, and fewer work have been done to quantify the wettability with presence of carbonated brines. For example, contact angle tests show that the rock surface turns to be strongly hydrophilic in carbonated water [92, 95]. Also, the salinity of carbonated brine is indicated to play a minor role on wettability alteration as results of contact angle tests in Fig. 12 of Teklu et al. [92]. However, to better understand wettability alteration in carbonated water, the following questions need to be addressed:

1. While pH variation is observed as one of main effects of low salinity EOR. How does the low pH of carbonated water affect wettability alteration for both sandstone and carbonate reservoirs?
2. Can CO_2-assisted EOR be expanded to reservoirs with high salinities in terms of wettability alteration towards more intermediate or water-wet systems?

Understanding of wettability alteration mechanism in carbonated water will provide an overall framework which would help to better manage and predict CO_2-assisted EOR means in fields.

Chapter 1. Drivers of pH Increase and Implications for Low Salinity Effect in Sandstone*

1.1 Abstract

Low salinity water flooding appears to be a cost-effective and environmentally friendly means to shift wettability of oil/brine/rock system towards more water-wet, thus improving hydrocarbon recovery. While the contribution of kaolinite (edge-charged clays) on low salinity effect has been extensively investigated, how basal-charged clays (e.g., illite, smectite, and chlorite) contributing to the low salinity effect remains unclear. We thus hypothesize that low salinity water facilitates ion exchange in the presence of basal charged clays, thus lifting off oil films from pore surfaces. To test the hypothsis, we performed a geochemical study using PHREEQC in light of double layer diffuse theory. We quantitatively interpreted the pH increase and low salinity effect from corefloods conducted by RezaeiDoust et al. [RezaeiDoust A, Puntervold T, Austad T. Chemical Verification of the EOR Mechanism by Using Low Saline/Smart Water in Sandstone. Energy & Fuels. 2011;25(5):2151-62.]. We demenstrate that low salinity water triggers a pH increase at the presence of basal-charged clays, thus a more water-wet because of ion exchange. We therefore expand the application envelope of low salinity water flooding to reservoirs with basal-charged clays.

Keywords: Low salinity water, Wettability, Basal-charged clays, pH increase, Surfacec complexation modelling

1.2 Introduction

Low emission energy (e.g., oil and natural gas) remains as important resources in this century [96]. As global energy demand continues to increase, the petroleum industry is constantly striving to develop economically viable techniques to maximize oil recovery [97]. One such technique what gains great interests from industry is termed low salinity water flooding, which is also called *LoSal* flooding by British Petroleum (BP) [3, 4], *Smart Water* flooding by its originators, Austad and co-workers, at the University of Stavanger, Saudi Aramco[5], and *Designer Water flooding* by Shell [6, 7]. While a number of mechanisms have been proposed to understand the low salinity effect, wettability alteration is thought to be the most agreed one. In this context, wettability of oil/brine/rock system thus is of vital importance because system wettability governs subsurface multiphase flow behaviour, remaining oil saturation distribution, thus hydrocarbon recovery.

While wettability alteration appears to be the main mechanism behind low salinity effect, the controlling factor(s) which drives this process has yet to be clearly defined, which in return brings uncertainties to manage and predict low salinity effect in field scale [24]. For example, BP conducted four sets of test at Endicott in Alaska North Slope, showing that residual oil saturation after high salinity water flooding decreased from 41 to 27% followed by low salinity water injection [25]. Yet, corefloods and single well field pilot tests conducted by STATOIL show a negligible low salinity effect in Snorre field at North Sea [26].

To constrain the uncertainty of the low salinity effect, multicomponent ion exchange (MIE) [98], double layer expansion [38], increased pH and reduced IFT similar to the alkaline flooding [14] have been proposed to decipher the controlling factor(s) of low salinity effect. For example, Austad et al. [73] hypothesized that low salinity likely triggers a substitution of Ca^{2+} by H^+, thus compensating the desorption of cations from clay surfaces. This hypothesis explains why low salinity water usually leads to a local pH increase. Low salinity water also likely facilitates the ion exchange between the embedded Na in phyllosilicate and H^+ [60], thus causing a local pH

increase [99]. In general, previous studies believe that presence of edge-charge dominated clays (e.g., kaolinite) is of vital importance to exhibit low salinity effect. This is because edge charges are sensitive to the increase of pH, which can be induced by low salinity water [60, 61]. This is also experimentally demonstrated by contact angle tests, showing that contact angle decreases dramatically from 60 to 30° with decreasing salinity from 142,431 to 1,424 mg/l [61]. Apart from contact angle test, this is also confirmed by surface complexation modelling [60] and field test [25]. Note: while the presence of kaolinite facilitates low salinity effect, the oil composition is also of vital importance to the wettability alteration. For example, oils with low low acid number (0.02 mg KOH/g) may show a little low salinity effect although with a high content of kaolinite (10% wt) in the reservoir[26].

Although the necessity of the presence of kaolinite to yield the low salinity effect is well agreed, this also raises the question: does reservoirs with basal charged clays (e.g., illite, smectite, and chlorite) prompt the low salinity effect? Previous study [RezaeiDoust A, Puntervold T, Austad T. Chemical Verification of the EOR Mechanism by Using Low Saline/Smart Water in Sandstone. Energy & Fuels. 2011;25(5):2151-62.] shows the low salinity effect from four outcrop cores with absence of kaolinite, but rich in basal charged clays, e.g., chlorite (1.9 wt%) and illite (8.4 wt%). However, Brady et al. [99] found the opposite, arguing that oil adsorption in the middle Bakken (rich in illite) decreases with increasing salinity of NaCl. Their results imply that low salinity water flooding likely does not work in reservoirs rich in basal charged clays. To understand the discrepancy and identify the controlling factor of low salinity effect in reservoirs rich in basal charged clays, we hypothesize that ion exchange prompts a pH increase, which in return decreases the bridges between oil/brine and brine/minerals, thus yields a favourable water-wet system. To test this hypothesis, we performed a geochemical study using the experimental data (e.g., oil and brine properties, and rock minerology) published by RezaeiDoust et al. [33]. We also compared our results with RezaeiDoust et al. [33] and Brady et al. [99].

1.3 Model description

While sandstone reservoirs contain many minerals such as quartz, feldspars, plagioclase, clay minerals appears to be the most active minerals due to their large surface area [60], which contact with oil directly at pore surfaces. This is the reason why it is of vital importance to understand the interaction of oil/brine/clays to gain a deeper understanding of low salinity effect. At pore-scale, basal-plane ion exchange adsorption and edge-charge bonding are the two main adsorption mechanisms [60]. Note: in this study, given that the rocks were rich in basal-charged minerals (illite and chlorite) with absence of edge-charged minerals (kaolinite) [33], only ion exchange reactions were considered in our thermodynamic model. We calculated the number of surface species and the bridging number [100] using PHREEQC[101] in light of diffuse double layer model. The input parameters to calculate the number of surface species at oil/brine and the bridge number between oil/brine and brine/minerals were listed in Table 1-1 and 1-2, respectively.

Table 1- 1 Oil Surface Complexation Model input parameters [60]

Geochemical reactions	log K_{298K}	Number
$-NH^+ = -N + H^+$	-6.0	1
$-COOH = -COO^- + H^+$	-5.0	2
$-COOH + Ca^{2+} = -COOCa^+ + H^+$	-3.8	3

Note: –NH represents nitrogen base groups present at the oil-water interface[102], and the concentration of nitrogen base groups can be characterized using base number. Moreover, –N is produced from the deprotonation of –NH$^+$ [99, 103].

Table 1- 2 Rock surface ion exchange input parameters [60, 99]

Geochemical reactions	log K_{298K}	Number
>Na + -NH$^+$ = >-NH + Na$^+$		4
>Na + -COOCa$^+$ = >-COOCa + Na$^+$		5
2>Na + Ca^{2+} = >Ca + 2Na$^+$	0.8 [a]	6
2>Na + Mg^{2+} = >Ca + 2Na$^+$	0.6 [a]	7
>Na + K$^+$ = >K + Na$^+$	0.7 [a]	8
>Na + H$^+$ = >H + Na$^+$	4.6 [b]	9

Note: [a] means a data from Lawrence Livermore National Laboratory thermo.com.v8.r6.230 thermodynamic database. [b] means a data from Wieland et al. for montmorillonite[104]. To calculate the amount of oil exchanged to clay surfaces, equilibrium constant need to be assumed for reaction (1) and (2). >Na, >K, and >Ca represent Na, K and Ca basal sites[99].

1.4 Experimental data from the literature [73]

1.4.1 Oil

Oil's acid number (AN) and base number (BN) are essential parameters to calculate the number of surface species at a given pH. The AN and BN of the experimental oil were 0.12 and 1.78 mg KOH/ g, corresponding to site density of 0.18 μmol/m^2 and 3.21 μmol/m^2, respectively. In our geochemical model, we assumed 1g oil in 1kg water with a surface area of 10m^2/g [61].

1.4.2 Brines

Brines used by RezaeiDoust et al [73] were listed in Table 1-3. FW means the formation water (connate water). LS-1, LS-2, LS-3, and LS-4 were low salinity water with different salinity level (Table 1-3), which were injected to B14, B15, B16 and B10 core plugs under tertiary mode, respectively, after formation water flooding.

Table 1- 3 Experimental brines for different corefloods [33]

Brines	Core samples	NaCl (mole/L)	CaCl$_2$ (mole/L)	KCl (mole/L)	MgCl$_2$ (mole/L)	Salinity (ppm)	Ionic strength (mole/L)
FW	-	1.54	0.09	0.0	0.0	100000	1.810
LS-1	B14	0.017	0.0	0.0	0.0	1000	0.0171
LS-2	B15	0.003	0.005	0.0	0.0	710	0.0171
LS-3	B16	0.0	0.0	0.017	0.0	1280	0.0171
LS-4	B10	0.005	0.0	0.0	0.003	640	0.676

1.4.3 Mineralogy

The presence of clay minerals is critical to exhibit low salinity effect [73, 105]. The clay compositions of the experimental core plugs were listed in Table 1-4, showing that these cores were rich in basal-charged clays, e.g., illite and chlorite, but with absence of kaolinite. Because the experimental cores had similar type and content of clays, we assume all samples contain the same amount of clay for the geochemical study. Note: the exchange capacity of illite and chlorite was assumed to be 400 and 300 µmol/g, respectively. The mass ratio of illite and chlorite was 4.5 in this geochemical study in line with the minerology of the experimental cores (Table 4). The surface area of clays ranges from 10 (kaolinite) to 100 (illite) m^2/g [106], and the clays site density are from 0.4 to 6.0 sites per nm^2 [106], equivalent to the range of 0.67 to 10 µmol/m^2. Thus, the amount of surface species for 1 g clays should be in a range of 6.7 to 1000 µmol. Given that the experimental cores were rich in basal charge clays, amount of 381.2 µmol/g was used in the geochemical study.

Table 1- 4 Clay content of outcrop core materials used in the core flooding experiments [33]

Core Name	Kaolinite (mass%)	Chlorite (mass %)	Illite (mass %)	Clays and micas (mass %)
B14	0.0	1.8	8.1	9.9
B15	0.0	1.9	8.4	10.3
B16	0.0	1.9	8.4	10.3
B10	0.0	1.9	8.6	10.5

1.4.4 Experimental procedure

This sections only provided a brief introduction of the experimental procedures. For a detailed description, the literature[33] can be referred. The dry cores were saturated with formation brine after evacuation. To fully saturate the core plugs, 20 PV (pore volume) of formation brine was injected into the cores until effluent pH and constant pressure drop reached in equilibrium. Subsequently, an amount of 2 PV oil was injected into the cores at 50 °C in both sides of the cores to establish the initial water saturation. Then the cores were placed in an aging cell at 60 °C for two weeks. After aging, an amount of 4 PV of high salinity brine was injected, followed by 7 PV of low salinity brine injection.

1.5 Results and Discussion

1.5.1 pH effect on number of surface species at Oil/Brine surfaces

pH strongly affected the number of surface species of $-NH^+$ at interfaces of oil/brine. For example, in the presence of formation brine, $-NH^+$ decreased dramatically from 3.16 µmol/m^2 to nearly 0 as pH increasing from 4 to 10 (Figure 1) in line with Brady et al. [60], who shows that $–NH^+$ decreases from 6.5 µmol/m^2 to nearly 0 as pH increasing from 4 to 9 in the presence of 1.0 M NaCl. This is attributed to the Reaction 1 shifting towards right-hand side, thus decreasing the number of $–NH^+$ with increasing pH. In these oil/brine/mineral systems, we believe that $–NH^+$ plays an important role in an oil-minerals adhesion. This is largely because high concentration of $–NH^+$ means great exchangeable sites (Reaction 1 and 4). Note: the number of surface species also means the surface concentration (Fig. 1-1).

However, in these oil/brine/mineral systems, the effect of pH on $–COO^-$ and $–COOCa^+$ was negligible. For example, in the presence of formation brine, the number of $–COO^-$ increased from 0 µmol/m^2 to 0.132 µmol/m^2 with pH increasing from 4 to 10. Likewise, the number of $–$

COOCa$^+$ increased slightly from 0.003 µmol/m^2 to 0.041 µmol/m^2 with pH increasing from 4 to 10. These results appear to contradict with Brady et al. [60] and Xie et al. [61], who reported that pH strongly affected the number of –COO$^-$ and –COOCa$^+$. This discrepancy is likely attributed to the composition of oils, to be more specific, the acid number and base number ratio. In this work, AN/BN is around 0.06, much smaller than 0.5 for Brady et al. [60] and 3.06 for Xie et al. [61]. Moreover, the competition of H$^+$ during the protonation and deprotonation for the Reaction 1 and Reaction 2 may be another reason to cause this discrepancy. When the deprotonation occurs, the relative larger number of –NH$^+$ will deprotonate more H$^+$, which will compensate the protonation of –COOH. Together, the surface species calculations confirm that the composition of oils is of vital importance to affect the interaction of oil/brine/rock system, thus wettability [107].

1.5.2 Ion type and concentration on the number of surface species at oil/brine interfaces

Ion type governed the type of surface species at oil/brine interfaces. For brines containing only monovalent cations, such as Na$^+$, K$^+$, the dominant type of surface species were –NH$^+$ and –COO$^-$ (Fig. 1-1). However, the –COOCa$^+$ and –COOMg$^+$ appeared at oil/brine interfaces in the presence of bivalent cations due to the Reaction 3 (Fig. 1-1 and 1-2). Note: ion type also decides exchangeable sites. For example, –NH$^+$ is an exchangeable group on oil/brine interfaces for the monovalent. If divalent cations, like Ca^{2+} and Mg^{2+}, are available in brines, –NH$^+$, –COOCa$^+$ and –COOMg$^+$ would be the exchangeable cations (Fig. 1-1). Note: Fig. 1-2 shows the concentration of surface species at oil/brine surfaces for the concentration from 0 to 0.4 µmol/m^2. Because the experimental oil had AN/BN around 0.06, the variation of –COO- and –COOCa$^+$ with pH is less pronounced compared to -NH$^+$ (Fig. 1-2).

Ion concentration heavily affected the surface species at oil/brine interfaces. For example, compared the formation water (100,000 ppm) with LS-2 (710 ppm) at pH=5, the concentration of –NH$^+$ were 2.81 µmol/m^2 and 2.19 µmol/m^2 in the presence of the formation brine and low salinity water, respectively, although brines had the same ion type. Note: the concentration of ions influence the activity of H$^+$. We believe that the high salinity compensates the degree of deprotonation, thus triggering more –NH$^+$ in the high salinity brine. Also note that the amount of surface concentration of –COO$^-$ and –COOCa$^+$ was much lower than –NH$^+$ particularly in low pH because for the experimental oil RezaeiDoust et al [33] used had high base number of 1.78 mg KOH/g oil, which is nearly 15 times of acid number (0.12mg KOH/g)
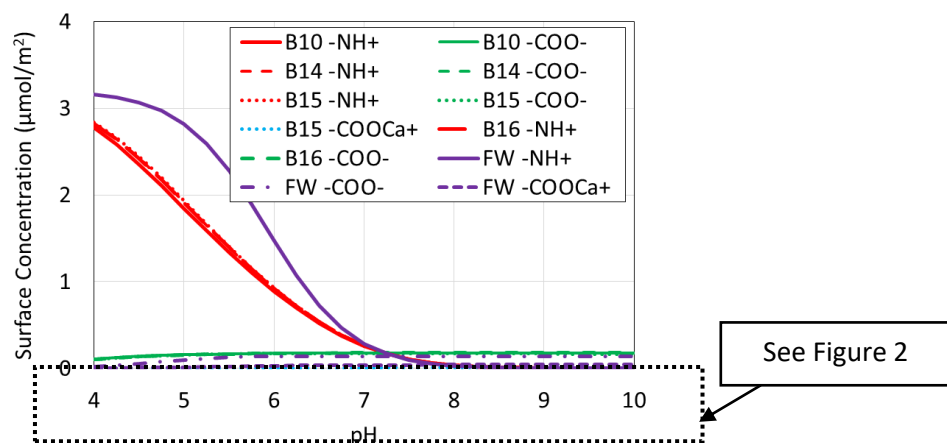
Fig. 1- 1 Concentration of surface species at oil/brine surfaces varies with increasing pH
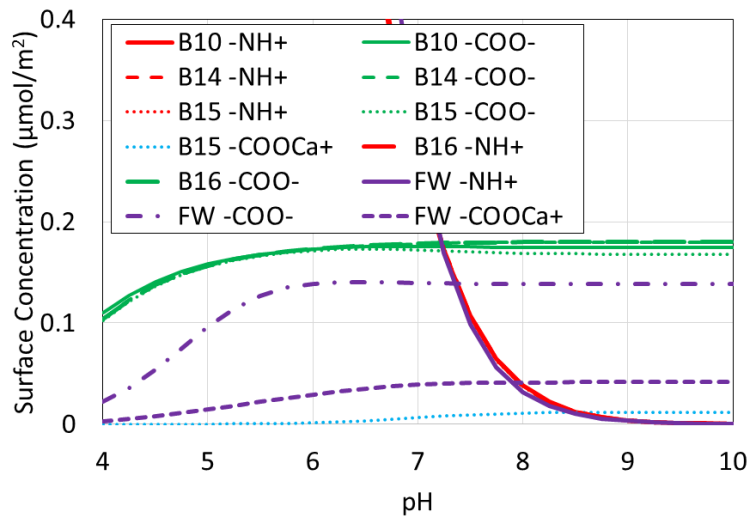
Fig. 1- 2 Concentration of surface species at oil/brine surfaces varies with increasing pH
(from Figure 1 for the concentration from 0 to 0.4 µmol/m^2)

1.5.3 pH effect on exchangeable sites at brine/mineral interfaces

pH strongly affected the exchangeable sites at interface of brine/mineral. To be more specific, exchangeable sites increased with increasing pH although the degree of increase gradually decreased as pH was greater than 7 (Fig. 1-3). This is because at low pH (pH<7), H$^+$ has a strong affinity towards the mineral surface. Therefore, amount of Na$^+$, K$^+$, Ca^{2+} and Mg^{2+} would be substituted by H$^+$ [73]. Yet, as pH was greater than 7, the concentration of H$^+$ decreased dramatically, thus less impact of pH on the exchangeable sites (Fig. 1-3).

1.5.4 Effect of Ion type on exchangeable sites at brine/mineral interfaces

Ion type strongly affected the number of exchangeable site (>Na) due to the competence of individual ion on the site adsorption. For example, B14 (NaCl) yielded a much greater >Na compared to B15 (NaCl+CaCl$_2$) and B10 (NaCl+MgCl$_2$) due to the presence of Ca^{2+} and Mg^{2+} which have a much stronger affinity than Na$^+$ [73]. This implies that at the same ionic strength, brines with presence of bivalent cations likely yield less exchangeable sites of >Na, thus less bridging number, which was calculated in Fig. 1-4. To be more specific, at pH=7, the concentration of >Na in B14 (NaCl) was 300.9 µmol/m^2, which was much higher than >Na (8.04 µmol/m^2) in the presence of B15 (NaCl+CaCl$_2$). This is because the concentration of Na$^+$ in B14 (NaCl) was five times higher than B15 (NaCl+CaCl$_2$), also B14 (NaCl) had no bivalent cations. Note: the bivalent cations have stronger affinity towards the mineral surfaces than monovalent cations [73], thus leading to the decrease of >Na.
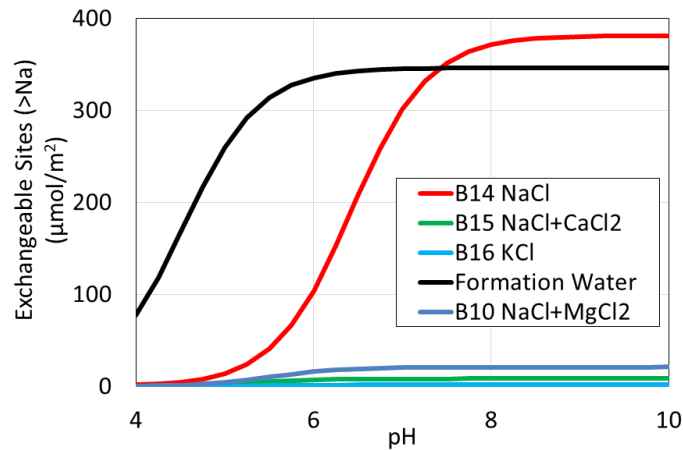
Fig. 1- 3 Exchangeable site density variation at clay surfaces with increasing pH in the presence of various experimental brines

1.5.5 pH effect on bridging product

While ion type and ionic strength slightly affected the bridging number as pH was lower than 6, bridging number decreased with increasing pH as pH was greater than 6, implying a more water-wet system (Fig. 1-4). For example, in the presence of formation brine, bridging number decreased dramatically from 3.34 $\mu mol/m^2$ to 0.21 $\mu mol/m^2$ as pH increasing from 5 to 10. In the presence of KCl (B16), bridging number decreased from 3.19 to 0.43 $\mu mol/m^2$ as pH increasing from 5 to 10. Similarly, in the presence of either $CaCl_2$, or $MgCl_2$, bridging number followed the same trend as formation brine. Note that as pH<6, the bridging number was relatively stable. This is because the number of exchangeable sites on brine/rock was higher than the number of surface species on the brine/oil per unit area. Therefore, all the $-NH^+$, $-COOCa^+$ exchanged with >Na based on the Reaction 4 and 5. In other words, the number of surface species (surface concentration) at oil/brine interfaces determines the bridging number at pH<6. Note: the dot points in Fig. 1-4 represent the bridging number in the presence of various brines at an average pH during low salinity water coreflooding experiments.
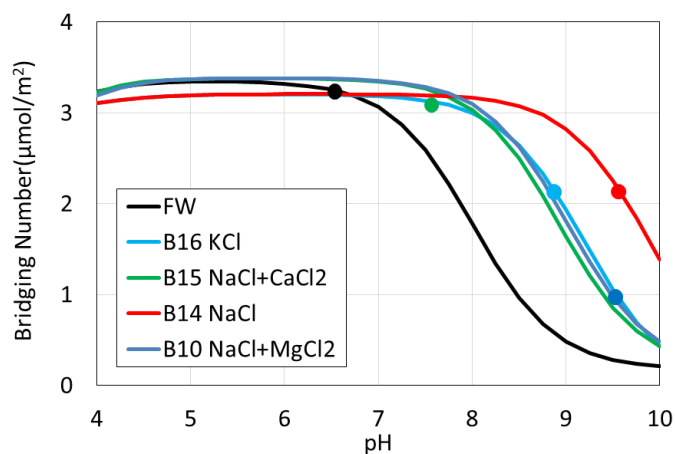
Fig. 1- 4 Bridging number variation with increasing pH in the presence of various experimental brines

1.6 Implications

1.6.1 Ion exchange mechanism triggers a pH increase during low salinity water flooding

Ion exchange triggers a pH increase during low salinity water flooding due to the Reaction 9, Table 2, $>Na + H^+ = >H + Na^+$ [60, 108]. This is also experimentally proved by RezaeiDoust et al [33] (Fig. 1-5) . For example, the initial pH during the formation brine injection was about 6.0 to 6.5 (Fig. 1-5). However, a pH increase appeared at 0.2 to 0.3 PV of low salinity water injection after 4 PV of formation brine injection. The finial pH during the low salinity water flooding for the four core plugs were in a range of 8.6 to 9.6, showing a pH increase of 2 to 3 (Fig. 1-5). Similar pH increase was also observed by Zhang et al. [109] who show an pH increase of 2-3 during low salinity water flooding. McGuire et al. [35] also observed an pH increase of 1 to 3. Likewise, Austad et al. [73] observed an ΔpH of 1.4-2.4 during low salinity water injection. Moreover, Lager et al. [98] found a pH increase of 1 to 3, and Xie et al. [18] observed a pH increase from 6 to 9 as ion tuned water injection. Note: the pH increase during low salinity water flooding predicted by PHREEQC was 8.09 to 8.47, slightly lower than the observed pH (8.6 to 9.6). This is likely attributed to the fact that in this study, only clay minerals were included to calculate the ion exchange without involving other minerals, like feldspar, plagioclase which may contribute to the increase in pH during low salinity water flooding [34].

Table 1- 5 Calculated pH and Core flooding pH

	B14	B15	B16	B10
Initial pH (Formation brine)	6.5-6.7	6.0-6.3	6.5-6.8	7.0-7.2
Core flooding pH	9.3-9.6	7.0-7.5	8.6-8.7	9.3-9.6
PHREEQC predicted pH in low salinity.	8.46-8.47	7.78-7.89	8.09-8.12	8.10-8.28

Note: the PHREEQC predicted pH in the formation brine was 7.2.
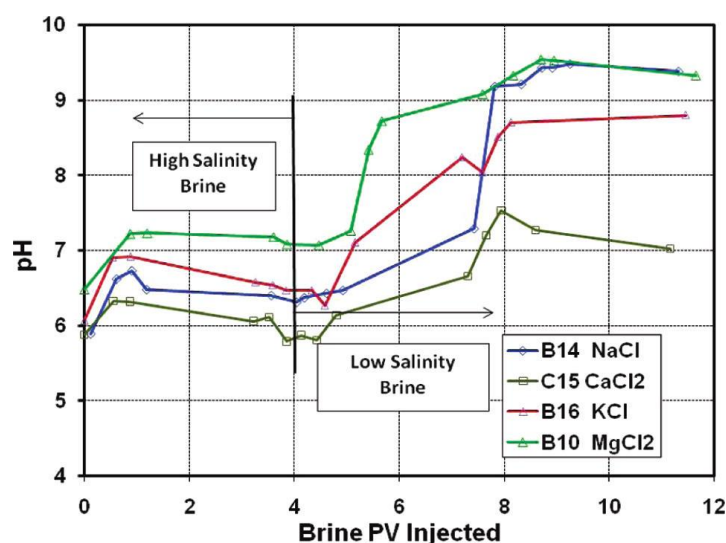
Fig. 1- 5 pH changes caused by different LS brine injection (Note: C15 in the legend means B15)

A pH increase during low salinity water flooding can be deciphered by the thermodynamic model [60]. The ion exchange reaction equilibrium constant, *pK* of Reaction 9 is 4.6, which is much higher than that of Reaction 6, 7, 8. Therefore, more H^+ adsorbing onto the clay surfaces occur when the ion exchange reaction equilibrium is disturbed by injecting low salinity water. Note: the equilibrium constant of the absorption of H^+ is much greater than other cations, e.g., Ca^{2+}, Mg^{2+}, Na^+ and K^+, implying that Ca^{2+}, Mg^{2+}, Na^+ and K^+ would be substituted by H^+ at low pH. Consequently, OH^- would be generated. We believe that the ion exchange process explains the question: why does low salinity water lead to a local pH increase in sandstone reservoirs. It is worth noting that a quantitative amount of substitution can be calculated together with pH increase using the thermodynamic model [60, 99].

1.6.2 Bridging number correlates with recovery factor

Bridging number scales with recovery factor. Fig. 1-7 shows that recovery factor increases with decreasing bridging number in the presence of low salinity water. This implies that bridging number may be used as an indicator to screen the potential reservoir candidates, and design the injected water chemistry [60]. For example, we plotted the recovery factors obtained by RezaeiDoust et al's (Fig. 1-6) [33] versus bridging number (Fig. 1-7). Note: a greater bridging number means a less water-wet system, thus a lower recovery factor. Fig. 1-7 shows that recovery factor decreases with increasing bridging number although the relationship between recovery factor and bridging number is not strongly linear. Fig. 1-7 also shows that the composition of the injected brine does not significantly affect the linear relationship between recovery factor and bridging number. Given the variation of pH of the effluents (Fig. 1-5), the standard deviation of bridging number was ± 2 µmol/m^2.

Given that we aimed to interpret the RezaeiDoust et al.'s coreflooding results in this work using surface complexation which appears to be one of the main mechanisms to decipher the controlling factors of low salinity effect. However, we also believe that double layer expansion likely plays a role in the interaction of oil/brine/illite because the two mechanisms (e.g., electrostatic forces [49, 53, 110] and physiochemical adsorption [99]) likely govern the system wettability. This may also explain why we observed a vertical spread in Fig. 1-7, which was discussed in the section below. Nevertheless, more quantitative work remains to be made to understand the relative contribution of surface complexation and double layer expansion on system wettability [111], thus hydrocarbon recovery.

Note: when we compare the ion exchange impact on the low salinity effect at a constant pH, a negative effect of ion exchange on the recovery can be observed [99]. This explains the question: why did Brady et al. observe an increase of adhesion between oil and illite with decreasing salinity at the same pH. However, due to the fact that low salinity water triggers a pH increase in reservoir condition, bridging number decreases with increasing pH, thus a more water-wet system. Also note the difference between bringing number and bond product sum. Bridging number means the electrostatic bridges (>-NH + >-COOCa) [99], which aims to define the ion exchange for basal-charged clays using the geochemical reactions listed in Table 1-2 [99]. However, the bond product sum ($[>AlOH_2^+][-COO^-]+[>Al:SiO^-][-NH^+]+[>Al:SiO^-][-COOCa^+]+[>Al:SiOCa^+][-COO^-]$) termed by Brady et al. [60] is an explicit approach to calculate the electrostatic force for edge charged clays, e.g., kaolintie, which is generated by the surface species at interface of oil/brine and brine/clays.
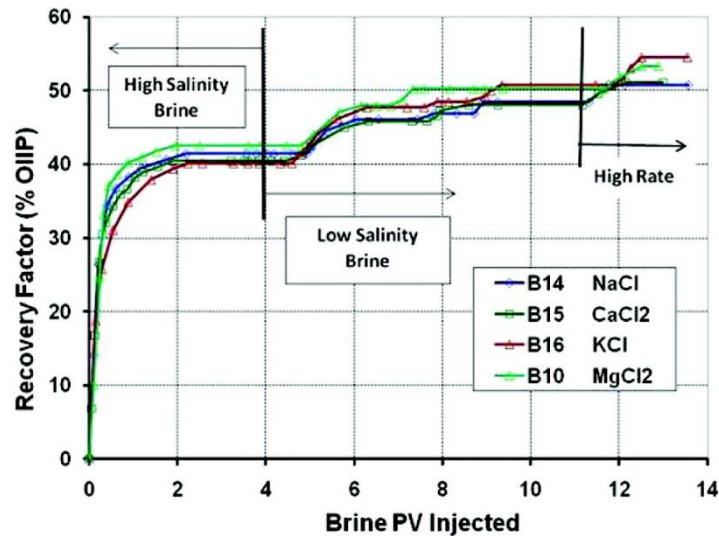
Fig. 1- 6 Recovery factor vs. injected brine pore volume

Although the recovery factor of RezaeiDoust et al.'s coreflooding results correlates with bridging number, the vertical spread in recovery factor is observable. Two potential explanations for the vertical spread are the following.

1. Ion exchange between $-NH^+$ and $>$Ca (B15), and $-NH^+$ and $>$K (B16) were not considered in this surface complexation model (Table 1-2). These ion exchanges may need to be considered in future although $-NH^+$ has less replacing power compared to Ca^{2+} and K^+ [112].

2. Double layer expansion force likely occurs during low salinity water flooding, which lifting up oil film adsorbed at pore surface due to an increase of disjoining pressure [53]. Note that B15 and B16 had the lowest ionic strength compared to B10 (Table 1-3), implying a more negative zeta potential [49, 113], thus increasing double layer expansion. This may explain why low salinity water yielded a greater oil recovery for core plug B15 and B16 although the relative contribution of double layer expansion and ion exchange remains to be open for discussion [111].

Besides the challenges to understand the relative contribution of double layer expansion and ion exchange, the edge and basal plan contribution on low salinity effect is also open for discussion. We believe that to examine the edge and basal plan contribution on low salinity effect, the following two experiments may need to be done in future.

1. Measure contact angles using muscovite surfaces, which are thought to be controlled by basal charges at the basal plains [114]. In this case, the effect of ion type and salinity on contact angle can be attributed to basal charges.

2. Measure zeta potential using muscovite powders at different pH. The zeta potential at different pH can be attributed to edge charges because muscovite powers may expose edge charges due to the huge amount of specific surface [114]. However, how to relate the zeta potential results to contact angle remains to be further explored.
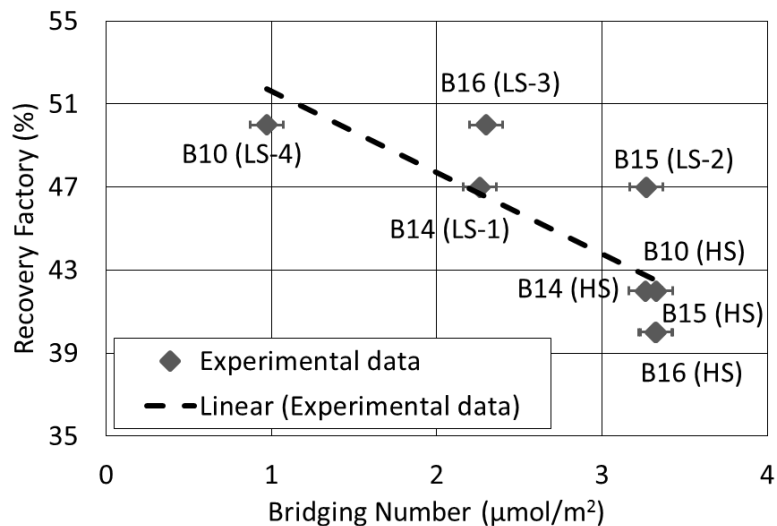
Fig. 1- 7 The relationship between the bridging number and Recovery Factor (Note: LS means low salinity water; HS means high salinity water. B14, B15, B16 and B10 are the labels of experimental core plugs for coreflooding experiments conducted by RezaeiDoust et al. (Energy & Fuels. 2011; 25(5):2151-62.))

1.7 Conclusions

Low salinity water flooding remains a cost-effective and environmentally friendly technique to enhance oil recovery. This is particularly true during the period of low oil prices. While wettabiilty alteration is thought to be the main mechanim, the controlling factor(s) which drives this process is still open for discussion. In this study, we thus hypothesize that low salinity water facilitates ion exchange, thus lifting off oil films from basal-charged clays (e.g., illite, chlorite, and semectite). To test the hypothsis, we performed a geochemical study using PHREEQC in light of double layer diffuse theory. We quantitatively interpreted the pH increase and low salinity effect from corefloods with absence of edge charged clays (e.g., kaolinite) [RezaeiDoust A, Puntervold T, Austad T. Chemical Verification of the EOR Mechanism by Using Low Saline/Smart Water in Sandstone. Energy & Fuels. 2011;25(5):2151-62.].

Our results confirm that basal-charged clays trigger a pH increase due to ion exchange ($>Na + H^+ = >H + Na^+$) during low salinity water flooding [60, 108]. We also demenstrate that oil recovery factor scales with bridging number, suggesting that bridging number may be used as an indicator to screen the potential reservoir candidates [60], and design the injected water chemistry. We thus expand the application envelope of low salinity water flooding to reservoirs rich in basal-charged clays. However, a quanative work remains to be made to understand the relative contribution of basal-charged clays and edge-charged clays on low salinity effect in sandstone reservoirs.

Chapter 2. Role of Ion Exchange in Low Salinity Water Flooding in Sandstone*

2.1 Abstract

Wettability alteration appears to be an important mechanism for low salinity water flooding, but two major challenges in predicting the low salinity effect are (1) to understand the contribution of ion exchange, surface complexation, and albite dissolution mechanisms, and (2) to quantify how the three mechanisms contribute to pH increase during low salinity water flooding. We thus modelled one-dimensional (1D) reactive transport, examining the ion exchange, surface complexation, and albite dissolution using PHREEQC, and compared with RezaeiDoust et al.'s [Energy & Fuels. 2011;25(5):2151-62.] experimental pH profiles during low salinity water injection.

We reasonably matched RezaeiDoust, et al.'s experimental pH profiles. We found that ion exchange, and albite dissolution significantly contribute to pH increase, and surface complexation mechanism plays a minor role in pH increase. Our results suggest that basal charged clays (e.g., illite, smectite, chlorite) and albite are minerals to trigger pH increase which decreases the bridging number (>-NH + >-COOCa) for basal charge clays, and also decrease the bonds ([>AlOH$_2^+$][-COO$^-$]+[>Al:SiO$^-$][-NH$^+$]+[>Al:SiO$^-$][-COOCa$^+$]+[>Al:SiOCa$^+$][-COO$^-$]) for edge charged clays (e.g., kaolinite). Our results provide insights to characterize the geochemical features of oil/brine/sandstone and shed light on constraining the intrinsic uncertainties of low salinity water EOR in sandstone reservoirs.

Keywords: Low salinity water flooding, Reactive transport, Ion exchange, Surface complexation, Albite dissolution

2.2 Introduction

Fossil fuel in particular oil remains an important resource in the rest of 21st century [115]. Low salinity water flooding appears to be a cost-effective and environmentally friendly mean to unlock the remaining oil resources after depletion and conventional water flooding [97, 116]. This is because low salinity water shifts relative permeability towards a lower residual oil saturation [117, 118], meaning increasing oil production rate and ultimate oil recovery [25, 119].

To better manage and predict low salinity water flooding in fields, several mechanisms have been proposed to describe how the low salinity water (LSW) improves oil recovery: fines mobilization [13], limited release of mixed-wet particles [13], increased pH and reduced IFT similar to the alkaline flooding [14], multi-component ion exchange (MIE) [4, 15-17], expansion of the double layer [18-20], salt-in effect [21], salting-out effect [22] and osmotic pressure [23].

Although the quantitative work remains to be made to decipher the relative contribution of the above mechanisms, wettability alteration towards more water-wet appears to be widely accepted [97, 116]. For example, many contact angle tests show that lowering salinity decreases contact angle thus more water-wet [18, 120]. Also, coreflooding experiments show that lowering salinity delays water breakthrough and improves ultimate oil recovery [33, 34, 121]. Moreover, core-scale history matching (core-scale numerical simulation) show that lowering salinity shifts relative permeabilities towards a lower residual oil saturation [122-124].

More importantly, existing coreflooding experiments show that the low salinity EOR-effect is always observed with effluent pH increase [33, 34]. For example, Zhang et al. [109] show an

pH increase of 2-3 during low salinity water flooding. McGuire et al. [35] also observed an pH increase of 1 to 3. Likewise, Austad et al. [73] observed an ΔpH of 1.4-2.4 during low salinity water injection. Moreover, Lager et al. [98] found a pH increase of 1 to 3, and Xie et al. [18] observed a pH increase from 6 to 9 during low salinity water injection. To decipher the controlling factor which governs pH increase during low salinity waterflooding, Austad et al. [73] hypothesized that low salinity likely triggers a substitution of Ca^{2+} by H^+, thus compensating the desorption of cations from clay surfaces. This hypothesis explains why low salinity water usually leads to a local pH increase. Low salinity water also likely facilitates the ion exchange between the embedded Na in phyllosilicate and H^+ [60], thus causing a local pH increase [99].

To decipher the factors controlling the pH shift during low salinity water flooding in sandstone reservoirs, a few mechanisms have been proposed from the geochemical perspective in the past decade. For example, Fjelde et al., (2012) [125] observed a pH increase from 7 to 8 from coreflooding experiments, and they conclude that ion exchange contributes to low salinity effect. To further quantify the pH increase due to ion exchange process, Dang et al. [29] performed geochemical modelling using CMG-GEM against Fjelde et al.'s coreflooding experiments. Their simulation results reveal that ion exchange process likely contributes to pH increase during low salinity water flooding. Besides, surface complexation modelling together with ion exchange were proposed by Brady et al. [36, 60, 77] to understand the interaction of oil-brine-rock thus quantifying wettability. However, until recently, to the best of our knowledge, there has been no direct geochemical modelling to quantify the relative contribution of the geochemical reactions (e.g., ion exchange, surface complexation and albite dissolution) on pH shift during low salinity water flooding thus wettability alteration.

In our previous work [126], we performed a static geochemical study using PHREEQC based on ion exchange mechanism, and we compared our results with RezaeiDoust et al.'s coreflooding data [33]. Our results quantitatively confirm that basal-charged clays (e.g., illite, smectite, chlorite) triggers a pH increase due to ion exchange (>Na + H^+ = >H + Na^+) during low salinity water flooding [60, 108]. However, we did not examine the relative contribution of ion exchange (for basal charged clays) and surface complexation (for edge charged clays, e.g., kaolinite) on pH increase. Also, we did not consider the pH increase due to ion exchange and dissolution of albite. This may be the reason why pH predicted PHREEEQC in our previous work is most 1.2 pH value lower than what RezaeiDoust et al. [33] observed from their coreflooding experiments. In this work, we aimed to quantify the relative contribution of three mechanisms on pH increase which directly governs the oil/brine/rock system wettability. To achieve this goal, we performed one dimensional reactive transport modelling using PHREEEQC. To validate our results, we also compared our results with RezaeiDoust et al.'s [33] pH profiles.

2.3 Experimental fluids and procedures from RezaeiDoust et al. (2011)

Because the experimental procedures and results was well documented in RezaeiDoust et al.'s work [RezaeiDoust A, Puntervold T, Austad T. Chemical Verification of the EOR Mechanism by Using Low Saline/Smart Water in Sandstone. Energy & Fuels. 2011;25(5):2151-62.]. Here we only briefly layout the experimental protocols.

2.3.1 Oil

Oil acid number (AN) and base number (BN) are essential parameters to calculate the number of surface species at a given pH. The AN and BN of the experimental oil were 0.12 and 1.78 mg KOH/ g, corresponding to site density of 0.18 µmol/m^2 and 3.21 µmol/m^2, respectively. In our geochemical model, we assumed 1g oil in 1kg water with a surface area of 10m^2/g [61].

2.3.2 Brines

Brines used by RezaeiDoust et al., [73] are listed in Table 2-1. FW means the formation water (connate water). LS-1, LS-2, LS-3, and LS-4 were low salinity water with different salinity level, which were injected to B14, B15, B16 and B10 core plugs under tertiary mode, respectively, after formation water flooding.

Table 2- 1 Experimental brines for different corefloods [33]

Brines	Core samples	NaCl (mol/L)	CaCl₂ (mol/L)	KCl (mol/L)	MgCl₂ (mol/L)	Salinity (ppm)	Ionic strength (mol/L)
FW	-	1.54	0.09	0.0	0.0	100000	1.810
LS-1	B14	0.017	0.0	0.0	0.0	1000	0.0171
LS-2	B15	0.003	0.005	0.0	0.0	710	0.0171
LS-3	B16	0.0	0.0	0.017	0.0	1280	0.0171
LS-4	B10	0.005	0.0	0.0	0.003	640	0.676

Outcrop cores provided by Total were used to conduct the coreflooding experiments with a length around 7.0 cm, and diameter of 3.8 cm. All experimental core plugs were evacuated and then saturated with formation brine (connate water). To obtain a stabilized pH at the outlet, twenty pore volume (PV) of formation brine was injected into each of the core plug. Subsequently, two PV of oil was injected from both ends of the core plug. Then the core plugs were placed in an oven to age for two weeks. After aging, formation brine (2 PV with flow rate 4 PV/d) was injected into core plugs followed by 7 PV of low salinity water injection with flow arte 4 PV/d. Effluent pH was monitored to examine how low salinity water affects aqueous solution pH.

2.4 Reactive transport modelling

2.4.2 Model description and assumptions

Given that 1D advective-dispersive transport was computed using an explicit finite difference algorithm in PHREEQC [101], to avoid numerical dispersion on both reactive and conservative species transport, forty cells were used in this study [127]. We employed 280 shifts to represent 7 PV low salinity water injection. We specified 1/160 day for each time step which was identical with the experimental injection rate 4 PV/d. Note: in our geochemical study, we did not consider the pH variation due to the reaction between the low salinity water and oil because the pH and composition of ionic aqueous solution are governed by the reactions between brine and rock [60].

Given that the pH variation of brine-oil mixture before and after contact with low salinity brine is negligible [120], implying that effect of surface complexation occurring at oil-brine surfaces on effluent pH variation is minor, we did not couple surface complexation at oil surface in our 1D reactive transport model while calculating the pH shift. Moreover, we also assumed that the effect of ion exchange between oil surface species and exchangeable sites at basal charged clays on pH variation is week. This is because this process occurs after ion exchange between cations in brines and exchangeable sites at clay minerals [99, 126].

According to Chen et al., (1997, Figure 2) [128] they show the pH and temperature-dependence of dissolution of albite. The albite dissolution rate is assumed to be $\log K = -15$ at

50ºC (K is albite dissolution rate), indicating albite dissolution rate of 10^{-15} mol $\times$ cm^{-2} $\times$ s^{-1}. Given that the reactions occurring in porous media with surface area of 20 m^2 for each of the core plug (with an assumption that specific area is 0.1 m^2/g [129] and weight of a core plug is 200g), the estimated rate of albite dissolution is 2 $\times$ 10^{-10} mol $\times$ s^{-1}. Estimated from equilibrium model, the amount of albite dissolution at equilibrium state is 9.2$\times$10^{-6} mol predicted by PHREEQC. Thus, the reaction time to reach equilibrium is around 12 hours. However, the duration of coreflooding experiments is around 24 for high salinity water flooding, and 48 hours for low salinity water flooding. We therefore can reasonably assume that the albite dissolution likely reached equilibrium during flooding period of time, which is also confirmed by constant effluent pH after four pore volume injection as shown in the Figure 2 of RezaeiDoust et al. [33]). Thus, we employed equilibrium model in our 1D reactive transport model instead of kinetic reaction model.

2.4.3 Geochemical reactions

Ion exchange (IE) and surface complexation reactions are two main geochemical mechanisms on the clay surface [60] in sandstone apart from mineral dissolution. The geochemical reactions for ion exchange and surface complexation are shown in Tables 2-2 and 2-3. In this study, we modelled the pH profile of core plugs which have 10% basal charged clays from RezaeiDoust et al [33]. To examine the how surface complexation contributes to pH increase, we also modelled 1D reactive transport with 10% edge charged clays (e.g., kaolinite) but without based charged clays. Note: most sandstone reservoirs have edge charged clays (kaolinite) less than mass fraction of 10%. Therefore, ten percent of kaolinite content in core plugs enables us to estimate the maximum pH increase contributed by surface complexation.

In our geochemical modelling, each cell is assigned with 0.2 mmol exchangeable sites (>Na), in total 80 mmol exchangeable sites throughout the core plugs based on an assumption of rock density with 2.6 g/cm^3. We assumed that the experimental rock density was around 2.6 g/cm^3. Given that the core plugs have 10 wt% of basal charged clays (e.g., illite and chlorite), 20 grams basal charged clays was specified in 1D reactive transport model. Because the cation exchange capacity (CEC) for illite and chlorite is in a range of 10 to 40 meq/100g [33], the exchangeable sites in the 1D reactive transport model are in a range of 2 to 8 mmol.

To calculate albite dissolution effect on pH shift, given that the mass concentration of albite is around 30 wt% in core plugs [34], an amount of albite (1.5 g) was assigned in each cell in our geochemical modelling. In the calculation, the albite is first equilibrated with formation brine. Then the low salinity brine is injected into the 1D reactive transport model. But it is worth noting that we did not couple albite dissolution kinetics in our 1D reactive transport. This is because RezaeiDoust et al.,'s (2011) coreflooding show that the effluent pH becomes stable after about 5 pore volumes of low salinity water injection, suggesting that geochemical reactions likely reach equilibrium state [130]. However, we believe that more quantitative work remains to be done in future to further constrain the geochemical models with coupling albite dissolution kinetics.

Table 2- 2 Rock surface ion exchange input parameters [60, 99]

Geochemical reactions	log K_{298K}	Number
2>Na + Ca^{2+} = >Ca + 2Na$^+$	0.8 [a]	1
2>Na + Mg^{2+} = >Ca + 2Na$^+$	0.6 [a]	2
>Na + K$^+$ = >K + Na$^+$	0.7 [a]	3
>Na + H$^+$ = >H + Na$^+$	4.6 [b]	4

Table 2- 3 Rock Surface Complexation Model-Input parameters

Geochemical reactions	log K_{298K}	Number
$>Al\text{-}O\text{-}H_2^+ = \; > Al\text{-}O\text{-}H + H^+$	-3.0	5
$> Al\text{-}O\text{-}H = \; > Al\text{-}O^- + H^+$	-3.8	6
$> Si\text{-}O\text{-}H = \; > Si\text{-}O^- + H^+$	-7.0	7
$> Al\text{-}O\text{-}H + Ca^{2+} = \; > Al\text{-}O\text{-}Ca^+ + H^+$	-9.7	8
$> Si\text{-}O\text{-}H + Ca^{2+} = \; > Si\text{-}O\text{-}Ca^+ + H^+$	-9.7	9
$> Al\text{-}O\text{-}H + CaOH^+ = \; > Al\text{-}O\text{-}CaOH + H^+$	-4.5	10
$> Si\text{-}O\text{-}H + CaOH^+ = \; > Si\text{-}O\text{-}CaOH + H^+$	-4.5	11

Note: [a] means a data from Lawrence Livermore National Laboratory thermo.com.v8.r6.230 thermodynamic database. [b] means a data from Wieland et al. for montmorillonite[104]. To calculate the amount of oil exchanged to clay surfaces, equilibrium constant need to be assumed for reaction (1) and (2). >Na, >K, and >Ca represent Na, K and Ca basal sites[99].

2.5 Results and Discussion

2.5.1 Effect of ion exchange and surface complexation on pH increase

Both ion exchange and surface complexation contributed to the pH increase, but ion exchange mechanism dominated the pH increase (Fig. 2-1 to 2-4), while we failed to successfully match the pH increase as we only considered ion exchange mechanism. For example, as NaCl solution (0.017 mol/L) was injected into the core plug (Fig. 2-1), ion exchange mechanism gave about 2 pH unit increase till reaching in equilibrium, whereas SCM gave about 1 pH increase. Likewise, when KCl solution (0.017 mol/L) was injected into the core plug (Fig. 2-2), ion exchange gave 1.9 pH increase, while surface complexation gave 1.0 pH increase. Similar to NaCl and KCl, ion exchange for B10 (NaCl 0.005 + $MgCl_2$ 0.003 mol/L) injection gave 0.7 pH increase, but surface complexation mechanism only gave 0.3. We believe the main reason of why ion exchange gave more impact on pH increase than surface complexation is: the Reaction 4 associated with ion exchange is much stronger than the Reactions 5 to 11 associated with surface complexation, confirming that basal-charged clays trigger a pH increase due to ion exchange ($>Na + H^+ = >H + Na^+$) [99] during low salinity water flooding. However, this also raises a question of why ion exchange contribution on pH increase was smaller than surface complexation as (NaCl 0.003 + $CaCl_2$ 0.005 mol/L) was injected into B15 (Fig. 2-4). We believe this is mainly because the increasing Ca^{2+} decreases the activity coefficient of H^+, which shifts the Reaction 5 towards left-hand side. Note: pH increase predicted by our geochemical study shows no abrupt pH increase which is not in line with experimental results (Fig. 2-1). This is largely because the experimental effluent may be diluted by the previous effluent which lowered the actual pH.
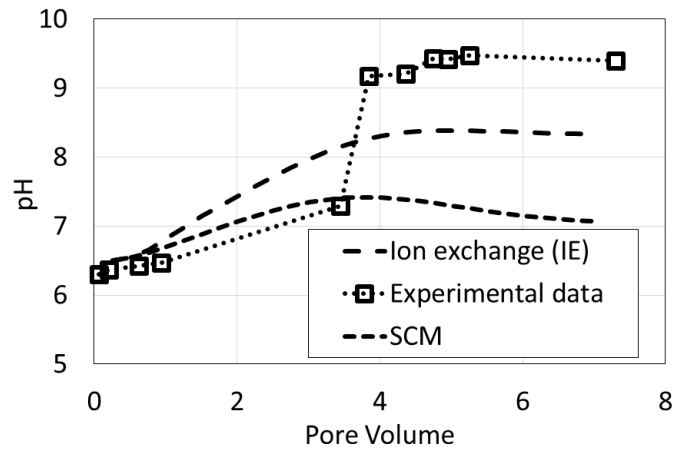
Fig. 2- 1 pH vs. pore volume with experimental data, ion exchange and surface complexation mechanisms for core plug B14 (NaCl 0.017 mol/L)
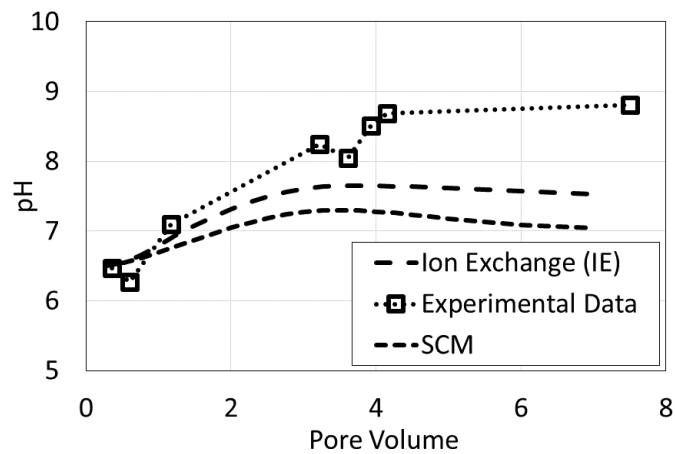
Fig. 2- 2 pH vs. pore volume with experimental data, ion exchange and surface complexation mechanisms for core plug B16 (KCl 0.017 mol/L)
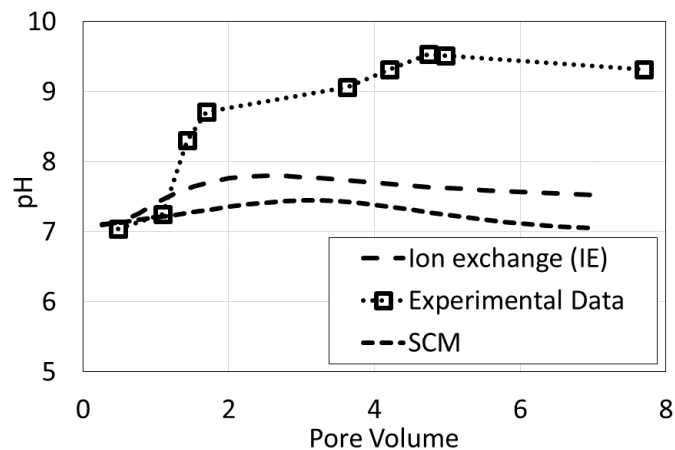
Fig. 2- 3 pH vs. pore volume with experimental data, ion exchange and surface complexation mechanisms for core plug B10 (NaCl 0.005 + MgCl$_2$ 0.003 mol/L)
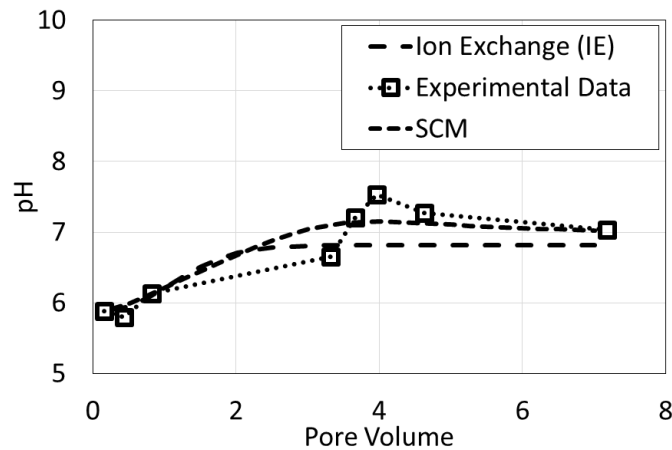
Fig. 2- 4 pH vs. pore volume with experimental data, ion exchange and surface complexation mechanisms for core plug B15 (NaCl 0.003 + CaCl$_2$ 0.005 mol/L)

2.5.2 Effect of ion type on pH increase

Ion type predicted by PHREEQC strongly affected the pH increase in line with RezaeiDoust et al.'s experiments [33], confirming that ion type needs to be thoroughly considered for low salinity water injection [53]. Our results show that monovalent cations (Na$^+$ and K$^+$) contributed to pH increase (1 to 2 pH value) more than divalent cations (less than 1 pH value) due to the ion exchange, implying that lowering divalent cations concentration should better facilitates low salinity effect. This is because increasing pH decreased bridging number (Brady et al. [99] and Chen et al. Fuel 2018, in press), meaning less adhesion between oil and rock surfaces.

2.5.3 Effect of albite dissolution on pH increase

While we quantified that the ion exchange dominates the pH increase during low salinity water injection, ion exchange mechanism alone failed to explain the pH increase which was observed by RezaeiDoust et al.[33]. pH increased predicted by PHREEQC was lower (1-1.3) than than experimental observation especially for monovalent cations injection (Fig. 2-1 and 2-2). To understand the pH increase difference between ion exchange and what RezaeiDoust et al. observed from coreflooding experiments, we hypothesized that plagioclase in particular albite (30.4 % wt %) in the core plugs as shown in Table 2-4 [34] would dissolve into the low salinity water, thus contributing to pH increase. To test our hypothesis, we conducted a geochemical study with ion exchange and albite dissolution using the geochemical reaction below. Note: the equilibrium constant for the albite dissolution is 2.7645 (llnl.database of PHREEQC).

$$NaAlSi_3O_8 + 4H^+ = Al^{3+} + Na^+ + 2H_2O + 3SiO_2$$
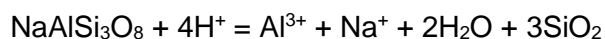
Our results show that the pH increase predicted by PHREEQC can be very close to the experimental pH profile (Fig. 2-5 to 2-7), confirming that albite dissolution contributes to the pH increase during low salinity water flooding. This also answers the question of why Strand et al. [34] observed a pH increase using core plugs with presence of plagioclase minerals, showing a significant LS EOR-effects. Note: due to the limited specific surface of albite, the contribution of surface complexation on oil-albite adhesion might be negligible, but the pH increase associated with albite presence can prompts ion exchange and surface complexation on the surface of edge charged clays [60, 61, 102], decreasing oil-minerals adhesion, thus leading to LS EOR-effects. Also note that the pH increase contributed by monovalent cations

(Na$^+$ and K$^+$) were more than the divalent cations (Ca^{2+}). This is largely because divalent cations may prevent albite dissolving into brines due to the strong affinity at the surface of albite. Also note that although albite dissolution was included to understand the pH increase, the pH increased given by PHREEQC was still slightly lower that the experimental data particularly for Na$^+$ and K$^+$. The following two reasons may account for the discrepancy.

1. Increasing temperature increases the albite dissolution rate [131], which was not considered in our geochemical study. All geochemical studies in this work were conducted at temperature of 25 ^{o}C rather the experimental temperature (40 ^{o}C). Equilibrium constants at various temperature may need to be computed in future.

2. Ion exchange between brine and albite was not considered in this work, which may contribute to pH increase.

Also, note that in our geochemical study, the pH increase in MgCl$_2$ injection predicted by PHREEQC with both albite dissolution and ion exchange on basal charged clays was in line with CaCl$_2$, but inconsistent with experimental results (see the Supporting Information). We assumed the presence of organic matter may arouse a significant pH increase due to the ion exchange at the organic matters which can provide 10 to 100 times cation exchangeable cations than clays [132]. However, we did not measure the organic matters in the core plug, so we cannot confirm this mechanism.

Table 2- 4 Mineralogy of core plug B14 [34]

Core No.	Illite/Mica (wt%)	Kaolinite (wt%)	Chlorite (wt%)	Tot. Clay (wt%)	Plagioclase (wt%)
B14	8.1	0	1.8	9.9	32.6

Note: In the literature, Strand et al., [34] reported that the minerology is homogeneous and all samples are similar in minerology. Thus, the mineralogy of is assumed to be same for all the core samples.
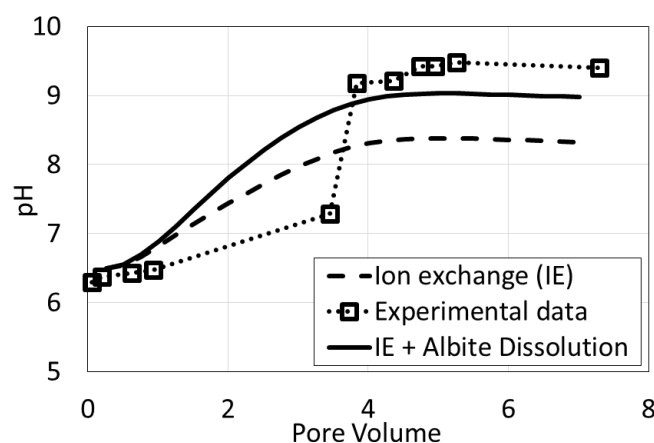
Fig. 2- 5 pH vs. pore volume with experimental data, ion exchange and albite dissolution mechanisms for core plug B14 (NaCl 0.017 mol/L). Note: the curve of IE + Albite Dissolution means the pH increase contributed by coupling albite dissolution and ion exchange.
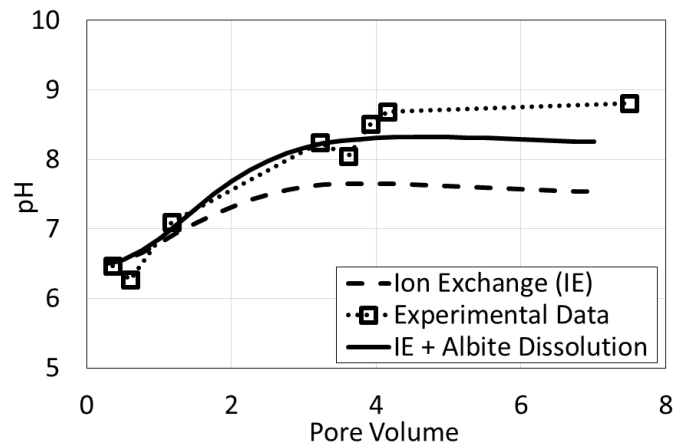
Fig. 2- 6 pH vs. pore volume with experimental data, ion exchange and albite dissolution mechanisms for core plug B16 (KCl 0.017 mol/L)
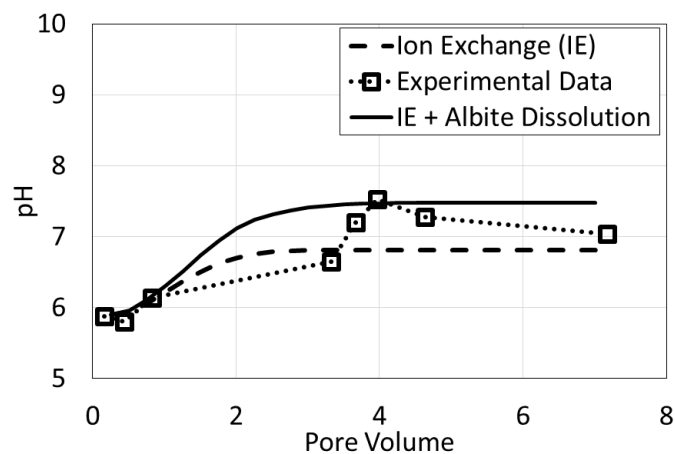
Fig. 2- 7 pH vs. pore volume with experimental data, ion exchange and albite dissolution mechanisms for core plug B15 (NaCl 0.003 + CaCl$_2$ 0.005 mol/L)

2.6 Implications and conclusion

Low salinity water flooding has been in the centre of attention as a cost-effective and environmentally friendly means [97]. Low salinity EOR-effects usually occur with pH increase [33, 34]. It is therefore of vital importance to identify and quantify the controlling factor(s) of pH increase, thus better manage and predict low salinity water flooding. We thus performed 1D reactive transport to quantify the ion exchange, surface complexation, and albite dissolution on pH increase during low salinity water flooding, and we compared our results with RezaeiDoust et al.'s experimental results.

Our results show that clays in particular basal-charged clays (e.g., illite, smectite, and chlorite) significantly contributes to pH increase due to ion exchange, confirming that the presence of clays is important to trigger low salinity EOR effect [33, 34, 60]. Surface complexation mechanism triggered by the presence of edge-charged clays (kaolinite) plays a minor role in pH increase. Albite is an important mineral which promotes pH increase due to albite dissolution and ion exchange [131]. Therefore, the presence of albite likely facilitates low salinity effect. This is not because the interaction between oil and albite significantly affects

29

system wettability thus incremental oil recovery. Rather, it is because the pH increase due to albite dissolution during low salinity water injection decreases the adhesion between oil and clay minerals (e.g., illite, smectite, chlorite, and kaolinite). This confirms that reservoirs rich in albite likely facilitates low salinity EOR-effect [34].

Together, our results imply that sandstone reservoirs with either presence of basal-charged clays or edge-charged clays may yield incremental oil recovery during low salinity water flooding. For basal charged clays, ion exchange mechanism triggers the decrease of bridging number between oil-clays (Brady et al. [99] and Chen et al. [126]). For edge-charged clays, lowering salinity decreases the bond product sum ($[>AlOH_2^+][-COO^-]+[>Al:SiO^-][-NH^+]+[>Al:SiO^-][-COOCa^+]+[>Al:SiOCa^+][-COO^-]$) [60, 61], meaning less oil-clays adhesion, thus low salinity effect. However, if reservoirs are rich in both basal-charged clays and edge charged clays, injecting low salinity very likely achieves more incremental oil recovery. Our results provide insights to characterize the geochemical features of oil-brine-sandstone and shed light on constraining the intrinsic uncertainties of low salinity water EOR in sandstone reservoirs.

2.7 Supplementary Information

2.7.1 pH profile on Sample B15

Fig. 2-8 shows the pH increase profiles vs. injected pore volume. Coupling basal charged ion exchange and albite dissolution failed to match the experimental data. We assumed that the presence of limited organic matter and calcite cement may trigger a pH increase due to the ion exchange and calcite dissolution. This is because organic matter could provide 10 to 100 times cation exchangeable cations than clays [132], and calcite dissolution would increase pH. However, we did not measure the organic matters in this core plug, so we cannot confirm this mechanism.
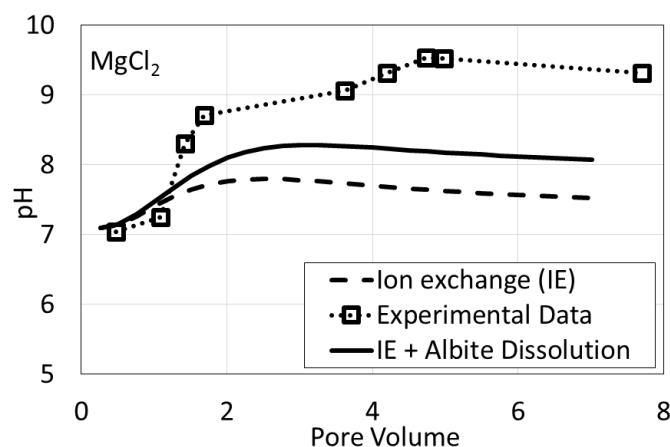
Fig. 2- 8 pH vs. pore volume with experimental data, ion exchange and albite dissolution mechanisms for core plug B15 (NaCl 0.003 + MgCl$_2$ 0.005 mol/L)

2.7.2 Example code for reactive transport simulation

```
DATABASE c:\phreeqc\database\LLNL.DAT
TITLE Transport and cation exchange.
SOLUTION 1-40 Initial solution for column
        units mol/L
        pH 5.9
        Na 1.54
        Ca 0.09
        Cl 1.72
END
SOLUTION 0
        units mol/L
        pH 7
        Na 0.003
        Ca 0.005
        Cl 0.013
END
EQUILIBRIUM_PHASES 1-40
        Albite  0  1.5
END
TRANSPORT
        -cells 40
        -lengths 0.00175
        -shifts 280
        -time_step 1/160 day
        -flow_direction forward
        -boundary_conditions flux flux
        -diffusion_coefficient 0
        -dispersivities 0.009
        -correct_disp true
        -punch_cells 40
```

-punch_frequency 10

        -print_cells 40

        -print_frequency 10

SELECTED_OUTPUT

        -file LSW

        -reset false

        -step

        -totals Na Cl K Ca

USER_PUNCH

        -heading Pore_vol

        10 PUNCH (STEP_NO + .5) / 40.

USER_GRAPH 1 Example 11

        -chart_title "CaCl Reactive Transport Ion Exchange"

        -headings PV pH

        -axis_titles "Pore volumes" "pH value"

        -axis_scale x_axis auto

        -axis_scale y_axis auto

        -start

        10 GRAPH_X (STEP_NO + .5) / cell_no

        20 GRAPH_Y -LA("H+")

        -end

END

Chapter 3. Electrostatic Characterization of -NH$^+$-Brine-Kaolinite System: Implications for Low Salinity Waterflooding in Sandstone Reservoirs*

3.1 Abstract:

Oil-Brine-Rock interaction appears to be an important physiochemical process, which governs multiphase flow and residual oil saturation during low salinity waterflooding in sandstone reservoirs. While it appears that electrostatic adhesion of oil polar components on clay edges and basal planes regulates oil-brine-rock interactions, relative contribution of adhesion on edge and basal planes remains unclear, thus presenting a substantial impediment to model and predict the low salinity effect. We thus coupled PEST and PHREEQC to model the quinoline adhesion against RezaeiDoust et al.,'s (Energy Fuels 2011, 25, 2151–2162) kaolinite-quinoline adsorption experimental data. We matched the experimental data by examining the adsorption capacity of quinoline on kaolinite basal and edges planes simultaneously. Our new calibrated model shows that basal adsorption ($>$Na + BaseH$^+$ = $>$BaseH + Na$^+$) dominates quinoline adsorption at low pH (pH=5). Rather, edge adsorption controls adsorption mechanism at high pH (pH=8). Furthermore, the model shows that salinity plays a minor role in adsorption at a controlled pH system. Our new model quantifies the relative contribution of basal and edge planes on basic component adhesion thus wettability at different pH and salinity, providing insights and new geochemical data to existing geochemical database, thereby better model and predict the wettability alteration during low salinity waterflooding.

3.2 Introduction

Low salinity waterflooding appears to be a cost-effective and environmentally friendly means for enhancing oil recovery in sandstone reservoirs. Extensive laboratory work have been done at multi-length-scale (from nanometre to kilometres) to understand the controlling factor(s) behind incremental oil recovery during low salinity waterflooding, which has been comprehensively reviewed by [133]. Existing results show that low salinity water injection triggers wettability alteration towards more water-wet as a result of weakening oil adhesion on clay minerals at pore surfaces [60, 126]. To characterize the interaction of oil-brine-rock system thereby wettability, electrical double layer theory (EDL) [53, 60, 110, 120]and surface complexation modelling [61, 74, 134] have been proposed and applied to quantify the wettability alteration process although uncertainties remain in sandstone reservoirs.

Lowering salinity likely drives zeta potential of oil-brine and brine-rock (clay minerals) to be strongly negative [113, 120, 135, 136], which in return shifts disjoining pressure from negative to positive due to increasing electrical double layer expansion thus more hydrophilic [18, 60, 61]. Lowering salinity also leads to an increase of Debye Length (i.e., characteristic length of thickness associated with diffuse electric double-layer) [137] thus the thickness of water film. For example, [138] measured zeta potential of clay minerals, and oils in the presence of various ion types and concentrations. Their results show that the zeta potential of oil-brine and brine-minerals become strongly negative while decreasing salinity and ionic strength. [53] used zeta potential data reported by [138], and calculated the disjoining pressure using extended Derjaguin-Landau-Verwey- Overbeek (DLVO) theory. They found that the disjoining pressure shifts from negative (attraction) in the presence of high salinity brines to positive (repulsion) in the presence of low salinity brine. [139, 140] observed that the adhesion force between modelled atomic force microscopy (AFM) tips and rock surface is a function of salinity.

They contribute the adhesion force reduction to the electrical double layer expansion and cation bridging effect. [141] further tested the adhesion force between tips (modified by –NH_2 and -COOH) and muscovite in different salinity brine. A positive adhesion force (repulsion) was observed in low salinity brine for both –COOH and –NH_2, which the adhesion force turns to be negative (attraction) in high salinity brine. However, while the electrical double layer theory together with disjoining pressure likely account for the physiochemical process of wettability alteration, integration of the theory to numerical modelling remains to be challenging. This is largely because disjoining pressure prediction to date does not give a quantitative physical parameter to interpolate the relative permeability curves of oil and brine although the trend of wettability shift would be predicted.

To be more practical to integrate the physiochemical process into reservoir numerical modelling, surface complexation modelling (SCM) has been performed to compute the surface chemical species at oil and minerals surfaces thus characterizing the wettability. For example, geochemical models were proposed to characterize the adhesion of oil on edge charged clays [60] and basal charged clays [99] separately. For edge charged clay minerals, [60] results show that surface complexation modelling predict the same trend as the electrical double layer theory. We further tested this conclusion at high temperature using an high acidic oil, and confirmed that both surface complexation model and electrical double layer predict the same trend although we observed a discrepancy in SCM and EDL results for high salinity brine and softened brine [61]. [99] also developed an ion exchange model to characterize the oil adhesion on illite, and compared with oil adsorption experimental data using middle Bakken shale as a function of pH and concentration of NaCl. We also used the ion exchange model to quantitatively interpret the pH increase and low salinity effect from corefloodings (kaolinite-free cores) conducted by [33]. While we correctly predicted the trend of pH increase in the effluent from corefloodings, the predicted pH by PHREEQC is at low side (see Table 5 in [126]). Meanwhile, we observed a vertical spread in the correlation between bridging number and recovery factor (see Fig. 7 in [126]). We believe that the existing discrepancy lies in the limitation of the present geochemical model with following assumptions:

(1) For edge charged clays (e.g., kaolinite), the oil adhesion only occurs at the edge charge. Similarly, for basal charged clays, the oil adhesion only takes place at basal plane.

(2) Oil adhesion is explicitly represented using the concept of bond product sum [60] although the concept of this model is groundbreaking.

(3) For basal planes, exchange constants was assumed to be 1 whilst modelling the ion exchange process between the basal planes and the oil surface.

Therefore, we believe that the existing geochemical models call for a closer examination in light of chemical adsorption theory. To be more specific, the relative contribution of edge plane and basal plane on oil adhesion need to characterized, and quantified for a given clay minerals. Moreover, the exchange constants of the ion exchange model need to be further quantified to better model and predict the oil adhesion on basal planes. Therefore, we modelled the oil adhesion through basal plane together with edge planes against RezaeiDoust et al.,'s (Energy Fuels 2011, 25, 2151–2162) kaolinite adsorption experimental data in presence of quinoline. It is worth noting that in this work, we only characterized the adhesion of basic component represented by quinoline on kaolinite surfaces through basal and edge planes. We matched the experimental data by examining the adsorption capacity through edge charges and basal charges of kaolinite at ambient condition. The adsorption reactions are assumed to be: (1) $>SiO^-$ + BaseH$^+$ = $>$SiO-BaseH; (2) $>AlO^-$ + BaseH$^+$ = $>$AlO-BaseH; (3) $>$Na + BaseH$^+$ = $>$BaseH + Na$^+$ as shown in the schematic diagram in Fig. 3-1. To quantify the adsorption reactions in particular the equilibrium isotherm, PEST and PHREEQC were coupled to

optimize the adsorption equilibrium. The optimized adsorption equilibrium was then used to compute the adsorbed kaolinite and compared with the experimental data obtained by [33].
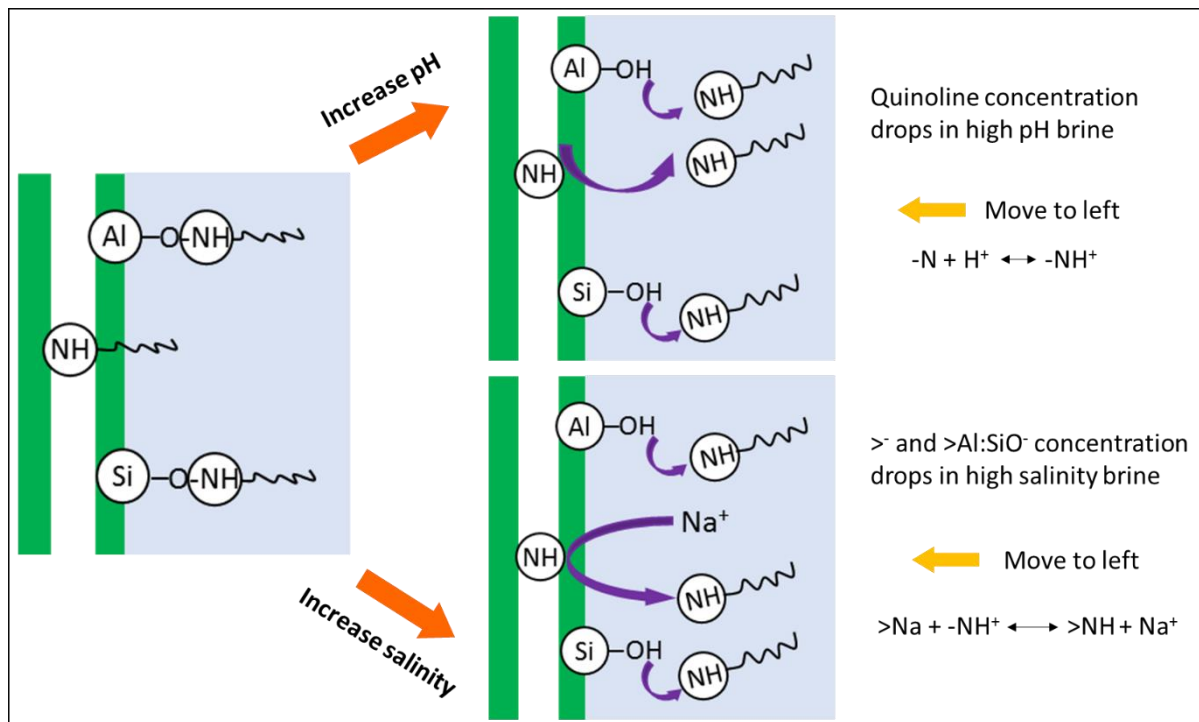
Fig. 3- 1 Schematic diagram of geochemical reactions taking place

3.3 Previous Experimental Results by RezaeiDoust et al. [33]

It is worth noting that in this paper, we aimed to investigate the relative contribution of the basal and edge plane on oil adhesion thus characterizing the adsorption equilibrium. We achieved by matching RezaeiDoust et al.,'s published experimental data (quinoline's adsorption on kaolinite powders) by coupling PEST and PHREEQC. Therefore, here we briefly documented the experimental fluids and procedures. For more detailed information in relation to experimental procedures, it can be referred to [33].

Given that kaolinite powers were used in the adsorption experiments, both edge and basal planes likely expose to the solution thus triggering quinoline's adsorption. To model this physico-chemical processes, surface complexation reactions and ion exchange reactions were coupled in the geochemical reactions to illustrate the reactions occurring on kaolinite edges and basal planes. Given the quinoline is dissolvable in brine, a solution species reaction is used to account for quinoline reactions in the brine.

3.3.1 Samples and fluids

To examine the adsorption of quinoline onto kaolinite powders, aqueous ionic solutions (30,000 ppm) listed in Table 3-1 were used. Then the test salinity brine is diluted from original brine (composition as in Table 3-1). For example, the original brine is diluted 6 times to get 5000ppm brine or diluted 2 times to get 15000ppm brine.. Given that pH also affects surface chemical species thus oil adhesion [60, 61, 126], aqueous ionic solutions with two different pH (5 and 8) were synthesized using NaOH or HCl. Quinoline solution was used to represent

basic material in crude oils, i.e., $-NH^+$ with concentration of 0.07mol/L. Kaolinite powders provided by VMR International were used in the adsorption measurements with weight percentage of 10–30wt% in solutions.

Table 3- 1 Composition of brine in the tests

	Na^+	Ca^{2+}	Mg^{2+}	Cl^-	TDS (g/L)
Concentration (mol/L)	0.355	0.045	0.045	0.534	30.0

3.3.2 Experimental procedures and results

The adsorption measurements were performed in a mixture of quinoline, kaolinite powders and brine as a function of pH and salinity as shown in Fig. 3-2. Each of adsorption test was repeated twice or three times to avoid experimental errors. Prior to the adsorption measurements, kaolinite powders (10-30 wt%) were mixed with a certain brine, and then rotated for two hours. Subsequently, quinoline (0.07 mol/L) was added into the mixture with rotation and equilibration for 24 hours. NaOH or HCl was added to adjust the pH. After the equilibration, diluted supernatant (100 times diluted) was measured by Shimadzu UV-1700 PharmaSpec UV – vis spectrophotometer with a wavelength of 312.5 nm to determine the adsorption. Then a calibration curve with a known concentration of quinoline was used to calculate quinoline concentration in the supernatant of diluted solution.

Fig. 3-2 shows that the adsorption of quinoline decreases with salinity for both pH 5 and 8. For example, at pH=5, the amount of quinoline adsorbed on kaolinite decreases from 4.5 to 3.7 mg/g as salinity increases from 0 to 25000 ppm. Similarly, at pH=8, the adsorption of quinoline declines from 2.1 to 0.8 mg/g with the same level of salinity increase. However, pH appears to control the adsorption of quinoline on kaolinite (Fig. 3-2) rather than salinity. For example, the amount of adsorption drops in a range of 3.3 to 2.4 mg/g when pH increases from 5 to 8 at a given salinity, which is two to three folds than the quinoline desorption made by salinity.
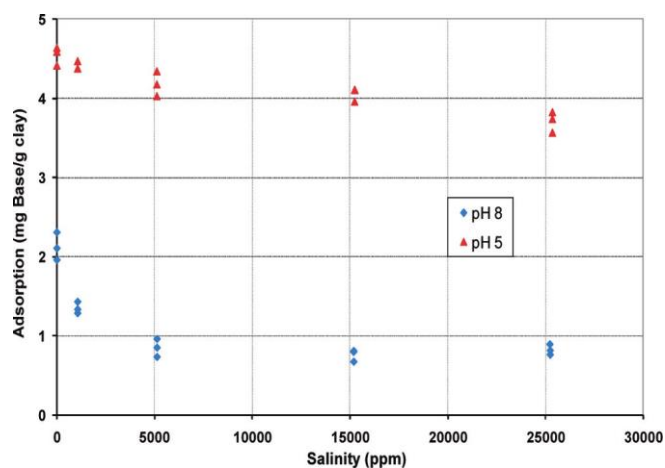
Fig. 3- 2 Quinoline adsorption/desorption as a function of salinity and pH [33]

3.4 Geochemical Modelling

3.4.1 Surface reactions at kaolinite surfaces

Given that the surface reactions occurring on kaolinite surface includes surface complexation reaction (occurring on edges) and ion exchange (occurring on basal plane). Reactions 1 to 7 are surface complexation reactions occurring on kaolinite edges in Table 3-2. Reactions 8 to 10 are ion exchange reactions on basal plane. While kaolinite edge surface complexation reactions dominate oil adhesion at pore network in porous media [74], kaolinite powders likely exhibit basal planes to trigger oil adhesion due to substantial specific area (10-30 m^2/g [142]) as a form of powders (with a CEC around 3-15 meq/100g [73]). Therefore, both surface complexation reactions and ion exchange reactions are taken into account to model quinoline adsorption on kaolinite powders.

Table 3- 2 Surface reactions input

Reactions occurring at edge planes		
Reaction	Equilibrium constant	Reaction No.
$>AlOH + H^+ = >AlOH_2^+$	3.0[a]	1
$>SiOH = >SiO^- + H^+$	-7.0[a]	2
$>AlOH = >AlO^- + H^+$	-3.8[a]	3
$>SiOH + Ca^{2+} = >SiOCa^+ + H^+$	-9.7[a]	4
$>AlOH + Ca^{2+} = >AlOCa^+ + H^+$	-9.7[a]	5
$>SiOH + Mg^{2+} = >SiOMg^+ + H^+$	-9.7[b]	6
$>AlOH + Mg^{2+} = >AlOMg^+ + H^+$	-9.7[b]	7
Reactions occurring at basal planes		
$>Na + H^+ = >H + Na^+$	4.6[c]	8
$2>Na + Ca^{2+} = >Ca + 2Na^+$	0.8[d]	9
$2>Na + Mg^{2+} = >Mg + 2Na^+$	0.6[d]	10

Note: Reaction equilibrium [a] is from [60]. [b] is assumed based on [143] [c] is from [104]. [d] is from thermo.com.V8.R6.230 thermodynamic database from Lawrence Livermore National Laboratory.

3.4.2 Quinoline-brine-kaolinite adsorption modelling

To model the quinoline-Brine-Kaolinite adhesion, quinoline surface species as a function of pH were calculated using the geochemical reaction: Quinoline + H$^+$ = QuinolineH$^+$ (*log K* = 4.9) [33]. Given that ion exchange process occurs between quinoline and kaolinite basal plane, we used geochemical reactions developed in literatures [99, 144, 145] to quantify the impact of basal plane on adhesion of quinolone and kaolinite. Moreover, to examine the relative contribution of edge and basal planes on oil adhesion, the geochemical reaction parameters in Table 3-2 were estimated by integrating geochemical simulator PHREEQC [101] and parameter estimation algorithm PEST [146]. It is worth noting that the quinoline is considered as a solution species in a brine, and its protonation process is calculated as an aqueous reaction. Adsorption process is modelled in two parts: (1) quinoline adsorption on kaolinite edge using surface complexation reactions, (2) quinoline adsorption on kaolinite basal planes using ion exchange reactions. After the geochemical reactions input the PHREEQC, the experimental results (i.e., observation data in PEST) are divided into two groups based on pH. Two observation groups (one pH is one group) are set in PEST. The average of adsorption

data at a given salinity is set as the observation data for PEST, which adjusts the input log k value until the optimal value is reached based on Gauss-Marguardt-Levenberg algorithm.

Table 3- 3 Parameter estimation for base adsorption on kaolinite surface

Reaction	Equilibrium constant	Adsorption location
$>SiO^- + BaseH^+ = >SiO\text{-}BaseH$	k_1	edge plane
$>AlO^- + BaseH^+ = >AlO\text{-}BaseH$	k_2	edge plane
$>Na + BaseH^+ = >BaseH + Na^+$	k_3	basal plane

To achieve computation algorithm mentioned above, the estimation process implemented in this work is illustrated in Fig. 3-3. Firstly, the parameters (log K) are defined in Table 3-3, and set in the "Template file" of PEST. Then the "Instruction file" was prepared to call the PEST thus reading the output file of PHREEQC. A "Control file" was built to call PEST for simulations, generating PHREEQC input file, and setting the stop criteria etc. After each run, PEST reads PHREEQC output value, and calculates parameters (log K) based on Gauss-Marguardt-Levenberg Algorithm until the minimum value of the objective function. The objective function here refers to the sum of squares of the weighted mismatches between observations and model generated counterparts. Otherwise, PEST would generate a new PHREEQC file to continue the optimisation until reaching the minimum of objective function.
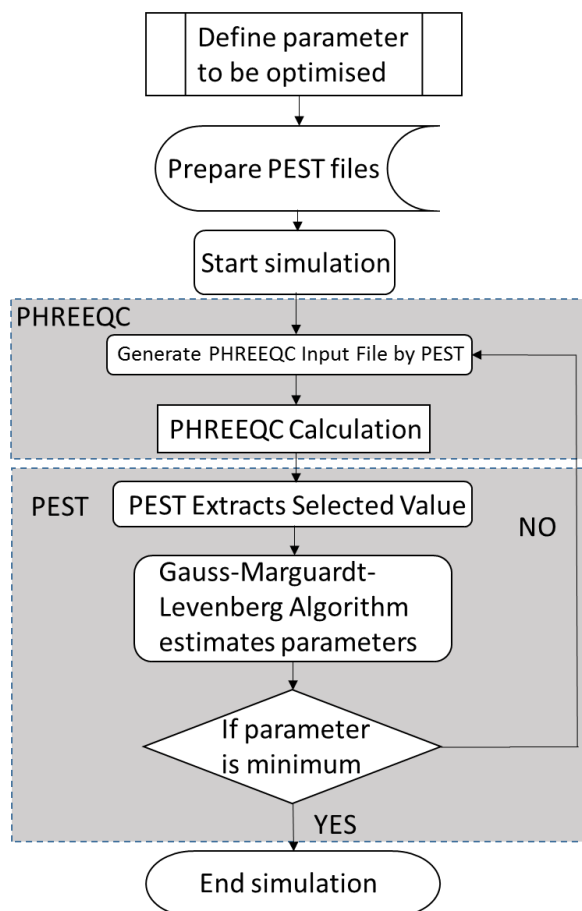
Fig. 3- 3 Schematic diagram to couple PHREEQC and PEST for estimating equilibrium constants between quinoline and kaolinite on edge and basal planes

3.5 Results and Discussion

3.5.1 Modelling Results: Effect of water chemistry on protonation of quinoline in brines

The amount of –NH$^+$ due to quinoline protonation slightly increases with salinity. For example, the protonated quinoline increases from 34.4 to 39.8 mmol when salinity increases from 0 to 25000 ppm at pH=5 (Fig. 3-4). The same trend is also observed by Brady et al. [60], who shows that the base component of oil increases from about 4.9 to 5.4 µmol/m^2 when brine salinity (NaCl brine) increases from 0.01 to 1.0 µmol/L.

While amount of –NH$^+$ increases slightly with salinity, pH controls the –NH$^+$, showing that –NH$^+$ increasing with lowering pH in line with existing calculations [59, 99, 126, 147]. For example, at a given salinity of 15,000 ppm, the amount of –NH$^+$ is 36.3 mmol at pH=5, whereas –NH$^+$ concentration is 0.08 mmol at pH=8. [99] calculated that the concentration is 5-7 µmol/m^2 at pH = 4, while it drops to less than 1 µmol/m^2 at pH = 8. [126] reported that the adsorption of functional groups (e.g., -COOCa$^+$ and –NH$^+$) on clay mineral (basal plane based) decreases from 3 to almost 0 µmol/m^2 when pH increases from 3 to 8.
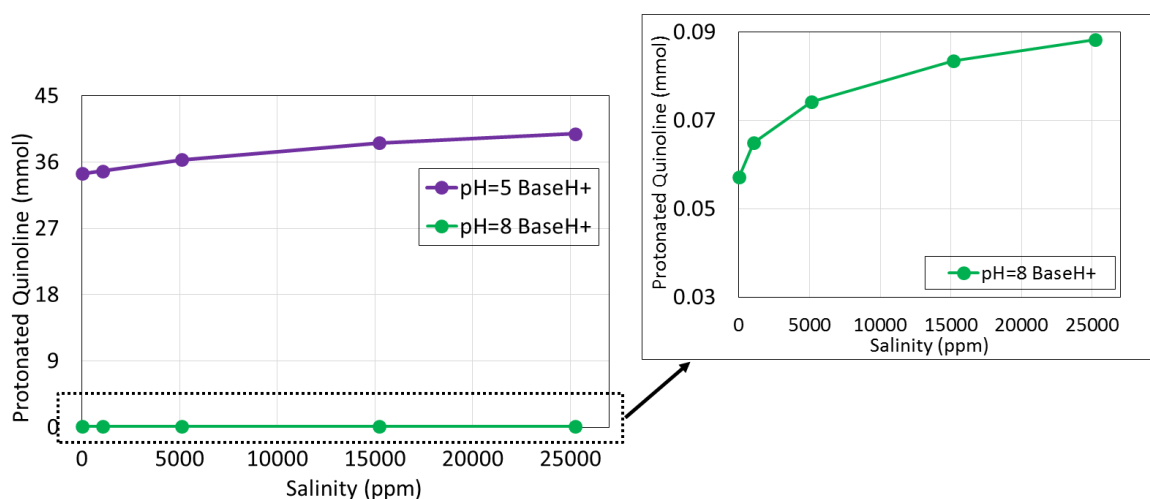
Fig. 3- 4 Protonation of quinoline in different brine

3.5.2 Modelling Results: Effect of water chemistry on surface species of kaolinite surfaces

On kaolinite edges, total site density of >Al:SiO$^-$ increases with salinity at a given pH (as shown in Fig. 3-5). At pH=8, the amount of >Al:SiO$^-$ increases from 3.4 to 6.8 mmol when salinity increases from 0 ppm to 25000 ppm, implying more binding sites available for quinoline adsorption, which in return promotes oil-wetting. Fig. 3-5 also implies that zeta potential of brine-kaolinite likely becomes more negative due to the increase of >Al:SiO$^-$ with salinity. However, this contradicts existing zeta potential results. For example, [49] reported that zeta potential is around -12 mV in 50,000 ppm brine for Berea sandstone. However, zeta potential turns to be -35 mV in 2,000 ppm brine. The contradiction may be attributed to the increase of pH in low salinity brine as a result of ion exchange, calcite and albite dissolution which has been well documented in our previous publications in geochemical modelling [59, 126]. The

pH increase has also been experimentally demonstrated. For example, [72] measured the pH in a synthetic sand columns (quartz with either illite or kaolinite) before and after low salinity injection, showing that effluent pH increases from 7 to around 9.8 after low salinity waterfloosing.

Apart from salinity effect, concentration of >Al:SiO$^-$ increases with pH, implying the increase of negative charges on kaolinite surfaces [49]. For example, the site concentration is 6.5 mmol in 15000 ppm brine at pH=5. However, the site concentration drops to 2.3 mmol in the same brine at pH=8. The decrease concentration of >Al:SiO$^-$ with pH can be explained by the chemical reactions in Table 2. Increasing pH or decreasing concentration of H$^+$ will move the deprotonation reaction of >AlOH and >SiOH to the right-hand side in line with [60], who reported that the concentration of >Al:SiO- increases from around 1 to about 3 µmol/m^2 in 1 mol/L NaCl when pH increases from 4 to 9. Fig. 3-5 also implies that pH increase triggered by low salinity waterflooding likely increases >Al:SiO$^-$ thus shifting kaolinite surface to be more negative charged, which in return lifts off oil films from kaolinite surfaces because oil surface usually is negative charged at high pH [49, 68, 138].
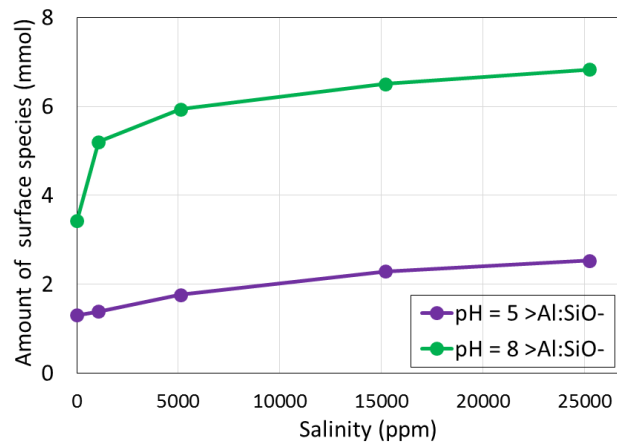
Fig. 3- 5 Amount of negatively charged surface species on kaolinite

3.5.3 Modelling Results: Effect of water chemistry on exchangeable site of kaolinite surfaces

The number of exchangeable site increases with salinity at a given pH (as shown in Fig. 3-6). For example, the exchangeable site >Na increases from nearly 0 to 0.9 mmol when salinity increases from 0 to 25000 ppm at pH=5. Similar, >Na increases from 0.9 to 4.0 mmol with increasing salinity from 0 to 25000 ppm at pH=9. This is largely because increasing salinity shifts Reactions 8 and 9 (in Table 3-2) towards left-hand side thus increasing >Na. The salinity dependant of exchangeable site implies that the adsorption of oil on basal plane of kaolinite surfaces would be a function of salinity [99].

Along with salinity impact, increasing the pH increases the number of exchangeable site at basal plane of kaolinite surfaces. For example, the exchangeable site increases from 3.94×10^{-3} to 3.94 mmol when pH increases from 5 to 8 at 15000 ppm. Analogously, >Na increases from 0.9 mmol to 4.1 mmol with same pH increase at salinity of 25,000 ppm. The trend of exchangeable site increase with pH at a given salinity is in line with our previous work [126] where shows that the exchangeable site (>Na) increases from nearly 0 to 400 µmol/m^2 with

pH increasing from 4 to 8. The pH dependent of the number of exchangeable sites is due to the Reaction 8 (Table 3-2) which shifts towards right-hand side with increasing pH.
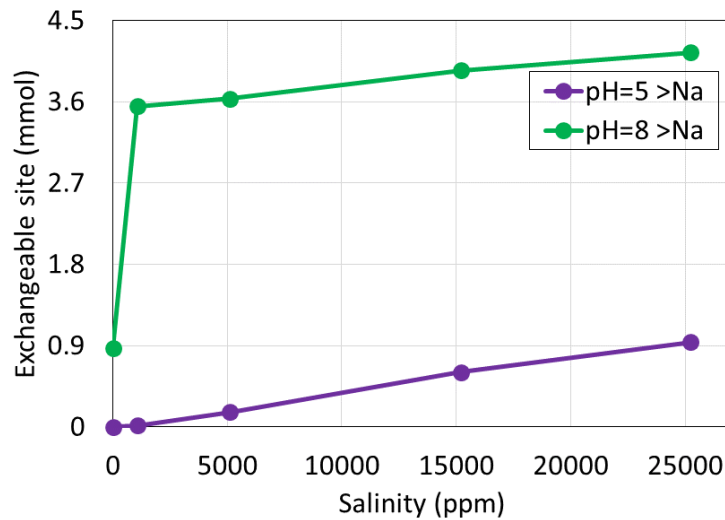
Fig. 3- 6 Amount of exchangeable site in different brines

3.5.4 Characterization of quinoline-brine-kaolinite adsorption model

To characterize the geochemical reactions proposed in Table 3-3, quinoline adsorption on kaolinite surfaces was modelled on basal and edge planes. Experimental data reported by [33] was matched as shown in Fig. 3-7 with the aid of coupling PEST and PHREEQC. The calibrated equilibrium constants for the geochemical reactions are listed in Table 3-4. Fig. 3-7 shows that the calculated adsorption of quinoline on kaolinite surfaces and observed value are well fitted as a function of salinity and pH. For example, in the presence of brine with 5000 ppm at pH=5, the calculated amount of adsorption is 4.09 mg/g in light of geochemical reactions proposed in Table 3-4 while the experimental observed adsorption is 4.16 mg/g with standard derivation less than 2%. Taken all of the data into consideration, the mean value of non-zero weighted residuals is 2.56×10^{-2}, which is lower than pre-set stop criteria (0.01 in this optimisation) thus reasonable results.
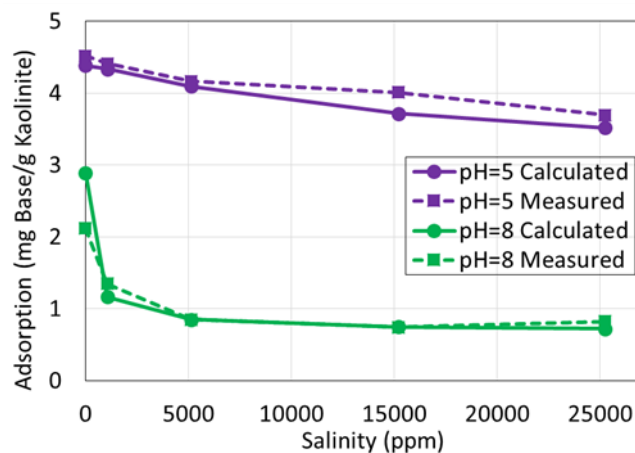
Fig. 3- 7 Measured adsorption results and calculated adsorption results

Table 3-4 shows the equilibrium constants of the geochemical reactions proposed in Table 3-3. The equilibrium constant for base component adsorption on $>SiO^-$ and $>AlO^-$ is 2.79 and 0.79, respectively. The equilibrium constant for ion exchange between quinoline and basal plane is 1.7, which is slightly greater than the parameters proposed by [99], who used 1 to model the adsorption of $-NH^+$ and $-COOCa^+$ on basal plane.

Table 3- 4 Adsorption equilibrium constants estimated results

Reaction	Equilibrium constant	Adsorption location
$>SiO^- + BaseH^+ = >SiO-BaseH$	2.79	Kaolinite edge adsorption
$>AlO^- + BaseH^+ = >AlO-BaseH$	0.79	Kaolinite edge adsorption
$>Na + BaseH^+ = >BaseH + Na^+$	1.70	Kaolinite basal adsorption

3.5.5 Adsorption analysis on basal and edge planes

To quantify the relative contribution of edge and basal planes on the adhesion, based on the equilibrium constants in Table 3-4, the adsorption of quinoline on kaolinite surfaces through edge and basal planes are plotted separately as a function of salinity and pH. Fig. 3-8 shows that adsorption slightly decreases with increasing salinity from both basal and edge planes at a given pH (as shown in Fig. 3-8). For example, when salinity increases from 0 to 25,000 ppm at pH = 5, quinoline adsorption declines from 2.4 to 1.9 mg/g from basal planes, and a decrease from 2.0 mg/g to 1.6 mg/g was observed from edges. Similar to pH =8, when salinity increases from 0 to 25,000 ppm, quinoline adsorption decreases from 1.2 to 0.01 mg/g from basal planes, and a decrease from 1.7 mg/g to 0.7 mg/g is shown from edges.

However, the relative contribution of basal and edge planes on adsorption varies at different pH. For example, at low pH=5, while both basal and edge planes render more adsorption compared to pH=8, the adsorption at basal plane remains to be 7-10 times greater than edge plane at pH=8. Taken together, these results imply that at reservoir condition of pH in a range of 5 to 6.5 due to dissolved CO_2 in crude oil and aqueous phase, sandstone reservoirs likely exhibit intermediate or less water-wet, which provides potential for wettability alteration. Nevertheless, low salinity water injection likely triggers pH increase due to ion exchange, calcite, and albite dissolution [33, 59, 99, 126, 148], thus decreasing the adhesion from both edge and basal planes. The adsorption in particular of the basic component, $-NH^+$, through basal planes would significantly decrease with the same range of pH increase. Therefore, it is of vital importance to integrate ion exchange model and surface complexation model to model the wettability alteration in sandstone reservoirs.
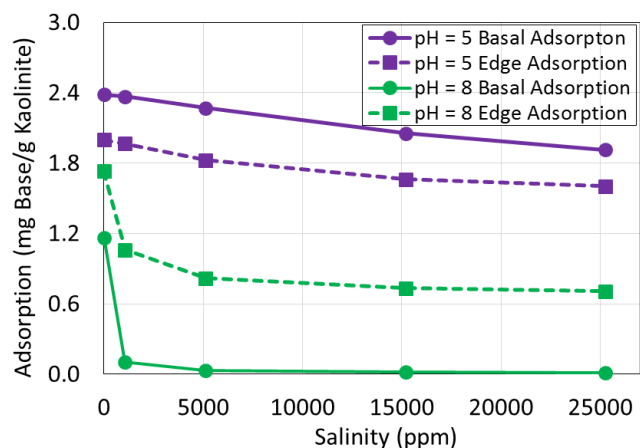
Fig. 3- 8 Adsorption on kaolinite edge and basal under different pH and salinity

3.6 Implications and Conclusions

While clay minerals in particular through basal and edge planes play an important role in oil-brine-sandstone system interaction thus wettability, the relative contribution of basal and edge planes on oil adhesion remains unclear, presenting a substantial impediment to manage and predict the performance of low salinity water in sandstone reservoirs. We thus coupled PEST and PHREEQC to model the oil adhesion against RezaeiDoust et al.,'s (Energy Fuels 2011, 25, 2151–2162) kaolinite-quinoline adsorption experimental data. We coupled interaction taking place between quinolone-basal plane and quinolone-edge plane using ion exchange model and surface complexation model developed by [74]. Moreover, to explicitly model the number of bonds between quinolone-kaolinite through basal and edge planes, we proposed a new geochemical model as shown in Table 3-4. By integrating PHREEQC and PEST, we successfully matched RezaeiDoust et al.,'s experimental data, which in return, enable us to derive equilibrium constants of the new geochemical model in Table 3-4. Our new calibrated model shows that the basal adsorption ($>Na + BaseH^+ = >BaseH + Na^+$) dominates quinoline adsorption at low pH (pH=5). Rather, the edge adsorption controls adsorption mechanism at high pH (pH=8). Furthermore, the model shows that salinity plays a minor role in adsorption at a controlled pH system. Taken together, our new model reveals that basal plane modelled by ion exchange would regulate oil-clay minerals adsorption at low pH (<5), whereas edge plane modelled by surface complexation reactions would take the control at high pH (>8). Our results may also explain why [149] observed less oil prevalent onto kaolinite in high salinity at pH = 8.0, and less oil removal from kaolinite in the presence of low salinity brine at pH = 6.3 from SEM-EDS images compared to silicate grains. This is largely because edge plane regulates oil-kaolinite adsorption at pH =8 which gives repulsion between $>Al:SiO^-$ and $-COO^-$. However, basal plane likely governs oil-kaolinite adsorption at pH=6 which triggers more bridges between oil-kaolinite in low salinity brine [99, 126]. Our new model quantifies the relative contribution of basal and edge planes on basic component adhesion thus wettability at different pH and salinity, providing insights and new geochemical data to existing geochemical database, thereby better model and predict the wettability alteration during low salinity waterflooding.

Chapter 4. Insights into the Wettability Alteration at Pore Scale during Low Salinity Water Flooding in Sandstone Using X-ray Micro Computed Tomography

4.1 Abstract

Wettability alteration appears to be an important physicochemical process for low salinity waterflooding in sandstone reservoirs. While fundamental principles in particular electrostatic origins have been proposed to characterize *in-situ* wettabiilty at sub-pore scale (molecular level), few studies have been done in pore-scale, and fewer had looked beyond the detachment of oil film from pore surfaces to constrain the uncertainty of low salinity effect at different length scale. We thus performed a pore-scale multiphase flow experiment on a sandstone core sample. We imaged the core sample at initial oil saturation, residual oil saturations after high salinity and low salinity water flooding. Moreover, we examined fluid occupancy maps and water cluster size distribution at pore-scale before and after low salinity waterflooding. Furthermore, we performed a geochemical study to relate physicochemical process at sub-pore scale to account for *in-situ* wettability alteration at pore-scale.

Micro-CT imaging shows that low salinity waterfloodng yielded 5% of residual oil saturation reduction after high salinity water flooding. Fluid occupancy maps within pore network show water film propagation at pore surface during low salinity water flooding, suggesting the oil film detachment from pore surfaces due to *in-situ* wettability alteration. Micro-CT imaging analysis also shows that the large size water cluster (greater than 10^7 μm^3) occupies 87.7% of water volume after high salinity water flooding, whereas the same size water cluster occupies 89.6% pore volume after low salinity water flooding, implying that water clusters coalesce into each other to transport in pore network during low salinity water flooding in line with fluid occupancy maps. Geochemical modelling predicts a pH increase (from 7 to 8.9) during low salinity water flooding largely due to ankerite and albite dissolution. Moreover, low salinity brine decreases adhesion of oil-kaolinite minerals, which is widely coated at pore surfaces based on SEM and XRD examinations, accounting for the *in-situ* wettability alteration thus oil film detachment. This study sheds light on the significance of geochemical controls over wettability alteration at pore-scale through water film propagation, thus providing insights in oil coalescence, transport, banking and eventually recovery of oil at different length scale.

4.2 Introduction

Low salinity water flooding appears to be an emerging means for improving oil recovery in sandstone reservoirs particularly at the period of low oil price. This is largely because low salinity injection would accelerate oil production by improving oil relative permeability whilst decreasing water relative permeability as a result of wettability alteration due to fluid-rock and fluid-fluid interactions [29, 31, 150]. To quantify the wettabiity alteration process on recovery of oil, various approaches have been proposed and developed in industry and academia. Industry aims to develop a *predictive strategy* and *screening tool* at core and reservoir scale, for example using well testing [151], field pilots [35], and special core analysis with combination of core-scale and reservoir scale numerical simulation using existing commercial reservoir simulation packages [30, 31]. Academia endeavours to characterize wettability alteration processes at sub-pore scale by the aid of atomic force microscopy [152, 153], zeta potential [49, 65, 68, 138, 154], contact angle experiments [65, 68, 76, 134, 155-157], molecular dynamics [55, 158], etc. However, the main challenges in low salinity water flooding in sandstone reservoirs lie in multi-length and multi-time scale nature [133], which means that

a certain mechanism at sub-pore scale, pore- and core-scale may not prevail in reservoir-scale during multiphase flow in subsurface, although the mechanism may work at a certain length scale. Therefore, there is a pressing need to identify controlling factor(s) of low salinity effect across all length scales. In particular, it is of vital importance to reveal multiple mechanisms which may act at different length scales simultaneously thus assisting detachment, coalescence, transport in pore network, oil-bank formation and eventually recovery of oil.

Therefore, a few works have been done at pore-scale to examine how multiple mechanisms act together to aid oil and brine transport and coalescence of oil at pore-scale. For example, Bartels et al. [80] imaged sandstone rocks during low salinity water flooding using fast X-Ray scanning. They reported that low salinity water flooding triggers emulsification (brine in oil emulsion) which contributes to incremental oil recovery. Moreover, they also confirm that the presence of clay minerals is important to yield the low salinity effect due to fluid-rock interactions [159]. Sandengen et al. [81] scanned sandstone mini-core plugs during the spontaneous imbibition (5 mol/L NaCl and distilled brine). They conclude that osmosis is a potential mechanism for the additional oil recovery. This is because water film expansion during spontaneous imbibition may provide channels for wettability modifiers (e.g., Ca^{2+}, Mg^{2+}, SO_4^{2-}) to access oil-brine-rock interfaces thus shifting wettability. To confirm the wettability alteration at pore-scale, Khishvand et al. [78] characterised the *in-situ* contact angle in sandstone pore network using micro-CT scanning. Their results show that contact angle of oil at pore surface decreases from 115° to 89° during low salinity water flooding, confirming that wettability is the main physicochemical process behind residual oil saturation reduction during low salinity water flooding. Shabaninejad et al. [160] analysed the oil and water occupancy in the pore network before and after low salinity water flooding. They concluded that oil film detachment occurs mainly on grain surfaces rather than aggregated clay.

Taken together, while a few works have been done at pore-scale, the existing accounts fail to link mechanisms at sub-pore and pore-scale. In this work, our objective was to gain a better understanding of the factors controlling the multiphase flow from sub-pore to pore-scale by addressing the following questions.

1. How does wettability alteration from contact angle measurements using substrates represent *in-situ* wettability alteration at pore-scale?
2. How does wettability alteration trigger oil detachment from pore surfaces thus coalescence and oil banking?
3. More importantly, can we link electrostatic adhesion at sub-pore scale to wettability alteration at pore-scale?

To address the above questions, we therefore performed a pore-scale multiphase flow experiment on a sandstone core sample. We imaged the core sample at initial oil saturation, residual oil saturations after high salinity and low salinity water flooding. Moreover, we examined the fluid occupancy maps and water cluster size distribution before and after low salinity waterflooding. Furthermore, we performed a geochemical study to relate physicochemical processes at sub-pore scale to *in-situ* pore-scale, thus mitigating the intrinsic uncertainty of low salinity water flooding at multiscale from centimetres to kilometres.

4.3 Materials and Methods

4.3.1 Core sample and fluids

A Berea sandstone was used in the Micro-CT core-flooding experiment with the mineralogy listed in Table 4-1, where quartz is the main mineral with 63.9% weight percentage, followed by ankerite $(Ca(Fe,Mg,Mn)(CO_3)_2)$ and albite with 18% and 8.5 % weight percentage,

respectively. The rock also contains clay minerals, mainly kaolinite (2.1%) and muscovite (3.8%).

Table 4- 1 XRD data for Berea sandstone

Mineral	Phases (wt%)
Quartz	63.9
Albite	8.5
Kaolinite	2.1
Muscovite	3.8
Clinochlore	0.6
Ankerite	18
Microcline	3.1

A crude oil with acid number of 4.0 mg KOH/g, and base number of 1.3 mg KOH/g was used in the Micro-CT core-flooding experiments. The mass fraction of asphaltenes and wax are listed in Table 4-2, which was analysed using gas chromatograph mass spectrometer (GC-MS). The composition of formation brine is listed in Table 4-3 with a total salinity of 142,431 ppm. Low salinity brine was obtained using 100 times diluted formation brine. To enhance CT contrast of oil and brine from CT images, 1-Iodooctane (from Sigma Aldrich, number 238295, 98% purity) was added into the oil with a mass percentage of 10%.

Table 4- 2 Experimental oil properties

Oil	Acid Number (mg KOH/g)	Base Number (mg KOH/g)	Asphaltenes wt%	Wax wt%	Viscosity mPa.s
	4.0	1.3	0.54	2.58	5.23

Table 4- 3 Composition of experimental brines

Brines	K^+	Na^+	Ca^{2+}	Mg^{2+}	Cl^-	HCO_3^-	SO_4^{2-}	TDS/ppm
Formation brine/FB	1152.0	47520.0	5840.0	771.0	86500.0	586.7	61.5	142431
Low salinity water/LSW	11.52	475.2	58.4	7.71	865	5.867	0.615	142.31

4.3.2 Experimental setup

4.3.2.1 Coreflooding flow cell

To perform Micro-CT core-flooding experiments, a cylindrical mini-core plug with diameter of 4.67 mm and length of 14.63 mm was drilled from a Berea core plug. Then the mini-core plug was loaded in a flow cell. Two tube fittings with size of 3/8 in. × 3/16 in (diameter) were used as the inlet and outlet of the Micro-CT coreflooding ends (as shown in Fig. 4-1). To avoid the fluid bypass, the core plug was covered with teflon and plastic shrinkage sleeve, which were heated to seal the core plug with the two metal ends. Additionally, to increase physical strength of the flow cell, plastic hardener was used to cover the core plugs and connect the two metal ends.
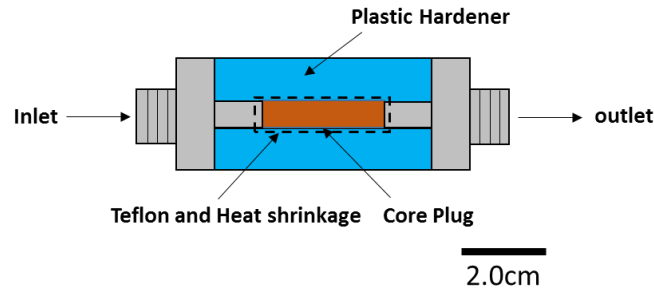
Fig. 4- 1 Schematic of flow cell for X-ray micro computed tomography

4.3.2.2 Micro-scale Coreflooding procedure

Prior to saturating the rock with brine, the micro-scale coreflooding system (as shown in Fig. 4-2) was vacuumed for 24 hours. The system was then saturated with formation brine for 24 hours. Subsequently, the sample was flooded using the crude oil to establish the initial oil saturation, S_{oi}, with an injection rate of 0.001 ml/min, equivalent of capillary number of 2.06×10^{-6} ($Ca = \dfrac{\mu v}{\sigma}$, The capillary number is selected according to Iglauer et al., [161, 162]. Two-hundred pore volumes (PV) of oil in total were injected into the mini-core plug. Once the initial oil saturation S_{oi} was established, the mini-core plug was imaged using X-Ray Micro CT at a resolution of 1.9628 μm per pixel. Later, the core plug was flooded with 100 PV high salinity brine at an injection rate of 0.005ml/min, followed by low salinity brine flooding with the same injection rate and the same number of PVs. The mini-core plug was imaged again at residual oil saturation (S_{or}) after high and low salinity water flooding. The Micro-CT images were processed with a beam hardening filter to eliminate beam hardening to get rid of ring effect. Subsequently, a median filter was applied to mitigate noise, and watershed segmentation was used to partition oil and brine phases in Avizo 9.5 (Segmented phases as shown in Fig. 4-3).
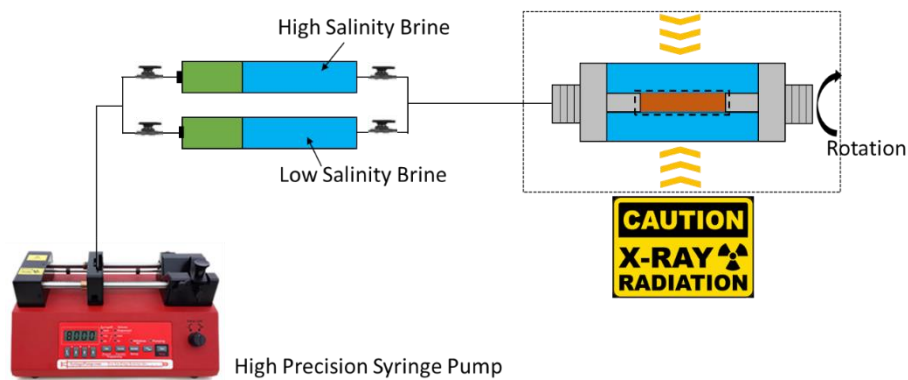
Fig. 4- 2 Schematic of Micro-CT coreflooding setup at ambient condition of temperature and pressure
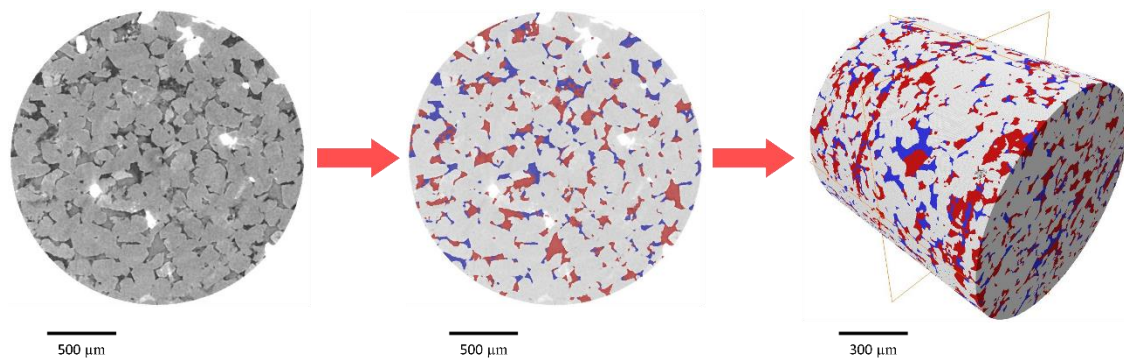
Fig. 4- 3 2D and 3D segmentation results. The left image is a gray scale image after reconstructing raw images, and the middle one is obtained after de-noising and segmentation. The right one is a segmented 3D image. Note that the 2D images are located at the middle of core plug with a slice number of 471 in 944 images.)

4.4 Results

4.4.1 Potential Imaging Artifacts

Prior to the segmentation of fluid from porous rock, images were processed by beam hardening filter to eliminate beam hardening effect. Subsequently, media filter was applied to de-noise and watershed segmentation was used to partition oil and brine phases in Avizo 9.5. It is worth noting that due to the close intensity range between doped-oil and rock matrix, while watershed segmentation approach was used to segment oil and water phase, artifacts remains. However, the artifacts at oil and rock partitioning does not prevent us from capturing the essence of the physics at pore surface, because the intensity difference between oil and rock can be recognized by watershed filter.

4.4.2 Responses to high and low Salinity water flooding

Low salinity water flooding at tertiary mode exhibited low salinity EOR-effect by further decreasing residual oil saturation after high salinity water flooding. For example, high salinity water flooding at secondary mode yielded 64.5% residual oil saturation after 100 PV flooding, whereas low salinity water flooding at tertiary mode further decreased residual oil saturation to 59.6% by 100 PV low salinity water injection, suggesting a more water-wet system (as shown in Table 4-4). Our result is also consistent with Shabaninejad et al., [160] who reported that low salinity water (100 times diluted Minnelusa reservoir brine) yields 3% of incremental oil recovery (Minnelusa formation oil) in a Berea sandstone reservoir rock using pore-scale X-ray CT. Similarly, Lebedeva et al. [163] observed additional 7% of oil saturation reduction in kaolinite coated sandpack in low salinity tertiary flooding compared with high salinity tertiary flooding. Interestingly, X-ray micro-CT also shows that the porosity of the rock increases from 21.7% to 23.0% after the low salinity water flooding, implying that mineral dissolution likely took place possibly on ankerite and albite minerals. To further test this, we performed reactive transport modelling to explore the potential mechanisms behind the porosity variation during low salinity water flooding in the subsection.

Table 4- 4. Processed phase properties from CT images

Injection sequence	Water saturation (%)	Oil Saturation (%)	Porosity (%)
high salinity water flooding at secondary mode	35.5	64.5	21.7
Low salinity water flooding at tertiary mode	40.4	59.6	23.0

4.4.3 Pore-scale displacement: Water film propagation at pore surfaces

Fig. 4-4 shows the water film propagation before and after low salinity waterflooding at different positions along the core plug from inlet to outlet. Fig. 4-4 shows that low salinity water flooding triggers water film enlargement at pore surfaces, implying that the size of clusters of remaining oil decreases after low salinity water flooding, which supports the reduction of oil saturation after low salinity waterflooding reported in Table 4-4. For example, at location A, the water film evolves along the pore surface, which likely connects the previously disconnected water ganglion [78, 80]. Same evolutions occur at other locations, e.g., the locations of B, C, D, E, F, G and H from Fig. 4-4. Besides, Fig. 4-4 also shows that some pore networks are not swept by high salinity water flooding, where exhibits no response to the subsequent low salinity waterflooding, e.g. locations I, J. This suggests that low salinity brine likely decreases the residual oil saturation at pore networks which are swept by high salinity waterflooding. This explains why low salinity water injection at tertiary mode likely gives less EOR potential compared to the secondary mode [71, 133, 164].
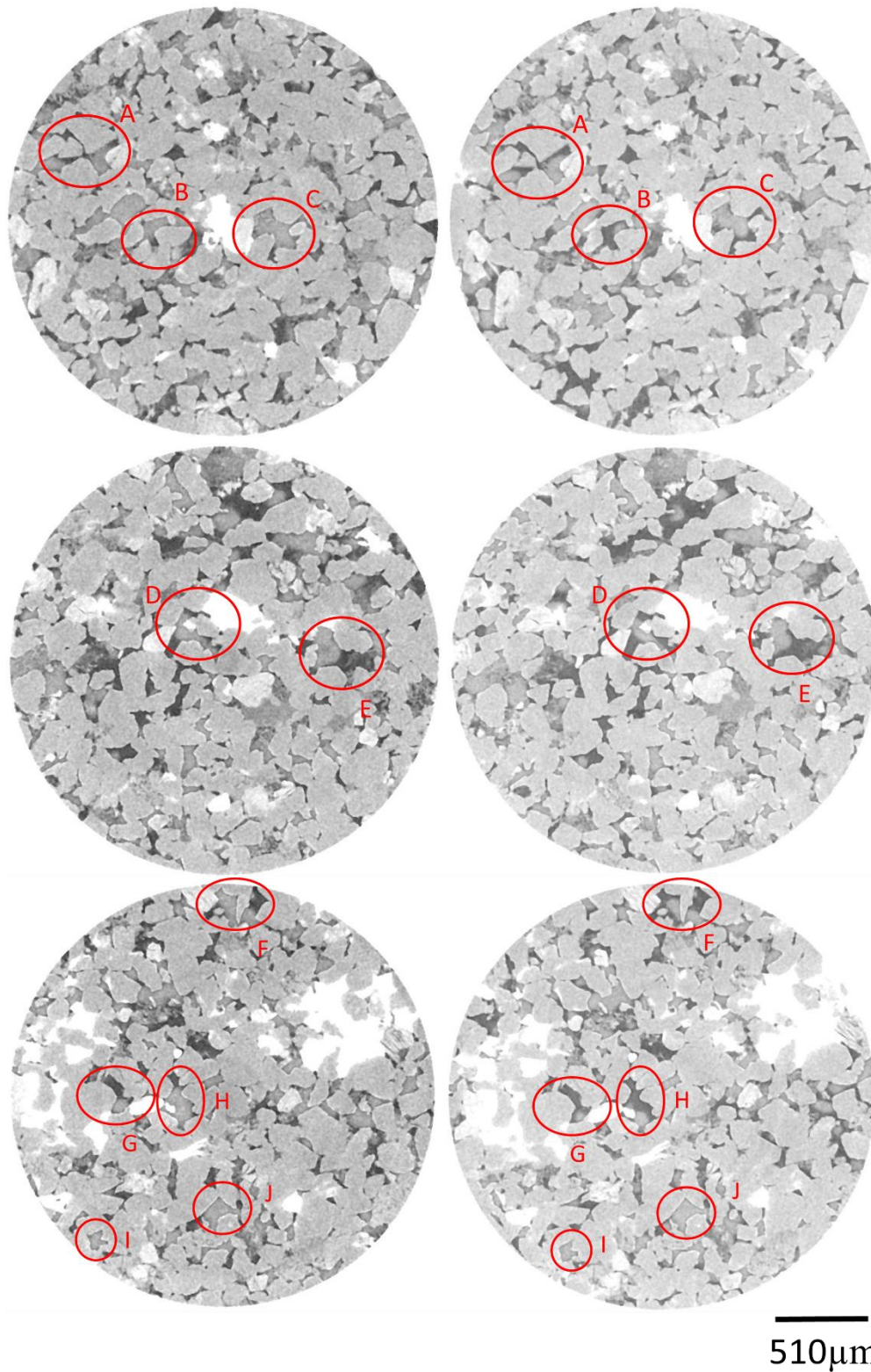
Fig. 4- 4 Water film propagation at pore scale near the inlet of the mini-core plug (Note: the left image is after high salinity water flooding, and the right image is after low salinity water flooding.)

4.5 Discussion

4.5.1 Geochemical controlled water film propagation

Water film propagation at pore surfaces indicates that wettability alteration processes take place during low salinity water flooding. Fig. 4-4 shows that the water film advances at the pore network surfaces during low salinity water flooding, implying a more hydrophilic pore surfaces. To decipher underlying mechanism(s) of wettability alteration at pore surfaces, SEM scanning was taken on Berea sandstone to reveal pore scale mineralogical distribution. As shown in Fig. 4-5, the pore surfaces are either coated with kaolinite minerals or exposed with quartz surfaces, and illite are distributed at pore throats. Previous studies show that kaolinite mineral promotes wettability alteration towards more water-wet in the presence of low salinity water, which has been observed at reservoir pilot scale [25] and interpreted using electrical double layer [49, 53, 138, 165] and surface complexation modelling [59, 74]. For examples, Nasralla et al. [49] conducted zeta potential measurements, showing that low salinity water shifts the zeta potential of brine-clays and brine-oil strongly negative and thus more hydrophilicity. Geochemical modelling shows that low salinity water can significantly decrease the number of the bridges (indicated by bond product sum) between kaolinite and oil thus increasing hydrophilicity [60, 61]. Our previous work also shows mineral dissolution (e.g., calcite and albite) can increase local pH by 1 to 2 units, which facilitates the bond-breaking between kaolinite and oil [59, 126]. To further confirm the geochemical controls over water film propagation in this work, we calculated the bond product sum between oil and kaolnite ($[>AlOH_2^+][-COO^-]+[>Al:SiO^-][-NH^+]+[>Al:SiO^-][-COOCa^+]+[>Al:SiOCa^+][-COO^-]$) in the presence of low salinity and high salinity brine with input parameters from reactions as shown in Table 4-5. The site density and surface area of kaolinite are 3.84 $\mu mol/m^2$ and 10 m^2/g, respectively. Our results show that high salinity brine gives a bund product sum of 2.97 $(\mu mol/m^2)^2$, whereas low salinity brine gives a bond product sum of 2.25 $(\mu mol/m^2)^2$, 24% decrease, indicating the wettability alteration process at pore surfaces.

Table 4- 5 Geochemical Parameters (After Brady et al. [60])

Reaction location	Reaction	Log K_{25oC}
Oil Surface	$-NH^+ = -N + H^+$	-6.0
	$-COOH = -COO^- + H^+$	-5.0
	$-COOH + Ca^{2+} = -COOCa^+ + H^+$	-3.8
Kaolinite Edges	$>AlOH_2^+ = >AlOH + H^+$	-3.0
	$>AlOH = >AlO^- + H^+$	-3.8
	$>SiOH = >SiO^- + H^+$	-7.0
	$>AlOH + Ca^{2+} = >AlOCa^+ + H^+$	-9.7
	$>SiOH + Ca^{2+} = >SiOCa^+ + H^+$	-9.7
	$>AlOH + CaOH^+ = >AlOCaOH + H^+$	-4.5
	$>SiOH + CaOH^+ = >SiOCaOH + H^+$	-4.5
Ion exchange on clay basal	$>Na + H^+ = >H + Na^+$	4.6
	$2>Na + Ca^{2+} = >Ca + 2Na^+$	0.21
Calcite dissolution	$CaCO_3 + H^+ = Ca^{2+} + HCO_3^-$	1.85
Dolomite dissolution	$CaMg(CO_3)_2 + 2H^+ = Ca^{2+} + Mg^{2+} + 2HCO_3^-$	2.5
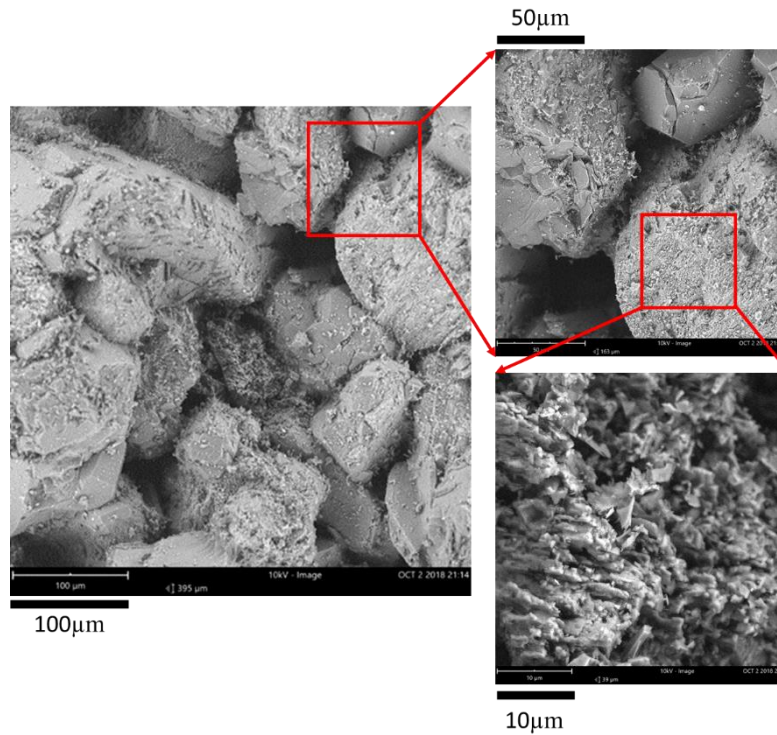
Fig. 4- 5 SEM image of Berea sandstone surfaces

4.5.2 Potential geochemical evidence of pH increase and ankerite Dissolution

Given that mineral dissolution in particular calcite/dolomite and albite would increase the pH during low salinity water flooding beside the ion exchange process, to understand the local pH increase during low salinity water flooding, we performed reactive transport modelling using PHREEQC [101]. Due to the fact that the core plug is rich in ankerite (18 wt%), we investigated the potential of pH increase as a result of ankerite dissolution during low salinity water flooding. Our results show that pH likely increases to 8.6-8.9 during the low salinity water flooding as shown in Fig. 4-6 after 8-9 PV low salinity water injection before reaching in equilibrium. It is worth noting that due to the lack of thermodynamic data for ankerite dissolution in PHREEQC, in our reactive transport modelling, calcite and dolomite were employed to indicate ankerite dissolution. This is largely because ankerite is a member of dolomite, which shows a similar geochemical surface species. Our previous work showed that pH increase would promote detachment of oil film from local pore surfaces through depressing ion exchange and supressing surface complexation reactions [59, 126, 141, 147], which further supports the reduction of residual oil saturation and water film propagation at pore surfaces.
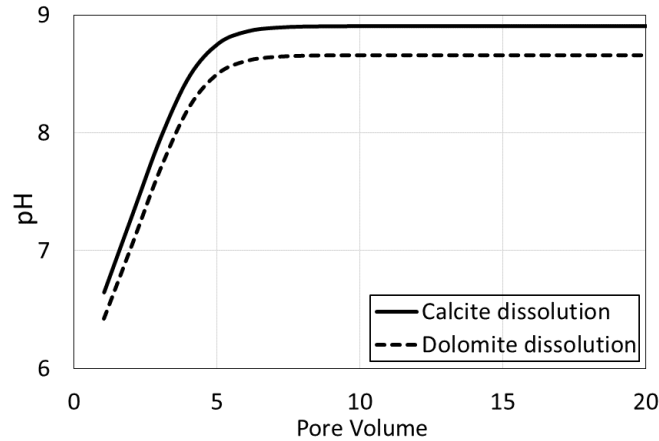
Fig. 4- 6 pH variation with pore volume during low salinity water injection due to mineral dissolution predicted by 1D reactive transport modelling using PHREEQC. The reaction column is composed of 10 cells. One thousand shifts were applied to model the reactive transport with a time step of 0.000335 day, which corresponds to 100 PV low salinity water injection at a rate of 0.005 ml/min. Prior to modelling the transport during low salinity waterflooding, the cells are saturated and equilibrated with formation brine.)

We also found that the volume of high density mineral (light mineral as show in Fig. 4-4) increases from 3.18×10^6 (0.44%) to 3.92×10^6 μm^3 (0.54%) after low salinity water flooding. It is worth noting that the high density mineral is ankerite which has high density element Fe and Mn as shown in Fig. 4-7. The increased volume of high density mineral may explain why the rock porosity slightly increases after low salinity water flooding. We are uncertain why the volume of ankerite increases after low salinity water flooding; perhaps this is because ankerite dissolution and clay adsorption. To be more specific, low salinity brine leads to ankerite dissolution thus releasing Fe^{2+} to the brine, which would be adsorbed on the clay minerals (kaolinite and muscovite) as shown in Reaction (1) [166]. Therefore, the ion exchange reaction occurs between Fe^{2+} in the brine and basal-charged clay surface (muscovite and illite). Moreover, the edge charged surface species >AlO⁻ and >SiO⁻ can also adsorb metal ions (Fe or Mn) from brines (See Fig. 8 in Gan et al. [143]). Taken together, the ion exchange process and adsorption through edges likely increases the volume of the high density minerals due to the high specific area of clays.

$$2\text{>Na} + Fe^{2+} = \text{>}_2\text{Fe} + 2Na^+ \quad logK= 0.4 \tag{1}$$
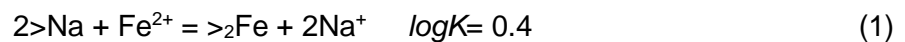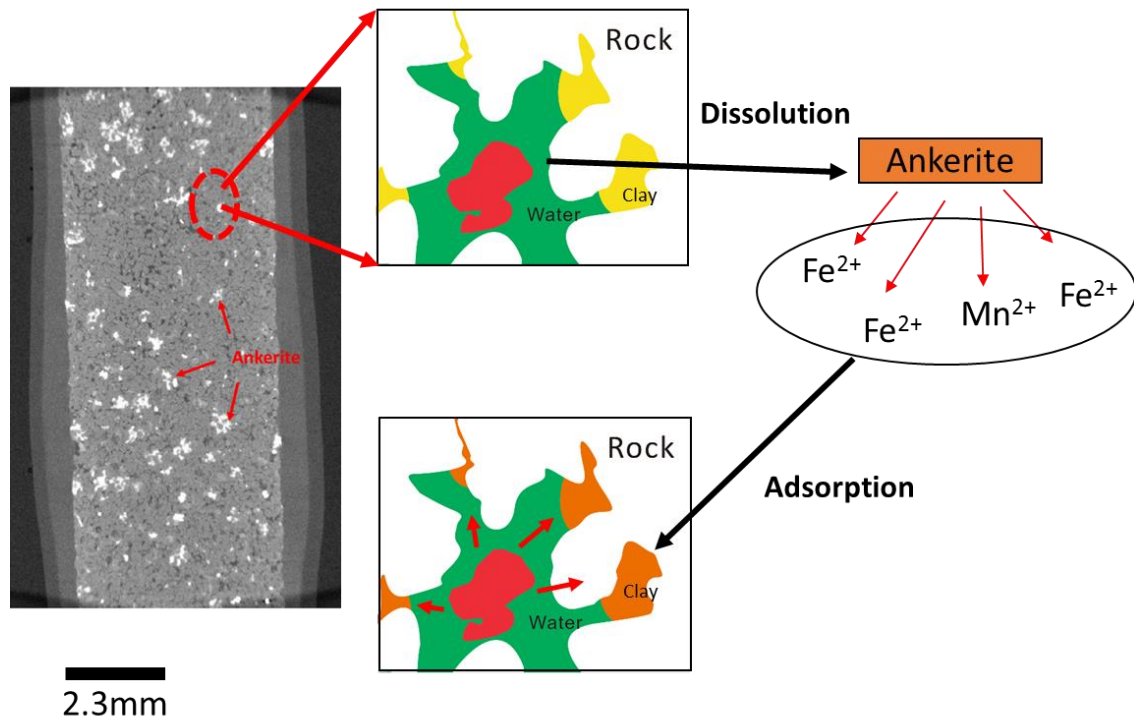
Fig. 4- 7 Ankerite distribution in Micro-CT image (The white parts (high CT number parts) are ankerite minerals)

4.5.3 Pore-scale displacement events during low salinity water flooding

To gain a deeper understanding of geochemistry controls over wettability alteration at pore scale, we also investigated the distribution of water clusters before and after low salinity water flooding. It is worth noting that the reason we examined the clusters of water is because water phase can be well partitioned from oil and rock in our Micro-CT images. Also, focusing on water clusters can help us to understand water film propagation at pore surfaces. Fig. 4-8 shows that the large size water cluster (greater than 10^7 μm^3) occupies 87.7% of water volume after high salinity water flooding, whereas the same size water cluster occupies 89.6% pore volume after low salinity water flooding, implying that water clusters coalesce into each other to transport in pore network during low salinity water flooding. The growing contiguous water clusters can be observed in Fig. 4-8, which shows that the volume of the large water clusters increases from 3.3×10^7 to 4.8×10^7 μm^3 (Figure 10, b), whereas the volume of the medium size water clusters (with size from 10000 μm^3 to 100000 μm^3), and small size water clusters (less than 10000 μm^3) decreases after low salinity water flooding. The decrease of medium and small water clusters likely triggers the water phase inter-connection at pore network to form large size water clusters due to *in-situ* wettability alteration attributed to water film propagation.

Fig. 4-8 also shows that volume of medium size water clusters decreases from 5.7×10^6 to 2.9×10^6 μm^3 (48.9% decrease). Yet, a less decrease (27.7%) is observed from small size water clusters. This implies that medium size water clusters is more responsive to water ganglion reconnection thus contributing to low salinity water flooding effect. Rather, small size water clusters are less responsive to water ganglion reconnection thus making a minor contribution to incremental oil recovery. This is largely because the small size water clusters would be by-passed by high salinity water flooding at secondary mode thus having limited contact area during the low salinity water flooding at tertiary mode. This explains why low

salinity water injection at tertiary mode likely gives less EOR potential compared to the secondary mode [71, 133, 164]. The water cluster behaviour is also consistent with Iglauer et al. [167], who observed that the residual oil clusters were located adjacent to rock surface in oil-wet system, while in the water-wet rock, the residual oil clusters were stranded towards the middle of larger pores, which agrees with the water phase movement in this research.
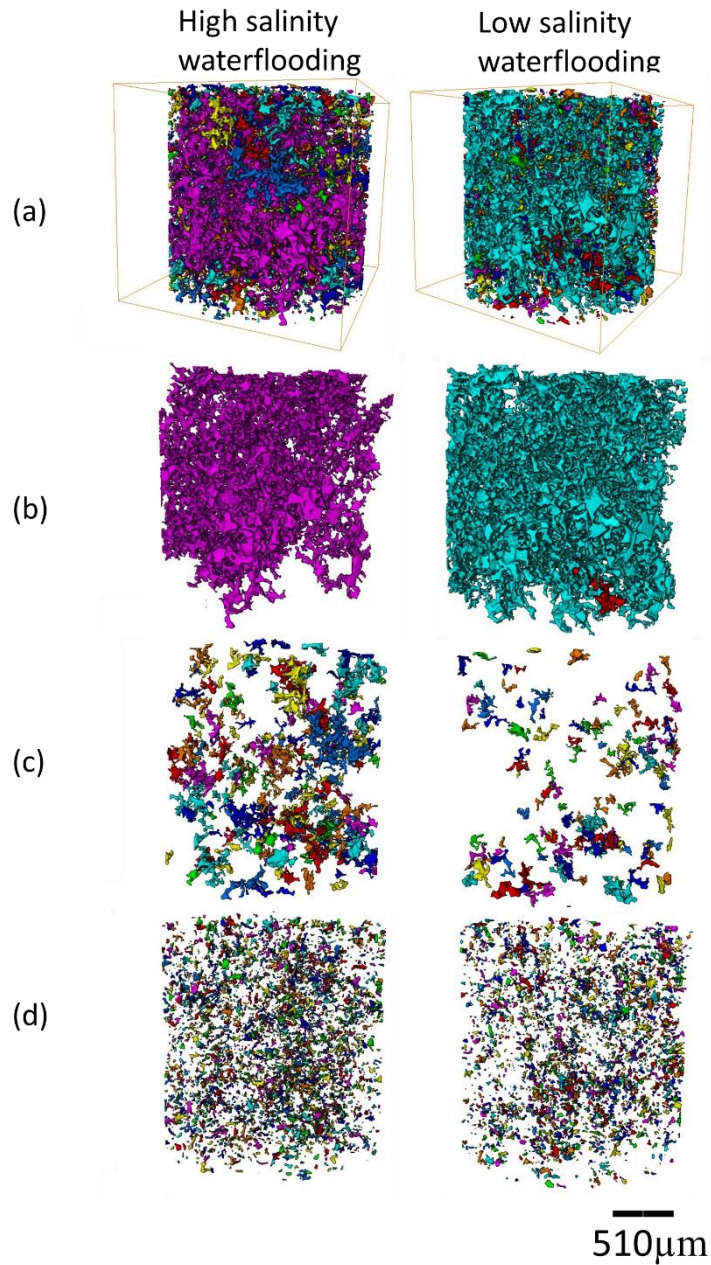
Fig. 4- 8 The variation of the volume of water clusters before and after low salinity water at pore network. (a): the volume of total water clusters, (b) large water clusters (size >100000 μm^3), (c) medium water clusters (size 10000-100000 μm^3), (d) small water clusters (size < 10000 μm^3). Different colours label the connectivity of water clusters.

Table 4- 6 The volume of water clusters with different size

Cluster Volume (μm^3)	HSW flooding secondary mode	LSW flooding tertiary mode	Variation
large size water clusters	33413776	48159763	44.1%
medium size water clusters	5700634	2914089	-48.9%
small size water clusters	4982003	3602545	-27.7%

Note: HSW and LSW refer to high salinity water and low salinity water.

4.6 Conclusions and Implications

Water-assisted Enhanced Oil Recovery termed low salinity water flooding appears to be a cost-effective means to achieve reservoir potential due to wettability alteration processes. While geochemical studies [36, 59, 76, 126, 147] and thermodynamic modelling [67] have been performed to relate the wettability alteration at sub-pore scale (contact angle and atomic force microscopy measurements [139, 153, 168, 169]) to core-scale, few studies have been done to identify the local wettability alteration prevailing at pore scale, and fewer have investigated how geochemical controls over wettability alteration at pore scale during low salinity water flooding. We thus performed a pore-scale multiphase flow experiment on a sandstone core sample. We imaged the core sample at initial oil saturation, residual oil saturations after high salinity and low salinity water flooding. Moreover, we examined fluid occupancy maps and water cluster size distribution at pore-scale before and after low salinity waterflooding. Furthermore, we performed a geochemical study to relate physicochemical process at sub-pore scale to account for *in-situ* wettability alteration at pore scale.

Our Micro-CT imaging shows that low salinity water yielded 5% of residual oil saturation reduction after high salinity water flooding in line with previous study [160, 163]. Fluid occupancy maps at pore scale show water film propagation at pore surface after low salinity water flooding, suggesting the oil film detachment from pore surface due to *in-situ* wettability alteration. This also explains why Khishvand et al. [78] observed contact angle decrease at pore-scale after low salinity water flooding. Moreover, geochemical modelling also predicts a pH increase to 8.9 during low salinity water flooding largely due to albite and ankerite dissolution, which facilitates *in-situ* wettability alteration [59, 60, 126, 147]. More importantly, surface complexation modelling shows less adhesion between oil and kaolinite minerals which likely leads to water film propagation at pore surfaces in the presence of low salinity water. We also found that the large size water cluster (greater than 10^7 μm^3) occupies 87.7% of water volume after high salinity water flooding, whereas the same size of the water cluster occupies 89.6% pore volume after low salinity water flooding, implying that water clusters coalesce into each other to transport in pore network during low salinity water flooding in line with fluid occupancy maps. Moreover, we also found that medium size water clusters is more responsive to water ganglion reconnection thus contributing to low salinity water flooding effect. Rather, small size water clusters are less responsive to water ganglion reconnection thus making a minor contribution to incremental oil recovery. Taken together, these findings imply that remaining oil in medium size clusters would be the main target to achieve low salinity EOR-effect. This study sheds light on the significance of geochemical controls over wettability alteration at pore-scale through water film propagation, thus providing insights in oil coalescence, transport, banking and eventually recovery of oil at different length scale.

Chapter 5. Oil/Water/Rock Wettability: Influencing Factors and Implications for Chemical Water Flooding in Carbonate Reservoirs*

5.1 Abstract

Wettability of the oil/brine/rock system is an essential petro-physical parameter which governs subsurface multiphase flow behaviour and the distribution of fluids, thus directly affecting oil recovery. Recent studies [24, 97, 116] show that manipulation of injected brine composition can enhance oil recovery by shifting wettability from oil-wet to water-wet in a process we term here "chemical water flooding". However, what factor(s) control system wettability has not been completely elucidated due to incomplete understanding of the geochemical system. To isolate and identify the key factors at play we used SO_4^{2-} free solutions to examine the effect of salinity (formation brine/FB, 10 times diluted formation brine/10dFB, and 100 times diluted formation brine/100dFB) on the contact angle of oil droplets at the surface of calcite. We then compared contact angle results with predictions of surface complexation by chemical water using PHREEQC software.

We demonstrate that the conventional dilution approach likely triggers an oil-wet system at low pH, which may explain why the chemical water EOR-effect is not always observed by injecting low salinity water in carbonated reservoirs. pH plays a fundamental role in the surface chemistry of oil/brine interfaces, and wettability. Our contact angle results show that formation brine triggered a strong water-wet system (35°) at pH 2.55, yet 100 times diluted formation brine led to a strongly oil-wet system (contact angle=175°) at pH 5.68. Surface complexation modelling correctly predicted the wettability trend with salinity; the bond product sum ($[>CaOH_2^+][-COO^-]$ + $[>CO_3^-][-NH^+]$ + $[>CO_3^-][-COOCa^+]$) increased with decreasing salinity. At pH < 6 dilution likely makes the calcite surface oil-wet, particularly for crude oils with high base number. Yet, dilution probably causes water wetness at pH > 7 for crude oils with high acid number.

Keywords: Chemical water flooding, Carbonate reservoirs, Wettability, Contact angle, Surface complexation modelling

5.2 Introduction

Carbonates rock host most of the world's oil reserves (> 60 %) [170], which are composed primarily of the minerals calcite and dolomite together with impurities, e.g., quartz, anhydrite, clay minerals, organic matter, and apatite [171]. However, average recovery typically is lower than 40%. Cost-effective and environmentally friendly techniques to enhance oil recovery from carbonates are therefore of broad scientific interest [68]. One such technique that has gained interest is to modify the injected water chemistry to shift reservoir wettability from oil-wet to water-wet in a process termed chemical water flooding, which is also called *LoSal* flooding by BP [3, 4], *Smart Water* flooding by its originators, Austad and co-workers, at the University of Stavanger, Saudi Aramco[5], and *Designer Water flooding* by Shell [6, 7].

Several mechanisms have been proposed to describe how the approach improves oil recovery in sandstones: fines mobilization [13], limited release of mixed-wet particles [13], increased pH and reduced IFT similar to the alkaline flooding [14], multi-component ion exchange (MIE) [4, 15-17], electrical double layer expansion [18-20], salt-in effect [21], salting-out effect [22] and osmotic pressure [23].

The chemical water effect in carbonate reservoirs is less clear, which limits application of chemical water in carbonated reservoirs [97]. Previous studies suggest that wettability alteration is the main mechanism for the chemical water effect in carbonated reservoirs, despite the fact that the specific factors controlling wettability have not been completely elucidated. For example, most reports suggest that chemical water shifts reservoir wettability from oil-wet towards water-wet, lifting oil films off the pore surface, whereas Al-Attar, etc. found the opposite [172], arguing that chemical water shifted reservoir wettability from water-wet to intermediate wetting, thereby increasing recovery. Sulphate apparently acts as a catalyst by adsorbing at pore surfaces more strongly than oil carboxylate groups, thereby changing the rock surface charge locally from positive to negative, and causing repulsion between oil carboxylate groups and pore surfaces [173]. As a consequence, reservoir rock wettability will be shifted from oil-wet to water-wet, thereby increasing oil recovery. However, there is still uncertainty about the nature of wettability change, with some reports suggesting it is double layer expansion, and others suggesting it is mineral dissolution [174].

We aimed to gain a deeper understanding of the factors governing the wettability of the oil/brine/carbonate system with a combination of approaches (e.g., contact angle test, surface complexation modelling, and geochemical modelling). Given that the conventional dilution approach is widely used in field, we particularly focused on the effect of salinity level on the wettability of oil/brine/carbonate system. We removed SO_4^{2-} ions from test solutions in order to isolate wettability controls in the absence of the specific effect of SO_4^{2-} [175].

We examined the effect of salinity level (formation brine/FB with salinity level at 252,244 ppm, 10 times diluted formation brine/10dFB, and 100 times diluted formation brine/100dFB), on contact angles of oil droplets at the surface of carbonates. To gain a deeper understanding of the geochemical reactions controlling the contact angle results, we used the geochemical speciation code PHREEQC (Parkhurst et al., 1999) to examine the impacts of calcite dissolution and surface complexation.

5.2.1 Rock Mineralogy

Rock mineralogy is essential to wettability alteration in carbonated reservoirs. X-ray diffraction (XRD) of rock samples used in the contact angle measurements showed 98.1 % calcite, 0.7% quartz, and 1.2% ankerite, but no detectable anhydrite ($CaSO_4$).

5.2.2 Brine Properties

To specifically focus on the salinity effect on system wettability, we removed SO_4^{2-} from all of the experimental brines. Formation brine (FB) was synthesised based on the composition of produced water from North Rumaila field having a salinity of 286,677 ppm [176]. Formation brine was then diluted by 10 times (10dFB) and 100 times using deionized water, to obtain low salinity brine (Table 5-1).

Table 5- 1 Composition of the brines used in contact angle measurements.

Brine	mg/L						TDS (ppm)	pH
	Na^+	Ca^{2+}	Mg^{2+}	K^+	Fe^{2+}	Cl^-		
Formation brine	74638	15200	4526	2013	303	155564	252244	2.55
10dFB	7463.8	1520	452.6	201.3	30.3	15556.4	25224.4	4.42
100dFB	746.4	152.0	45.3	20.1	3.0	1555.6	2522.4	5.68

Note that the brines used in this study had low pH values (Table 5-1) due to the reaction of Iron(II) chloride ($FeCl_2$) in water, which resulted in formation of ferrous, and chloride ions. This process resulted in the removal of hydroxyl ions from the solution, leaving hydrogen ions in excess, which made the solution acidic.

5.2.3 Experimental Crude Oil

The experimental crude oil was extracted from Stag field located in Commonwealth waters on the North West shelf of Western Australia. To avoid the precipitation and plugging by particulates in the crude oil during injection of crude oil, the crude oil was filtered using 12-micron paper filter. The properties of the crude oil are given in Table 5-2. Note: the experimental oil had a higher base number (1.02 mg KOH/g) than acid number (0.50 mg KOH/g), suggesting that concentration of $–NH_2^+$ at oil surface may be two times greater than $–COO^-$ [83]. This implies that the bond between carbonate and amine group, $[>CO_3^-][-NH^+]$, may play an important role in system wettability.

Table 5- 2 Properties of crude oil

Property	Unit	Result
density	g/cm^3	0.94
API gravity	°API	18.50
Specific Gravity 260/60°F	-	0.94
Acid number	mg KOH/g	0.50
Base number	mg KOH/g	1.02
Kinematic viscosity @ 20°C	cSt	122.50
Kinematic viscosity @ 40°C	cSt	37.26
Asphaltene content	% mass	0.14
Water content	% volume	0.15
Wax content	% mass	<5

5.2.4 Contact Angle Test

To investigate the effect of water chemistry on wettability of carbonate, we tested the contact angle on the rock with crude oil and aqueous ionic solutions using Vinci IFT-700 (Fig. 1). The experimental temperature and pressure was at 60 °C and 2000 psi, respectively. Contact angle tests were conducted using the sessile droplet method. Note: all of the contact angle results were recorded after equilibrium was reached, i.e. the contact angle did not change over 48 hours. Also note that while the substrate roughness, contact angle hysteriss, and preparation procedure all may affect the the macroscopoic contact angle [155], the philosophy

of the contact angle test in this study was to highlight the actual trend of the contact angle with salinity rather than the exact initial value of the contact angle.
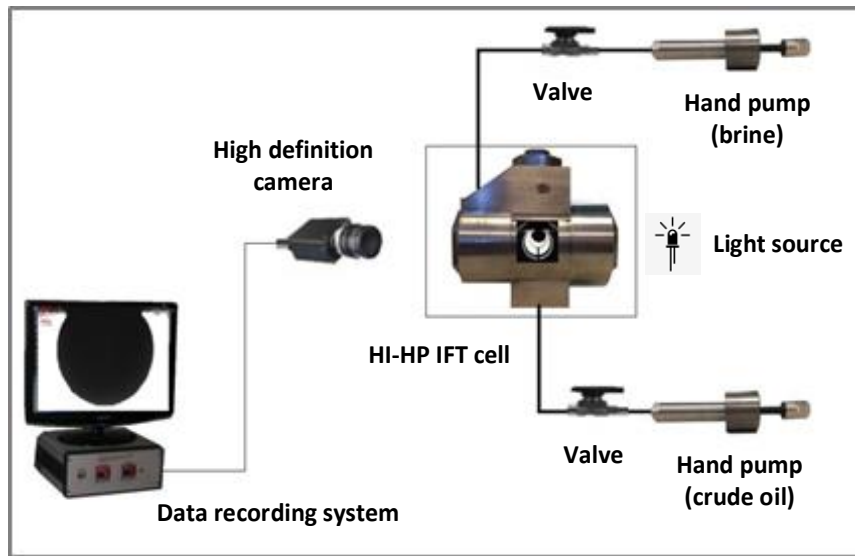
Fig. 5- 1 Schematic of contact angle and interfacial tension apparatus.

To obtain representative contact angles, the rock substrates were exposed to air plasma for 10 min to remove organic surface contamination [177]. Note that the aged sample were obtained by putting a clean sample in a beaker with crude oil in an oven at 90°C for eight weeks to restore wettability. After completing the aging process, samples were dried in the oven and cleaned for 15 min in an air plasma for the second time before measuring the contact angle. Subsequently, the substrates were placed in the HT-HP cell and vacuumed before the cell was filled with brine. Temperature and pressure was set at 60 °C and 2000 psi, respectively. After a state of equilibrium was achieved in the system (constant pressure and temperature), a drop of crude oil (0.04 - 0.06 ml) was introduced through a 0.6 mm diameter needle at the bottom of the cell into the brine environment. Then the droplet was released from the needle and placed on the substrate to measure the contact angle.

5.3 Results and Discussion

5.3.1 Effect of Water Chemistry on Contact Angle

The contact angle between oil and the carbonate substrate increased with decreasing salinity, implying that dilution shifts the wettability of oil/brine/carbonate towards more oil-wet. This may explain why the dilution approach does not always trigger chemical water EOR-effect. For example, the contact angle on un-aged carbonate substrate increased from 30 to 81° with decreasing salinity from FB to 100dFB (Fig. 5-3). A similar trend was also observed with aged carbonate substrate; the contact angle shifted from 35 to 175 ° with decreasing the salinity level from FB to 100dFB.

Although we observed a similar trend in contact angle alteration for both aged and un-aged rock samples, the effect of reduction in salinity on wettability was much more profound on aged substrate compared to un-aged substrate. Our results are in line with Al-Attar et al. [178] who reported that the contact angle increased with the decrease in the salinity level. For example, they observed the contact angle increased from 45° in the presence of FB (197,000 ppm), to 70° when salinity was reduced to 1,000 ppm. They also argue that a shift in carbonate

wettability from water wet to intermediate condition triggered incremental oil recovery. Similar results were reported by Mohsenzadeh et al. [179] who found that dilution led to oil-wetting. Successive dilution of FB increased the contact angle from 63° in FB (203,000 ppm), to 130° in 20dFB, shifting wettability from water-wet to oil-wet. However, the literature results also provides examples of the opposite behavior, low salinity brine shifting wettability of carbonate rocks from oil-wet to preferentially water-wet [155, 180-182]. For example, Mahani et al. [155] reported that contact angles was decreased by 5-17° as high salinity fromation brine was switched over to sea water after 40 hours, which can be interpreted by surface complexation modelling. For example, as pH above 6 at the oil/brine interface, –COO⁻ increases and –COOCa⁺ decreases in sea water compared to formation brine because of the decrease of the Ca^{2+}, thereby –COO^- dominates the surface charges at the oil/brine interface. At brine/calcite surface, much more >$CaSO_4^-$ would be generated in the presence of sea water simply because the concentration of SO_4^{2-} in sea water was 14 times higher than that of in the formation brine (e.g., 234 mg/l in FB, 3384 mg/l in SW),. As a consequence, the repulsive force between the oil/brine and brine/calcite increases, shifting the wettability toward more water-wet in the sea water. Note: the pH from Mahani et al.'s test for the fluids before and after the contact angle test did not change (pH for FW=6.9, and pH for SW=8.0).
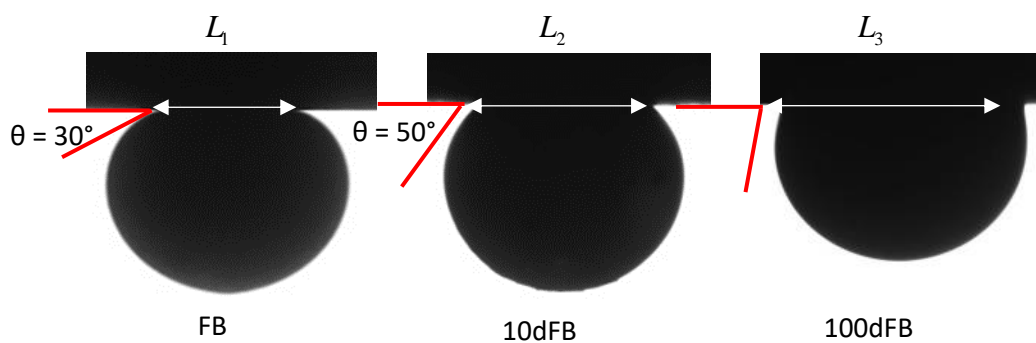
Fig. 5- 2 Contact angle of various brine and oil on the un-aged carbonate sample.
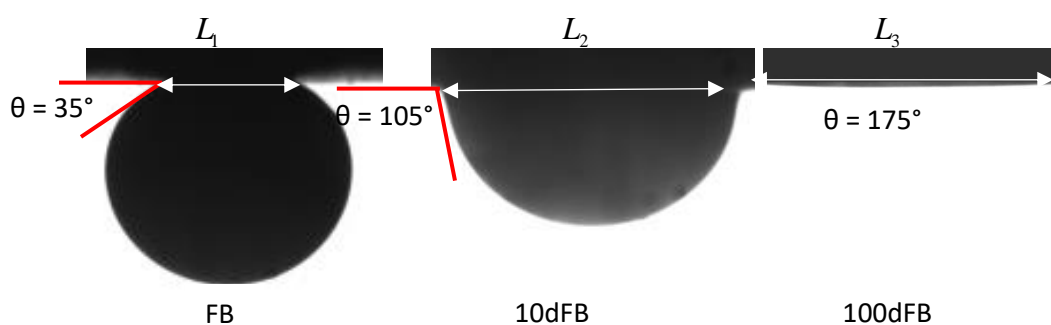
Fig. 5- 3 Contact angle of various salinity level and oil on the aged carbonate sample.

Note that L means the diameter of the oil droplet on the surface of the calcite, which is an indication of the affinity of the oil phase on the surface of calcite. The greater L is, the system is more oil-wet [155]. (Note: the initial pH of the FB, 10dFB, and 100dFB was 2.55, 4.42, and 5.68, respectively, see Table 5-1)

5.3.2 Surface Complexation Modelling

The surface complexation model developed by Brady et al. [83, 99] was applied to calculate the number of charged species that are thought to cause local adhesion of the oil/brine interface to the brine/calcite interface, hence wetting. The bond product sum counts the number of electrostatic connections between the two. Surface complexation modelling (and DLVO theory) presumes an electric double layer at each interface and the existence of charged surface species whose concentrations depend upon the chemical makeup of the water and the oil and mineral surface [61]. In the surface complexation model, the calcite surface area was assumed as 10 m^2/g with site density of 10 µmol/m^2 [83]. The chemical reactions on the surface of calcite can be described by the following reactions (Table 5-1). We used 25°C Log K for all of the chemical reactions in Table 5-3 because water chemistry dominates the surface complexation of the oil/brine/rock system and temperature plays a secondary effect [61]. The surface species concentrations were calculated using PHREEQC version 3.3.9 (Parkhurst and Appelo 2013) and a diffuse layer surface model.

Table 5- 3 Surface complexation model input parameters [83, 174, 183, 184]

Interface	Reaction	Log K_{25oC}	Reaction
oil/brine	-NH$^+$ = -N + H$^+$	-6.0	1
	-COOH = -COO$^-$ + H$^+$	-5.0	2
	-COOH + Ca^{2+} = -COOCa$^+$ + H$^+$	-3.8	3
calcite/brine	>CaOH + H$^+$ = >CaOH$_2^+$	11.85	4
	>CaOH + HCO$_3^-$ = >CaCO$_3^-$ + H$_2$O	5.8	5
	>CaOH$_2^+$ + SO$_4^{2-}$ = >CaSO$_4^-$ + H$_2$O	2.1	6
	>CO$_3$H = >CO$_3^-$ + H$^+$	-5.1	7
	>CO$_3$H + Ca^{2+} = >CO$_3$Ca$^+$ + H$^+$	-2.6	8
	>CO$_3$H + Mg^{2+} = >CO$_3$Mg$^+$ + H$^+$	-2.6	9

Where ">" denotes a site on the carbonate surface while "-" denotes a site on the oil surface.

5.3.2.1 Effect of Salinity on Number of Oil/Brine Surface Species

Salinity level strongly affected the calculated number of surface chemical groups at the oil/brine interface at a given pH (Fig 5-4). For example, the number of -NH$^+$ groups increased with increasing salinity at low pH (<5.5), yet at pH>5.5, the number of –NH$^+$ groups decreased with increasing salinity. The same trend was predicted by Brady et al. [83] who showed that the calculated number of –NH$^+$ oil groups increases sharply with increasing NaCl, whereas the number of –NH$^+$ groups decreases slightly with increasing the salinity level for a BN/AN = 10 oil at 100 °C. They also reported that for pH < 5.7, oil surface charge is dominated by –NH$^+$ groups, showing that increasing ionic strength increases the number of –NH$^+$ groups at the oil/brine interface, attributing it to –NH$^+$ surface activity coefficient increases with salinity [60].

The calculated concentration of –COOCa$^+$ increased with increasing salinity, in part because the concentration of Ca^{2+} increased, at a given pH (>5.5) (Fig. 5-4). However, increasing monovalent cation concentrations likely decreases the concentration of –COOCa$^+$ by decreasing the activity coefficient of dissolved Ca^{2+}. For example, Brady et al. [60] calculated that with constant concentration (5mM) of CaCl$_2$, the concentration of –COOCa$^+$ increased with decreasing NaCl from 1 M to 0.01 M.

pH also strongly affected the number of oil/brine surface groups. For instance, the number of –NH$^+$ groups decreased sharply with increasing pH particularly at pH < 6.5 (Reaction 1). Fig.

5-4 also shows that the effect of pH on the concentration of –NH$^+$ groups was much more pronounced than the effect of salinity. Increasing pH also increases the calculated number of –COOCa$^+$ groups (Reaction 3). Yet, the numbers of all of the surface chemical groups (–COOCa$^+$, –COO$^-$, and –NH$^+$) remained constant at pH > 8 (Fig. 5-4).

Our results imply that –NH$^+$ dominates the surface charges at low pH level (pH < 5.5), whereas –COOCa$^+$ and –COO$^-$ govern oil surface chemistry at pH > 6. Therefore, we believe that the dilution likely triggers oil-wet system at low pH < 5.5, particularly for crude oils with high base number. Dilution probably leads to water-wetting at for crude oils with high acid number at pH > 7.
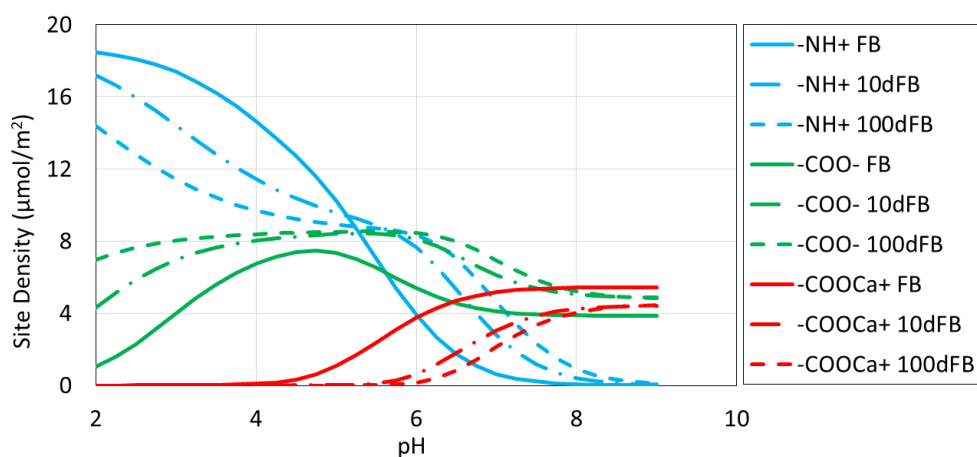
Fig. 5- 4 Number of oil surface chemical groups versus pH and dilution.

5.3.2.2 Effect of Salinity on Number of Rock/Brine Surface Species

To understand oil/brine/carbonate wettability we must characterize speciation at the brine/carbonate surface. We calculated the number of calcite surface species as a function of salinity and pH. We found that salinity strongly affected the number of >CO$_3^{2-}$ and >CO$_3$Ca$^+$ groups at a given pH (Fig. 5-5). For example, the number of >CO$_3^{2-}$ groups was calculated to increase with decreasing salinity at a given pH. However, the number of >CO$_3$Ca$^+$ groups increases with increasing salinity, and increased Ca^{2+} (Reaction 8). The concentration of >CO$_3$Mg$^+$, similar to >CO$_3$Ca$^+$, also increased with increasing salinity (Because the concentration of Mg^{2+} in each of the brines was 2 times less than that of Ca^{2+}, the variation of the >CO$_3$Mg$^+$ with pH was not shown in Fig. 5-5). Similar results were reported by Mahani et al. [84] who showed that the surface concentration of >CO$_3$Mg$^+$ decreased with decreasing salinity. For example, 100 times diluted seawater prompted a 0.2 µmol/m^2 decrease in >CO$_3$Mg$^+$ groups at pH < 8, but the trend of the decrease became more pronounced at pH > 8 owing to Reaction 7 moving to the right at high pH.

The calculated number of >CaOH$_2^+$ groups was largely insensitive to pH and salinity. The same trend was calculated by Brady et al. [83] who showed that the surface concentration of >CaOH$_2^+$ varied little with pH from 5.3 to 8. Increasing pH increased the calculated number of >CO$_3^-$ groups up to pH ~ 6; pH had less of an effect at higher pH. Fig. 5-5 shows that the effect of salinity on the number of >CO$_3^-$ groups was much greater than the effect of pH.
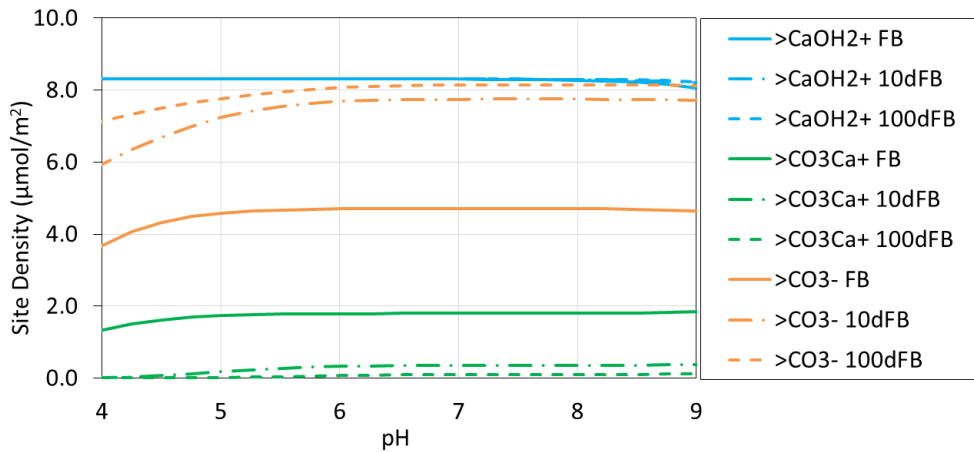
Fig. 5- 5 Site density of calcite surface groups versus pH and dilution.

5.3.2.3 Effect of Salinity on Electrostatic Bridges between Oil and Rock

Oil-wetness is thought to be correlated with the number of electrostatic bonds between oil and rock [83, 102]. We used our calculations above to quantify the number of electrostatic bonds, and wetting, by summing the number of oil/rock electrostatic pairs. For example, the concentration product $[>CO_3^-][-NH^+]$, is the bond product quantifying the number of electrostatic bonds between oil $-NH^+$ groups and calcite $>CO_3^-$ groups. Salinity level strongly affected the calculated individual bond products, and the bond product sum ($[>CO_3^-][-NH^+]$ + $[>CO_3^-][-COOCa^+]$ + $[>CaOH_2^+][-COO^-]$). For example, the bond product $[>CO_3^-][-NH^+]$ increased with decreasing salinity (Figure 6) because the calculated number of $>CO_3^-$ groups increases substantially with decreasing salinity despite $-NH^+$ decreasing with decreasing salinity level at pH < 5.5. The bond product $[>CO_3^-][-COOCa^+]$ increased with increasing salinity at pH < 7.3, but increased with salinity at pH > 7.3. Each change occurred because of the salinity and pH effects on the number of bond product surface species present at the oil and calcite interface. Given that the experimental oil used in this study had a low acid number, 0.50 mg KOH/g, compared to the base number, 1.02 mg KOH/g, a slight change of $[>CO_3^-][-COOCa^+]$ bond product did not affect the trend of variation of the bond product sum. The bond product of $[>CaOH_2^+][-COO^-]$ was tightly controlled by the variation of site density of $-COO^-$ owing to a negligible change of the $>CaOH_2^+$ along with pH and salinity level.

The bond product sum results show that lowering the salinity level triggered greater bond product sum, which varies at a different pH level. This implies that decreasing the salinity level triggers more oil-wet system at a given pH level, explaining why the chemical water effect was not always observed using the conventional dilution approach. The surface complexation modelling also correctly predicted the wetting characteristic of the oil/brine/calcite system in this study, showing that FB, 10dFB and 100dFB yielded a bond product sum of 29, 136 and 140 (μmol/m^2) ^{2} for the oil/brine/calcite system in line with the contact angel test (Fig. 5-2 and 5-3). Note: the great the bond product means more oil-wet system. However, our surface complexation modelling raises two questions: why does the aging process affect the wetting characteristics of the oil/brine/calcite system for the same bond product sum predicted by surface complexation modelling, and why did 100dFB exhibit a slight increase in bond product sum compared to 10dFB, but the contact angle increased tremendously? The potential explanation for the discrepancy is that:

In situ pHs during the contact angel test were on the low side due to deprotonation [61] (see Reaction 1-3 and 7-9). Therefore, the in situ pH likely shifted towards left-hand side, which in return gives a greater difference of bond product sum for the 10dFB and 100dFB.
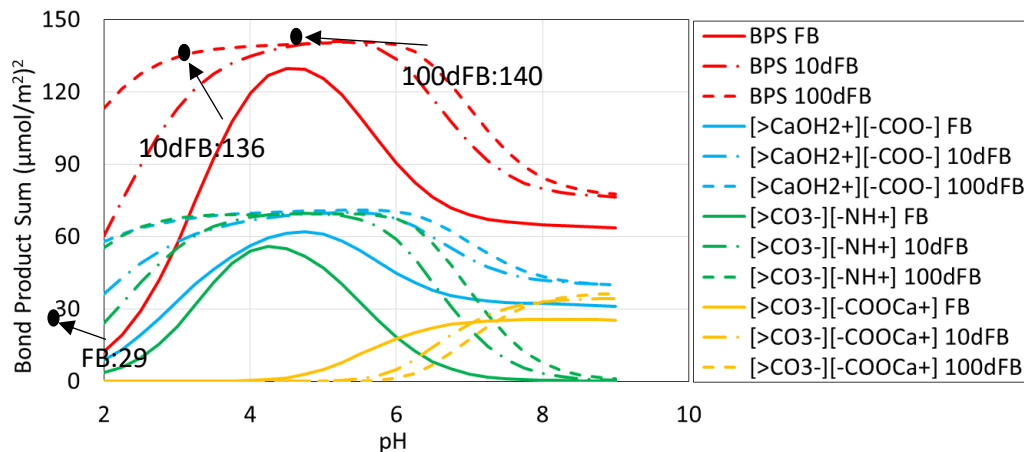
Fig. 5- 6 Bond product between the interface of oil/brines and brines/carbonate versus pH.

5.4 Implications

Wettability of the oil/brine/rock system is a fundamental petro-physical parameter, governing the subsurface multi-phase flow behaviour, thus oil recovery [185]. To better model and manage the chemical water flooding, we need to know more about the surface chemistry of the system [24]. We therefore used a combination of approaches (contact angel and surface complexation modelling) to identify how the water chemistry, pH, salinity level and the oil compositions (acid number and base number) control the wettability of the system. We also demonstrate that the surface complexation modelling contributes to a deeper understanding of the factors controlling the wettability of the oil/brine/rock system.

Our contact angle and surface complexation modelling both identify that water chemistry, salinity both affect the interaction of the oil/brine and brine/carbonate, yet pH level plays a fundamental role. This is because pH strongly affects surface chemistry of the oil/brine regardless of the magnitude of oil acid number and base number. For a high acid number oil, dilution likely causes chemical water EOR effect. This is because the functional chemical groups, [-COO$^-$] from oil surface and [>CO$_3$$^-$] from rock surface, increase with decreasing the salinity, which in return generating repulsive force, thus a more water-wet system. For a high base number oil, the functional chemical group of [-NH$^+$] from oil interface dominates the surface charge of oil interface at low pH level. Moreover, [>CO$_3$Ca$^+$] favours the high salinity level. Together, a high salinity level chemical water renders a water-wet system, which explains why the conventional dilution approach does not always yield an incremental oil recovery compare to formation brine.

We also confirm that chemical water can shift the wettability with an absence of SO$_4$$^{2-}$. In other words, the presence of SO$_4$$^{2-}$ in the aqueous ionic solution is not necessary to observe the chemical water EOR effect. This is not because SO$_4$$^{2-}$ does not affect the surface geochemical reaction, rather it is because the wettability of the system is governed by the water chemistry, pH, salinity level and the oil compositions (acid number and base number) as a whole instead of an individual ion. Therefore, we argue that surface chemical modelling should be applied to

screen the potential reservoir candidate, and provide a framework to design the injected water chemistry for a given oil/brine/rock system. Moreover, note that PHREEQC calculations (not described here) point to relatively little calcite dissolution during contact angle measurements in consistent with Nasralla et al. who did a more extensive studies disproving any calcite dissolution link to wettability [186, 187].

5.5 Conclusions

Our study demonstrates that the wetting characteristics of oil/brine/calcite system is strongly influenced by the surface chemistry of oil/brine and brine/calcite, which is governed by the composition of crude oil (e.g., acid number and base number), and water chemistry (pH, salinity level and the composition of the aqueous ionic solutions). We used a crude oil with base number (BN=1.02 mg KOH/g) and acid number (AN=0.5 mg KOH/g). We tested the contact angle on aged and un-aged carbonate rocks, with crude oil and aqueous ionic solutions under pressure of 2,000 psi and temperature of 60 $^{\circ}$C. We independently calculated the concentrations of charged surface species, and electrostatic bridges between the oil and the calcite.

Formation brine caused a strongly water-wet system (contact angle=35°), yet 100 times diluted formation brine led to a strong oil-wet system (contact angle=175°). The surface complexation modelling correctly predicted the trend of the wetting characteristic in the presence of various salinity level, showing that the bond product sum increased with decreasing salinity. Our results suggest that that at pH < 6, all other things being equal, conventional dilution approach likely prompts oil-wetness particularly for the crude oil with high base number. Dilution probably causes water wetness at pH > 7 for crude oils with high acid number. In this work, while we did not explicitly convert the bond product sum to the wettability of the system, or the oil recovery in an actual oil reservoir, bond product sum allows us to put boundaries on injected water chemistry controlled oil recovery, and quantify the key factors governing wetting characteristics of the oil/brine/calcite system.

Chapter 6. Insights into the Wettability Alteration of CO_2-Assisted EOR in Carbonate Reservoirs*

6.1 Abstract

Wettability of oil-brine-carbonate system is an important petro-physical parameter, which governs subsurface multiphase flow and residual oil saturation. CO_2-assisted EOR techniques have been identified as cost-effective and environmentally friendly means to unlock remaining hydrocarbon resources from carbonate reservoirs. While wettability alteration appears to be one of the main mechanisms during CO_2-assisted EOR implementation, the controlling factor(s) of wettability alteration at molecular level remains unclear. We thus hypothesized that excess of H^+ as a result of water uptake of CO_2 increases hydrophilicity of oil-brine-carbonate systems. More specifically, the surface charge properties will be alterated to more positive due to the increase of H^+ in the brine. To test this hypothesis, we measured oil contact angles on calcite surfaces in the presence of non-carbonated brine, carbonated brine, and acidic brine (pH=3). We also performed surface complexation modelling to examine how the surface chemistry controls over wettability of oil/brine/carbonate system using PHREEQC. Our contact angle results show that both carbonated brine and acidic brine gave a contact angle of 24° and 22°, respectively, while non-carbonated brine gives a contact angle of 73° in 1 mol/L $CaCl_2$ brines. Same trend was also observed in synthesized formation brine, showing that non-carbonated formation brine yielded a contact angle of 69° while both acidic formation brine and carbonated formation brine gave a contact angle of 37°. Experimental results show that both carbonated brine, and acidic brine significantly decreased contact angle compared to non-carbonated brine, suggesting a strong water-wet system. Surface complexation modelling shows that for both carbonated water and acidic water, $>CaOH_2^+$ dominates surface charges at calcite surfaces, and $-NH^+$ governs surface charges on oil surfaces. Together, these two processes increase repulsive forces thus hydrophilicity. Our study sheds light on the significant influence of excess H^+ due to water uptake of CO_2 on oil-brine-carbonate system wettability thus enhancing hydrocarbon recovery in carbonate reservoirs.

6.2 Introduction

As global energy demand continues to increase, the petroleum industry is constantly striving to develop economically viable techniques to maximize oil recovery in carbonate reservoirs [97]. This is largely because carbonates rock host most of the world's oil reserves (> 60 %) [170]. However, the conventional EOR technique can only recover up to 40% of origin oil in place (OOIP) [188], whereas considerable high capital investment would be required for additional oil recovered by chemical-EOR method (e.g., polymer flooding, surfactant flooding, and alkaline flooding, etc.). Therefore, water and CO_2-assisted EOR techniques (e.g., low salinity water flooding [13, 83, 134, 155, 189], carbonated water flooding [190-193], etc.) have emerged to boost oil recovery. Besides, carbonated water injection can not only enhance oil recovery, but also helps to reduce anthropogenic emission of CO_2, mitigating greenhouse effect [194, 195].

Carbonated water flooding yields considerable incremental oil recovery than conventional water flooding [87, 196-200]. For example, Mehran et al. [198] showed that more than 10% of OOIP was achieved by injecting carbonated water. Nader et al. [87] injected carbonated water at secondary mode under various operational pressure, and achieved 80% of OOIP. Apart from coreflooding experiments, residual oil saturation reduction was also observed at pore-scale by carbonated brine injection. For example, Alizadeh et al. [197] observed 40.7% of

incremental oil recovery by injecting carbonated brine at tertiary mode from micro-scale core-flooding experiments.

A few mechanisms have been proposed to decipher the controlling factor of carbonated water flooding, including (a) promote oil-swelling [201], (b) reduce oil viscosity [201], (c) mitigate gravity segregation as a result of reducing the density difference between oil and water [202], (d) lower oil interfacial tension [203], (e) gas exsolution [193], (f) new phase generation between oil/water [94, 204]. Although the above mechanisms partly account for the incremental oil recovery achieved by carbonated water, wettability alteration appears to be an important mechanism behind carbonated water injection. For example, Teklu et al. [92] measured oil contact angle on carbonate rocks in the presence of seawater and carbonated seawater. They observed that seawater without carbonation gave contact angle of 116.6°, whereas carbonated seawater gave contact angle of 40.8°. Fjelde et al. [205] conducted spontaneous imbibition and coreflooding experiments using chalk plugs, and examined the water-wet area before and after CO_2-WAG process using sulphate wettability test They observed that the water-wet area increases up to 3 times after CO_2-WAG process. Sohrabi et al. [192] also revealed wettability alteration during carbonated water injection during micromodel experiments.

Previous observations over wettability alteration call for a closer examination of surface chemistry control over wettability of oil-carbonated brine-carbonate systems at a molecular level. We thus hypothesized that excess H^+ as a result of CO_2 dissolution increases hydrophilicity of oil-brine-carbonate systems. To test this hypothesis, we measured oil contact angles on calcite surfaces in the presence of non-carbonated brine, carbonated brine, and acidic brine (pH=3). We also performed surface complexation modelling to examine the surface chemistry controls over wettability of oil/brine/carbonate system using PHREEQC version 3.30 [101].

6.3 Experimental procedures

6.3.1 Oil

An oil (acid number = 1.7, base number = 1.2 mg KOH/g) was used to test the contact angles in the presence of non-carbonated brine, acidic water (pH=3), and carbonated brine. Gas chromatograph mass spectrometer (GC-MS) was used to examine the oil properties, showing that the oil was comprised of asphaltenes (37.1 wt %), naphthenes (26.3 wt %), wax (3.8 wt %) and sulphur (3.9 wt %) with density of 0.89 g/cm^3 at 20°C. Our previous work [111, 134, 153] show that asphaltenes adsorption is reversible on calcite surface.

6.3.2 Brine preparation

Calcite chloride ($CaCl_2$) with concentration of 1 mol/L was used. Contact angles in the three different aqueous solutions were measured, including non-carbonated brine, acidic water, and carbonated brine. Note that non-carbonated brine means 1 mol/L $CaCl_2$ at pH=7; acidic water means 1 mol/L $CaCl_2$ at pH=3 (pH adjusted by adding HCl); and carbonated water which was obtained with water ($CaCl_2$, 1 mol/L) uptake of CO_2 at temperature of 25 ^{o}C and pressure of 3000 psi. It is estimated that the concentration of CO_2 is 3.65mol/L based on PHREEQC equilibrium calculation at experimental pressure and temperature.

To prepare carbonated brines, an aqueous ionic solution (1.0 mol/L $CaCl_2$) was prepared and loaded in a reactor (AMAR Autoclaves/Reactors/Pressure Vessels) as shown in Fig. 6-1, Carbon dioxide (CO_2) was injected and pressurized in the reactor through a syringe pump (Vinci BFSP 500-15) with an aid of an air compressor (AFP P100084 Gas Booster). The brine and CO_2 are kept under 3000 psi in the reactor chamber at 25°C for nearly 12 hours until the

equilibrium is reached (when pressure is stable). After the equilibration, Valve 1 is opened to transfer carbonated brine to the accumulator. The pressure of accumulator is controlled by a back pressure regulator under 3000 psi. Acidic brine is obtained by adding HCl (analytical grade, 99.95%) to non-carbonated water (1.0 mol/L $CaCl_2$) until pH reached to 3, which is monitored by a pH meter (Checker pH tester HI98103) at 25°C.
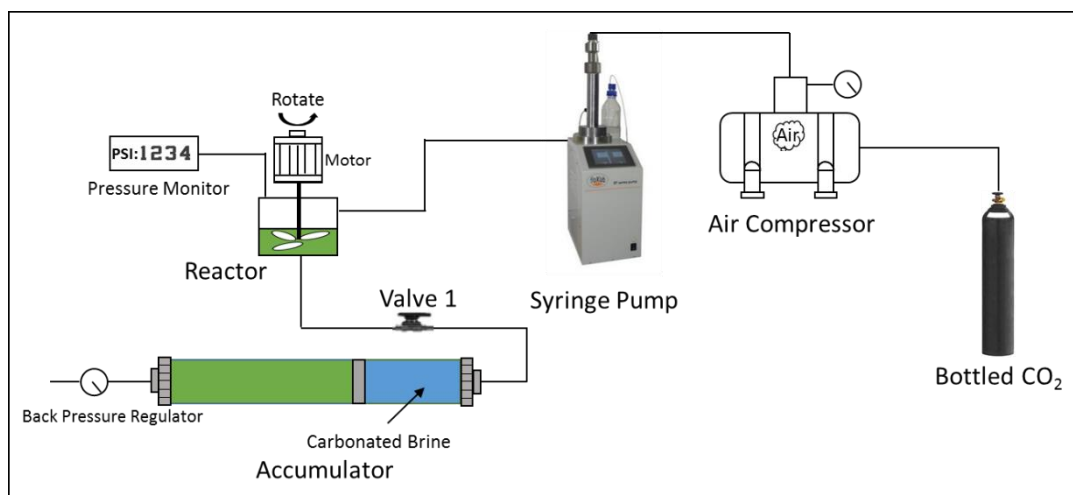
Fig. 6- 1 Schematic diagram of carbonated water preparation

6.3.3 Calcite substrates

Calcite minerals (Iceland Spar, as shown in Fig. 5-2) supplied by Ward's Science are used in our contact angle measurements. Our X-Ray Diffraction (XRD) test shows that the composition of substrates were 100% calcite. Prior to experiments, substrates are cleaned with solvents (e.g., toluene and methanol) to remove any traces of organic and inorganic contaminants. Substrates were then rinsed with equilibrated deionised water to prevent undesired dissolution and dried in an oven at temperature of 60 °C.

6.3.4 Experimental procedure

The contact angle measurements were conducted using Vinci IFT 700 as shown in Fig. 1 in Sari et al. [65]. However, to conduct contact angle measurements in the presence of carbonated brine, we modified the setup as shown in Fig. 6-3. A substrate (after solvents cleaning, dried in an oven at 60 °C and cool down at 25 °C) was mounted inside of the high-pressure and high-temperature (HPHT) cell, and placed under vacuum for 12 hours until the pressure inside of the cell dropped to 0.1 bar. During vacuuming process, valve 3 and 4 were kept open to vacuum the system while all other valves were closed.

For contact angle tests in carbonated water, the valve 4 was closed but keeping the valve 5 open to pressurize the system with N_2 to 3000 psi. After pressurization, the cell was disconnected from vacuum pump and N_2 source. The syringe pump was then set to constant pressure model (3500psi) to introduce the carbonated water into the cell. Meanwhile, the valve 3 was carefully opened to release the N_2 until the cell is full of carbonated water. The valve 1 kept closed after the cell is filled with carbonated brine. Then the cell was left for half an hour. Subsequently, a drop of crude oil was introduced by the hand pump onto the substrate from the bottom of the cell through a capillary needle (0.64 mm diameter). Afterwards, the contact angle of oil on the substrate was monitored till reaching the equilibrium over two hours.

For non-carbonated brine and acidic brine, the brine was injected directly after the system was vacuumed without pressurizing the system with N_2. After the cell was pressurized to 3000 psi with non-carbonated brine or acidic brine, the syringe pump is stopped, a drop of crude oil was introduced onto the substrate from a hand pump. For all contact angle tests, three droplets were introduced to minimize the system error and avoid environmental disturbance.

pH measurements were performed to track the pH variation during the contact angle measurements. A substrate was placed in a beaker with a bulk volume (55 ml) of acidic brine (1mol/L $CaCl_2$, pH=3). The substrate dimension is shown in the Fig. 6-2. The beaker was sealed with plastic wrapper to avoid solution evaporation, whereas it was punctured to release the accumulated CO_2 inside of the beaker. The brine was stirred to guarantee homogeneity for pH measurements. Each pH was measured twice by the pH meter to avoid experimental errors and environmental disturbance.
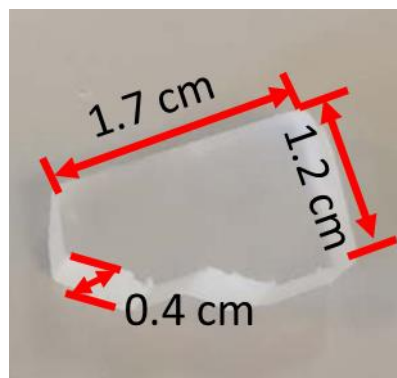
Fig. 6- 2 The calcite substrate was used for pH measurements. Note that this was not the same substrate for contact angle measurements, but the size and the dimension of the substrate is comparable to the substrate for contact angle measurements.
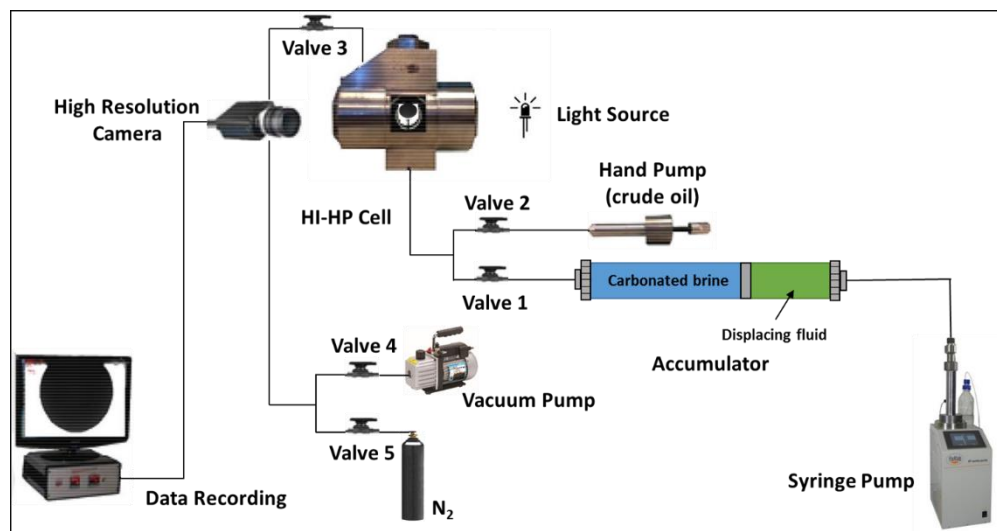
Fig. 6- 3 Schematic diagram of contact angle measurements.

6.4 Calcite surface reactivity

In our geochemical models, we did not consider interactions between non-polar oil and calcite surfaces, e.g., hydrogen bonding, Van der Waals interaction, and ligand bridging, etc. [17]. Instead, we assume that acidic and amine functional groups governs the electrostatic surface species at oil surfaces, which dominates the adhesion force between oil and rock surfaces [56-58]. We believe that this assumption is reasonable because water chemistry of water-assisted EOR (e.g., carbonated water and low salinity water) governs the interaction of polar part and rock surfaces [206-208], but the interaction between non-polar oil and calcite surfaces plays a secondary effect in water assisted EOR [13, 209].

A surface complexation model developed by Brady et al. [83, 99] was applied to identify the individual charged species that give rise to the variation of the site density at the interface of oil/brine and brine/calcite. In the surface complexation model, the calcite surface area was assumed as 0.11 m^2/g with site density of 5 sites/nm^2 [84]. The chemical reactions on the surface of calcite can be described by the following reactions (Table 6-1). The surface species were calculated by PHREEQC version 3.30 [101].

Table 6- 1 Aqueous speciation reactions [101] and Surface complexation model input parameters [83, 174, 183, 184]

Reaction location	Chemical Reaction	Log_{10} K_{25oC}
Brine	CO_2 (g) = CO_2 (aq)	-1.47
	$CO_2(aq) + H_2O = H_2CO_3$	-2.59
	$H_2CO_3 = H^+ + HCO_3^-$	-3.76
	$HCO_3^- = H^+ + CO_3^{2-}$	-10.33
	$CaCO_3(s) = Ca^{2+} + CO_3^{2-}$	-8.48
At the interface of oil/brine	$-NH^+ = -N + H^+$	-6.0
	$-COOH = -COO^- + H^+$	-5.0
	$-COOH + Ca^{2+} = -COOCa^+ + H^+$	-3.8
At the interface of brine/calcite	$>CaOH + H^+ = >CaOH_2^+$	11.85
	$>CaOH + HCO_3^- = >CaCO_3^- + H_2O$	5.8
	$>CaOH_2^+ + SO_4^{2-} = >CaSO_4^- + H_2O$	2.1
	$>CO_3H = >CO_3^- + H^+$	-5.1
	$>CO_3H + Ca^{2+} = >CO_3 Ca^+ + H^+$	-2.6

Where ">" represents a negatively charged site on the carbonate surface and "-" represents the carbon chain of oil. It is worth noting that we assumed that calcite dissolution and pH change during the contact angle tests were negligible. We verified the assumption by performing pH measurement.

6.5 Results and Discussion

6.5.1 Effect of non-carbonated water, carbonated water and acidic water on wettability

Both acidic water and carbonated water increase water-wetness compared to non-carbonated water, implying that lowering pH likely shifts system wettability towards more water-wet. For example, non-carbonated brine gives a contact angle of 73°. Yet, the acidic water and carbonated water give contact angle of 22° and 24° respectively (Fig. 6-4). Similar experimental results were observed by Teklu et al. [92], who reported that carbonated

seawater (pH=5.5 at atmospheric condition) gives a contact angle of 36.1°, whereas seawater (pH=6.6) gives a contact angle of 133.6°. Note that the carbonated seawater used in Teklu et al.'s [92] contact angle experiments were depressurized effluent from carbonated seawater flooding at pressure of 2500 psi. Therefore, more divalent cations, e.g., Ca^{2+} and Mg^{2+} would appear in the carbonated seawater effluent due to the calcite dissolution thus increasing $>CO_3Ca^+$, and $>CO_3Mg^+$ at calcite surfaces [83, 210], and $>COOCa^+$ at oil surfaces during contact angle tests [83, 134]. We believe that this surface chemistry variation contributes to the strongly water-wet system apart from pH decreasing from 6.6 to 5.5.

	Non-Carbonated water	Acidic water	Carbonated water
Contact Angle	$\theta = 73°$	$\theta = 22°$	$\theta = 24°$
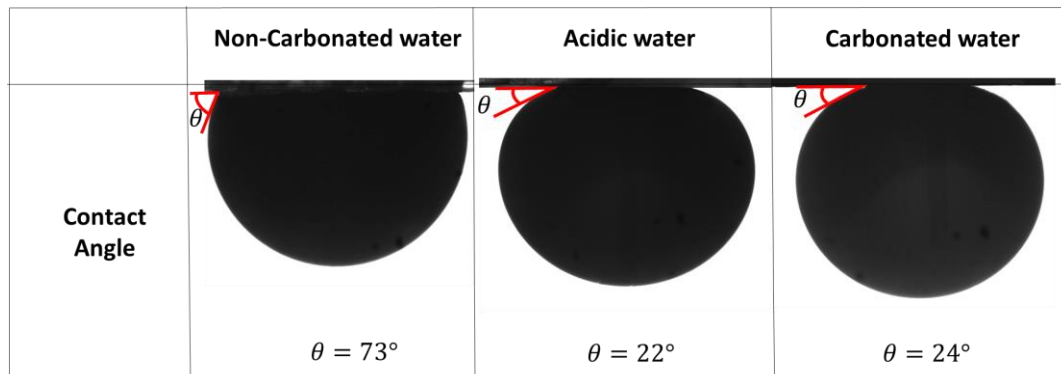
Fig. 6- 4 The contact angle in different brines (The contact angles were measured multiple times. The typical values are selected to present here)

To substantiate that pH did not change dramatically as a result of calcite dissolution while measuring contact angle in the presence of acidic water, we indeed recorded the pH variation with time at ambient condition using substrate in same dimension of substrate for contact angle measurements. pH test showed pH value changed from 3.0 to 6.18 with 72 hours for acid water (Figure 5). Within the first 12h, the pH increased from 3.0 to 4.4. The final recorded pH value was 6.18, which is well fitted to results predicted by PHREEQC batch reaction calculation (6.19). The reason for the slow pH increase is largely because of small specific area of the calcite substrate [153] . It is worth noting that the *in-situ* pH would be lower for carbonated brine than the recorded pH because of a sealed system, where the generated CO_2 can't be released [132]. Therefore, we can reasonably assume that the difference of *in-situ* pH in the presence of acidic water and carbonated water is negligible during tests period (10 hours).
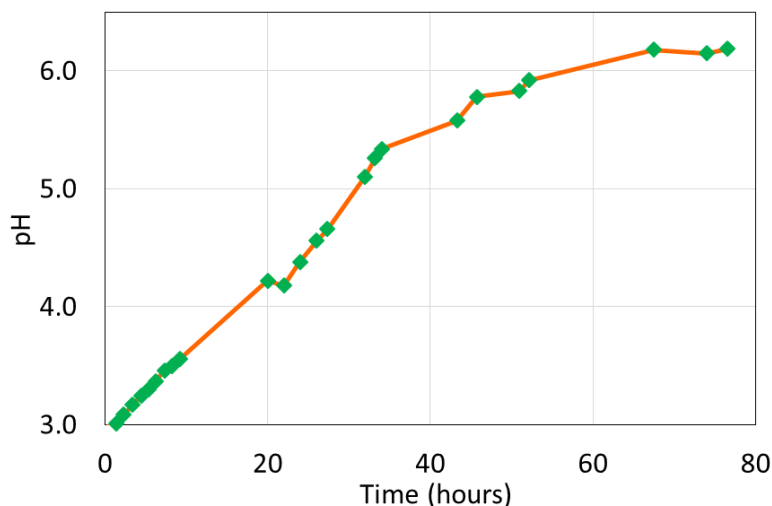
Fig. 6- 5 pH changes of acidic 1mol/L $CaCl_2$ brine with bulk calcite submerged

Table 6- 2 The pH of the three brines.

	1 mol/L $CaCl_2$ Brine	Carbonated Brine (PHREEQC calculation)	Acidic Brine (pH at 12 hours)
pH	7	4.05	4.4

Note that non-carbonated brine refers to 1 mol/L $CaCl_2$ at pH=7; acidic brine refers to 1 mol/L $CaCl_2$ at pH=3; and carbonated brine with a PHREEQC estimated pH of 4.05 refers to brine ($CaCl_2$, 1 mol/L) uptake of CO_2 at temperature of 25 ℃ and pressure of 3000 psi.

6.5.2 Calcite/Brine surface species

To understand how surface chemistry controls over wettability alteration of oil/brine/calcite. We calculated surface species on calcite in the presence of non-carbonated brine and carbonated brine (Fig. 6-6). Our results show that surface species of calcite/brine surface change dramatically with water chemistry and pH. For non-carbonated water, $>CaOH_2^+$ site abundance remains almost constant as pH increases from 2 to 8 in line with Chen et al. [134] and Brady et al. [83]. The number of $>CaOH_2^+$ drops from 5.0 µmol/m^2 to 4.2 µmol/m^2 when pH increase to 10. Note that the presence of sulfate (SO_4^{2-}) can significantly affect the number of $>CaOH_2^+$ with increasing pH [211], thus oil/brine/calcite system wettability. The number of $>CaCO_3^-$ (a pair species of $>CaOH^{2+}$), slightly increases with increasing pH as pH is greater than 5 due to calcite dissolution, which introduces CO_3^{2-} and HCO_3^{2-}. This is confirmed by the slight increase of $>CO_3Ca^+$ with increasing pH. The number of $>CO_3^-$, a pair with $>CO_3Ca^+$, gradually drops as pH is greater than 5, which is also attributed to the increase of $>CO_3Ca^+$. It is worth noting that the concentration of $>CaOH_2^+$ is almost 5 times higher than $>CaCO_3^-$ because of larger equilibrium constant for generation of $>CaOH_2^+$ than $>CaCO_3^-$ (see Table 6-1).

Calcite surface species would be different in the carbonated brine. For carbonated brine, water uptake of CO_2 enables $>CaOH_2^+$ to drop from 4.6 to almost 0 µmol/m^2 when pH increases from 4 to 10. It is worth noting that the carbonated and non-carbonated water at same pH have different water chemistry because dissolution of CO_2 generates HCO_3^-. Therefore, in carbonated water, $>CaOH_2^+$ decreases sharply with increasing pH due to generation of HCO_3^-

in the brine as shown in Fig. 6-2. In carbonated water, $>CO_3Ca^+$ increases sharply with increasing pH compared to non-carbonated water due to calcite dissolution as a result of the water uptake of CO_2 (Reaction 8). In return, the number of $>CO_3^{2-}$ (a pair of $>CO_3Ca^+$) becomes lower in carbonated water compared to non-carbonated water.

It has been identified that SO_4^{2-} can increase the number of surface species ($>CaSO_4^-$) at calcite surfaces thus increasing hydrophilicity duing low salinity water flooding due to anhydrite dissolution [175, 212]. Our calcite surface species calculation reveals that excess H^+ can also significantly increase system hydrophilicity as a result of water uptake of CO_2. This is because low pH can decrease the number of $>CO_3^-$ at calcite surface, and increase $-NH^+$ at oil surfaces which in return triggers repulsion force and less number of electrostatic bridges between oil and calcite surfaces [83, 134]. Therefore, lowering pH by adding HCl may serve as carbonated water flooding, but a more quantitative work remains to be made to examine the effect calcite dissolution on reservoir integrity.
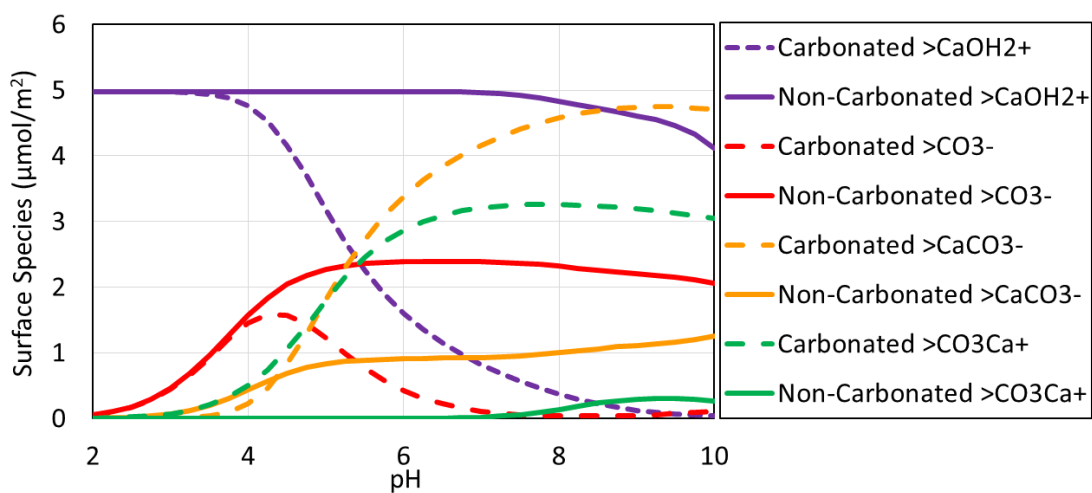
Fig. 6- 6 Calcite/Brine surface species for carbonated brine and non-carbonated brine

6.5.3 Oil/Brine surface species

While the number $-NH^+$ change is negligible in the presence of non-carbonated and carbonated brine at given pH, pH shift significantly affects $-NH^+$. Fig. 6-7 shows that $-NH^+$ decreases dramatically with increasing pH due to the reaction moving towards right-hand side in line with Brady et al. [60, 102]. For non-carbonated brine, $-COO^-$ increase at low pH (pH<4.6), then decreases with further increasing pH to 10 due to the Reaction 2 moving towards right-hand side. Meanwhile, $-COOCa^+$ (a pair of $-COO^-$) increases with increasing pH. $-COOCa^+$ and $-COO^-$ in carbonated brine exhibit similarly to non-carbonated brine except at pH=7.5. After pH reaching 7.5, $-COOCa^+$ decreases, but $-COO^-$ increases with further increasing pH. This is due to the deposition of $CaCO_3$ at pH above 7.5. At high pH, HCO_3^- will be converted to CO_3^{2-} thus precipitating as $CaCO_3$, which in return decreasing $-COOCa^+$ and increasing $-COO^-$ at oil surfaces. Note that $-COOCa^+$ and $-COO^-$ are pair surface species on oil surfaces [102].
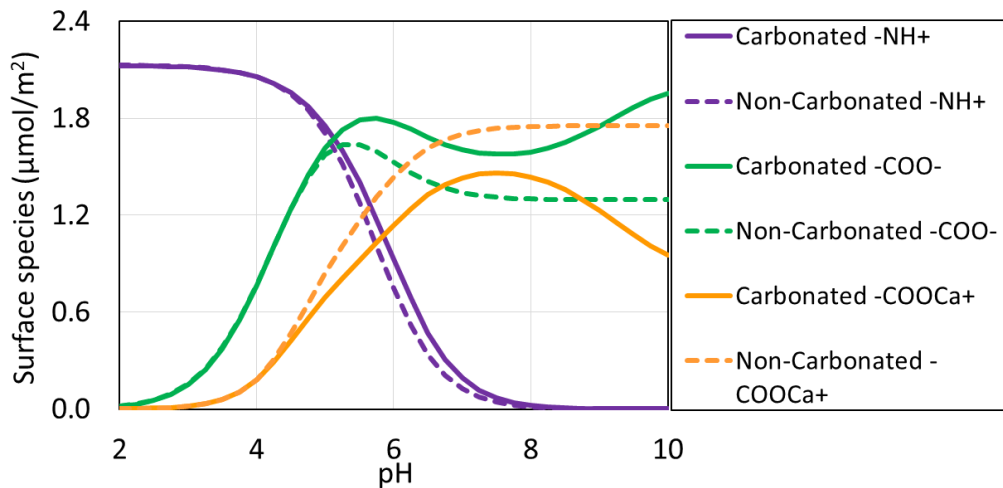
Fig. 6- 7 Oil/Brine surface species for carbonated brine and non-carbonated brine. For polarized oil, $-NH^+$, $-COO^-$, and $–COOCa^+$ are the three main surface species at oil surfaces [60, 102]. We modelled the number of surface species change with non-carbonated brine and carbonated brine with a range of pH.

6.5.4 Bond Product Sum

To quantify the adhesion of oil-calcite, we used the concept of Bond Product Sum (BPS) proposed by Brady et al. [83, 213]. BPS was proposed to quantify the electrostatic bonding between oppositely charged oil and calcite surface pair species, $-NH^+$ and $>CO_3^-$, $-NH^+$ and $>CaCO_3^-$, $-COOCa^+$ and $>CO_3^-$, $-COOCa^+$ and $>CaCO_3^-$, $-COO^-$ and $>CaOH_2^+$, and $-COO^-$ and $>CO_3Ca^+$. A quantitative measure of electrostatic attraction can be mathematical expressed as $[-NH^+] [>CO_3^-] + [-NH^+] [>CaCO_3^-] + [-COOCa^+] [>CO_3^-] + [-COOCa^+] [>CaCO_3^-] + [-COO^-] [>CaOH_2^+] + [-COO^-] [>CO_3Ca^+]$; where bracketed terms are calculated surface concentrations (mol/m^2).

Our results show that BPS varies with pH for both non-carbonated brine and carbonated brine. For carbonated water, increasing pH from 2 to 5.5 increases BPS from 0.2 to 15.6 $(μmol/m^2)^2$. Afterwards, BPS decreases slightly with further increasing pH from 5.5 to 10. Similar trend of BPS with pH is also observed in the presence of Non-carbonated brine. Our results shows that a relatively high BPS appears at pH in a range of 5.5 to 6.5, suggesting strong adhesion of oil-calcite at reservoir conditions (Fig. 6-8). However, the strong adhesion decreases with further increasing pH or decreasing pH. This supports the potential of low salinity EOR-Effect because low salinity water usually increases pH from 1 to 3 thus decreasing BPS [83]. Moreover, Fig. 6-8 also supports carbonated water flooding as a result of water uptake of CO_2, showing that further decreasing pH indeed decreases BPS thus increasing water-wetness and incremental oil recovery. Moreover, Figure 8 shows that acidic water may act as same as carbonated brine at low pH because the BPS for both brines are almost overlapped, suggesting the same adhesion force between oil-calcite. This means that manually manipulating injected brine pH likely reduces residual oil saturation due to wettability alteration. This is also consistent with our previous study [65], showing that high salinity brine (252,244 ppm without carbonation) at low pH (2.55) triggers a strongly water-wet system (oil/brine/carbonate). This could be a good news for fields where are lack of CO_2 resources although calcite dissolution effect on petro-physical properties may need to be evaluated. Besides, for carbonate reservoirs with huge amount of anhydrite, acidic water or carbonated water flooding may also trigger anhydrite dissolution thus increasing SO_4^{2-} in aqueous phase

[214], which in return leads to the increase of $>CaSO_4^-$ at calcite surfaces [83, 210] (also see Reaction 6 in Table 6-1). Consequently, calcite surfaces perhaps become less positive charges, thereby less water-wet. We believe that further investigation over the effect of calcite and anhydrite dissolution on surface chemistry is required for a given reservoir.
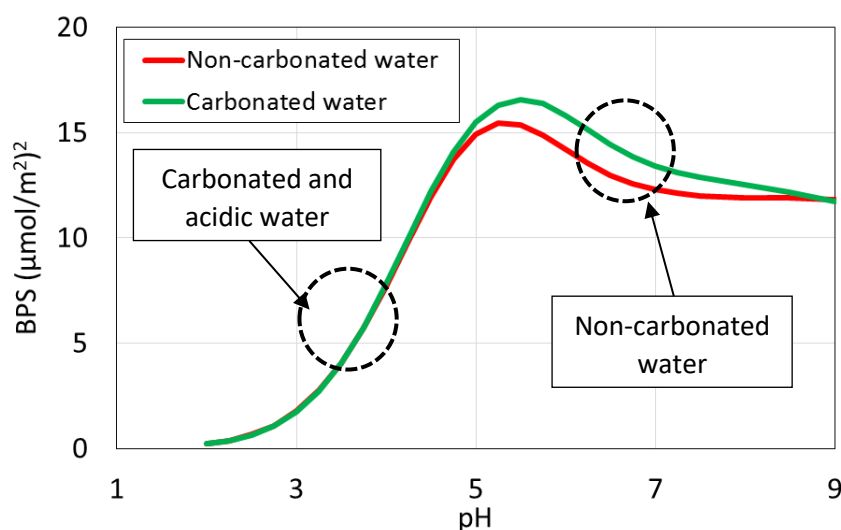
Fig. 6- 8 BPS for different brine with various pH

6.5.5 Confirmation of results under *in-situ* condition

To further test our hypothesis, we conducted contact angle measurements using porous carbonate reservoir rocks (minerology as shown in Table 6-3) in the presence of formation brine (composition as shown in Table 6-4) and another crude oil (AN=4.0 mg/g, BN=1.3 mg/g, dengsity = 0.85 g/cm^3). The same procedure was followed to obtain carbonated formation brine and acidic formation brine. During the measurement, all the pressure and temperature were kept the same. The concentration of CO_2 in formation brine is 4.04 mol/L with a pH of 4.39. Our results show that acidic formation brine and carbonated formation brine give a contact angle of 37°, whereas non-carbonated brine gives a contact angle of 69° (Fig. 6-9). The results further confirm that the results derived in mono component $CaCl_2$ brine on Iceland Spar pure mineral. It shows that excess of H^+ in the aqueous ionic solution increases hydrophilicity of oil-brine-carbonate.

Table 6- 3 XRD minerology composition of formation rock [65]

Minerology	Weight Percentage
Calcite	98.1%
Quartz	0.7%
Ankerite	1.2%

Table 6- 4 Composition of formation brines

Brines	K^+	Na^+	Ca^{2+}	Mg^{2+}	Cl^-	HCO_3^-	SO_4^{2-}	TDS/ppm
Formation brine/FB	1152.0	47520.0	5840.0	771.0	86500.0	586.7	61.5	142431

To examine the potential impact of asphaltene precipitation and soaking time of carbonated water on contact angle, all the tests were performed with a soaking time up to 100 hours. We

observed a minor contact angle variation during the test (less than 3° increase), implying that asphaltene precipitation and soaking time during the contact angle measurements play a negligible role in recorded contact angle.

	Non-carbonated water	Acidic water	Carbonated water
Contact Angle	$\theta = 69°$	$\theta = 37°$	$\theta = 37°$
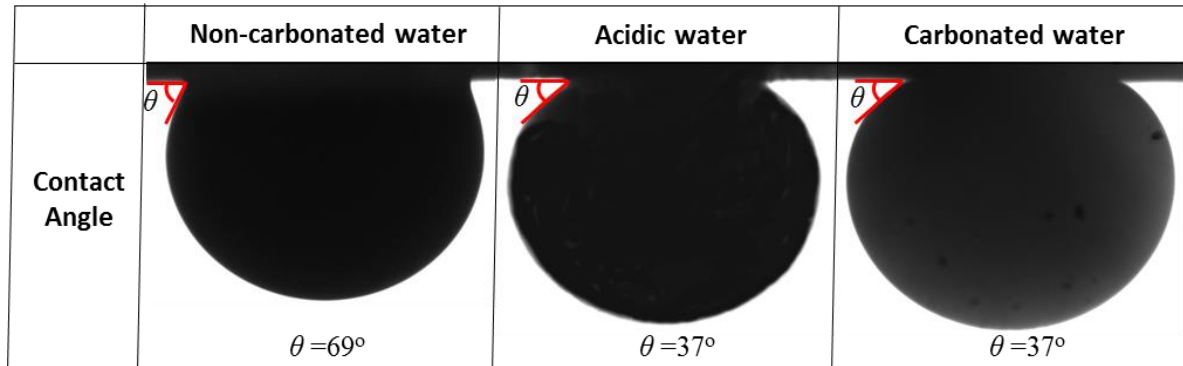
Fig. 6- 9 Wettability changes in formation brine, acidic formation brine and carbonated formation brine (The volume of the drop size is in a range of 17 mml to 19 mml)

6.6 Implications and Conclusions

Our contact angle results show that both carbonated water and acidic water can significantly increase water-wetness. Carbonated water shifted contact angle from 73° to 24° in line with Teklu et al.[92, 215] and Seyyedi et al. [95]. Also, acidic water shifted contract angle from 73° to 22° in line with our previous study [211]. Our surface complexation modelling predicts the same trend as the experiments, showing that $>CaOH_2^+$ (at calcite surfaces) and $-NH^+$ (at oil surfaces) dominate surface charges at low pH thus decreasing the bonds between oil-calcite. We therefore argue that H^+ adsorption due to water uptake of CO_2 on the interface of oil/brine and brine/carbonate governs wettability alteration during CO_2-assisted EOR techniques. Our study sheds light on the significant influence of excess H^+ due to water uptake of CO_2 on oil-brine-carbonate system wettability thus enhancing hydrocarbon recovery in carbonate reservoirs.

Chapter 7. Electrostatic Origins of CO₂-Increased Water Wetness in Carbonate Reservoirs*

7.1 Abstract

Injecting CO_2 into oil reservoirs appears to be cost-effective and environmentally friendly due to decreasing the use of toxic chemicals and cutting back on the greenhouse gas emission released. However, there is a pressing need for new algorithms to characterize oil/brine/rock system wettability, thus better predict and manage CO_2 geological storage and enhanced oil recovery in oil reservoirs. We coupled surface complexation/CO_2 and calcite dissolution model, and accurately predicted measured oil-on-calcite contact angles in NaCl and $CaCl_2$ solutions with and without CO_2. Contact angles decreased in carbonated water indicating increased water-wetness under carbonation. Lowered salinity increased water-wetness as did Ca^{2+}. Water-wetness correlates with independently calculated oil-calcite electrostatic bridging. The link between the two may be used to better implement CO_2 EOR in fields. Our new algorithm provide insights into the transport, the clean-up of the hydrocarbon contaminants in soils.

7.2 Introduction

Oil will be an important energy source for the rest of the 21st century [96] and carbonate reservoirs host most of the world's oil (> 60 %) [170]. However, the recovery factor is low (<40%) [216], so there is enormous motivation to improve recovery cost-effectively, and with environmentally friendly techniques if possible. CO_2 EOR is attractive because it produces more oil without the expense of toxic chemicals (e.g., polymers, surfactants, or additives) while sequestering residual CO_2 in the subsurface. CO_2 EOR techniques include miscible [217] and immiscible continuous injection [218, 219], carbonated water flooding [191], huff and puff injection (injecting CO_2 in a single well and producing from the well after CO_2 equilibration with the crude oil) [220, 221], and water-alternating-CO_2 injection [92, 222, 223]. CO_2 techniques work through some combination of immiscible drive, first contact miscible drive, vaporizing-gas drive, condensing-gas drive, and vaporizing-condensing gas drive, and multiple-contact miscible drive. At the microscopic level, these processes can: promote oil-swelling, reduce oil viscosity, mitigate gravity segregation by reducing the density difference between oil and water, and, lower oil interfacial tension, all of which can increase oil recovery. The net impact of CO_2 addition can be quite large, amounting to recovery of an extra 4-15 % of the original oil in place in conventional reservoirs [224]. Moreover, CO_2 huff-n-puff can achieve 14 % additional oil recovery from unconventional reservoirs [225]. While much is known about the effect of CO_2 on oil fluid properties, the mechanistic links between CO_2 and oil adhesion, that is reservoir wettability, is unclear. Wettability helps determine oil recovery by controlling reservoir relative permeabilities, capillary pressure, and residual saturations.

Teklu et al. [92] showed that dissolving CO_2 into seawater decreases oil contact angles on calcite, thus increasing water-wetness. Decreased salinity also decreases contact angles. Teklu et al. [92] noted several potential explanations for their contact angle trends and called for a closer examination of the surface controls over wettability alteration. Venkatraman et al. [226] used Gibbs free-energy function to integrate phase-behaviour computations and geochemical reactions to find equilibrium composition, but quantitative work remains to be made to understand how dissolved CO_2 governs oil-brine-calcite interaction, thus wettability. Here we constrain surface chemical controls over wettability in carbonate reservoirs undergoing CO_2 EOR by interpreting new oil-on-calcite contact angles in the presence of

model reservoir brines containing NaCl and $CaCl_2$ using a coupled surface complexation/CO_2 and mineral dissolution model.

7.3 Results

Figure 1 shows oil-on-calcite contact angles measured at 25°C and 3000 psi pressure in model brines under carbonated and non-carbonated conditions. Carbonated water lowers contact angles and produces a strongly water-wet system regardless of salinity and ion type compared to non-carbonated water. For example, non-carbonated 1 mol/L NaCl yielded a contact angle of 120°, meaning an oil-wet system. However, carbonated 1 mol/L NaCl gave a contact angle of 39°, meaning a strongly water-wet system. Similarly, Teklu et al. [92] observed a contact angle shift from 116.6 - 133.6° (non-carbonated seawater, pH=6.6) to 36.1 - 40.8° (carbonated seawater, pH=5.5 at atmospheric condition). A secondary effect of lowered salinity decreasing contact angles and moving the system towards water wetness is also seen in Fig. 7-1, and was observed before by Teklu et al. [92]. Divalent cations (Ca^{2+}) gave a lower contact angle compared to monovalent cations (Na^+) regardless of concentration.

	1 mol/L NaCl	0.01 mol/L NaCl	1 mol/L CaCl$_2$	0.01 mol/L CaCl$_2$
Non-carbonated Brine	$\theta = 120°$	$\theta = 55°$	$\theta = 73°$	$\theta = 43°$
Carbonated Brine	$\theta = 39°$	$\theta = 23°$	$\theta = 24°$	$\theta = 23°$
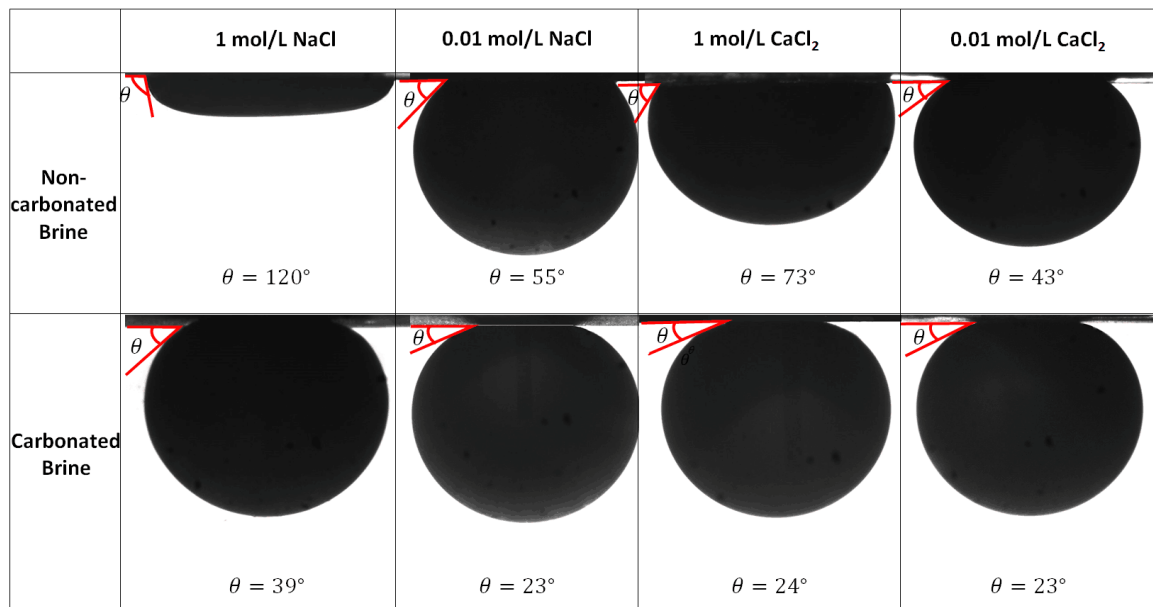
Fig. 7- 1 Oil-on-calcite contact angles in the presence of carbonated and non-carbonated brines.

To understand how carbonation increases water-wetness, we develop a geochemical model that couples CO_2 dissolution, mineral dissolution, and oil and calcite surface chemistry (Table 7-1). CO_2 and calcite dissolution into brines is calculated by a standard equilibrium approach. Oil surface species are assumed to be $-NH^+$, $-COO^-$ and $-COOCa^+$ [60, 83, 102], polar surface groups expressed at, and attached to, the oil-water interface. Calcite surface species are assumed to be $>CO_3^-$, $>CaCO_3^-$, $>CaOH_2^+$, and $>CO_3Ca^+$ [67, 83, 134, 210] (Fig. 7-2); where ">" denotes a calcite surface species. The primary electrostatic bridges between oppositely charged oil and calcite surface species are then the pairs, $-NH^+$ and $>CO_3^-$, $-NH^+$ and $>CaCO_3^-$, $-COOCa^+$ and $>CO_3^-$, $-COOCa^+$ and $>CaCO_3^-$, $-COO^-$ and $>CaOH_2^+$, and $-COO^-$ and $>CO_3Ca^+$. A quantitative measure of electrostatic attraction is termed the bond product sum [83, 213], BPS, which is equal to $[-NH^+] [>CO_3^-] + [-NH^+] [>CaCO_3^-] + [-COOCa^+] [>CO_3^-] + [-COOCa^+] [>CaCO_3^-] + [-COO^-] [>CaOH_2^+] + [-COO^-] [>CO_3Ca^+]$; where bracketed terms are calculated surface concentrations (mol/m²).
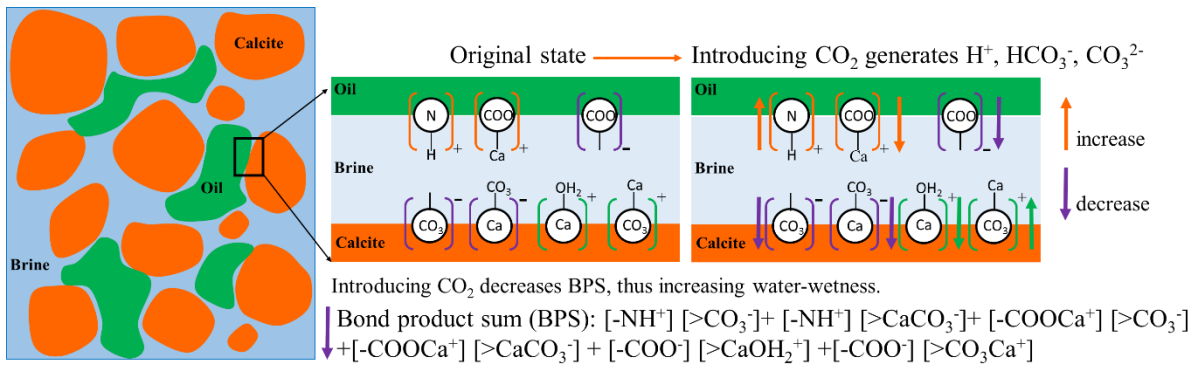
Fig. 7- 2 Schematic of surface chemistry alteration during CO_2 EOR.

7.3.1 Speciation of Oil/Brine Interfaces

Fig. 7-3 and 7-4 show calculated oil surface speciation in non-carbonated and carbonated NaCl and $CaCl_2$ brines. Calculation outputs are listed in Table 7-2 and 7-3 in Supporting Information.
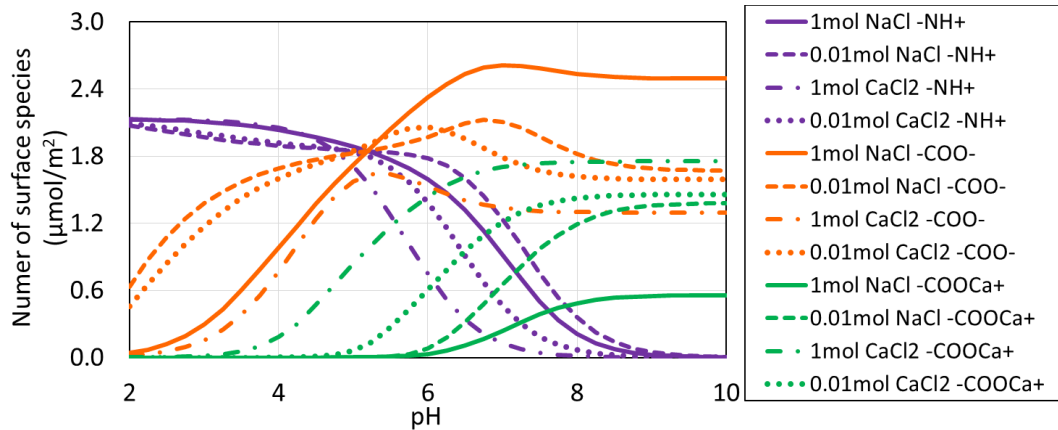
Fig. 7- 3 pH-dependent oil surface speciation in non-carbonated brine.

The calculated amount of $-NH^+$ decreases with increasing pH regardless of ion type and salinity for both non-carbonated and carbonated brines as pH controls the amount of $-NH^+$ through Reaction 1 (Table 7-1) shifting to the left [60, 99]. The calculated amount of $-COO^-$ increases with increasing pH but decreases due to the formation of $–COOCa^+$ for non-carbonated brines (Fig. 7-3). The same trend is observed in carbonated brines (Fig. 7-4), but with an increase of $-COO^-$ with increasing pH due to the formation of CO_3^{2-}, which decreases Ca^{2+}. Note: the amount of $–COOCa^+$ depends on dissolved Ca levels and to a lesser extent ionic strength because of their effect on surface species concentrations and the Ca^{2+} activity coefficient [60].   Keep in mind that surface speciation responds to dissolved phase concentrations that, through calcite equilibria, are set by pH and amount of carbonation (*in situ* P_{CO2}). For example, Ca^{2+} levels and ionic strength are higher at low pH and in carbonated brine. The PHREEQC surface complexation calculation tracks each of the competing factors while maintaining equilibrium with calcite.
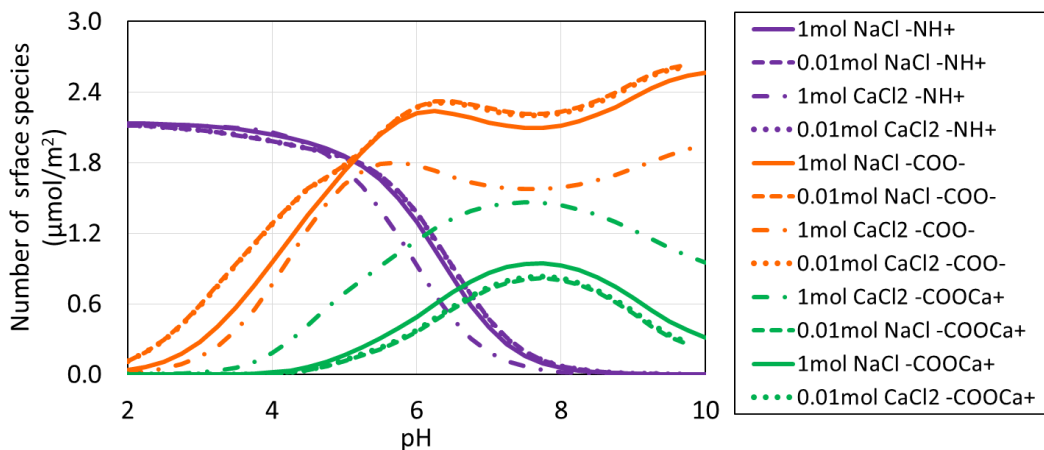
Fig. 7- 4 pH-dependent oil surface speciation in carbonated brine.

7.3.2 Speciation of Calcite/Brine Interfaces

Fig. 7-5 and 7-6 show calculated calcite surface speciation in non-carbonated and carbonated NaCl and CaCl$_2$ brines. Calculation outputs are listed in Table 7-4 and 7-5 in Supporting Information. Note that the legends in Fig. 7-5 to 7-8 refer to initial solution compositions. Final solution compositions are influenced by calcite dissolution and P$_{CO2}$. Because in the CaCO$_3$-H$_2$O-CO$_2$ system CO$_2$, pH, and Ca^{2+} are coupled, ionic strength is particularly sensitive to pH and P$_{CO2}$-dependent calcite dissolution reactions. So for example, calcite dissolution in the pH < 4 causes calculated ionic strengths to be well above 1M.

In both non-carbonated and carbonated solutions, low pH calcite surface charge is dominated by >CaOH$_2$$^+$. >CaOH$_2$$^+$ is the most abundant surface species at high pH as well in non-carbonated solutions. Increasing pH favors a decrease in >CaOH$_2$$^+$ and an increase in >CaCO$_3$$^-$, >CO$_3$$^-$, and >CO$_3Ca^+$ given available Ca^{+2}. In carbonated solutions, high pHs and bicarbonate prompt appreciable formation of >CaCO$_3$$^-$, >CO$_3$$^-$, and >CO$_3Ca^+$.

Two shifts that stand out between the non-carbonated and carbonated cases are the conversion of >CaOH$_2$$^+$ to >CaCO$_3$$^-$ and >CO$_3$$^-$ to >CO$_3$Ca$^+$ with increasing CO$_2$. These reactions are driven by respectively the higher bicarbonate and calcium levels in CO$_2$-charged brine:

$$>CaOH_2^+ + HCO_3^- \leftrightarrow >CaCO_3^- + H_2O$$
$$>CO_3^- + Ca^{+2} \leftrightarrow >CO_3Ca^+$$
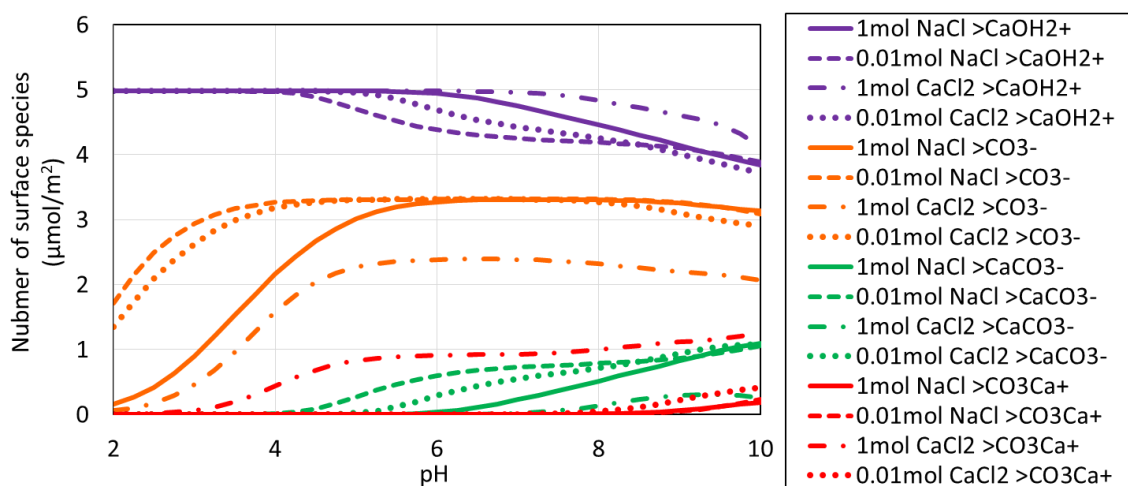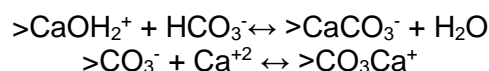
Fig. 7- 5 pH-dependent calcite surface speciation in non-carbonated brine.
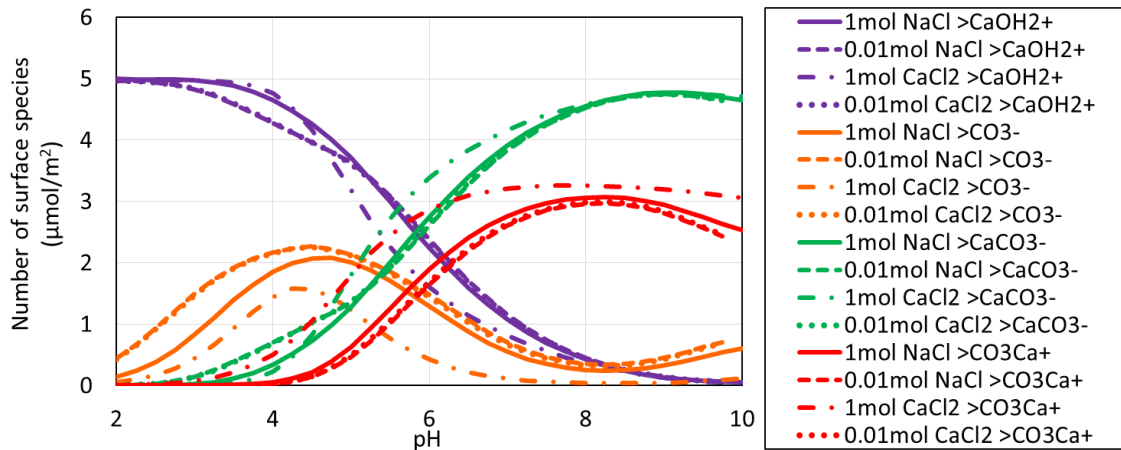
Fig. 7- 6 pH-dependent calcite surface speciation in carbonated brine.

7.3.3 Calculation of Oil-on-Calcite Wetting

We combined the calculated oil and calcite speciation above into a bond product sum, BPS, the number of electrostatic bridges between the oil and calcite. Again, the bond product sum is a measure of electrostatic attraction between oil and calcite, is proportional to measured contact angles (Chen et al. Fuel, 2018, in press and Xie et al. unpublished), and is therefore a useful predictor of wetting. For our system, the bond product sum is the total of six concentration products that quantify the strength of six electrostatic bridges between oppositely charged oil and calcite species, as noted above. For natural systems containing sulfate the BPS would also include, for example, a $[>CaSO_4^-][-NH^+]$ term.

Fig. 7-7 and 7-8 show the bond product sum for non-carbonated and carbonated conditions. Calculation outputs are listed in Table 6 and 7 of Supporting Information. The most important electrostatic bridges are $[>CaOH_2^+]$ $[-COO^-]$, $[>CO_3^-]$ $[-COOCa^+]$, and $[>CaCO_3^-]$ $[-COOCa^+]$; the first of these bridges provides most of the oil-calcite electrostatic linking.
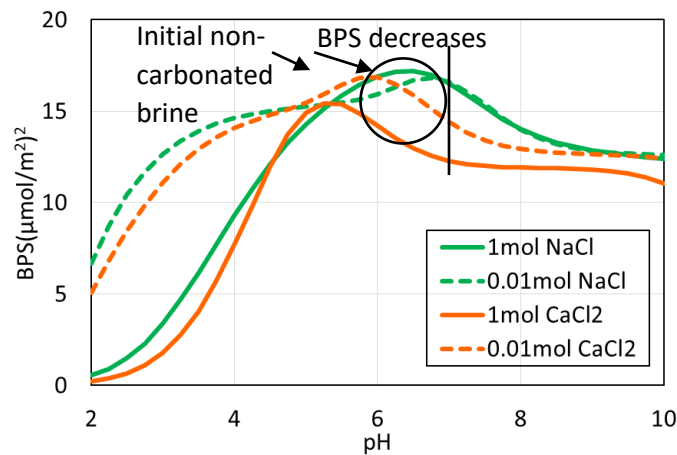
Fig. 7- 7 Bond Product Sum vs. pH in non-carbonated brine. The PHREEQC calculated pH of non-carbonated brine with calcite in equilibrium for 1 mol/L NaCl, CaCl$_2$, and 0.01 mol/L NaCl, CaCl$_2$, were 9.8, 8.2, 9.0, and 9.9 at P$_{CO2}$=0 psi, and 25 ºC. The initial pH of all fluids before equilibration with calcite was 7.
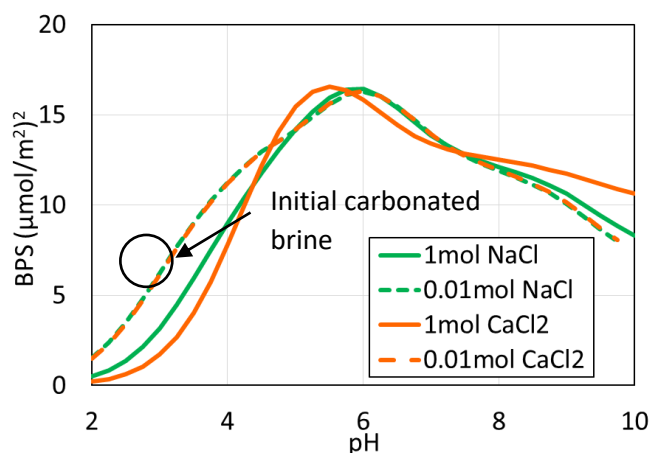
Fig. 7- 8 Bond Product Sum vs. pH for carbonated brine. The PHREEQC calculated pH of carbonated brine for 1 mol/L NaCl, $CaCl_2$, and 0.01 mol/L NaCl, $CaCl_2$, were 4.9, 4.1, 4.9, and 4.8 at P_{CO2}=3000 psi, and 25°C after equilibration with calcite. The calculated pre-calcite equilibration brine pH was 3.0, 2.6, 3.0, and 3.0 for 1 mol/L NaCl, $CaCl_2$, and 0.01 mol/L NaCl, $CaCl_2$, respectively, at P_{CO2}=3000 psi, and 25 °C.

The pH in non-carbonated brines increased from 7 to 10 after equilibration with calcite which decreases the BPS (Fig. 7-7) and the contact angle (Fig. 7-1). In contrast, in carbonated brines the pH decreases to less than 4 which decreases the BPS (Fig.7-8) and the contact angle (Fig. 7-1), pointing to a more water-wet system. The pH difference between calcite-equilibrated carbonated and non-carbonated brine largely accounts for why Teklu et al. [92] and we observed a dramatic contact angle decrease in carbonated brine (Fig.7-1). Specifically, electrostatic adhesion decreases with carbonation because of a decrease in pH. In a carbonate reservoir the reduction in electrostatic adhesion with carbonation ultimately means greater oil recovery because it causes an increase in oil relative permeability [227].

7.4 Implications and Conclusions

Our coupled surface complexation/CO_2 and mineral dissolution model provides a mechanistic rationale for the CO_2-induced wettability shift, and a means for coupling such observations into larger reservoir simulators. The latter might provide a path for more effectively tuning CO_2 EOR to increase oil recovery from carbonate reservoirs. That being said, uncertainties remain. The surface complexation modelling might be improved by developing a more precise picture of the oil-water interface chemistry, specifically by verifying more closely the identities and surface acidity constants of surface polar groups e.g. through zeta potential measurements. The impact of salinity on oil and calcite surface complexation in high TDS solutions must be verified. Alternative calcite surface complexation stoichiometries than those in Table 7-1 exist [67]. Our preliminary calculations using the calcite surface stoichiometries of Song et al. [67] predict the same trends seen above although the absolute values of the calculated BPS are different. We believe that our new algorithm provide insights into the transport, the clean-up of the hydrocarbon contaminants in soils.

7.5 Methods

7.5.1 Substrates

Calcite minerals supplied by Ward's Science were used in the contact angle tests. X-Ray Diffraction (XRD) tests confirmed that the composition of substrates were 100% calcite. To avoid any hysteresis and contamination the natural mineral surfaces (cleavage) were used as pendent spots.

Prior to experiments, substrates were cleaned with solvents (e.g., toluene and methanol) to remove any traces of organic and inorganic contaminants. Substrates were then rinsed with equilibrated deionised water to prevent undesired dissolution and dried in an oven at moderate temperature of 60°C.

7.5.2 Liquids preparation

Texas crude oil from the United States was used in contact angle tests. Chemical analysis of crude oil indicated the acid and base number were 1.7 and 1.2 mg KOH/g, respectively. To prepare carbonated brines, 1.0 mole and 0.01 mole of NaCl and $CaCl_2$ brines were prepared and individually loaded in a reactor. CO_2 gas was injected in the reactor through a syringe pump with the aid of a compressor and mixed with the brine at 3000 psi and 25°C until the brine was saturated with CO_2 gas. Saturated brine was transferred into an accumulator and maintained under pressure until the experiment was carried out.

7.5.3 Experimental procedure

Contact angle experiments were measured using a Vinci IFT apparatus (see Figure 1 in Xie et al. [61]). All contact angles were measured at 3000 psi and 25°C conditions. Calcite substrates were mounted on the apparatus turn table and placed inside the high pressure high temperature (HPHT) cell and sealed and vacuumed until state of vacuum was attained. The pressure cell was then filled with the desired brine and pressurised to 3000 psi. Subsequently, the experimental oil was slowly and steadily introduced into the cell through a capillary needle (0.64 mm diameter) until a droplet was formed. The droplet was then released on the substrate, and integrated software was utilised to measure left and right contact angles between substrate and the oil droplet. Contact angles were continuously recorded until equilibrium was achieved where contact angle became stable. This process was repeated for CO_2-saturated brines. Throughout the experiment test pressure was closely monitored and maintained to prevent depressurisation of cell, and desaturation of the brine.

7.5.4 Simulation methods

Surface complexation modelling (and DLVO theory) presumes an electric double layer at each interface and the existence of charged surface species whose concentrations depend upon the chemical makeup of the water and the oil and mineral surface [61]. Surface equilibria and constants [83, 174, 183, 184] are listed in Table 7-1. The surface species concentrations were calculated using PHREEQC version 3.3.9 (Parkhurst and Appelo 2013) and a diffuse layer surface model. The calcite surface site density was assumed to be 5 sites/nm^2 [210]. The oil/calcite surface area was set to 0.11 m^2/g [84].

Table 7- 1 Surface complexation model input parameters

Interfaces	Reaction	Log $K_{25°C}$	Reaction
Oil/Brine Interface	$-NH^+ = -N + H^+$	-6.0	1
	$-COOH = -COO^- + H^+$	-5.0	2
	$-COOH + Ca^{2+} = -COOCa^+ + H^+$	-3.8	3
Calcite/Brine Interface	$>CaOH + H^+ = >CaOH_2^+$	11.85	4
	$>CaOH + HCO_3^- = >CaCO_3^- + H_2O$	5.8	5
	$>CaOH_2^+ + SO_4^{2-} = >CaSO_4^- + H_2O$	2.1	6
	$>CO_3H = >CO_3^- + H^+$	-5.1	7
	$>CO_3H + Ca^{2+} = >CO_3 Ca^+ + H^+$	-2.6	8
	$>CO_3H + Mg^{2+} = >CO_3 Mg^+ + H^+$	-2.6	9

"$>$" represents the negatively charged site on the carbonate surface while the "$-$" represents the negatively charged site on the oil surface.

7.6 Supporting materials

Fig. 7-9 shows the BPS in the carbonated brines using Song et al.'s [67] model with CO_2 and mineral dissolution using alternative calcite surface stoichiometries. Song et al.'s model predicts the same trend as our model, showing that carbonated brines gave a much lower BPS compared to in-situ reservoir condition (pH 6-7) although the absolute value is different.
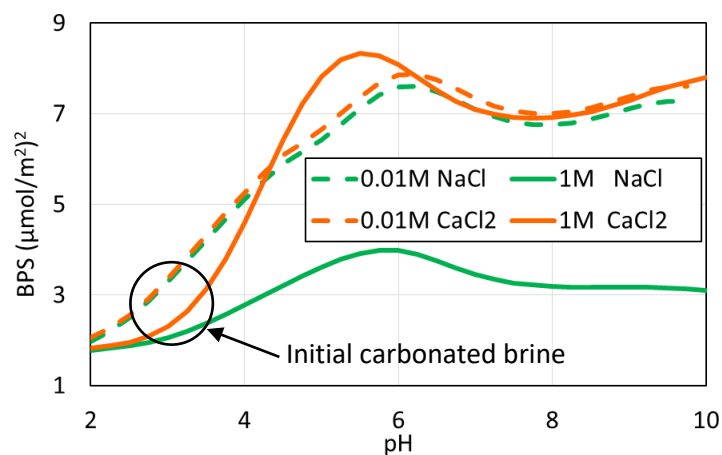
Fig. 7- 9 Bond Product Sum for the carbonated system using Song et al.'s [67] model with CO_2 and mineral dissolution using alternative calcite surface stoichiometries.

Table 7- 2 pH-dependent oil surface speciation in non-carbonated brine.

	Oil surface species in non-carbonated brine for Figure 3 in article file											
pH	$-NH^+$ ($\mu mol/m^2$)				$-COO^-$ ($\mu mol/m^2$)				$-COOCa^+$ ($\mu mol/m^2$)			
	$CaCl_2$	$CaCl_2$	NaCl	NaCl	$CaCl_2$	$CaCl_2$	NaCl	NaCl	$CaCl_2$	$CaCl_2$	NaCl	NaCl
	1M	0.01M	1M	0.01M	1M	0.01M	1M	0.01M	1M	0.01M	1M	0.01M
2.00	2.13	2.09	2.13	2.08	0.02	0.45	0.04	0.63	0.00	0.00	0.00	0.00
2.25	2.13	2.07	2.13	2.05	0.03	0.65	0.07	0.87	0.00	0.00	0.00	0.00
2.50	2.13	2.05	2.12	2.02	0.05	0.84	0.12	1.08	0.01	0.00	0.00	0.00
2.75	2.12	2.03	2.12	1.99	0.09	1.01	0.19	1.25	0.01	0.00	0.00	0.00
3.00	2.12	2.01	2.11	1.97	0.15	1.17	0.30	1.38	0.02	0.00	0.00	0.00
3.25	2.11	1.98	2.10	1.95	0.25	1.31	0.43	1.48	0.03	0.00	0.00	0.00
3.50	2.10	1.96	2.08	1.93	0.38	1.42	0.60	1.57	0.06	0.00	0.00	0.00
3.75	2.08	1.94	2.06	1.91	0.56	1.52	0.79	1.64	0.10	0.00	0.00	0.00
4.00	2.05	1.92	2.03	1.89	0.77	1.60	0.98	1.69	0.18	0.00	0.00	0.00
4.25	2.01	1.90	2.00	1.88	1.00	1.67	1.18	1.73	0.31	0.00	0.00	0.00
4.50	1.95	1.88	1.97	1.87	1.24	1.73	1.37	1.77	0.47	0.01	0.00	0.00
4.75	1.85	1.86	1.93	1.86	1.44	1.78	1.55	1.80	0.65	0.02	0.00	0.00
5.00	1.71	1.83	1.88	1.85	1.57	1.84	1.72	1.83	0.84	0.06	0.00	0.00
5.25	1.52	1.79	1.83	1.84	1.63	1.92	1.89	1.86	1.01	0.14	0.00	0.00
5.50	1.28	1.70	1.77	1.83	1.64	1.99	2.04	1.88	1.17	0.27	0.01	0.01
5.75	1.01	1.57	1.69	1.81	1.59	2.05	2.19	1.92	1.31	0.43	0.02	0.03

6.00	0.75	1.38	1.59	1.78	1.53	2.06	2.33	1.97	1.44	0.61	0.03	0.08
6.25	0.52	1.16	1.47	1.71	1.46	2.02	2.44	2.04	1.54	0.78	0.06	0.18
6.50	0.34	0.91	1.32	1.61	1.41	1.96	2.53	2.09	1.62	0.95	0.11	0.32
6.75	0.21	0.67	1.13	1.44	1.37	1.87	2.59	2.12	1.67	1.09	0.17	0.48
7.00	0.13	0.47	0.92	1.24	1.34	1.79	2.61	2.11	1.70	1.21	0.24	0.65
7.25	0.07	0.30	0.70	1.00	1.32	1.72	2.61	2.05	1.73	1.30	0.31	0.82
7.50	0.04	0.19	0.50	0.76	1.31	1.67	2.59	1.97	1.74	1.36	0.38	0.97
7.75	0.02	0.11	0.33	0.54	1.30	1.64	2.56	1.89	1.74	1.40	0.44	1.10
8.00	0.01	0.07	0.21	0.36	1.30	1.62	2.54	1.82	1.75	1.42	0.49	1.19
8.25	0.01	0.04	0.13	0.23	1.30	1.61	2.52	1.76	1.75	1.44	0.52	1.26
8.50	0.00	0.02	0.08	0.14	1.30	1.60	2.51	1.73	1.75	1.45	0.53	1.31
8.75	0.00	0.01	0.04	0.08	1.30	1.60	2.50	1.70	1.75	1.45	0.54	1.34
9.00	0.00	0.01	0.02	0.05	1.30	1.59	2.50	1.69	1.75	1.46	0.55	1.36
9.25	0.00	0.00	0.01	0.03	1.30	1.59	2.49	1.68	1.75	1.46	0.55	1.37
9.50	0.00	0.00	0.01	0.02	1.30	1.59	2.49	1.68	1.75	1.46	0.56	1.37
9.75	0.00	0.00	0.00	0.01	1.30	1.59	2.49	1.67	1.75	1.46	0.56	1.38
10.00	0.00	0.00	0.00	0.00	1.30	1.59	2.49	1.67	1.75	1.46	0.56	1.38

Table 7- 3 pH-dependent oil surface speciation in carbonated brine.

Oil surface species in carbonated brine for Figure 4 in article file											
pH	−NH$^+$ (µmol/m^2)				−COO$^-$ (µmol/m^2)				−COOCa$^+$ (µmol/m^2)			
	CaCl$_2$ 1M	CaCl$_2$ 0.01M	NaCl 1M	NaCl 0.01M	CaCl$_2$ 1M	CaCl$_2$ 0.01M	NaCl 1M	NaCl 0.01M	CaCl$_2$ 1M	CaCl$_2$ 0.01M	NaCl 1M	NaCl 0.01M
2.00	2.13	2.12	2.13	2.12	0.02	0.11	0.04	0.12	0.00	0.00	0.00	0.00
2.25	2.13	2.11	2.13	2.11	0.03	0.19	0.06	0.19	0.00	0.00	0.00	0.00
2.50	2.12	2.10	2.13	2.10	0.05	0.29	0.11	0.29	0.01	0.00	0.00	0.00
2.75	2.12	2.09	2.12	2.09	0.09	0.42	0.18	0.43	0.01	0.00	0.00	0.00
3.00	2.12	2.08	2.11	2.08	0.15	0.58	0.27	0.59	0.02	0.00	0.00	0.00
3.25	2.11	2.06	2.10	2.06	0.24	0.76	0.41	0.76	0.03	0.00	0.00	0.00
3.50	2.10	2.04	2.09	2.04	0.37	0.93	0.57	0.94	0.06	0.00	0.00	0.00
3.75	2.08	2.01	2.07	2.01	0.55	1.11	0.76	1.12	0.11	0.00	0.01	0.00
4.00	2.06	1.98	2.04	1.98	0.77	1.28	0.96	1.28	0.18	0.01	0.02	0.01
4.25	2.02	1.95	2.01	1.95	1.00	1.44	1.16	1.44	0.29	0.02	0.04	0.02
4.50	1.96	1.92	1.97	1.92	1.24	1.58	1.36	1.58	0.42	0.04	0.06	0.04
4.75	1.87	1.89	1.92	1.89	1.45	1.67	1.55	1.68	0.56	0.08	0.11	0.07
5.00	1.75	1.85	1.86	1.85	1.62	1.78	1.73	1.78	0.69	0.12	0.17	0.12
5.25	1.60	1.78	1.77	1.79	1.73	1.91	1.90	1.91	0.81	0.17	0.23	0.16
5.50	1.40	1.69	1.66	1.69	1.79	2.05	2.04	2.05	0.92	0.23	0.31	0.22
5.75	1.18	1.55	1.50	1.56	1.80	2.18	2.16	2.18	1.03	0.30	0.39	0.28
6.00	0.93	1.37	1.30	1.38	1.78	2.27	2.22	2.28	1.14	0.38	0.49	0.36
6.25	0.68	1.15	1.07	1.16	1.73	2.31	2.24	2.32	1.24	0.48	0.60	0.46
6.50	0.47	0.91	0.82	0.92	1.68	2.31	2.22	2.32	1.33	0.57	0.70	0.56
6.75	0.31	0.67	0.59	0.68	1.64	2.28	2.18	2.30	1.39	0.67	0.79	0.65
7.00	0.19	0.46	0.40	0.47	1.60	2.25	2.14	2.26	1.43	0.74	0.86	0.73
7.25	0.11	0.30	0.26	0.31	1.59	2.22	2.11	2.23	1.45	0.80	0.91	0.78

pH												
7.50	0.07	0.19	0.16	0.20	1.58	2.20	2.10	2.22	1.46	0.83	0.94	0.81
7.75	0.04	0.12	0.10	0.12	1.58	2.20	2.10	2.22	1.46	0.84	0.94	0.82
8.00	0.02	0.07	0.06	0.07	1.59	2.22	2.12	2.24	1.44	0.82	0.93	0.80
8.25	0.01	0.04	0.04	0.05	1.62	2.26	2.15	2.27	1.40	0.78	0.89	0.76
8.50	0.01	0.03	0.02	0.03	1.65	2.31	2.21	2.33	1.36	0.72	0.83	0.70
8.75	0.01	0.02	0.01	0.02	1.70	2.38	2.27	2.40	1.30	0.63	0.75	0.62
9.00	0.00	0.01	0.01	0.01	1.75	2.46	2.35	2.47	1.23	0.54	0.66	0.52
9.25	0.00	0.01	0.00	0.01	1.81	2.54	2.44	2.55	1.15	0.43	0.55	0.41
9.50	0.00	0.00	0.00	0.00	1.87	2.59	2.50	2.61	1.08	0.34	0.45	0.32
9.75	0.00	0.00	0.00	0.00	1.92	2.62	2.54	2.63	1.01	0.27	0.38	0.26
10.00	0.00		0.00		1.96		2.56		0.95		0.32	

Table 7- 4 pH-dependent calcite surface speciation in non-carbonated brine.

	Calcite surface speciation in non-carbonated brine (Figure 5, in article file)															
pH	$>CaOH^{2+}$ ($\mu mol/m^2$)				$>CO_3^-$ ($\mu mol/m^2$)				$>CaCO_3^-$ ($\mu mol/m^2$)				$>CO_3Ca^+$ ($\mu mol/m^2$)			
	$CaCl_2$	$CaCl_2$	NaCl	NaCl	$CaCl_2$	$CaCl_2$	NaCl	NaCl	$CaCl_2$	$CaCl_2$	NaCl	NaCl	$CaCl_2$	$CaCl_2$	NaCl	NaCl
	1M	0.01M	1M	0.01M	1M	0.01M	1M	0.01M	1M	0.01M	1M	0.01M	1M	0.01M	1M	0.01M
2.00	4.98	4.98	4.98	4.98	0.06	1.35	0.16	1.71	0.00	0.00	0.00	0.00	0.01	0.00	0.00	0.00
2.25	4.98	4.98	4.98	4.98	0.11	1.74	0.27	2.15	0.00	0.00	0.00	0.00	0.01	0.00	0.00	0.00
2.50	4.98	4.98	4.98	4.98	0.18	2.09	0.42	2.49	0.00	0.00	0.00	0.00	0.02	0.00	0.00	0.00
2.75	4.98	4.98	4.98	4.98	0.29	2.39	0.63	2.75	0.00	0.00	0.00	0.00	0.04	0.00	0.00	0.00
3.00	4.98	4.98	4.98	4.98	0.46	2.63	0.90	2.94	0.00	0.00	0.00	0.00	0.07	0.00	0.00	0.00
3.25	4.98	4.98	4.98	4.98	0.69	2.83	1.21	3.08	0.00	0.00	0.00	0.00	0.12	0.00	0.00	0.00
3.50	4.98	4.98	4.98	4.98	0.97	2.99	1.53	3.17	0.00	0.00	0.00	0.00	0.19	0.00	0.00	0.00
3.75	4.98	4.98	4.98	4.98	1.28	3.10	1.85	3.23	0.00	0.00	0.00	0.01	0.30	0.00	0.00	0.00
4.00	4.98	4.98	4.98	4.97	1.58	3.18	2.16	3.26	0.00	0.00	0.00	0.02	0.44	0.00	0.00	0.00
4.25	4.98	4.98	4.98	4.94	1.84	3.24	2.43	3.29	0.00	0.00	0.00	0.04	0.57	0.00	0.00	0.00
4.50	4.98	4.98	4.98	4.89	2.04	3.27	2.67	3.30	0.00	0.00	0.00	0.09	0.69	0.00	0.00	0.00
4.75	4.98	4.97	4.98	4.81	2.18	3.29	2.86	3.30	0.00	0.01	0.00	0.18	0.78	0.00	0.00	0.00
5.00	4.98	4.96	4.98	4.71	2.27	3.30	3.01	3.31	0.00	0.02	0.00	0.28	0.83	0.00	0.00	0.00
5.25	4.98	4.92	4.98	4.61	2.33	3.31	3.12	3.31	0.00	0.06	0.00	0.37	0.87	0.00	0.00	0.00
5.50	4.98	4.86	4.97	4.52	2.36	3.31	3.20	3.31	0.00	0.12	0.01	0.46	0.89	0.00	0.00	0.00
5.75	4.98	4.78	4.96	4.44	2.38	3.32	3.24	3.31	0.00	0.20	0.02	0.54	0.90	0.00	0.00	0.00
6.00	4.98	4.69	4.94	4.38	2.39	3.32	3.27	3.31	0.00	0.29	0.04	0.60	0.91	0.00	0.00	0.00
6.25	4.98	4.61	4.91	4.34	2.39	3.32	3.29	3.31	0.00	0.37	0.07	0.64	0.92	0.00	0.00	0.00
6.50	4.97	4.54	4.87	4.30	2.39	3.32	3.30	3.32	0.01	0.44	0.11	0.68	0.92	0.00	0.00	0.00
6.75	4.97	4.48	4.81	4.27	2.39	3.32	3.31	3.32	0.01	0.50	0.17	0.71	0.93	0.00	0.00	0.00
7.00	4.96	4.43	4.75	4.25	2.39	3.31	3.31	3.32	0.02	0.55	0.23	0.73	0.93	0.01	0.00	0.00
7.25	4.94	4.39	4.68	4.24	2.38	3.31	3.31	3.32	0.04	0.59	0.30	0.75	0.94	0.01	0.00	0.00
7.50	4.92	4.34	4.61	4.22	2.37	3.30	3.31	3.32	0.06	0.63	0.37	0.76	0.95	0.02	0.01	0.00
7.75	4.88	4.30	4.54	4.20	2.35	3.29	3.31	3.32	0.09	0.67	0.44	0.77	0.98	0.03	0.01	0.00
8.00	4.84	4.26	4.46	4.19	2.32	3.27	3.31	3.31	0.14	0.72	0.52	0.79	1.00	0.05	0.01	0.01
8.25	4.78	4.21	4.39	4.18	2.29	3.25	3.30	3.31	0.19	0.76	0.59	0.80	1.03	0.07	0.02	0.01
8.50	4.72	4.15	4.31	4.16	2.26	3.21	3.29	3.30	0.23	0.82	0.67	0.82	1.06	0.11	0.03	0.02
8.75	4.67	4.08	4.23	4.13	2.23	3.16	3.28	3.29	0.27	0.88	0.75	0.84	1.09	0.16	0.05	0.03
9.00	4.61	4.01	4.15	4.11	2.21	3.10	3.25	3.27	0.30	0.94	0.83	0.87	1.12	0.22	0.07	0.05
9.25	4.55	3.93	4.06	4.07	2.18	3.04	3.23	3.24	0.31	1.00	0.91	0.90	1.14	0.28	0.09	0.08

9.50	4.46	3.86	3.98	4.01	2.16	2.99	3.20	3.20	0.31	1.05	0.98	0.95	1.17	0.33	0.13	0.12
9.75	4.32	3.79	3.91	3.95	2.12	2.94	3.16	3.15	0.29	1.08	1.05	1.00	1.20	0.38	0.16	0.18
10.00	4.12	3.72	3.84	3.89	2.06	2.91	3.13	3.09	0.26	1.08	1.10	1.06	1.26	0.41	0.19	0.23

Table 7- 5 pH-dependent calcite surface speciation in carbonated brine.

Calcite surface speciation in carbonated brine for Figure 6 in article file															
pH	>CaOH^{2+} (µmol/m^2)				>CO$_3^-$ (µmol/m^2)				>CaCO$_3^-$ (µmol/m^2)				>CO$_3$Ca$^+$ (µmol/m^2)			
	CaCl$_2$	CaCl$_2$	NaCl	NaCl	CaCl$_2$	CaCl$_2$	NaCl	NaCl	CaCl$_2$	CaCl$_2$	NaCl	NaCl	CaCl$_2$	CaCl$_2$	NaCl	NaCl
	1M	0.01 M	1M	0.01 M	1M	0.01 M	1M	0.01 M	1M	0.01 M	1M	0.01 M	1M	0.01 M	1M	0.01 M
2.00	4.97	4.97	4.99	4.97	0.06	0.43	0.15	0.44	0.00	0.00	0.00	0.01	0.01	0.00	0.00	0.00
2.25	4.97	4.96	4.99	4.96	0.10	0.65	0.24	0.67	0.00	0.01	0.00	0.01	0.01	0.00	0.00	0.00
2.50	4.97	4.94	4.99	4.94	0.17	0.91	0.38	0.93	0.00	0.03	0.00	0.03	0.02	0.00	0.00	0.00
2.75	4.97	4.90	4.98	4.90	0.28	1.20	0.58	1.22	0.00	0.07	0.01	0.07	0.04	0.00	0.00	0.00
3.00	4.97	4.84	4.97	4.83	0.45	1.47	0.83	1.49	0.01	0.14	0.02	0.14	0.07	0.00	0.00	0.00
3.25	4.96	4.73	4.94	4.72	0.67	1.71	1.11	1.73	0.02	0.24	0.05	0.25	0.13	0.00	0.01	0.00
3.50	4.94	4.60	4.88	4.59	0.93	1.91	1.39	1.92	0.04	0.38	0.11	0.39	0.21	0.01	0.01	0.01
3.75	4.88	4.45	4.79	4.44	1.21	2.06	1.65	2.06	0.10	0.53	0.21	0.54	0.34	0.01	0.03	0.01
4.00	4.76	4.29	4.65	4.28	1.45	2.16	1.85	2.17	0.23	0.69	0.34	0.70	0.51	0.03	0.06	0.03
4.25	4.52	4.13	4.48	4.12	1.58	2.23	2.00	2.24	0.47	0.85	0.52	0.86	0.75	0.07	0.11	0.06
4.50	4.16	3.96	4.27	3.96	1.57	2.26	2.07	2.27	0.83	1.03	0.73	1.03	1.05	0.15	0.22	0.14
4.75	3.69	3.81	4.01	3.81	1.44	2.21	2.08	2.22	1.30	1.18	0.98	1.18	1.42	0.29	0.39	0.28
5.00	3.18	3.62	3.71	3.63	1.23	2.12	2.01	2.13	1.81	1.37	1.29	1.36	1.80	0.50	0.63	0.47
5.25	2.69	3.36	3.36	3.39	0.99	1.99	1.88	2.01	2.29	1.62	1.63	1.60	2.15	0.76	0.93	0.72
5.50	2.26	3.05	2.99	3.08	0.77	1.83	1.70	1.86	2.72	1.93	2.00	1.90	2.45	1.06	1.26	1.01
5.75	1.90	2.71	2.61	2.74	0.58	1.65	1.50	1.68	3.09	2.28	2.38	2.25	2.69	1.37	1.58	1.33
6.00	1.60	2.35	2.25	2.38	0.43	1.45	1.29	1.48	3.38	2.64	2.75	2.61	2.87	1.69	1.89	1.64
6.25	1.36	2.00	1.91	2.04	0.31	1.23	1.08	1.27	3.63	2.99	3.09	2.95	3.00	1.98	2.17	1.93
6.50	1.15	1.68	1.60	1.71	0.22	1.03	0.87	1.06	3.84	3.31	3.40	3.28	3.10	2.24	2.41	2.20
6.75	0.97	1.39	1.32	1.42	0.16	0.84	0.70	0.87	4.01	3.60	3.67	3.57	3.16	2.45	2.61	2.42
7.00	0.82	1.13	1.08	1.16	0.11	0.67	0.55	0.70	4.16	3.85	3.91	3.83	3.21	2.63	2.76	2.60
7.25	0.68	0.91	0.87	0.93	0.08	0.54	0.44	0.57	4.29	4.07	4.12	4.05	3.24	2.77	2.89	2.75
7.50	0.57	0.73	0.70	0.74	0.06	0.44	0.35	0.46	4.41	4.26	4.29	4.24	3.25	2.88	2.97	2.85
7.75	0.46	0.57	0.55	0.58	0.05	0.37	0.29	0.39	4.50	4.41	4.44	4.40	3.26	2.94	3.03	2.93
8.00	0.37	0.44	0.43	0.45	0.04	0.33	0.26	0.35	4.58	4.54	4.55	4.53	3.26	2.98	3.06	2.97
8.25	0.29	0.34	0.33	0.34	0.04	0.32	0.24	0.34	4.64	4.63	4.65	4.62	3.25	2.99	3.07	2.97
8.50	0.22	0.25	0.24	0.26	0.04	0.33	0.25	0.35	4.69	4.70	4.72	4.69	3.24	2.97	3.05	2.95
8.75	0.17	0.19	0.18	0.19	0.04	0.37	0.28	0.39	4.72	4.74	4.76	4.74	3.22	2.92	3.01	2.90
9.00	0.12	0.14	0.13	0.14	0.05	0.43	0.33	0.45	4.74	4.75	4.78	4.75	3.20	2.83	2.94	2.81
9.25	0.09	0.10	0.10	0.11	0.06	0.51	0.40	0.53	4.75	4.74	4.77	4.74	3.17	2.72	2.85	2.70
9.50	0.07	0.08	0.08	0.08	0.08	0.60	0.47	0.62	4.75	4.70	4.74	4.70	3.13	2.59	2.74	2.57
9.75	0.05	0.07	0.06	0.07	0.09	0.69	0.55	0.71	4.73	4.65	4.70	4.65	3.09	2.46	2.63	2.43
10.0	0.04		0.05		0.11		0.61		4.71		4.65		3.05		2.53	

Table 7- 6 Bond Product Sum vs. pH for the non-carbonated system.

BPS values for non-carbonated brine (Figure 7, in article file)				
pH Value	1M CaCl$_2$	0.01M CaCl$_2$	1M NaCl	0.01M NaCl
2.00	0.22	5.08	0.54	6.69
2.25	0.38	6.83	0.91	8.74
2.50	0.65	8.45	1.48	10.41
2.75	1.09	9.88	2.29	11.69
3.00	1.76	11.10	3.37	12.66
3.25	2.74	12.11	4.69	13.38
3.50	4.06	12.93	6.18	13.92
3.75	5.73	13.57	7.74	14.32
4.00	7.70	14.08	9.29	14.61
4.25	9.85	14.47	10.76	14.83
4.50	11.96	14.79	12.09	15.00
4.75	13.73	15.09	13.26	15.13
5.00	14.92	15.45	14.27	15.25
5.25	15.44	15.93	15.14	15.35
5.50	15.37	16.46	15.86	15.47
5.75	14.89	16.83	16.44	15.64
6.00	14.23	16.87	16.89	15.92
6.25	13.55	16.53	17.15	16.31
6.50	12.99	15.91	17.20	16.68
6.75	12.57	15.17	16.99	16.82
7.00	12.29	14.45	16.52	16.60
7.25	12.11	13.85	15.89	16.07
7.50	12.01	13.39	15.20	15.37
7.75	11.95	13.05	14.55	14.64
8.00	11.92	12.79	14.02	14.00
8.25	11.90	12.56	13.60	13.52
8.50	11.88	12.32	13.29	13.18
8.75	11.86	12.07	13.05	12.96
9.00	11.81	11.82	12.87	12.83
9.25	11.74	11.56	12.72	12.75
9.50	11.61	11.31	12.60	12.69
9.75	11.39	11.08	12.50	12.66
10.00	11.05	10.86	12.42	12.62

Table 7- 7 Bond Product Sum for the carbonated system.

BPS values for carbonated brine (Figure 8, in article file)				
pH Value	1M CaCl$_2$	0.01M CaCl$_2$	1M NaCl	0.01M NaCl
2.00	0.21	1.49	0.50	1.53
2.25	0.37	2.33	0.83	2.38
2.50	0.63	3.42	1.36	3.49
2.75	1.05	4.73	2.13	4.81
3.00	1.72	6.16	3.17	6.24
3.25	2.69	7.61	4.47	7.68
3.50	4.03	8.96	5.94	9.02
3.75	5.75	10.17	7.50	10.21
4.00	7.80	11.21	9.02	11.24
4.25	10.01	12.12	10.45	12.13
4.50	12.19	12.96	11.78	12.95
4.75	14.08	13.54	13.03	13.53
5.00	15.47	14.20	14.18	14.16
5.25	16.29	14.93	15.19	14.88
5.50	16.56	15.63	15.96	15.58
5.75	16.36	16.14	16.40	16.11
6.00	15.83	16.30	16.42	16.28
6.25	15.13	16.05	16.04	16.05
6.50	14.43	15.46	15.38	15.47
6.75	13.84	14.71	14.61	14.72
7.00	13.40	13.94	13.88	13.95
7.25	13.08	13.27	13.27	13.27
7.50	12.86	12.73	12.80	12.72
7.75	12.69	12.30	12.44	12.28
8.00	12.53	11.94	12.13	11.91
8.25	12.36	11.58	11.83	11.55
8.50	12.17	11.19	11.50	11.14
8.75	11.96	10.71	11.11	10.66
9.00	11.73	10.13	10.62	10.07
9.25	11.46	9.44	10.04	9.36
9.50	11.18	8.73	9.42	8.64
9.75	10.90	8.05	8.82	7.96
10.00	10.65		8.29	

Table 7- 8 Bond Product Sum for the carbonated system using Song et al.'s [67] model with CO2 and mineral dissolution using alternative calcite surface stoichiometry.

Song's SCM BPS values for Figure 9 in supplementary informaiton				
pH Value	1M $CaCl_2$	0.01M $CaCl_2$	1M NaCl	0.01M NaCl
2.00	1.82	2.05	1.78	1.97
2.25	1.87	2.26	1.82	2.20
2.50	1.95	2.55	1.88	2.50
2.75	2.09	2.92	1.95	2.86
3.00	2.31	3.36	2.06	3.29
3.25	2.65	3.84	2.20	3.75
3.50	3.13	4.33	2.37	4.22
3.75	3.79	4.81	2.57	4.68
4.00	4.61	5.26	2.78	5.11
4.25	5.51	5.69	2.99	5.51
4.50	6.42	6.09	3.21	5.89
4.75	7.21	6.35	3.42	6.15
5.00	7.81	6.65	3.62	6.43
5.25	8.19	7.00	3.79	6.76
5.50	8.33	7.37	3.92	7.11
5.75	8.28	7.68	3.99	7.41
6.00	8.08	7.85	3.97	7.58
6.25	7.80	7.86	3.89	7.60
6.50	7.51	7.74	3.75	7.49
6.75	7.27	7.55	3.59	7.30
7.00	7.09	7.34	3.45	7.10
7.25	6.98	7.17	3.34	6.93
7.50	6.92	7.05	3.26	6.82
7.75	6.90	7.00	3.21	6.76
8.00	6.91	7.00	3.19	6.75
8.25	6.96	7.04	3.18	6.80
8.50	7.04	7.13	3.17	6.88
8.75	7.16	7.25	3.18	6.99
9.00	7.29	7.38	3.18	7.10
9.25	7.44	7.52	3.17	7.22
9.50	7.58	7.59	3.16	7.27
9.75	7.70	7.61	3.13	7.27
10.00	7.79	5.70	3.10	4.92

Table 7- 9 Brine chemistry of carbonated and non-carbonated brines in various ion type and salinity (This was computed using PHREEQC with consideration of calcite dissolution and water uptake of CO2 for carbonated brine)

	1 mol/L $CaCl_2$		1 mol/L NaCl		0.01 mol/L $CaCl_2$		0.01 mol/L NaCl	
	non-carbonated	carbonated	non-carbonated	carbonated	non-carbonated	carbonated	non-carbonated	carbonated
H^+	6.32×10^{-9}	1.00×10^{-4}	1.28×10^{-10}	3.7×10^{-5}	1.1×10^{-9}	3.78×10^{-5}	1.39×10^{-10}	3.62×10^{-5}
Ca^{2+}	9.69×10^{-1}	9.43×10^{-1}	4.34×10^{-4}	9.43×10^{-2}	1.00×10^{-2}	6.28×10^{-2}	1.45×10^{-4}	5.68×10^{-2}
Na^+	-	-	9.93×10^{-1}	9.15×10^{-1}	-	-	9.99×10^{-3}	9.02×10^{-3}
Cl^-	2.01	2.02	9.93×10^{-1}	9.94×10^{-1}	2.00×10^{-2}	2.00×10^{-2}	9.99×10^{-3}	9.98×10^{-3}
$CaHCO^{3+}$	6.68×10^{-6}	1.06×10^{-1}	1.25×10^{-7}	3.67×10^{-2}	8.95×10^{-7}	3.35×10^{-2}	1.11×10^{-7}	3.19×10^{-2}
$CaCl^+$	7.60×10^{-2}	7.42×10^{-2}	1.90×10^{-5}	3.94×10^{-3}	2.30×10^{-5}	8.28×10^{-5}	2.05×10^{-7}	3.80×10^{-5}
HCO^{3-}	2.78×10^{-6}	4.54×10^{-2}	1.07×10^{-4}	1.51×10^{-1}	1.38×10^{-5}	1.39×10^{-1}	9.68×10^{-5}	1.45×10^{-1}
$NaCO_3^-$	-	-	1.05×10^{-4}	4.62×10^{-7}	-	-	1.07×10^{-6}	5.03×10^{-9}
CO_3^{2-}	1.09×10^{-7}	1.12×10^{-7}	1.84×10^{-4}	9.3×10^{-7}	1.04×10^{-6}	5.29×10^{-7}	4.63×10^{-5}	5.66×10^{-7}

Table 7- 10 Surface potential of oil-brine and brine-calcite in carbonated and non-carbonated brine (This is also computed using PHREEQC at the corresponding brines in Table 9)

	1 mol/L $CaCl_2$ brine		1 mol/L NaCl brine		0.01 mol/L $CaCl_2$ brine		0.01 mol/L NaCl brine	
	non-carbonated	carbonated	non-carbonated	carbonated	non-carbonated	carbonated	non-carbonated	carbonated
pH	8.21	4.02	9.85	4.91	9.05	4.87	9.92	4.91
Surface Potential (oil-brine) (mV)	14.55	56.72	-80.68	19.32	-31.33	20.90	-83.00	19.03
Surface Potential (brine-calcite) (mV)	63.76	64.10	-7.12	37.17	41.15	40.09	-9.46	38.27

Chapter 8. Excess H+ Increases Hydrophilicity during CO2-Assisted Enhanced Oil Recovery in Sandstone Reservoirs*

8.1 Abstract

CO_2-assisted enhanced oil recovery (EOR) appears to be a cost-effective and environmentally friendly means to unlock remaining oil resources from sandstone reservoirs. While wettability alteration due to water uptake of CO_2 has been identified as one of the primary mechanisms to govern subsurface multiphase flow thus residual oil saturations, few work has been done to explore the leading factor of wettability alteration, and fewer work has looked beyond the quantitative characterization of this physical process. We hypothesized that water uptake of CO_2 provides excess H+ which decreases electrostatic bridges of oil-brine-sandstone system thus increasing hydrophilicity. To test our hypothesis, we conducted three sets of contact angle measurements in non-carbonated and carbonated brines using muscovite substrates at pressure of 3000 psi and temperature of 25^oC. Moreover, we performed a geochemical study to quantify how excess H+ governs electrostatic bridges in oil-brine-muscovite system bearing with basal charged clays.

Our contact angle measurements show that non-carbonated water gave a contact angle of 118°, whereas carbonated brine gave a contact angle of 30°, implying a strong hydrophilic system. Geochemical modelling demonstrates that excess H+ substantially substitutes exchangeable cations (>Na) embedded in muscovite thus decreasing electrostatic bridges between oil-brine-muscovite. This work provides a first quantitative investigation on how water uptake of CO_2 depresses ion exchange process between oil-brine-muscovite and thus leading to wettability alteration.

Keywords: Carbonated water, Wettability alteration, Ion exchange, Contact angle, Geochemistry modelling

8.2 Introduction

While conventional water flooding technique has been widely implemented to maintain reservoir pressure, thereby improving oil recovery for more than an half century, up to 70% of Original Oil in Place (OOIP) remains in reservoirs after water flooding [134]. Current chemical-Enhanced Oil Recovery (e.g., polymer flooding, surfactant flooding, and alkaline flooding, etc.) at tertiary mode can further unlock the residual oil in a range of 10 to 15% of OOIP. However, these chemical-EOR involves chemical injection which likely gives rise to environmental and economic concerns particularly in the periods of low oil price [11]. Therefore, cost-effective and environmental friendly techniques are of extensive scientific interest [68]. One such technique is CO_2-assisted Enhanced Oil Recovery, which involves CO_2 immiscible and miscible flooding, CO_2 huff-n-puff in tight oil and shale oil reservoirs, and carbonated water flooding. Existing results from spontaneous imbibition and coreflooding experiments have shown that CO_2-assisted EOR can yield additional oil recovery of 10 to 15% of OOIP under secondary and tertiary mode (Table 8-1). Given all of these CO_2-EOR processes involve *in-situ* carbonated water due to water uptake of CO_2 at reservoir conditions. It is thereby of vital importance to understand how carbonated water affects subsurface multiphase flow behaviour thus residual oil saturation. Previous studies (Table 8-1) show that while measureable incremental oil recovery has been confirmed during CO_2-assisted EOR implementation, the controlling mechanism behind this remains unclear. However, the mechanisms can be divided into two categories. One is related to oil-CO_2 interactions, which are associated with solution gas drive, IFT and oil viscosity decrease thus lower mobility of oil

[228], CO_2-diffusion [229] and oil swelling [191], etc. The other one is associated with oil-carbonated water-rock interactions thus wettability alteration [92, 230].

We reckon that oil-CO_2 interaction does contribute to incremental oil recovery due to decreasing IFT and increasing oil mobility, but in this paper, we particularly focused on wettability alteration mechanism which governs subsurface multiphase flow and residual oil saturation. To understand the contribution of wettability alteration process on incremental oil recovery during carbonated water flooding, wettability alteration at core-scale has been identified by Sohrabi et al., [95, 192] who reported that carbonated water flooding at tertiary mode yields additional 15% of OOIP (Original Oil in Place). They argue that the reduction of pH due to water uptake of CO_2 likely affects surface charges on oil-brine-rock system thus wettability. Besides, they also believe that dissolution of CO_2 in oil and destabilization of polar component will in part cause wettability alteration [192]. Moreover, Grape et al., [228] and Fjelde et al., [231] did spontaneous imbibition tests, reporting that the carbonated brine exhibits 8% and 28% to 31% additional oil recovery respectively as well as increasing imbibition rate. Grape et al., [228] did spontaneous imbibition test and observed an additional 8% of OOIP from sandstone due to increasing hydrophilicity. Fjelde et al., [231] did spontaneous imbibition test and sulphate wettability test, which shows the increase of water-wet area in core plugs, confirming the wettability alteration towards more water-wet during carbonated water flooding.

Wettability alteration at pore scale has also been experimentally revealed by contact angle tests and artificial pore network flooding in the presence of carbonated water. For example, Seyyedi et al., [95] did contact angle measurements on mica surfaces, showing that system wettability shifts from intermediate-wet to water-wet. Sharbatian et al., [232] confirmed that system hydrophilicity increases with CO_2 partial pressure using a micro-model. Seyyedi et al., [94] found that carbonated water injection decreases residual oil saturation using an artificial pore network model. They conclude that the wettability alteration is an important mechanism apart from the new gaseous phase generation.

However, much of the existing work up to now has been descriptive in nature and no single study exists which quantitatively characterizes the physical nature of the oil-carbonated brine-rock interactions thus quantifying the wettability alteration during CO_2-assisted EOR implementation. To quantify the interaction of oil-brine-rock, Brady et al. (2016) developed an ion exchange model to predict the adhesion between oil and illite, and our previous work confirm that ion exchange process contributes to incremental oil recovery by decreasing electrostatic bridges between oil and basal charged clays during low salinity water flooding [126]. Molecular dynamic calculations were performed to investigate the desorption of decane and decanoatethe on montmorillonite [55], showing that cation bridge likely contributes to the organic matter adsorption. However, little is known about how excess H^+ due to water uptake of CO_2 affects ion exchange process, and what is not yet clear is the impact of excess H^+ on wettability alteration during CO_2-assisted EOR implementation.

We therefore hypothesized that the ion exchange processes between oil-brine interface and rock-brine interface (-NH$^+$ + >Na = >(-NH) + Na$^+$ and –COOCa$^+$ + >Na = >(–COOCa) + Na$^+$) would be depressed due to decreasing the number of exchangeable sites in basal charged clays in presence of carbonated water (as shown in Fig. 8-1). To test this hypothesis, we conducted three sets of contact angle measurements with presence of non-carbonated brine, carbonated brine and carbonated low salinity brine using a crude oil. Moreover, we performed a geochemical study to quantify the surface species at oil, exchangeable sites on muscovite, and electrostatic bridges in various brine.
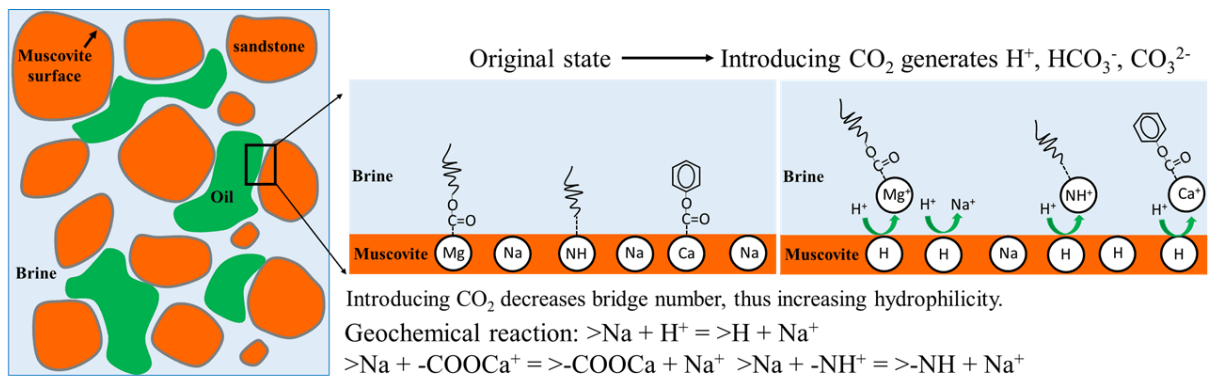
Fig. 8- 1 Schematic graph for carbonated water impact on wettability alteration (After Brady et al. [99]).

Table 8- 1 Literature CO2-assisted EOR and Proposed mechanisms

Researchers	Experimental Method	Rock and clay type	Recovery factor (%)	Incremental oil recovery (%)		Proposed mechanism(s)
				Secondary mode	Tertiary mode	
Grape et al. [228]	Spontaneous imbibition	Sandstone (basal charged)	6% to 8% additional oil recovered	-	-	Increase oil mobility. Reduce IFT. Solution gas drive. Pore throat dissolution
Dong et al.[200]	Carbonated waterflooding	Sandstone	60% to 94%	9% to 26%	3% to 35%	-
Kechut et al.[229]	Carbonated waterflooding	Sandstone	60.6% for secondary 58.4% for tertiary model	19%	9.2%	CO_2 diffusion is important
Van et al.[233]	Water-alternating-CO_2 flooding	Berea sandstone	Highest recovery factor is 52.33%	-	-	-
Li et al.[234]	CO_2 flooding	Tight sandstone	50-65%	-	-	-
Mahdavi et al. [89]	Carbonated waterflooding	Sandstone with fracture	57.1%, additional 13.45% oil recovered	9.4%	7.3%	-
Mosavat et al.[87]	Carbonated waterflooding	Sandstone	78.76%	19.02%	-	-
Mahzari et al.[190]	In-situ WAG	Glass micro model	56% OOIP secondary mode, 51% OOIP tertiary mode	-	-	New gaseous phase formation
Mosavat et al.[191]	Carbonated waterflooding	Sandstone	91.1% for secondary mode, 89.7 for tertiary mode	9.4%	7.7%	CO2 dissolution induced oil swelling and viscosity reduction
Potter et al.[230]	CO_2 flooding	Sandstone	-	-	-	Wettability alteration
Riazi et al.[235]	Carbonated waterflooding	Glass micro model	51% for secondary mode, 67% for tertiary mode	18%	16%	Oil swelling and coalescence of oil ganglia
Seyyedi et al.[236]	Carbonated waterflooding	Glass micro model	90%	-	-	Gaseous new phase
Seyyedi et al.[94]	Carbonated waterflooding	Berea sandstone	75.26% secondary mode	6.19%	-	New gaseous phases formation
Seyyedi et al. [237]	Carbonated waterflooding	Sandstone	44.9% recovery for secondary mode and	13.5%	10%	Formation of new gaseous phase; Wettability alteration

			48.4% for tertiary mode			
Shu et al.[238]	Carbonated waterflooding	Berea sandstone	28.8% additional oil recovery	-	-	-
Sohrabi et al.[201]	Carbonated waterflooding	Berea sandstone	Alomost 60% for secondary and tertiary mode	13%	15%	New fluid phase formation
Sohrabi et al. [198]	Carbonated waterflooding	Sandstone	60.6% for secondary model, 67.6 for tertiary mode	19%	9.2%	Viscosity reduction
Teklu et al. [92]	Water-alternating CO_2 flooding	Sandstone and carbonate	81.8% to 83.4%	-	14.2% to 38.5%	Wettability alteration

8.3 Materials and Methods

8.3.1 Experimental procedures

8.3.1.1 Fluids

Three brines were used in contact angle measurements. The composition for each of the brine is listed in Table 8-2. To prepare carbonated brine, the non-carbonated brine was loaded in a reactor (AMAR Autoclaves/Reactors/Pressure Vessels). Subsequently, carbon dioxide (CO_2, 99.9 mol%, from BOC Australia, food grade, gas code-082) was injected and pressurized in the reactor through a syringe pump (Vinci BFSP 500-15) with an aid of a compressor (AFP P100084 Gas Booster). The brine and CO_2 were kept under 3000 psi at 25°C until they reached thermodynamic equilibrium. Then, the carbonated brine was transferred to an accumulator for contact angle measurements.

Table 8- 2 Water composition in the experiments

Brines	Water compositions	CO_2 Concentration (mol/L)	pH
Non-carbonated high salinity brine	1mol/L NaCl + 50 mmol/L $CaCl_2$	-	7
Carbonated high salinity brine	1mol/L NaCl + 50 mmol/L $CaCl_2$ + CO_2	5.45	2.66
Non-carbonated low salinity brine	0.01mol/L NaCl + 0.5 mmol/L $CaCl_2$ + CO_2	6.85	2.79

Note: The CO_2 concentration and pH are calculated at equilibrium state by PHREEQC

A crude oil (dead oil without dissolved gas) with acid number of 1.7 mg KOH/g and base number of 1.2 mg KOH/g for the contact angle measurements. Gas chromatograph mass spectrometer (GC-MS) analysis shows that the oil is composed of wax (3.8wt %), naphthenes (26.3wt %) and sulphur (3.9 wt %). Oil density is 0.89 g/cm^3. More information in relation to the oil properties can be found in Xie et al. [111, 147, 153].

8.3.1.2 Rock Samples

Clay minerals largely control the interaction of oil-brine-sandstone reservoirs thus wettability [116], and basal charged clays (e.g., illite, smectite and chlorite) are common minerals in sandstone reservoirs [239]. In contact angle experiments, fresh muscovite surfaces were acquired by cleaving the muscovite sheet prior to introducing an oil droplet on mineral surfaces. To examine the wettability alteration on sandstone bearing basal charged clays, cleaved muscovite sheets (Provided by Ward's Natural Science) were used in contact angle measurements. This is because muscovite has similar chemical structure as the basal charged clays [240]. In addition, muscovite has cation exchange capacity (CEC) 3-4 times greater than kaolinite.

Given that surface roughness likely affects contact angle, prior to the measurement of contact angle, the surface roughness was examined using atomic force microscopy (AFM) (WITec, ALPHA 300 RA for combined Raman-AFM imaging). The AFM test shows that the surface roughness of muscovite is in a range of 0 to 2.5 nm (see Fig. 8-1 in [147]), which is much less than the thickness of water film on muscovite surface [241]. Therefore, the influence of surface roughness on contact angle can be reasonably eliminated.

The contact angle measurements were conducted on a Vinci IFT equipment (Vinci IFT 700) as shown in Fig. 8-2. The sample was loaded on a mental substrate and put inside of the high-temperature and high-pressure (HTHP) cell. Then the system was vacuumed for 12 hours before introducing bulk fluids. Prior to the contact angle tests, the crude oil was loaded in a hand pump. When the pressure of the cell was stabilized, the valve 2 was opened to introduce an oil droplet by aid of the hand pump. It is worth noting that before introducing the oil droplet onto the substrate, the first a few droplets were released to avoid any emulsion in lines. The oil droplet was also double-checked before introducing it onto the muscovite surface for a reasonable contact angle recording. To measure the contact angle in non-carbonated water, the brine was introduced directly into the unpressurized cell and pressurized it to 3000 psi. Afterwards, the cell was pressurized up to 3000 psi, and an oil droplet was later introduced onto the mineral substrate by means of a hand pump. To measure the contact angle in carbonated water, the cell was firstly pressurized using N_2 to a pressure of 3000 psi. Then the carbonated brine was injected into the cell from the bottom of the cell through a capillary needle (0.64 mm diameter) whilst adjusting the valve 3 on the top of the cell thus displacing N_2 until the cell was filled with carbonated water. The contact angle was then monitored and recorded by an integrated software. Stable contact angle value was recorded until contact angle did not change with time.
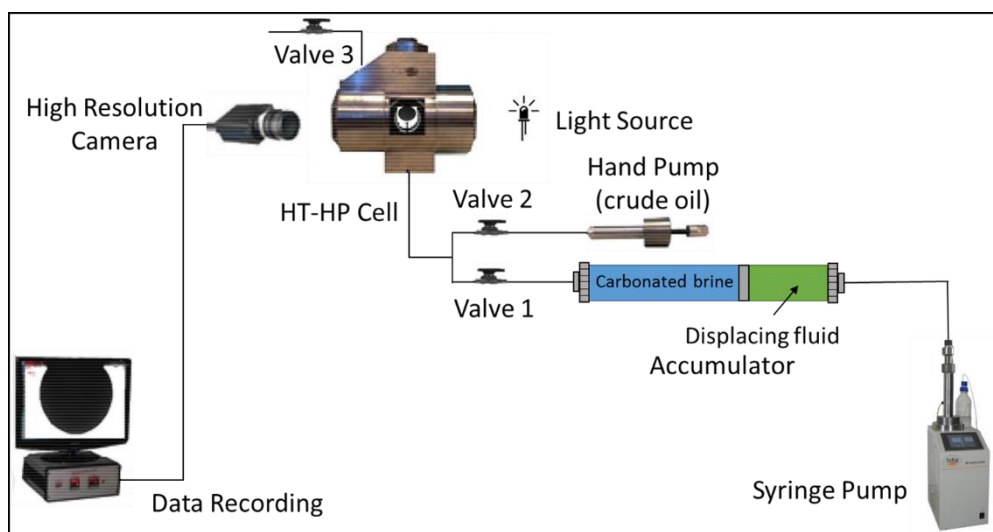

Fig. 8- 2 Schematic diagram of contact angle measurement (HT-HP cell) in non-carbonated and carbonated water

During the contact angle measurements, the system was left for up to 10 hours. The oil droplet size and contact angle was monitored continuously during test period of time. During the test period, oil drop size and contact values keep constant. Because of time independent of oil droplet size and contact angle values, we can reasonably assume that the system is equilibrated during the test. In addition, we did measure viscosity of an oil (with high content of wax) in the presence of carbonated water using a capillary viscometer (CVL 1000 from Sanchez Technologies). Our results show that viscosity decreases with amount of CO_2 dissolving into the brine. However, we only observed this viscosity decrease after we mixed the carbonated brine with oil using a reactor which the mixture is stir for 10 hours with a certain pressure. But we did not observe measureable viscosity decrease without stirring for a long

time. We therefore assumed that the viscosity of the oil during the contact angle measurements should not make a significant change. Moreover, existing literature data shows that the wettability is governed by interaction of oil-brine-rock [60, 138], rather than viscosity. Therefore, we believe that viscosity variation effect on contact angle should be negligible.

8.3.2 Geochemical modelling

8.3.2.1 Oil-brine-muscovite Reactions

To quantity the process of interaction between oil-brine-muscovite, we performed a geochemical study using ion exchange models proposed by Brady et al. [99]. Considering the contact angle will be stable after about 30 minutes, we assume that the polar adsorption will equilibrate during the test period (10 hours). We calculated the number of species on oil surfaces, and exchangeable sites on muscovite surfaces using PHREEQC [101]. The input equilibrium constants for the geochemical study are listed in Table 8-3 and 8-4.

Table 8- 3 Oil Surface Complexation Model input parameters [60]

Geochemical reactions	log K_{298K}	Number
$-NH^+ = -N + H^+$	-6.0	1
$-COOH = -COO^- + H^+$	-5.0	2
$-COOH + Ca^{2+} = -COOCa^+ + H^+$	-3.8	3

Note: –N represents nitrogen base groups present at oil interfaces [102] which is characterized using base number. $-NH^+$ is produced from the protonation of –N [99, 103].

Table 8- 4 Rock surface ion exchange input parameters [60, 99]

Geochemical reactions	log K_{298K}	Number
$>Na + -NH^+ = >-NH + Na^+$	1	4
$>Na + -COOCa^+ = >-COOCa + Na^+$	1	5
$2>Na + Ca^{2+} = >Ca + 2Na^+$	0.8 [a]	6
$>Na + H^+ = >H + Na^+$	4.6 [b]	7

Note: [a] means a data from Lawrence Livermore National Laboratory thermo.com.v8.r6.230 thermodynamic database. [b] means a data from Wieland et al. for montmorillonite[104]. To calculate the amount of oil exchanged to clay surfaces, equilibrium constant of 1 is assumed for reaction (1) and (2). >Na, >K, and >Ca represent Na, K and Ca basal sites [99]. Also, we estimated the amount of exchangeable site within the contact area between an oil drop and muscovite is 0.3 μmol which is calculated by multiplication of cation exchange capacity of muscovite (300 meq/kg) and the mass contact between oil and muscovite (0.01g). It is worth noting that the absolute exchangeable site within the contact area is not important. Rather, the trend of the electrostatic bridges variation with pH provides insights to understand how excess H^+ contributes to oil-carbonated brine-muscovite intercalations thus wettability.

8.3.2.2. Carbonated Water Chemistry

Carbonated water chemistry would significantly affect oil-carbonated brine-muscovite interactions thereby wettability. To compute the carbonated water chemistry due to water uptake of CO_2, the following CO_2 dissolution reactions (Table 8-5) with equilibrium constants were considered in our geochemical modelling at experimental pressure (3000 psi) and temperature (25 °C).

For pressure effect on gas solution, PHREEQC calculates the solubility of gas using $m = K\dfrac{\varphi P}{\gamma}$,

where m is the molarity of dissolved gas; γ is an activity coefficient in water; K is the

equilibrium constant; P (MPa) is the gas partial pressure; and φ is the fugacity coefficient. The fugacity coefficient is calculated using the Peng-Robinson equation of state [242]. More details about gas solubility calculation can be found in PHREEQC manual [101].

Table 8- 5 Solution batch reaction constants

Reaction	$Log_{10} K$	Units
$CO_{2(g)} = CO_{2(aq)}$	-1.47	mol/L atm
$CO_{2(aq)} + H_2O = H_2CO_3$	-2.59	-
$H_2CO_3 = H^+ + HCO_3^-$	-3.76	mol/L
$HCO_3^- = H^+ + CO_3^{2-}$	-10.33	mol/L
$H_2O = H^+ + OH^-$	-14	$(mol/L)^2$
$CaCO_3 = Ca^{2+} + CO_3^{2-}$	-8.48	$(mol/L)^2$
$CaOH^+ = Ca^{2+} + OH^-$	-1.22	mol/L
$CaHCO_3^+ = Ca^{2+} HCO_3^-$	-1.11	mol/L
$NaHCO_3 = Na^+ + HCO_3^-$	0.25	mol/L
$NaCO_3^- = Na^+ + CO_3^{2-}$	-1.27	mol/L

Note: The equilibrium constants are from Yutkin et al., [243] at temperature of 25°C.

8.4 Results and discussion

8.4.1 Experimental Results-Effect of Carbonated and Non-carbonated Brines on Contact Angle

Carbonated brine significantly decreases contact angle, implying a strongly water-wet system in line with existing report [92, 95, 232, 244]. For example, Fig. 8-1 shows that carbonated water gives a much lower contact angle (24.8° and 26.2°) compared to non-carbonated water (118°). Existing literature data also show that CO_2 dissolution will increase the hydrophilicity. For instance, Teklu et al., [92] did contact angle tests on Berea sandstone, showing that the contact angle decreases from 94.6° in seawater to 60° in carbonated seawater. Moreover, Al-Mutairi et al., [244] also found that contact angle decreases from 97.5° to 69.3° with increasing CO_2 exposure time. Yang et al., [245] found that and increasing CO_2 partial pressure from 0.38 MPa and 33.49 MPa would decrease the contact angle from 115° and 60°. Together, our contact angle tests and literature data all confirm the hydrophilicity increase in the presence of carbonated brine.

Salinity plays a minor role in contact angle in the presence of carbonated brine. Fig. 8-3 shows that the carbonated water regardless of salinity gives a strongly water-wet system. For example, high salinity brine gives a contact angle of 24.8°, and carbonated low salinity brine yields a contact angle of 26.2°. Both carbonated brines show a strong hydrophilic surface regardless of salinity. Our results are in line with Teklu et al., [92] who measured contact angle in carbonated seawater and carbonated low salinity water on Berea sandstone. They reported that both carbonated brines exhibit a water-wet system regardless of salinity. For instance, they show that the contact angles are 46.5° and 60° in the presence of depressurized carbonated low salinity brine and carbonated seawater, respectively.

We hypothesized that the minor dependence of salinity on wettability in the presence of carbonated water is attributed to the fact that excess H^+ due to water uptake of CO_2 can significantly reduce electrostatic bridges between oil and muscovite. This was well verified by geochemical modelling which is listed in the section below. We believe that the wetness independence of salinity will expand the application envelop of carbonated water flooding in reservoirs with high salinity formation brine.
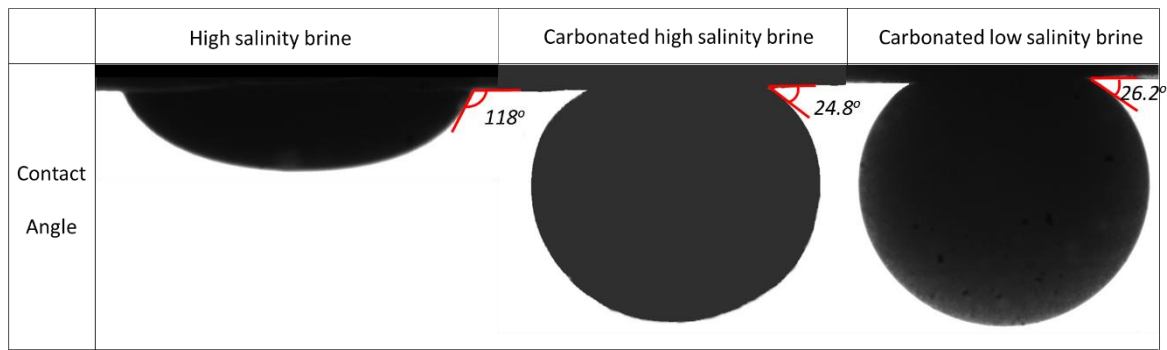
Fig. 8- 3 Contact angle in different brines

8.4.2. Modelling Results: Effect of Non-Carbonated and Carbonated Brines on Oil Surface Chemistry

Given that oil surface chemistry significantly affects oil-brine-rock interactions, we calculated the oil surface species in the presence of non-carbonated and carbonated brines. We found that while both salinity and pH play an important role in surface species, whereas carbonation plays a negligible role in $-NH^+$ at a given pH (pH <5). Rather, decreasing salinity decreases $-NH^+$ at low pH (Fig. 8-4). This is because at low pH, carbon dioxide in part exists in the form of H_2CO_3 in brine [132]. In return, salinity has more impact on the H^+ activity coefficient than the H_2CO_3. This is confirmed by the computation of $-NH^+$ in the presence of carbonated low salinity brine, which gives lower $-NH^+$ compared to carbonated high salinity brine. However, when pH is greater than 5, carbonated high salinity water increases $-NH^+$ compared to non-carbonated high salinity water at a given pH. This is largely because the carbon exists in the form of HCO_3^- at this pH range, which depresses H^+ activity. Also, carbonated low salinity gives a greater $-NH^+$ compared to carbonated high salinity brine due to the fact that lowering salinity increases the activity of H^+ thus shifting Reaction 1 towards left-hand side.

Similar to $-NH^+$, carbonation plays a negligible role in $-COO^-$ at low pH (pH <5), but decreasing salinity increases $-COO^-$ (Figure 4), implying that salinity plays a major role in $-COO^-$ regardless of carbonation . This is again due to the fact that carbon dioxide exists in the form of H_2CO_3 in brine [132]. In return, this has more impact on the H^+ activity coefficient than the H_2CO_3. However, when pH increases to 5, carbonated high salinity brine increases $-COO-$ compared to non-carbonated high salinity brine because a presence of HCO_3^- in carbonated brine may lower the activity of Ca^{2+}. This triggers an impediment of Reaction 3 shifting towards right-hand side, thus leaving $-COO^-$ at the oil surfaces, which is well supported by computed $-COOCa^+$ variation with pH (Figure 4).

Carbonation gives almost zero $-COOCa^+$ due to generating excess H^+, implying that the bridge between $-COOCa^+$ and $>Na$ from muscovite surfaces can be significantly reduced, thus increasing hydrophilicity. Figure 2 shows that at low pH (pH<5), a negligible amount of $-COOCa^+$ was computed for all three brines. This is largely because the high concentration of H^+ compensates the deprotonation of $-COOH$ (see Reactions 2 in Table 1). However, as pH > 5, carbonated high salinity brine increases $-COOCa^+$ compared to non-carbonated high salinity brine, but decreasing salinity decreases $-COOCa^+$ due to decreasing Ca level.
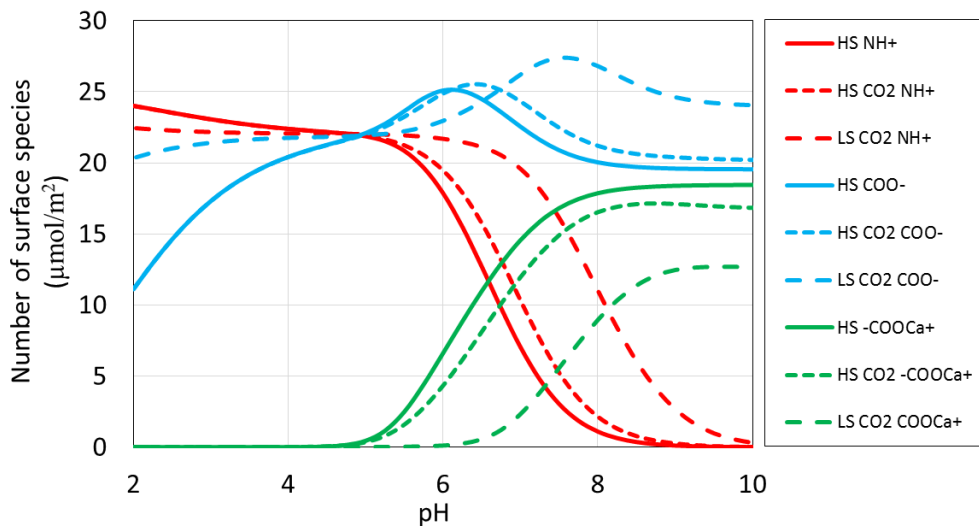
Fig. 8- 4 Oil/brine surface surfaces in different brine

Table 8- 6 Oil surface species at equilibrium condition

	Non-carbonated high salinity water	Carbonated high salinity water	Carbonated low salinity water
pH	7.02	2.66	2.79
-NH$^+$ (μmol/m^2)	7.7×10^{-2}	23.4	22.1
-COO$^-$ (μmol/m^2)	19.2	15.6	21.4
-COOCa$^+$ (μmol/m^2)	18.0	2.9×10^{-5}	5.4×10^{-5}

Note: This table shows the surface species distribution without adjustment of pH by adding NaOH or HCl. The pH is determined by the mica-brine bath reaction. We also assumed that the brine pH and composition is determined only by rock-brine interaction equilibrium state. The oil surface species is determined by the water composition after rock-brine interaction reaching in equilibrium.

8.4.3 Impact of Non-carbonated Brine and Carbonated on Exchangeable Sites

Carbonation significantly decreases exchangeable sites on muscovite surfaces, implying a substantial decrease of oil adsorption, thus more hydrophilicity. For example, non-carbonated formation brine gives an exchangeable site of 0.289 μmol/m^2, whereas carbonated high salinity and carbonated low salinity give an exchangeable site of 2.25×10^{-3} μmol/m^2 and 4.1×10^{-5} μmol/m^2, respectively. This is largely because excess H$^+$ as a result of water uptake of CO$_2$ substitutes exchangeable site >Na from muscovite surfaces [99, 126]. This is also in line with Helling et al., [246] who measured the cation exchange capacity (CEC) of soils under variable pHs. Their experiments show that the CEC drops from 213 to 36 meq/100g when pH decreases from 8 to 2.5 for all soil samples. This trend agrees well with our calculation in Figure 5, which shows that the increase of the concentration of H$^+$ decreases the exchangeable site on clay surface significantly. It is worth noting that more available exchangeable sites means more sites available for oil adsorption [126].

Increasing salinity increases exchangeable sites although salinity plays a minor role in the presence of carbonated water compared to non-carbonated water. For example, carbonated high salinity brine gives exchangeable site of 2.25×10^{-3}μmol/m^2, whereas carbonated low salinity brine gives 4.1×10^{-5}μmol/m^2 (Fig. 8-5). This is mainly because high salinity water shifts

the Reaction 6 in Table 8-4 towards right-hand side. This is in line with our previous results [126], showing that exchangeable site on basal charged clays is about 40 times in high salinity brine compared to low salinity water. However, it is worth noting that carbonation can significantly compensate the salinity effect on exchangeable sites due to the strong affinity of H^+ towards exchangeable sites on rock surfaces, which is quantified by equilibrium constant shown in Reactions 6 and 7 in Table 8-4.
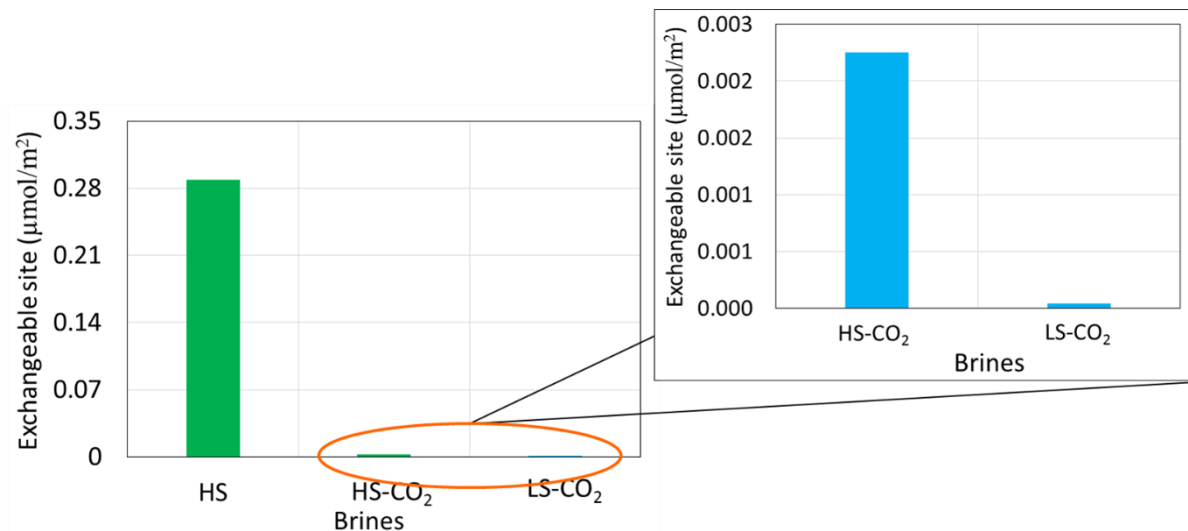

Fig. 8- 5 Exchangeable sites on mica in high salinity and low salinity brine (HS-CO$_2$ and LS-CO$_2$ are for carbonated high salinity brine and carbonated low salinity brine). Note that we did not compute the exchangeable site variation with pH in the presence of carbonated brines. This is because a huge amount of HCl and NaOH need to be added to balance *in-situ* pH, thus losing the representation of primitive brine.

8.4.3 Modelling Results: Effect of Carbonated and Non-Carbonated water on Bridging Number between Oil and Mica Surfaces

Carbonated water can significantly decrease bridging number between oil and muscovite (Fig. 8-6), implying increasing hydrophilicity. For example, carbonated high salinity water and carbonated low salinity water gives a bridging number of 5.36×10^{-14} and 9.08×10^{-14} mol/m^2. Yet, non-carbonated high salinity water gives 6.78×10^{-12} mol/m^2, 100 times more than carbonated water. The low bridging number in the presence of carbonated brine is due to the reaction 7 (Table 8-4) which shifts towards right-hand side thus decreasing exchangeable site (Na level) due to water uptake of CO_2. Moreover, given the Reaction 7 shifts towards right-hand side, the increase of Na^+ likely shifts Reactions 4 and 5 towards left-hand side, thus further decreasing bridges (>-NH, and >-COOCa). The prediction from our computation results is in line with our contact angle measurements, showing that carbonated brine gave a contact angle of 30°, whereas the non-carbonated brine gave a contact angle of 118°. Our results are also supported the existing literatures [33, 144, 247], showing that the desorption of quinoline on kaolinite and montmorillonite is accelerated with the increase of the concentration of H^+. For example, Helmy et al., [248] observed that the adsorption of quinoline is 0.6 mmol/g at pH 2, and 2.3 mmol/g at pH 7 on Na- montmorillonite. The desorption of base component indicates that the oil component with positive charges, e.g., -NH$^+$, -COOCa$^+$ likely detach from sandstone surface with presence of excess H^+, which explains why the sandstone

surface tends to be more water-wet in carbonated brine. The pH dependant of wettability is also supported by Drummond et al., [168], who observed that the muscovite surface turns to be more water wet with the increase concentration of H^+. Together, both the adsorption test and contact angle test confirm that the wettability is a function of H^+ concentration, which supports our hypothesis.

Salinity level plays a minor role in bridging number in carbonated brine although lowering salinity slightly increased bridging number (Fig. 8-6). For example, carbonated high salinity brine gives a bridging number of 5.36×10^{-14} mol/m^2, and carbonated low salinity brine yields a bridging number of 9.08×10^{-14} mol/m^2, showing 100 times lower than the bridging number in the presence of non-carbonated brine. The bridging number also predicts the same trend as contact angle measurements, showing that carbonated high salinity brine gave a contact angle of 24.8°, and carbonated low salinity brine gave a contact angle of 26.2°. The reason for the insensitivity of salinity in carbonated brine is due to the fact that excess H^+ shifts the Reaction 7 towards right-hand side thus less >Na available for bridging of the Reaction 4 and 5. This implies that carbonated brine can significantly shift oil-brine-sandstone system wettability towards strongly water-wet due to water uptake of CO_2.
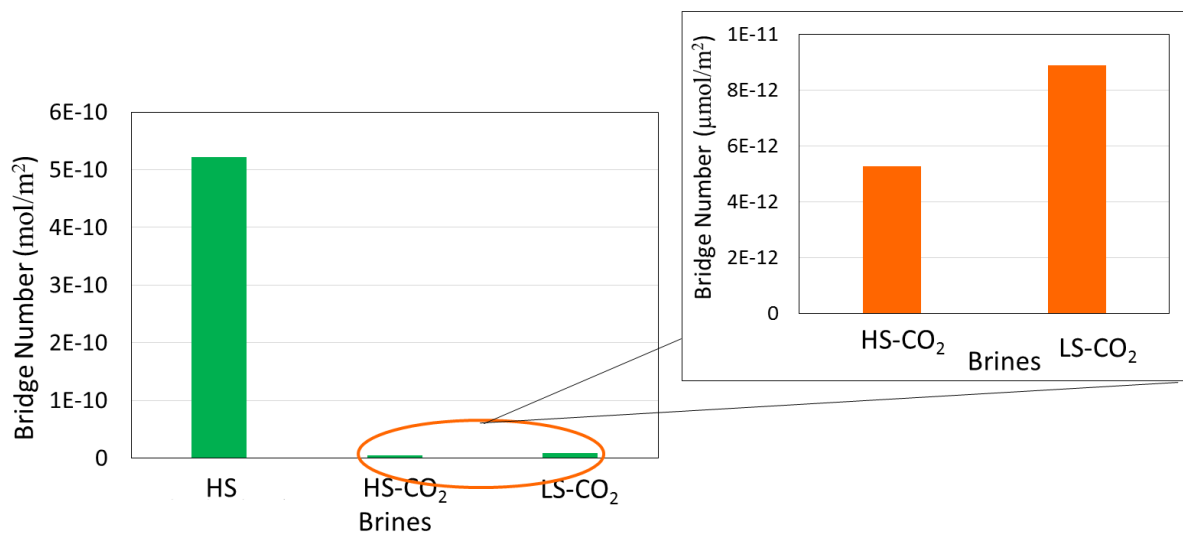

Fig. 8- 6 Bridge number in different brines (e.g., high salinity brine, carbonated high salinity brine and carbonated low salinity brine)

8.5 Implications and Conclusions

CO_2-assisted enhanced oil recovery (EOR) appears to be cost-effective and environmentally friendly to further achieve reservoir potential after conventional water flooding. While extensive special core analysis (e.g., contact angle measurements, spontaneous imbibition and coreflooding experiments) indicate that wettability alteration plays an important role in incremental oil recovery, few work have been done to characterize and quantify the wettability alteration process particularly from the geochemical perspective. We thus hypothesized that CO_2 uptake in water provides excess H^+ which decreases electrostatic bridges of oil-brine-sandstone system thus increasing hydrophilicity. To test the hypothesis, we conducted contact angle measurements in the presence of non-carbonated and carbonated brine. Moreover, we performed a geochemical study to verify our hypothesis.

Our contact angle measurements show that carbonated brine significantly decreases contact angle regardless of salinity, implying a strongly water-wet system in line with existing report [92, 95, 232, 244]. To be more specific, carbonated water gives a much lower contact angle (24.8° and 26.2°) compared to non-carbonated water (118°). Geochemical modelling shows that ion exchange process (as shown in Fig. 8-1) will be significantly depressed in carbonated brine as a result of excess H^+, which in return reduces the exchangeable sites (>Na) on mica surfaces thus the number of bridges between oil and muscovite. Taken together, our results suggest that carbonation can increase hydrophilicity of oil-brine-rock system regardless of salinity thus expanding the application envelope of carbonated water flooding in reservoirs with high salinity. This work contributes to existing knowledge of wettability alteration during carbonated water flooding by providing a quantitative analysis on adhesion of oil-brine-rock system.

Chapter 9. Conclusions, Recommendations and Outlook for Future Work

Water-assisted EOR (e.g. low salinity waterflooding, carbonated waterflooding) appears to be a cost-effective, environmental friendly oil recovery means. To explain the underlying mechanism of low salinity EOR-Effect, the wettability alteration has been identified as the main driver. However, the prediction of wettability alteration remains challenging at different length scale. In particular, the principle of shifting the relative permeability curves at core and reservoir scale remains undefined. This research work aimed to quantify the oil-brine-rock interactions thus wettability from geochemical perspective. This aim has been achieved with a combination of contact angle measurements (sub-pore scale) and micro-CT imaging (pore-scale) together with geochemical modelling with the following conclusions.

9.1 Conclusions and application

9.1.1 Wettability characterization in sandstone from sub-pore to pore-scale

A combination of coreflooding experiments and geochemical modelling confirm that basal-charged clays trigger a pH increase due to ion exchange (>Na + H$^+$ = >H + Na$^+$) during low salinity water flooding [60, 108]. We also demenstrate that oil recovery factor scales with bridging number defined by Brady et al., [60], suggesting that bridging number may be used as an indicator to screen the potential reservoir candidates thus designing the injected water chemistry. The application envelop of low salinity water flooding therefore may be expanded to reservoirs rich in basal-charged clays.

One dimensional reactive transport modelling confirms that basal-charged clays (e.g., illite, smectite, and chlorite) significantly contributes to pH increase, followed by mineral dissolution (albite) and surface complexation mechanism. Therefore, the presence of albite likely facilitates low salinity effect. This is not because the interaction between oil and albite significantly affects system wettability thus incremental oil recovery. Rather, it is because the pH increase due to albite dissolution during low salinity water injection decreases the adhesion between oil and clay minerals (e.g., illite, smectite, chlorite, and kaolinite).

The new calibrated model shows that the basal adsorption (>Na + BaseH$^+$ = >BaseH + Na$^+$) dominates base component adsorption at low pH (pH=5). Rather, the edge adsorption controls adsorption mechanism at high pH (pH=8). Furthermore, the model shows that salinity plays a minor role in adsorption at a controlled pH system. The new model reveals that basal plane modelled by ion exchange would regulate oil-clay minerals adsorption at low pH (<5), whereas edge plane modelled by surface complexation reactions would take the control at high pH (>8).

The Micro-CT imaging shows that low salinity water yielded 5% of residual oil saturation reduction after high salinity water flooding in line with previous study [160, 163]. Fluid occupancy maps at pore scale show water film propagation at pore surface after low salinity water flooding, suggesting the oil film detachment from pore surface due to *in-situ* wettability alteration. Moreover, geochemical modelling also predicts a pH increase to 8.9 during low salinity water flooding largely due to albite and ankerite dissolution, which facilitates *in-situ* wettability alteration [59, 60, 126, 147]. More importantly, surface complexation modelling shows less adhesion between oil and kaolinite minerals which likely leads to water film propagation at pore surfaces in the presence of low salinity water. We also found that the large size water cluster (greater than 10^7 μm^3) occupies 87.7% of water volume after high salinity water flooding, whereas the same size of the water cluster occupies 89.6% pore volume after

low salinity water flooding, implying that water clusters coalesce into each other to transport in pore network during low salinity water flooding in line with fluid occupancy maps. Moreover, we also found that medium size water clusters is more responsive to water ganglion reconnection thus contributing to low salinity water flooding effect. Rather, small size water clusters are less responsive to water ganglion reconnection thus making a minor contribution to incremental oil recovery. Taken together, these findings imply that remaining oil in medium size clusters would be the main target to achieve low salinity EOR-effect.

9.1.2 Wettability alteration on calcite surface in low salinity brines

Geochemical modelling shows that wetting characteristics of oil/brine/calcite system is strongly influenced by the surface chemistry of oil/brine and brine/calcite, which is governed by the composition of crude oil (e.g., acid number and base number), and water chemistry (pH, salinity level and the composition of the aqueous ionic solutions). A combination of contact angle measurements and surface complexation modelling shows that suggests that at pH < 6, conventional dilution approach likely prompts oil-wetness particularly for the crude oil with high base number. Dilution probably causes water wetness at pH > 7 for crude oils with high acid number.

9.1.3 Mechanism of wettability alteration in carbonated brines

Contact angle results show that both carbonated water and acidic water can significantly increase water-wetness. Our surface complexation modelling predicts the same trend as the experiments, showing that $>CaOH_2^+$ (at calcite surfaces) and $-NH^+$ (at oil surfaces) dominate surface charges at low pH thus decreasing the bonds between oil-calcite. We therefore argue that H^+ adsorption due to water uptake of CO_2 on the interface of oil/brine and brine/carbonate governs wettability alteration during CO_2-assisted EOR techniques. Our study sheds light on the significant influence of excess H^+ due to water uptake of CO_2 on oil-brine-carbonate system wettability thus enhancing hydrocarbon recovery in carbonate reservoirs.

We also further confirm the role of pH on wettability alteration on mica surface in carbonated brines. Our contact angle measurements show that carbonated brine significantly decreases contact angle regardless of salinity, implying a strongly water-wet system in line with existing report [92, 95, 232, 244]. To be more specific, carbonated water gives a much lower contact angle (24.8° and 26.2°) compared to non-carbonated water (118°). Geochemical modelling shows that ion exchange process (as shown in Fig. 8-1) will be significantly depressed in carbonated brine as a result of excess H^+, which in return reduces the exchangeable sites (>Na) on mica surfaces thus the number of bridges between oil and muscovite. Taken together, our results suggest that carbonation can increase hydrophilicity of oil-brine-rock system regardless of salinity thus expanding the application envelope of carbonated water flooding in reservoirs with high salinity. This work contributes to existing knowledge of wettability alteration during carbonated water flooding by providing a quantitative analysis on adhesion of oil-brine-rock system.

The geochemical modelling shows that the pH plays a major role on wettability alteration in carbonated brines in oil-brine-carbonate system. Under low pH, the $>CaOH_2^+$ and $-NH^+$ would domain the calcite surface and oil surface respectively. Therefore, the repulsive force would govern the oil-brine-calcite interface, which may lead to a hydrophilic calcite surface in carbonated brines.

9.2 Recommendation and outlook for future work

Although the water cluster distribution and *in-situ* contact angle results prove that wettability alteration can take place at pore-scale, how wettability alteration takes place and how the wettability alteration affects pore scale flow need to be further explored. From my perspective, at least the following two works need to be conducted in future.

1. Coupling geochemical reaction with multiphase flow at pore-scale to predict how geochemical controls fluids flow at pore space.

2. Coupling geochemical reaction with reservoir simulator to interpolate relative permeability curves, thus predicting the low salinity effect in field scale.

3. A new geochemical model for acidic component adhesion through basal and edge-charged planes need to be developed followed the same methodology which is presented in Chapter 3. Subsequently, to predict the shift of relative permeability curves at core and reservoir scale, the new geochemical model needs to be incorporated into the existing reservoir numerical simulators thus better managing and predicting low salinity EOR-Effect.

References

1.   Willhite, G.P., *Waterflooding.* 1986.
2.   Xie, X., et al., *Improved oil recovery from carbonate reservoirs by chemical stimulation.* SPE Journal, 2005. **10**(03): p. 276-285.
3.   Jerauld, G., et al., *Modeling low-salinity waterflooding.* SPE Reservoir Evaluation & Engineering, 2008. **11**(6): p. 1000-1012.
4.   Lager, A., et al., *Low Salinity Oil Recovery-An Experimental Investigation1.* Petrophysics, 2008. **49**(1).
5.   Al-sofi, A.M. and A.A. Yousef, *Insight into Smart-Water Recovery Mechanism through Detailed History Matching of Coreflood Experiments.* 2013, Society of Petroleum Engineers.
6.   Ayirala, S.C., et al., *A Designer Water Process for Offshore Low Salinity and Polymer Flooding Applications.* 2014, Society of Petroleum Engineers.
7.   Cense, A., et al., *Direct Visualization of Designer Water Flooding in Model Experiments.* 2014, Society of Petroleum Engineers.
8.   Akhmetgareev, V. and R. Khisamov, *40 Years of Low-Salinity Waterflooding in Pervomaiskoye Field, Russia: Incremental Oil*, in *SPE European Formation Damage Conference and Exhibition.* 2015, Society of Petroleum Engineers: Budapest, Hungary. p. 27.
9.   Fjelde, I., et al., *Secondary and Tertiary Low Salinity Water Floods: Experiments and Modeling*, in *EAGE Annual Conference & Exhibition incorporating SPE Europec.* 2013, Society of Petroleum Engineers: London, UK. p. 15.
10.   Morrow, N. and J. Buckley, *Improved Oil Recovery by Low-Salinity Waterflooding.* 2011.
11.   Wei, B., et al., *Mechanistic Study of Oil/Brine/Solid Interfacial Behaviors during Low-Salinity Waterflooding Using Visual and Quantitative Methods.* Energy & Fuels, 2017. **31**(6): p. 6615-6624.
12.   Yildiz, H.O. and N.R. Morrow, *Effect of brine composition on recovery of Moutray crude oil by waterflooding.* Journal of Petroleum Science and Engineering, 1996. **14**(3): p. 159-168.
13.   Tang, G.-Q. and N.R. Morrow, *Influence of brine composition and fines migration on crude oil/brine/rock interactions and oil recovery.* Journal of Petroleum Science and Engineering, 1999. **24**(2–4): p. 99-111.
14.   McGuire, P., et al. *Low Salinity Oil Recovery: An Exciting New EOR Opportunity for Alaska's North Slope.* 2005.
15.   Lee, S.Y., et al., *Low Salinity Oil Recovery: Increasing Understanding of the Underlying Mechanisms*, in *SPE Improved Oil Recovery Symposium.* 2010: Tulsa, Oklahoma, USA.
16.   Seccombe, J., et al. *Improving Wateflood Recovery: LoSalTM EOR Field Evaluation.* 2008.
17.   A.Lager, K.J.W., C.J.J.Black, M.Singleton, K.S.Sorbie, *Low salinity oil recovery-an experimental investigation.* SCA2006-36, 2006.
18.   Xie, Q., et al., *Ions tuning water flooding experiments and interpretation by thermodynamics of wettability.* Journal of Petroleum Science and Engineering, 2014. **124**: p. 350-358.
19.   Nasralla, R.A. and H.A. Nasr-El-Din, *Double-Layer Expansion: Is It A Primary Mechanism of Improved Oil Recovery by Low-Salinity Waterflooding?*, in *SPE Improved Oil Recovery Symposium.* 2012, Society of Petroleum Engineers: Tulsa, Oklahoma, USA.
20.   Ligthelm, D., et al. *Novel Waterflooding Strategy By Manipulation Of Injection Brine Composition.* 2009.

21. RezaeiDoust, A., et al., *Smart water as wettability modifier in carbonate and sandstone: A discussion of similarities/differences in the chemical mechanisms.* Energy & fuels, 2009. **23**(9): p. 4479-4485.
22. Lashkarbolooki, M., et al., *Low salinity injection into asphaltenic-carbonate oil reservoir, mechanistical study.* Journal of Molecular Liquids, 2016. **216**: p. 377-386.
23. Sandengen, K. and O. Arntzen. *Osmosis During Low Salinity Water Flooding.* in *IOR 2013-From Fundamental Science to Deployment.* 2013.
24. Myint, P.C. and A. Firoozabadi, *Thin liquid films in improved oil recovery from low-salinity brine.* Current Opinion in Colloid & Interface Science, 2015. **20**(2): p. 105-114.
25. Seccombe, J., et al., *Demonstration of Low-Salinity EOR at Interwell Scale, Endicott Field, Alaska*, in *SPE Improved Oil Recovery Symposium.* 2010: Tulsa, Oklahoma, USA.
26. Skrettingland, K., et al., *Snorre Low-Salinity-Water Injection--Coreflooding Experiments and Single-Well Field Pilot.* SPE Reservoir Evaluation & Engineering, 2011(04).
27. Dang, C., et al., *Application of Artificial Intelligence for Mechanistic Modeling and Probabilistic Forecasting of Hybrid Low Salinity Chemical Flooding*, in *SPE Annual Technical Conference and Exhibition.* 2018, Society of Petroleum Engineers: Dallas, Texas, USA. p. 25.
28. Dang, C., et al., *Modeling and Optimization of Low Salinity Waterflood.* 2015, Society of Petroleum Engineers.
29. Dang, C., et al., *Mechanistic modeling of low salinity water flooding.* Journal of Petroleum Science and Engineering, 2016. **146**: p. 191-209.
30. Dang, C.T.Q., et al., *Modeling Low Salinity Waterflooding: Ion Exchange, Geochemistry and Wettability Alteration*, in *SPE Annual Technical Conference and Exhibition.* 2013, Society of Petroleum Engineers: New Orleans, Louisiana, USA. p. 22.
31. Esene, C., et al., *Modeling investigation of low salinity water injection in sandstones and carbonates: Effect of Na+ and SO42−.* Fuel, 2018. **232**: p. 362-373.
32. Pouryousefy, E., Q. Xie, and A. Saeedi, *Effect of multi-component ions exchange on low salinity EOR: Coupled geochemical simulation study.* Petroleum, 2016. **2**(3): p. 215-224.
33. RezaeiDoust, A., T. Puntervold, and T. Austad, *Chemical Verification of the EOR Mechanism by Using Low Saline/Smart Water in Sandstone.* Energy & Fuels, 2011. **25**(5): p. 2151-2162.
34. Strand, S., et al., *Impact of Plagioclase on the Low Salinity EOR-Effect in Sandstone.* Energy & Fuels, 2014. **28**(4): p. 2378-2383.
35. McGuire, P.L., et al., *Low Salinity Oil Recovery: An Exciting New EOR Opportunity for Alaska's North Slope.* 2005, Society of Petroleum Engineers.
36. Brady, P.V. and J.L. Krumhansl, *A surface complexation model of oil–brine–sandstone interfaces at 100 °C: Low salinity waterflooding.* Journal of Petroleum Science and Engineering, 2012. **81**: p. 171-176.
37. Abdulla, F., et al., *First EOR Trial using Low Salinity Water Injection in the Greater Burgan Field, Kuwait*, in *SPE Middle East Oil and Gas Show and Conference.* 2013, Society of Petroleum Engineers: Manama, Bahrain. p. 15.
38. Ligthelm, D.J., et al., *Novel Waterflooding Strategy By Manipulation Of Injection Brine Composition.* 2009, Society of Petroleum Engineers.
39. Tang, G.Q. and N.R. Morrow, *Salinity, Temperature, Oil Composition, and Oil Recovery by Waterflooding.* 1997.
40. Zhang, P. and T. Austad, *Wettability and oil recovery from carbonates: Effects of temperature and potential determining ions.* Colloids and Surfaces A: Physicochemical and Engineering Aspects, 2006. **279**(1–3): p. 179-187.
41. Zhuoyan, Z., et al., *Evaluation of the Potential of High-Temperature, Low-Salinity Polymer Flood for the Gao-30 Reservoir in the Huabei Oilfield, China: Experimental*

and Reservoir Simulation Results, in *Offshore Technology Conference*. 2015, Offshore Technology Conference: Houston, Texas, USA. p. 19.

42.   Xie, Q., et al., *Low Salinity Waterflooding in Low Permeability Sandstone: Coreflood Experiments and Interpretation by Thermodynamics and Simulation*, in *SPE Asia Pacific Enhanced Oil Recovery Conference*. 2015, Society of Petroleum Engineers: Kuala Lumpur, Malaysia. p. 17.

43.   Masalmeh, S.K., *Determination of Waterflooding Residual Oil Saturation for Mixed to Oil-Wet Carbonate Reservoir and its Impact on EOR*, in *SPE Reservoir Characterization and Simulation Conference and Exhibition*. 2013, Society of Petroleum Engineers: Abu Dhabi, UAE. p. 14.

44.   Kuznetsov, D., et al., *Low-Salinity Waterflood Simulation: Mechanistic and Phenomenological Models*, in *SPE Asia Pacific Enhanced Oil Recovery Conference*. 2015, Society of Petroleum Engineers: Kuala Lumpur, Malaysia. p. 19.

45.   Jerauld, G.R., et al., *Modeling Low-Salinity Waterflooding.* SPE Reservoir Evaluation & Engineering, 2008. **11**(06): p. 1000-1012.

46.   Farzaneh, S.A., et al., *A Case Study of Oil Recovery Improvement by Low Salinity Water Injection*, in *Abu Dhabi International Petroleum Exhibition & Conference*. 2017, Society of Petroleum Engineers: Abu Dhabi, UAE. p. 43.

47.   Amiri, S. and A. Gandomkar, *Influence of electrical surface charges on thermodynamics of wettability during low salinity water flooding on limestone reservoirs.* Journal of Molecular Liquids, 2018.

48.   Mahani, H., et al., *Driving Mechanism of Low Salinity Flooding in Carbonate Rocks*. 2015, Society of Petroleum Engineers.

49.   Nasralla, R.A. and H.A. Nasr-El-Din, *Impact of cation type and concentration in injected brine on oil recovery in sandstone reservoirs.* Journal of Petroleum Science and Engineering, 2014. **122**: p. 384-395.

50.   Yousef, A.A., S. Al-Saleh, and M.S. Al-Jawfi, *Improved/Enhanced Oil Recovery from Carbonate Reservoirs by Tuning Injection Water Salinity and Ionic Content*, in *SPE Improved Oil Recovery Symposium*. 2012, Society of Petroleum Engineers: Tulsa, Oklahoma, USA. p. 18.

51.   Al Maskari, N., Q. Xie, and A. Saeedi, *Role of Basal-charged Clays in Low Salinity Effect in Sandstone Reservoirs: Adhesion Force on Muscovite using Atomic Force Microscope.* Energy & Fuels, 2019.

52.   Hassenkam, T., et al., *Could Atomic-Force Microscopy Force Mapping Be a Fast Alternative to Core-Plug Tests for Optimizing Injection-Water Salinity for Enhanced Oil Recovery in Sandstone?* 2016.

53.   Xie, Q., et al., *Extended DLVO-based estimates of surface force in low salinity water flooding.* Journal of Molecular Liquids, 2016. **221**: p. 658-665.

54.   Zhao, J., et al., *Molecular Dynamics Simulation of the Salinity Effect on the n-Decane/Water/Vapor Interfacial Equilibrium.* Energy & Fuels, 2018. **32**(11): p. 11080-11092.

55.   Underwood, T., et al., *Molecular Dynamic Simulations of Montmorillonite–Organic Interactions under Varying Salinity: An Insight into Enhanced Oil Recovery.* The Journal of Physical Chemistry C, 2015. **119**(13): p. 7282-7294.

56.   Brown, C.E. and E.L. Neustadter, *The Wettability of Oil/Water/Silica Systems With Reference to Oil Recovery.* 1980.

57.   Buckley, J.S., K. Takamura, and N.R. Morrow, *Influence of Electrical Surface Charges on the Wetting Properties of Crude Oils.* 1989.

58.   Dubey, S.T. and P.H. Doe, *Base Number and Wetting Properties of Crude Oils.* 1993.

59.   Chen, Y., Q. Xie, and A. Saeedi, *Role of ion exchange, surface complexation, and albite dissolution in low salinity water flooding in sandstone.* Journal of Petroleum Science and Engineering, 2019. **176**: p. 126-131.

60.   Brady, P.V., et al., *Electrostatics and the Low Salinity Effect in Sandstone Reservoirs.* Energy & Fuels, 2015. **29**(2): p. 666-677.

61. Xie, Q., et al., *The low salinity effect at high temperatures.* Fuel, 2017. **200**: p. 419-426.

62. Al-Sarihi, A., A. Zeinijahromi, and P. Bedrikovetsky, *Low-salinity waterflooding in non-polar oil.* The APPEA Journal, 2018. **58**(2): p. 660-663.

63. Chen, L., et al., *Zeta potential of limestone in a large range of salinity.* Colloids and Surfaces A: Physicochemical and Engineering Aspects, 2014. **450**: p. 1-8.

64. Vinogradov, J., M.D. Jackson, and M. Chamerois, *Zeta potential in sandpacks: Effect of temperature, electrolyte pH, ionic strength and divalent cations.* Colloids and Surfaces A: Physicochemical and Engineering Aspects, 2018. **553**: p. 259-271.

65. Sari, A., et al., *Drivers of Low Salinity Effect in Carbonate Reservoirs.* Energy & Fuels, 2017. **31**(9): p. 8951-8958.

66. Takeya, M., et al., *Predicting the electrokinetic properties of the crude oil/brine interface for enhanced oil recovery in low salinity water flooding.* Fuel, 2019. **235**: p. 822-831.

67. Song, J., et al., *Surface complexation modeling of calcite zeta potential measurements in brines with mixed potential determining ions (Ca2+, CO32−, Mg2+, SO42−) for characterizing carbonate wettability.* Journal of Colloid and Interface Science, 2017. **506**: p. 169-179.

68. Jackson, M.D., D. Al-Mahrouqi, and J. Vinogradov, *Zeta potential in oil-water-carbonate systems and its impact on oil recovery during controlled salinity water-flooding.* Scientific Reports, 2016. **6**: p. 37363.

69. Xie, Q., et al., *Potential Evaluation of Ion Tuning Waterflooding for a Tight Oil Reservoir in Jiyuan OilField: Experiments and Reservoir Simulation Results*, in *SPE Asia Pacific Enhanced Oil Recovery Conference*. 2015, Society of Petroleum Engineers: Kuala Lumpur, Malaysia. p. 16.

70. Khaledialidusti, R. and J. Kleppe, *Surface-Charge Alteration at the Carbonate/Brine Interface During Single-Well Chemical-Tracer Tests: Surface-Complexation Model.* SPE Journal, 2018. **Preprint**(Preprint): p. 14.

71. Zhang, Y. and N.R. Morrow, *Comparison of Secondary and Tertiary Recovery With Change in Injection Brine Composition for Crude-Oil/Sandstone Combinations*. 2006, Society of Petroleum Engineers.

72. Al-Saedi, H.N., et al., *Insights into the role of clays in low salinity water flooding in sand columns.* Journal of Petroleum Science and Engineering, 2019. **174**: p. 291-305.

73. Austad, T., A. Rezaeidoust, and T. Puntervold, *Chemical Mechanism of Low Salinity Water Flooding in Sandstone Reservoirs*. 2010, Society of Petroleum Engineers.

74. Brady, P.V., J.L. Krumhansl, and P.E. Mariner, *Surface Complexation Modeling for Improved Oil Recovery*. 2012, Society of Petroleum Engineers.

75. Chen, Y., Q. Xie, and A. Saeedi, *Electrostatic characterization of -NH+-brine-kaolinite system: Implications for low salinity waterflooding in sandstone reservoirs.* Journal of Petroleum Science and Engineering, 2019.

76. Chen, Y., et al., *Excess H+ Increases Hydrophilicity during CO2-Assisted Enhanced Oil Recovery in Sandstone Reservoirs.* Energy & Fuels, 2019. **33**(2): p. 814-821.

77. Brady, P.V. and J.L. Krumhansl, *Surface Complexation Modeling for Waterflooding of Sandstones*. 2013.

78. Khishvand, M., et al., *In situ characterization of wettability alteration and displacement mechanisms governing recovery enhancement due to low-salinity waterflooding.* Water Resources Research, 2017. **53**(5): p. 4427-4443.

79. Song, W. and A.R. Kovscek, *Functionalization of micromodels with kaolinite for investigation of low salinity oil-recovery processes.* Lab on a Chip, 2015. **15**(16): p. 3314-3325.

80. Bartels, W.B., et al., *Fast X-Ray Micro-CT Study of the Impact of Brine Salinity on the Pore-Scale Fluid Distribution During Waterflooding*. 2017.

81. Sandengen, K., et al., *Osmosis as Mechanism for Low-Salinity Enhanced Oil Recovery.* SPE Journal, 2016. **21**(04): p. 1227-1235.

82.	Moosavi, S.R., et al., *Impact of monovalent and divalent cationic and anionic ions on wettability alteration of dolomite rocks.* Journal of Molecular Liquids, 2019. **281**: p. 9-19.

83.	Brady, P.V. and G. Thyne, *Functional Wettability in Carbonate Reservoirs.* Energy & Fuels, 2016. **30**(11): p. 9217-9225.

84.	Mahani, H., et al., *Electrokinetics of Carbonate/Brine Interface in Low-Salinity Waterflooding: Effect of Brine Salinity, Composition, Rock Type, and pH on ζ-Potential and a Surface-Complexation Model.* 2016.

85.	Shiraki, R. and T.L. Dunn, *Experimental study on water–rock interactions during CO2 flooding in the Tensleep Formation, Wyoming, USA.* Applied Geochemistry, 2000. **15**(3): p. 265-279.

86.	Bagci, A., *Immiscible CO2 flooding through horizontal wells.* Energy Sources, Part A, 2007. **29**(1): p. 85-95.

87.	Mosavat, N. and F. Torabi, *Performance of Secondary Carbonated Water Injection in Light Oil Systems.* Industrial & Engineering Chemistry Research, 2014. **53**(3): p. 1262-1273.

88.	Alizadeh, A., M. Ioannidis, and M. Piri. *CO2-saturated brine flooding: an effective process for mobilization and recovery of waterflood residual oil.* in *International Symposium of the Society of Core Analysts, Austin, Texas, USA.* 2011.

89.	Mahdavi, S. and L. James, *Investigation of Water Flooding and Carbonated Water Injection (CWI) in a Fractured Porous Media.* SCA Conference paper, 2017.

90.	Shoaib, S. and B.T. Hoffman, *CO2 Flooding the Elm Coulee Field*, in *SPE Rocky Mountain Petroleum Technology Conference.* 2009, Society of Petroleum Engineers: Denver, Colorado. p. 11.

91.	Iglauer, S., C.H. Pentland, and A. Busch, *CO2 wettability of seal and reservoir rocks and the implications for carbon geo-sequestration.* Water Resources Research, 2015. **51**(1): p. 729-774.

92.	Teklu, T.W., et al., *Low-salinity water-alternating-CO2 EOR.* Journal of Petroleum Science and Engineering, 2016. **142**: p. 101-118.

93.	Seyyedi, M. and M. Sohrabi, *Pore-Scale Investigation of Crude Oil/CO2 Compositional Effects on Oil Recovery by Carbonated Water Injection.* Industrial & Engineering Chemistry Research, 2017. **56**(6): p. 1671-1681.

94.	Seyyedi, M., M. Sohrabi, and A. Sisson, *Experimental investigation of the coupling impacts of new gaseous phase formation and wettability alteration on improved oil recovery by CWI.* Journal of Petroleum Science and Engineering, 2017. **150**: p. 99-107.

95.	Seyyedi, M., M. Sohrabi, and A. Farzaneh, *Investigation of Rock Wettability Alteration by Carbonated Water through Contact Angle Measurements.* Energy & Fuels, 2015. **29**(9): p. 5544-5553.

96.	Pierre Gadonneix, A.S., Liu,Tie'nan, *2013 World Energy Issues Monitor*, in *Pierre Gadonneix.* 2013, World Energy Council: London W1B 5LT, United Kingdom.

97.	Al-Shalabi, E.W. and K. Sepehrnoori, *A comprehensive review of low salinity/engineered water injections and their applications in sandstone and carbonate rocks.* Journal of Petroleum Science and Engineering, 2016. **139**: p. 137-161.

98.	Lager, A., et al., *Low Salinity Oil Recovery - An Experimental Investigation1.* 2008.

99.	Brady, P.V., et al., *Altering wettability to recover more oil from tight formations.* Journal of Unconventional Oil and Gas Resources, 2016. **15**: p. 79-83.

100.	Parkhurst, D.L. and C. Appelo, *User's guide to PHREEQC (Version 2): A computer program for speciation, batch-reaction, one-dimensional transport, and inverse geochemical calculations.* 1999.

101.	Parkhurst, D.L. and C. Appelo, *Description of input and examples for PHREEQC version 3—a computer program for speciation, batch-reaction, one-dimensional transport, and inverse geochemical calculations.* US geological survey techniques and methods, book, 2013. **6**: p. 497.

102. Brady, P.V. and J.L. Krumhansl, *A surface complexation model of oil–brine–sandstone interfaces at 100°C: Low salinity waterflooding.* Journal of Petroleum Science and Engineering, 2012. **81**(0): p. 171-176.

103. Brady, P.V. and J.L. Krumhansl, *Surface Complexation Modeling for Waterflooding of Sandstones.* SPE Journal, 2013. **18**(02).

104. Erich Wieland, H.W. and Y. Albinsson, *A SURFACE CHEMICAL MODEL OF THE BENTONITE-WATER INTERFACE AND ITS IMPLICATIONS FOR MODELLING THE NEAR FIELD CHEMISTRY IN A REPOSITORY FOR SPENT FUEL.* 1994.

105. Schembre, J.M., G.Q. Tang, and A.R. Kovscek, *Wettability alteration and oil recovery by water imbibition at elevated temperatures.* Journal of Petroleum Science and Engineering, 2006. **52**(1–4): p. 131-148.

106. Langmuir, D.L., *Aqueous Environmental Geochemistry.* 1996: Prentice-Hall: Upper Saddle River, NJ,.

107. Wu, J., et al., *Effect of specific functional groups on oil adhesion from mica substrate: Implications for low salinity effect.* Journal of Industrial and Engineering Chemistry, 2017.

108. Vaidya, R.N. and H.S. Fogler, *Formation damage due to colloidally induced fines migration.* Colloids and Surfaces, 1990. **50**(Supplement C): p. 215-229.

109. Zhang, Y., X. Xie, and N.R. Morrow. *Waterflood performance by injection of brine with different salinity for reservoir cores.* in *SPE Annual Technical Conference and Exhibition.* 2007. Society of Petroleum Engineers.

110. Xie, Q., et al., *Low Salinity Waterflooding in Low Permeability Sandstone: Coreflood Experiments and Interpretation by Thermodynamics and Simulation.* 2015, Society of Petroleum Engineers.

111. Xie, Q., et al., *A pH-Resolved Wettability Alteration: Implications for CO2-Assisted EOR in Carbonate Reservoirs.* Energy & Fuels, 2017.

112. Mengel, K. and E.A. Kirkby, *Principles of plant nutrition.* Principles of plant nutrition., 1978.

113. Xie, Q., et al., *Investigation of Electrical Surface Charges and Wettability Alteration by Ions Matching Waterflooding.* International Symposium of the Society of Core Analysts, 2012.

114. Zhao, H., et al., *Probing surface charge potentials of clay basal planes and edges by direct force measurements.* Langmuir, 2008. **24**(22): p. 12899-12910.

115. Longwell, H.J., *The future of the oil and gas industry: past approaches, new challenges.* World Energy, 2002. **5**(3): p. 100-104.

116. Sheng, J.J., *Critical review of low-salinity waterflooding.* Journal of Petroleum Science and Engineering, 2014. **120**: p. 216-224.

117. Nasralla, R.A., et al., *Potential of Low-Salinity Waterflood To Improve Oil Recovery in Carbonates: Demonstrating the Effect by Qualitative Coreflood.* SPE Journal, 2016.

118. Zhuoyan, Z., et al., *Evaluation of the Potential of High-Temperature, Low-Salinity Polymer Flood for the Gao-30 Reservoir in the Huabei Oilfield, China: Experimental and Reservoir Simulation Results.* 2015, Offshore Technology Conference.

119. Patil, S.B., et al., *Low Salinity Brine Injection for EOR on Alaska North Slope (ANS)*, in *International Petroleum Technology Conference.* 2008: Kuala Lumpur, Malaysia.

120. Nasralla, R.A. and H.A. Nasr-El-Din, *Double-Layer Expansion: Is It a Primary Mechanism of Improved Oil Recovery by Low-Salinity Waterflooding?* SPE Reservoir Evaluation & Engineering, 2014. **Volume 17**(Issue 01, 2014): p. Pages 49-59.

121. Nasralla, R.A. and H.A. Nasr-El-Din, *Coreflood Study of Low Salinity Water Injection in Sandstone Reservoirs*, in *SPE/DGS Saudi Arabia Section Technical Symposium and Exhibition.* 2011: Al-Khobar, Saudi Arabia.

122. Xie, Q., et al., *Potential Evaluation of Ion Tuning Waterflooding for a Tight Oil Reservoir in Jiyuan OilField: Experiments and Reservoir Simulation Results.* 2015, Society of Petroleum Engineers.

123. Liu, Y., et al., *Evaluation of the Potential of Low Salinity Water Flooding in the High Temperature and High Salinity Dong-He-Tang Reservoir in the Tarim Oilfeild, China:*

Experimental and Reservoir Simulation Results. 2016, Society of Petroleum Engineers.

124. Masalmeh, S.K., et al., *LOW SALINITY FLOODING: EXPERIMENTAL EVALUATION AND NUMERICAL INTERPRETATION.* SCA2013-022, 2013.

125. Fjelde, I., S.M. Asen, and A.V. Omekeh, *Low Salinity Water Flooding Experiments and Interpretation by Simulations*. 2012, Society of Petroleum Engineers.

126. Chen, Y., et al., *Drivers of pH increase and implications for low salinity effect in sandstone.* Fuel, 2018. **218**: p. 112-117.

127. C.A.J.Appelo, *PHREEQC.*

128. Chen, Y. and S.L. Brantley, *Temperature-and pH-dependence of albite dissolution rate at acid pH.* Chemical Geology, 1997. **135**(3-4): p. 275-290.

129. Nishiyama, N. and T. Yokoyama, *Does the reactive surface area of sandstone depend on water saturation?—The role of reactive-transport in water film.* Geochimica et Cosmochimica Acta, 2013. **122**: p. 153-169.

130. Plummer, L., T. Wigley, and D. Parkhurst, *The kinetics of calcite dissolution in CO 2-water systems at 5 degrees to 60 degrees C and 0.0 to 1.0 atm CO 2.* American journal of science, 1978. **278**(2): p. 179-216.

131. Chen, Y. and S.L. Brantley, *Temperature- and pH-dependence of albite dissolution rate at acid pH.* Chemical Geology, 1997. **135**(3): p. 275-290.

132. Appelo, C.A.J. and D. Postma, *Geochemistry, groundwater and pollution*. 2004: CRC press.

133. Bartels, W.B., et al., *Literature review of low salinity waterflooding from a length and time scale perspective.* Fuel, 2019. **236**: p. 338-353.

134. Chen, Y., et al., *Oil/water/rock wettability: Influencing factors and implications for low salinity water flooding in carbonate reservoirs.* Fuel, 2018. **215**: p. 171-177.

135. Nasralla, R.A. and H.A. Nasr-El-Din, *Impact of Electrical Surface Charges and Cation Exchange on Oil Recovery by Low Salinity Water*, in *SPE Asia Pacific Oil and Gas Conference and Exhibition*. 2011: Jakarta, Indonesia.

136. Xie, Q., et al., *Primary Mechanism of Improved Oil Recovery by Low Salinity Waterflooding: Double Layer Expansion or Multicomponent Ionic Exchange?*, in *SCA2013-85*, S.o.C. Analysts, Editor. 2013: Napa California.

137. Israelachvili, J.N., *Chapter 14 - Electrostatic Forces between Surfaces in Liquids*, in *Intermolecular and Surface Forces (Third Edition)*. 2011, Academic Press: San Diego. p. 291-340.

138. Nasralla, R.A. and H.A. Nasr-El-Din, *Double-Layer Expansion: Is It a Primary Mechanism of Improved Oil Recovery by Low-Salinity Waterflooding?* 2014.

139. Liu, Z.L., et al., *Insights into the Pore-Scale Mechanism for the Low-Salinity Effect: Implications for Enhanced Oil Recovery.* Energy & Fuels, 2018. **32**(12): p. 12081-12090.

140. Hilner, E., et al., *The effect of ionic strength on oil adhesion in sandstone – the search for the low salinity mechanism.* Scientific Reports, 2015. **5**: p. 9933.

141. Xie, Q., et al., *Effect of electrical double layer and ion exchange on low salinity EOR in a pH controlled system.* Journal of Petroleum Science and Engineering, 2019. **174**: p. 418-424.

142. Mitchell, J.K. and K. Soga, *Fundamentals of soil behavior*. Vol. 3. 2005: John Wiley & Sons New York.

143. Gan, W. and Q. Liu, *Coagulation of bitumen with kaolinite in aqueous solutions containing Ca2+, Mg2+ and Fe3+: Effect of citric acid.* Journal of Colloid and Interface Science, 2008. **324**(1): p. 85-91.

144. Zachara, J.M., et al., *Quinoline sorption to subsurface materials: role of pH and retention of the organic cation.* Environmental science & technology, 1986. **20**(6): p. 620-627.

145. Burgos, W.D., et al., *Adsorption of quinoline to kaolinite and montmorillonite.* Environmental engineering science, 2002. **19**(2): p. 59-68.

146. Doherty, J., *PEST: a unique computer program for model-independent parameter optimisation.* Water Down Under 94: Groundwater/Surface Hydrology Common Interest Papers; Preprints of Papers, 1994: p. 551.

147. Pooryousefy, E., et al., *Drivers of low salinity effect in sandstone reservoirs.* Journal of Molecular Liquids, 2017.

148. Al-Saedi, H.N., R.E. Flori, and S.K. Al-Jaberi, *Eliminate the role of clay in sandstone: EOR low salinity water flooding.* Journal of Petroleum Exploration and Production Technology, 2018.

149. Shabaninejad, M., et al., *Pore-Scale Analysis of Residual Oil in a Reservoir Sandstone and Its Dependence on Water Flood Salinity, Oil Composition, and Local Mineralogy.* Energy & Fuels, 2017. **31**(12): p. 13221-13232.

150. Qiao, C., et al., *A Mechanistic Model for Wettability Alteration by Chemically Tuned Waterflooding in Carbonate Reservoirs.* 2015.

151. Li, M., et al., *A Magnetic Resonance Study of Low Salinity Waterflooding for Enhanced Oil Recovery.* Energy & Fuels, 2017. **31**(10): p. 10802-10811.

152. Hassenkam, T., et al., *Pore scale observation of low salinity effects on outcrop and oil reservoir sandstone.* Colloids and Surfaces A: Physicochemical and Engineering Aspects, 2011. **390**(1–3): p. 179-188.

153. Xie, Q., et al., *pH effect on wettability of oil/brine/carbonate system: Implications for low salinity water flooding.* Journal of Petroleum Science and Engineering, 2018. **168**: p. 419-425.

154. Sari, A., et al., *Low salinity water flooding in high acidic oil reservoirs: Impact of pH on wettability of carbonate reservoirs.* Journal of Molecular Liquids, 2019. **281**: p. 444-450.

155. Mahani, H., et al., *Insights into the Mechanism of Wettability Alteration by Low-Salinity Flooding (LSF) in Carbonates.* Energy & Fuels, 2015. **29**(3): p. 1352-1367.

156. Mahani, H., et al., *Electrokinetics of Carbonate/Brine Interface in Low-Salinity Waterflooding: Effect of Brine Salinity, Composition, Rock Type, and pH on ζ-Potential and a Surface-Complexation Model.* SPE Journal, 2017. **22**(01): p. 53-68.

157. Nasralla, R.A., M.A. Bataweel, and H.A. Nasr-El-Din, *Investigation of Wettability Alteration and Oil-Recovery Improvement by Low-Salinity Water in Sandstone Rock.* 2013.

158. Mehana, M. and M.M. Fahes, *Investigation of Double Layer Expansion in Low-Salinity Waterflooding: Molecular Simulation Study*, in *SPE Western Regional Meeting*. 2018, Society of Petroleum Engineers: Garden Grove, California, USA.

159. Bartels, W.-B., et al., *Oil Configuration Under High-Salinity and Low-Salinity Conditions at Pore Scale: A Parametric Investigation by Use of a Single-Channel Micromodel.* SPE Journal, 2017. **22**(05): p. 1362-1373.

160. Shabaninejad, M., J. Middleton, and A. Fogden, *Systematic pore-scale study of low salinity recovery from Berea sandstone analyzed by micro-CT.* Journal of Petroleum Science and Engineering, 2018. **163**: p. 283-294.

161. Iglauer, S., et al., *X-ray tomography measurements of power-law cluster size distributions for the nonwetting phase in sandstones.* Physical Review E, 2010. **82**(5): p. 056315.

162. Iglauer, S., A. Paluszny, and M.J. Blunt, *Simultaneous oil recovery and residual gas storage: A pore-level analysis using in situ X-ray micro-tomography.* Fuel, 2013. **103**: p. 905-914.

163. Lebedeva, E.V. and A. Fogden, *Micro-CT and Wettability Analysis of Oil Recovery from Sand Packs and the Effect of Waterflood Salinity and Kaolinite.* Energy & Fuels, 2011. **25**(12): p. 5683-5694.

164. Winoto, W., et al., *Secondary and Tertiary Recovery of Crude Oil from Outcrop and Reservoir Rocks by Low Salinity Waterflooding*, in *SPE Improved Oil Recovery Symposium*. 2012, Society of Petroleum Engineers: Tulsa, Oklahoma, USA. p. 13.

165. Fauziah, C.A., et al., *Carbon Dioxide/Brine, Nitrogen/Brine, and Oil/Brine Wettability of Montmorillonite, Illite, and Kaolinite at Elevated Pressure and Temperature.* Energy & Fuels, 2019. **33**(1): p. 441-448.
166. Charlet, L. and C. Tournassat, *Fe (II)-Na (I)-Ca (II) cation exchange on montmorillonite in chloride medium: evidence for preferential clay adsorption of chloride–metal ion pairs in seawater.* Aquatic Geochemistry, 2005. **11**(2): p. 115-137.
167. Iglauer, S., et al., *Comparison of residual oil cluster size distribution, morphology and saturation in oil-wet and water-wet sandstone.* Journal of Colloid and Interface Science, 2012. **375**(1): p. 187-192.
168. Drummond, C. and J. Israelachvili, *Surface forces and wettability.* Journal of Petroleum Science and Engineering, 2002. **33**(1): p. 123-133.
169. Hassenkam, T., et al., *The low salinity effect observed on sandstone model surfaces.* Colloids and Surfaces A: Physicochemical and Engineering Aspects, 2012. **403**: p. 79-86.
170. Klemme, H., Ulmishek, G. F, *Effective petroleum source rocks of the world: stratigraphic distribution and controlling depositional factors (1).* AAPG Bulletin, 1991(75): p. 1809–1851.
171. Reeder, R.J. and M.S.o. America, *Carbonates: mineralogy and chemistry.* 1983: Mineralogical Society of America.
172. Al-Attar, H.H., et al., *Low-salinity flooding in a selected carbonate reservoir: experimental approach.* Journal of Petroleum Exploration and Production Technology, 2013. **3**(2): p. 139-149.
173. Austad, T., et al., *Conditions for a low-salinity Enhanced Oil Recovery (EOR) effect in carbonate oil reservoirs.* 2012. p. 569-575.
174. Hiorth, A., L.M. Cathles, and M.V. Madland, *The Impact of Pore Water Chemistry on Carbonate Surface Charge and Oil Wettability.* Transport in Porous Media, 2010. **85**(1): p. 1-21.
175. Zhang, P., M.T. Tweheyo, and T. Austad, *Wettability Alteration and Improved Oil Recovery in Chalk: The Effect of Calcium in the Presence of Sulfate.* Energy & Fuels, 2006. **20**(5): p. 2056-2062.
176. Kuraimid, Z.K., *Treatment of Produced Water in North Rumela Oil Field for Re-Injection Application.* Society of Petroleum Engineers.
177. Iglauer, S., et al., *Contamination of silica surfaces: Impact on water–CO2–quartz and glass contact angle measurements.* International Journal of Greenhouse Gas Control, 2014. **22**: p. 325-328.
178. Al-Attar, H.H., et al., *Low Salinity Flooding in a Selected Carbonate Reservoir: Experimental Approach.* 2013, Society of Petroleum Engineers.
179. Mohsenzadeh, A., P. Pourafshary, and Y. Al-Wahaibi, *Oil Recovery Enhancement in Carbonate Reservoirs Via Low Saline Water Flooding in Presence of Low Concentration Active Ions; A Case Study.* Society of Petroleum Engineers.
180. Alameri, W., et al., *Wettability Alteration During Low-Salinity Waterflooding in Carbonate Reservoir Cores.* Society of Petroleum Engineers.
181. Alotaibi, M.B., R. Azmy, and H.A. Nasr-El-Din, *Wettability Challenges in Carbonate Reservoirs.* Society of Petroleum Engineers.
182. AlQuraishi, A.A., S.N. AlHussinan, and H.Q. AlYami, *Efficiency and Recovery Mechanisms of Low Salinity Water Flooding in Sandstone and Carbonate Reservoirs.* Offshore Mediterranean Conference.
183. Pokrovsky, O.S., J. Schott, and F. Thomas, *Dolomite surface speciation and reactivity in aquatic systems.* Geochimica et Cosmochimica Acta, 1999. **63**(19–20): p. 3133-3143.
184. Van Cappellen, P., et al., *A surface complexation model of the carbonate mineral-aqueous solution interface.* Geochimica et Cosmochimica Acta, 1993. **57**(15): p. 3505-3518.
185. Hirasaki, G.J., *Wettability:fundamentals and surface forces.* SPE Formation Evaluation, 1991c. **6**(2): p. 217-226.

186.   Nasralla, R.A., et al., *Potential of Low-Salinity Waterflood To Improve Oil Recovery in Carbonates: Demonstrating the Effect by Qualitative Coreflood.* 2016.

187.   Nasralla, R.A., J.R. Snippe, and R. Farajzadeh, *Coupled Geochemical-Reservoir Model to Understand the Interaction Between Low Salinity Brines and Carbonate Rock.* 2015, Society of Petroleum Engineers.

188.   Downs, H. and P. Hoover, *Enhanced oil recovery by wettability alteration: Laboratory and field pilot waterflood studies.* 1989, ACS Publications.

189.   Standnes, D.C. and T. Austad, *Wettability alteration in chalk: 2. Mechanism for wettability alteration from oil-wet to water-wet using surfactants.* Journal of Petroleum Science and Engineering, 2000. **28**(3): p. 123-143.

190.   Mahzari, P., et al., *Carbonated water injection under reservoir conditions; in-situ WAG-type EOR.* Fuel, 2018. **217**: p. 285-296.

191.   Mosavat, N. and F. Torabi, *Micro-optical analysis of carbonated water injection in irregular and heterogeneous pore geometry.* Fuel, 2016. **175**: p. 191-201.

192.   Sohrabi, M., et al., *A Thorough Investigation of Mechanisms of Enhanced Oil Recovery by Carbonated Water Injection*, in *SPE Annual Technical Conference and Exhibition.* 2015, Society of Petroleum Engineers: Houston, Texas, USA.

193.   Alizadeh, A.H., et al., *Multi-scale experimental study of carbonated water injection: An effective process for mobilization and recovery of trapped oil.* Fuel, 2014. **132**: p. 219-235.

194.   Ren, B., et al., *Monitoring on CO_2 migration in a tight oil reservoir during CCS-EOR in Jilin Oilfield China.* Energy, 2016. **98**: p. 108-121.

195.   Damen, K., et al., *Identification of early opportunities for CO_2 sequestration—worldwide screening for CO_2-EOR and CO_2-ECBM projects.* Energy, 2005. **30**(10): p. 1931-1952.

196.   Mosavat, N. and F. Torabi, *Experimental evaluation of the performance of carbonated water injection (CWI) under various operating conditions in light oil systems.* Fuel, 2014. **123**(Supplement C): p. 274-284.

197.   Alizadeh, A.H., et al., *Multi-scale experimental study of carbonated water injection: An effective process for mobilization and recovery of trapped oil.* Fuel, 2014. **132**(Supplement C): p. 219-235.

198.   Sohrabi, M., et al., *Coreflooding Studies to Investigate the Potential of Carbonated Water Injection as an Injection Strategy for Improved Oil Recovery and CO_2 Storage.* Transport in Porous Media, 2012. **91**(1): p. 101-121.

199.   Sohrabi, M., et al., *Safe storage of Co2 together with improved oil recovery by Co2-enriched water injection.* Chemical Engineering Research and Design, 2011. **89**(9): p. 1865-1872.

200.   Dong, Y., et al., *An Experimental Investigation of Carbonated Water Flooding.* Society of Petroleum Engineers.

201.   Sohrabi, M., et al., *A Thorough Investigation of Mechanisms of Enhanced Oil Recovery by Carbonated Water Injection.* 2015, Society of Petroleum Engineers.

202.   Mahdavi, S. and L. James, *Investigation of Water Flooding and Carbonated Water Injection (CWI) in a Fractured Porous Media.*

203.   Yang, D., P. Tontiwachwuthikul, and Y. Gu, *Interfacial Tensions of the Crude Oil + Reservoir Brine + CO_2 Systems at Pressures up to 31 MPa and Temperatures of 27 °C and 58 °C.* Journal of Chemical & Engineering Data, 2005. **50**(4): p. 1242-1249.

204.   Seyyedi, M., P. Mahzari, and M. Sohrabi, *A comparative study of oil compositional variations during CO_2 and carbonated water injection scenarios for EOR.* Journal of Petroleum Science and Engineering, 2018. **164**: p. 685-695.

205.   Fjelde, I. and S.M. Asen, *Wettability alteration during water flooding and carbon dioxide flooding of reservoir chalk rocks*, in *SPE EUROPEC/EAGE Annual Conference and Exhibition.* 2010, Society of Petroleum Engineers: Barcelona, Spain.

206.   Buckley, J.S., Y. Liu, and S. Monsterleet, *Mechanisms of Wetting Alteration by Crude Oils.* SPE Journal, 1998(03).

207. Buckley, J.S., et al., *Asphaltenes and Crude Oil Wetting - The Effect of Oil Composition.* SPE Journal, 1997(06).

208. Dubey, S. and P. Doe, *Base number and wetting properties of crude oils.* SPE Reservoir Engineering, 1993. **8**(3): p. 195-200.

209. Suijkerbuijk, B., et al., *Fundamental Investigations into Wettability and Low Salinity Flooding by Parameter Isolation*, in *SPE Improved Oil Recovery Symposium*. 2012, Society of Petroleum Engineers: Tulsa, Oklahoma, USA.

210. Mahani, H., et al., *Electrokinetics of Carbonate/Brine Interface in Low-Salinity Waterflooding: Effect of Brine Salinity, Composition, Rock Type, and pH on ζ-Potential and a Surface-Complexation Model.* SPE Journal, 2016.

211. Xie, Q., et al., *A pH-Resolved Wettability Alteration: Implications for CO2-Assisted EOR in Carbonate Reservoirs.* Energy & Fuels, 2017. **31**(12): p. 13593-13599.

212. Strand, S., E.J. Høgnesen, and T. Austad, *Wettability alteration of carbonates— Effects of potential determining ions (Ca2+ and SO42−) and temperature.* Colloids and Surfaces A: Physicochemical and Engineering Aspects, 2006. **275**(1): p. 1-10.

213. Y.Q. Chen, Q.X., A. Sari, P.V. Brady, A. Saeedi, *Oil/Water/Rock Wettability: Influencing Factors and Implications for Low Salinity Water Flooding in Carbonate Reservoirs.* Fuel, 2018: p. In press.

214. Austad, T., et al., *Low Salinity EOR Effects in Limestone Reservoir Cores Containing Anhydrite: A Discussion of the Chemical Mechanism.* Energy & Fuels, 2015. **29**(11): p. 6903-6911.

215. Teklu, T.W., et al., *Low-salinity Water-alternating-CO2 Flooding Enhanced Oil Recovery: Theory and Experiments*. 2014, Society of Petroleum Engineers.

216. Downs, H.H., P., *Enhaced recovery by wettability alteration. In Oil Field Chemistry: Enhanced recovery and production stimulation 396 ch.* Vol. 32. 1989, American Chemical Society.

217. Le Van, S. and B.H. Chon, *Effects of salinity and slug size in miscible CO2 water-alternating-gas core flooding experiments.* Journal of Industrial and Engineering Chemistry, 2017.

218. Zheng, S. and D. Yang, *Pressure Maintenance and Improving Oil Recovery by Means of Immiscible Water-Alternating-CO2 Processes in Thin Heavy-Oil Reservoirs.* 2013.

219. Mohd Shafian, S.R., et al., *Enhancing the Efficiency of Immiscible Water Alternating Gas (WAG) Injection in a Matured, High Temperature and High CO2 Solution Gas Reservoir - A Laboratory Study*. 2013, Society of Petroleum Engineers.

220. Zuloaga, P., et al., *Performance evaluation of CO2 Huff-n-Puff and continuous CO2 injection in tight oil reservoirs.* Energy, 2017. **134**(Supplement C): p. 181-192.

221. Pu, W., et al., *Experimental investigation of CO2 huff-n-puff process for enhancing oil recovery in tight reservoirs.* Chemical Engineering Research and Design, 2016. **111**(Supplement C): p. 269-276.

222. Ramanathan, R., A.M. Shehata, and H.A. Nasr-El-Din, *Water Alternating CO2 Injection Process - Does Modifying the Salinity of Injected Brine Improve Oil Recovery?* 2015, Offshore Technology Conference.

223. Wilson, A., *CO2 Low-Salinity Water Alternating Gas: A Promising New Approach for EOR.* 2015.

224. Kuuskraa, V.A., et al., *Improving domestic energy security and lowering CO2 emissions with "next generation" CO2-enhanced oil recovery (CO2-EOR).* National Energy Technology Laboratory, Pittsburgh, PA, USA, 2011.

225. Ma, J., et al., *Enhanced light oil recovery from tight formations through CO2 huff 'n' puff processes.* Fuel, 2015. **154**(Supplement C): p. 35-44.

226. Venkatraman, A., et al., *Modeling Effect of Geochemical Reactions on Real-Reservoir-Fluid Mixture During Carbon Dioxide Enhanced Oil Recovery.* SPE Journal, 2017.

227. Hirasaki, G. and D.L. Zhang, *Surface Chemistry of Oil Recovery From Fractured, Oil-Wet, Carbonate Formations.* SPE Journal, 2004.

228.   Grape, S., S. Poston, and J. Osoba, *Imbibition Flooding with CO2-Enriched Water.* SCA Conference paper, 1990.

229.   Kechut, N.I., M. Sohrabi, and M. Jamiolahmady, *Experimental and Numerical Evaluation of Carbonated Water Injection (CWI) for Improved Oil Recovery and CO2 Storage*, in *SPE EUROPEC/EAGE Annual Conference and Exhibition.* 2011, Society of Petroleum Engineers: Vienna, Austria.

230.   Potter, G.F., *The Effects of CO2 Flooding on Wettability of West Texas Dolomitic Formations.* 1987, Society of Petroleum Engineers.

231.   Fjelde, I. and S.M. Asen, *Wettability alteration during water flooding and carbon dioxide flooding of reservoir chalk rocks.* 2010, Society of Petroleum Engineers.

232.   Sharbatian, A., et al., *Full Characterization of CO2–Oil Properties On-Chip: Solubility, Diffusivity, Extraction Pressure, Miscibility, and Contact Angle.* Analytical Chemistry, 2018. **90**(4): p. 2461-2467.

233.   Le Van, S. and B.H. Chon, *Effects of salinity and slug size in miscible CO2 water-alternating-gas core flooding experiments.* Journal of Industrial and Engineering Chemistry, 2017. **52**: p. 99-107.

234.   Li, S., et al., *Evaluation of four CO2 injection schemes for unlocking oils from low-permeability formations under immiscible conditions.* Fuel, 2018. **234**: p. 814-823.

235.   Riazi, M., M. Sohrabi, and M. Jamiolahmady, *Experimental Study of Pore-Scale Mechanisms of Carbonated Water Injection.* Transport in Porous Media, 2011. **86**(1): p. 73-86.

236.   Seyyedi, M., P. Mahzari, and M. Sohrabi, *An integrated study of the dominant mechanism leading to improved oil recovery by carbonated water injection.* Journal of Industrial and Engineering Chemistry, 2017. **45**: p. 22-32.

237.   Seyyedi, M., et al., *Quantification of oil recovery efficiency, CO2 storage potential, and fluid-rock interactions by CWI in heterogeneous sandstone oil reservoirs.* Journal of Molecular Liquids, 2018. **249**: p. 779-788.

238.   Shu, G., et al., *Improvement of CO2 EOR performance in water-wet reservoirs by adding active carbonated water.* Journal of Petroleum Science and Engineering, 2014. **121**: p. 142-148.

239.   Guidotti, C.V., *Micas in metamorphic rocks.* Reviews in Mineralogy and Geochemistry, 1984. **13**(1): p. 357-467.

240.   Hansen, G., A.A. Hamouda, and R. Denoyel, *The effect of pressure on contact angles and wettability in the mica/water/n-decane system and the calcite+stearic acid/water/n-decane system.* Colloids and Surfaces A: Physicochemical and Engineering Aspects, 2000. **172**(1): p. 7-16.

241.   Lee, S.Y., et al., *Low Salinity Oil Recovery: Increasing Understanding of the Underlying Mechanisms*, in *SPE Improved Oil Recovery Symposium.* 2010, Society of Petroleum Engineers: Tulsa, Oklahoma, USA. p. 11.

242.   Peng, D.-Y. and D.B. Robinson, *A new two-constant equation of state.* Industrial & Engineering Chemistry Fundamentals, 1976. **15**(1): p. 59-64.

243.   Yutkin, M.P., et al., *Bulk and surface aqueous speciation of calcite: implications for low-salinity waterflooding of carbonate reservoirs.* SPE Journal, 2017.

244.   Al-Mutairi, S.M., et al., *An experimental investigation of wettability alteration during CO2 immiscible flooding.* Journal of Petroleum Science and Engineering, 2014. **120**(Supplement C): p. 73-77.

245.   Yang, D., Y. Gu, and P. Tontiwachwuthikul, *Wettability Determination of the Crude Oil−Reservoir Brine−Reservoir Rock System with Dissolution of CO 2 at High Pressures and Elevated Temperatures.* Energy & Fuels, 2008. **22**(4): p. 2362-2371.

246.   Helling, C.S., G. Chesters, and R.B. Corey, *Contribution of Organic Matter and Clay to Soil Cation-Exchange Capacity as Affected by the pH of the Saturating Solution1.* Soil Science Society of America Journal, 1964. **28**: p. 517-520.

247.   Ainsworth, C.C., J.M. Zachara, and R.L. Schmidt, *Quinoline sorption on Na-montmorillonite: Contributions of the protonated and neutral species.* 1987.

248.   Helmy, A., S. De Bussetti, and E. Ferreiro, *Adsorption of quinoline from aqueous solutions by some clays and oxides.* Clays Clay Miner, 1983. **31**(1): p. 29-36.

Appendix 1

In this section, attribution tables for all publications are presented here to illustrate contribution from all co-authors.

Paper **"Drivers of pH increase and implications for low salinity effect in sandstone"**, Fuel 218, 112-117.

Authors: Yongqiang Chen[1], Quan Xie[1], Wanfen Pu[2], Ali Saeedi[1]

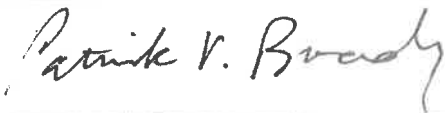[1] Department of Petroleum Engineering, Curtin University, 6151 Kensington, Western Australia.

[2] State Key Laboratory of Oil and Gas Reservoir Geology and Exploitation, Southwest Petroleum University, Chengdu, Sichuan 610500, China

Name	conception and design	Acquisition of data & method	Data conditioning & manipulation	Analysis & statistical method	Interpretation & discussion	Final approval
Yongqiang Chen	×	×	×	×	×	
Signature: Yongqiang CHEN						
Quan Xie			×	×	×	×
Signature:						
Wanfen Pu					×	
Signature:						
Ali Saeedi						×
Signature:						
I acknowledge that these represent my contribution to the above research output.						

Paper "**Role of ion exchange, surface complexation, and albite dissolution in low salinity water flooding in sandstone**", Journal of Petroleum Science and Engineering 176, 126-131.

Authors: Yongqiang Chen[1], Quan Xie[1], Ali Saeedi[1]

[1] Department of Petroleum Engineering, Curtin University, 6151 Kensington, Western Australia.

Name	conception and design	Acquisition of data & method	Data conditioning & manipulation	Analysis & statistical method	Interpretation & discussion	Final approval
Yongqiang Chen	×	×	×	×	×	
Signature: Yongqiang CHEN						
Quan Xie			×	×	×	×
Signature: Samdie						
Ali Saeedi						×
Signature: AliSaeedi						
I acknowledge that these represent my contribution to the above research output.						

Paper "**Electrostatic characterization of -NH$^+$-brine-kaolinite system: Implications for low salinity waterflooding in sandstone reservoirs**", Journal of Petroleum Science and Engineering 179, 539-545.

Authors: Yongqiang Chen[1], Quan Xie[1], Ali Saeedi[1]

[1] Department of Petroleum Engineering, Curtin University, 6151 Kensington, Western Australia.

Name	conception and design	Acquisition of data & method	Data conditioning & manipulation	Analysis & statistical method	Interpretation & discussion	Final approval
Yongqiang Chen	✗	✗	✗	✗	✗	
Signature: *Yongqiang CHEN*						
Quan Xie	✗		✗	✗	✗	✗
Signature: *Sanxie*						
Ali Saeedi						✗
Signature: *Ali Saeedi*						
I acknowledge that these represent my contribution to the above research output.						

Paper "Oil/water/rock wettability: Influencing factors and implications for low salinity water flooding in carbonate reservoirs", Fuel 215, 171-177.

Authors: Yongqiang Chen[1], Quan Xie[1], Ahmad Sari[1], Patrick V Brady[2], Ali Saeedi[1]

[1] Department of Petroleum Engineering, Curtin University, 6151 Kensington, Western Australia.
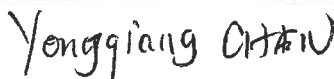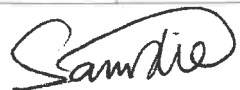
[2] Sandia National Laboratories, Albuquerque, New Mexico, 87185-0754, United States.

Name	conception and design	Acquisition of data & method	Data conditioning & manipulation	Analysis & statistical method	Interpretation & discussion	Final approval
Yongqiang Chen	×	×	×	×	×	
Signature:	*Yongqiang CHAN*					
Quan Xie			×	×	×	×
Signature:	*Sam Xie*					
Ahmad Sari		×				
Signature:	*(signature)*					
Patrick V Brady				×	×	
Signature:	*Patrick V. Brady*					
Ali Saeedi						×
Signature:	*A Saeedi*					
I acknowledge that these represent my contribution to the above research output.						

Paper "**Insights into the wettability alteration of CO2-assisted EOR in carbonate reservoirs**", Journal of Molecular Liquids 279, 420-426.

Authors: Yongqiang Chen[1], Ahmad Sari[1], Quan Xie[1], Ali Saeedi[1]

[1] Department of Petroleum Engineering, Curtin University, 6151 Kensington, Western Australia.

Name	conception and design	Acquisition of data & method	Data conditioning & manipulation	Analysis & statistical method	Interpretation & discussion	Final approval
Yongqiang Chen	×	×	×	×	×	
Signature: *Yongqiang CHEN*						
Ahmad Sari		×				
Signature:						
Quan Xie	×		×	×	×	×
Signature: *Sam Xie*						
Ali Saeedi						×
Signature: *Ali Saeedi*						
I acknowledge that these represent my contribution to the above research output.						

Paper "**Electrostatic Origins of CO 2-Increased Hydrophilicity in Carbonate Reservoirs**", Scientific reports 8 (1), 17691.

Authors: Yongqiang Chen[1], Ahmad Sari[1], Quan Xie[1], Patrick V Brady[2], Md Mofazzal Hossain[1], Ali Saeedi[1]

[1] Department of Petroleum Engineering, Curtin University, 6151 Kensington, Western Australia.

[2] Sandia National Laboratories, Albuquerque, New Mexico, 87185-0754, United States.

Name	conception and design	Acquisition of data & method	Data conditioning & manipulation	Analysis & statistical method	Interpretation & discussion	Final approval
Yongqiang Chen	×	×	×	×	×	
Signature: *Yongqiang CHEN*						
Ahmad Sari		×				
Signature:						
Quan Xie			×	×	×	×
Signature:						
Patrick V Brady				×	×	
Signature: *Patrick V. Brady*						
Md Mofazzal Hossain				×	×	
Signature:						
Ali Saeedi						×
Signature: *Ali Saeedi*						

I acknowledge that these represent my contribution to the above research output.

Paper "Excess H+ Increases Hydrophilicity during CO2-Assisted Enhanced Oil Recovery in Sandstone Reservoirs", Energy Fuels 2019, 33, 2, 814-821.

Authors: Yongqiang Chen[1], Ahmad Sari[1], Quan Xie[1], Ali Saeedi[1]

[1] Department of Petroleum Engineering, Curtin University, 6151 Kensington, Western Australia.

Name	conception and design	Acquisition of data & method	Data conditioning & manipulation	Analysis & statistical method	Interpretation & discussion	Final approval
Yongqiang Chen	×	×	×	×	×	
Signature: *Yongqiang CHEN*						
Ahmad Sari		×				
Signature:						
Quan Xie			×	×	×	×
Signature:						
Ali Saeedi						×
Signature:						
I acknowledge that these represent my contribution to the above research output.						

Appendix 2

In this section, the copyright agreements between the author and journals are included to reuse the author's own publication in this thesis.

RightsLink®

Home | Create Account | Help | LIVE CHAT
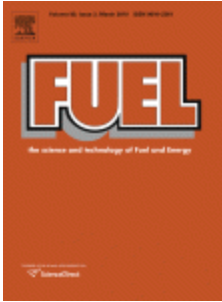
Title: Drivers of pH increase and implications for low salinity effect in sandstone

Author: Yongqiang Chen,Quan Xie,Wanfen Pu,Ali Saeedi

Publication: Fuel

Publisher: Elsevier

Date: 15 April 2018

© 2018 Elsevier Ltd. All rights reserved.

BACK | CLOSE WINDOW

Title: Role of ion exchange, surface complexation, and albite dissolution in low salinity water flooding in sandstone

Author: Yongqiang Chen, Quan Xie, Ali Saeedi

Publication: Journal of Petroleum Science and Engineering

Publisher: Elsevier

Date: May 2019

BACK | CLOSE WINDOW

RightsLink®

| Home | Create Account | Help | LIVE CHAT |

Title: Electrostatic characterization of -NH+-brine-kaolinite system: Implications for low salinity waterflooding in sandstone reservoirs

Author: Yongqiang Chen,Quan Xie,Ali Saeedi

Publication: Journal of Petroleum Science and Engineering

Publisher: Elsevier

Date: August 2019

LOGIN

If you're a copyright.com user, you can login to RightsLink using your copyright.com credentials.

Already **a RightsLink user** or want to learn more?

| BACK | CLOSE WINDOW |

Title: Oil/water/rock wettability: Influencing factors and implications for low salinity water flooding in carbonate reservoirs

Author: Yongqiang Chen,Quan Xie,Ahmad Sari,Patrick V. Brady,Ali Saeedi

Publication: Fuel

Publisher: Elsevier

Date: 1 March 2018

© 2017 Elsevier Ltd. All rights reserved.

BACK   CLOSE WINDOW

RightsLink®

Home | Create Account | Help | LIVE CHAT

Title: Insights into the wettability alteration of CO2-assisted EOR in carbonate reservoirs

Author: Yongqiang Chen,Ahmad Sari,Quan Xie,Ali Saeedi

Publication: Journal of Molecular Liquids

Publisher: Elsevier

Date: 1 April 2019

© 2019 Elsevier B.V. All rights reserved.

BACK | CLOSE WINDOW

Copyright Clearance Center

RightsLink®

SPRINGER NATURE

Title:	Electrostatic Origins of CO2-Increased Hydrophilicity in Carbonate Reservoirs
Author:	Yongqiang Chen et al
Publication:	Scientific Reports
Publisher:	Springer Nature
Date:	Dec 6, 2018

Copyright © 2018, Springer Nature

Creative Commons

RightsLink®

Copyright Clearance Center

| Home | Create Account | Help | LIVE CHAT |

ACS Publications Most Trusted. Most Cited. Most Read.

Title: Excess H Increases Hydrophilicity during CO2-Assisted Enhanced Oil Recovery in Sandstone Reservoirs

Author: Yongqiang Chen, Ahmad Sari, Quan Xie, et al

Publication: Energy & Fuels

Publisher: American Chemical Society

Date: Feb 1, 2019

Copyright © 2019, American Chemical Society

Quick Price Estimate

Permission for this particular request is granted for print and electronic formats, and translations, at no charge. Figures and tables may be modified. Appropriate credit should be given. Please print this page for your records and provide a copy to your publisher. Requests for up to 4 figures require only this record. Five or more figures will generate a printout of additional terms and conditions. Appropriate credit should read: "Reprinted with permission from {COMPLETE REFERENCE CITATION}. Copyright {YEAR} American Chemical Society." Insert appropriate information in place of the capitalized words.

I would like to...	reuse in a Thesis/Dissertation ▼
Requestor Type	Author (original work) ▼
Portion	Full article ▼
Format	Print and Electronic ▼
Will you be translating?	No ▼
Select your currency	USD - $ ▼
Quick Price	Click Quick Price

This service provides permission for reuse only. If you do not have a copy of the article you are using, you may copy and paste the content and reuse according to the terms of your agreement. Please be advised that obtaining the content you license is a separate transaction not involving Rightslink.

| QUICK PRICE | CONTINUE |

To request permission for a type of use not listed, please contact the publisher directly.